Experimental and Theoretical Investigation of the Crack Behavior of RC-slabs Subjected to Biaxial Bending

Daguang Han

Acknowledgement

Daguang Han

Universität der Bundeswehr München

Fakultät für Bauingenieur- und Vermessungswesen

Thema der Dissertation:

Experimental and Theoretical Investigation of the Crack Behavior of RC-slabs Subjected to Biaxial Bending

Verfasser: M.Sc. Daguang Han

Promotionsausschuss:

Vorsitzender: Univ.-Prof. Dr.-Ing. Ingbert Mangerig

1. Berichterstatter: Univ.-Prof. Dr.-Ing.Manfred Keuser

2. Berichterstatter: Univ.-Prof. Dr.-Ing. Oliver Fischer, TU München

Tag der Prüfung: 15. Dezember 2011

Mit der Promotion erlangter akademischer Grad:

Doktor der Ingenieurwissenschaften (Dr.- Ing.)

Neubiberg, den 15. Dezember 2011

Abstract

The flexural cracking behavior of reinforced concrete (RC) members, such as beams and slabs, is an important issue for serviceability limit state design. It has also a significant influence on the load bearing capacity of the structures. To date, the influence of the transverse reinforcement (TR) on the cracking properties of RC slabs subjected to uniaxial and biaxial bending has not been well understood. No experimental investigations of the influencing mechanism of TR parameters on the cracks have been carried out. Hence, design equations involving the influence of TR for the flexural cracking behavior are not available in the current codes of practice.

This thesis presented a comprehensive study on the influence of transverse reinforcement on the cracking patterns of RC slabs, including both slab-strips under uniaxial bending and also slabs subjected to biaxial bending. The variations in the tests include:

- Transverse reinforcement concrete cover (TR-cover);
- Transverse reinforcement spacing (TR-spacing);
- Transverse reinforcement direction to principle bending stress (TR-direction); and
- Transverse reinforcement position to longitudinal reinforcement (TR-position).

For each case, three different concrete types, including normal strength concrete, high strength concrete and lightweight concrete were also taken into account. Two series of experimental investigations, that is, uniaxial and biaxial bending tests, were performed, respectively. More than 8000 test data for the average crack spacing and the maximum crack width were obtained.

The experimental work on slab-strips subjected to uniaxial bending reveals that TR-cover TR-spacing as well as TR-direction has a considerable influence on the cracking behavior of the members.

- TR-cover and TR-spacing influence crack spacing and width;
- TR-direction influences the propagation of cracks intersected with TR;
- Concrete types influences the crack spacing and width related to the bond-slip relationship between steel and concrete.

Based on the experimental observations and theoretical analysis, new calculation equations for the average crack spacing and maximum crack width of RC slabs subjected to uniaxial bending were proposed. These equations take into account the influence of the transverse reinforcement and also the concrete types. A comparison of the calculated and experimental data indicates that the proposed design models provide a much better prediction of average crack spacing and maximum crack width than that

given by various codes, such as FIB Model Code 2010, DIN EN 1992-1-2011, DIN 1045-1-2008 and ACI 318-2008.

In the experiment on RC slabs under biaxial bending, the experimental observations verify that the different TR-cover in two orthogonal directions result in a different numbers of TR-induced cracks. The inclined orthogonal reinforcement net does not lead to a change of overall direction of cracks. In general, the influence of transverse reinforcement on the cracking behavior of the slab under biaxial bending is in good agreement with that in uniaxial bending. Moreover, due to the biaxial bending stress, a reverse relationship of decreasing bond-slip stress on perpendicular direction and increasing crack spacing and width was found in the experiment. Based on the mechanism analysis of interaction between the transverse reinforcement and the surrounding concrete, new models were developed to predict the average crack spacing and the maximum crack width of RC slabs under biaxial bending taking into account the TR-cover and TR-direction in two orthogonal directions and concrete types. In comparison with the design provisions, the new design equations can describe the cracking behavior of RC slabs subjected to biaxial bending in a more accurate way.

The work in this thesis is beneficial for the correctly understanding the influence of transverse reinforcement on the flexural cracking of reinforced concrete members and also helps to achieve a rational evaluation and design for the serviceability limit state

Table of Contents

1 Introduction

1.1 Background

Due to the low tensile strength of concrete, cracking in Reinforced Concrete (RC) structures subjected to various loadings is unavoidable. Wider cracks may not only affect visual aesthetics of building structures, but also expose tensile or shear reinforcement to the environment, which may lead to corrosion. In other words, crack width is one of the most significant factors affecting nonlinear behavior of RC structure. Hence, it should be effectively predicted and controlled.

The reasons of cracking in the concrete are numerous and complex, but cracks occurred mostly due to one or more of the following actions:

(a) Cracking due to the settlement of plastic concrete;

(b) Cracking due to the volumetric change;

(c) Cracking due to bending stresses resulting from the applied load or reaction forces.

Generally, action-(c) is one of the most common reasons causing flexural cracks in construction and considered by current design codes for concrete structures. In this case, cracks occur in the tension zone of transverse reinforcement element (TR-element) subjected to bending and expand under external loads or reaction forces once the rupture modulus of the concrete is exceeded. Behaviors of these flexural cracks are influenced by many variables and factors of reinforced concrete beams and slabs. Investigation of these factors affecting on crack pattern, spacing and width is the foundation of controlling cracks.Equation Chapter (Next) Section 1

On the basis of investigation for many years, it is well accepted that the bond strength between steel reinforcement and concrete is the main influencing factor for cracking behavior in recent research developments [1]. The second important factor for cracking behavior is the stress in the reinforcement. It has been confirmed by studies of Gergely and Lutz [2] and [3]. In their study, the crack width is proportional to the steel stress. Furthermore, experiments by Broms [4] and others have shown that the crack spacing and crack width are related to the concrete cover, which is measured from the centre of the bar to the face of the concrete.

The obtained investigation results helped people to decrease crack width with suitable techniques and methods. To control cracks width when designing a RC element, a number of approximate, semi-theoretical, and empirical approaches and formulas have been presented and developed for predicting the flexural crack spacing and width. These proposed approaches and formulas contained a different set of variables for RC structures under various loads. In early theories, crack widths were believed to depend on the bond strength between concrete and reinforcement [5]. The crack spacing was predicted by the concrete tensile strength and the tension reinforcement ratio. The crack width was

generally supposed to be the reinforcement extension between two cracks. In recent approaches, flexural crack width is primarily a function of steel stress [2, 3] and the relative distance from the neutral axis to the tensile reinforcement [4]. Above factors were considered partially or entirely by current codes. For example, formulas of the FIB Model Code 2010 (Draft)[6] and DIN1045-1 are based on Bond-slip mechanism, which considered the stress transfer mechanism between concrete and reinforcement to estimate crack spacing and width. Thus, parameters of bond strength, steel diameters, steel ratio and steel stress were considered by current codes.

The formulas of DIN EN 1992-1-2011 are developed based on the Combination Model, which combines Bond-slip mechanism and No-slip mechanism. Concrete cover is considered additionally as a parameter to estimate crack spacing.

Due to the complexity of stress and displacement between concrete and steel, an empirical equation to estimate crack width is directly adopted by ACI 318-2008, which involves a series of parameters, such as steel stress, the side and bottom side covers, strain gradient from the steel level to the tension face and effective concrete area.

In 1970s, Beeby [7] found that a crack could be induced roughly in the region of TR and the crack will be induced along TR. Further investigations were conducted by other researchers [8-10]. Mr. Rizkalla [10] tested 18 reinforced concrete specimens to study the influence of TR spacing on crack behavior, and presented expressions to predict the crack spacing of RC members subjected to axial tension. However, although TR was proved to affect crack spacing significantly, it was not considered as a parameter in above current codes.

Furthermore, most formulas in these codes are based on test results of RC element subjected to tension loads. However, RC element under bending load is more common in practical construction. For example, the box grider beam of bridge constriction is shown in Figure 1-1, bridge slab in two orthogonal directions and the slab in the loading bearing area under the column supports are subjected to bending stress. This bending stress situation are very different with tension. Thus, crack behaviors of them are very different. Especially the RC-slabs subjected to biaxial bending. The Figure 1-2 [11] shows a comparison of different load-deformation curves of RC element subjected to uniaxial and biaxial bending, respectively. It indicates that when subjected to biaxial bending, cracking load of RC tensile element decreased and thus a different load-deformation curve is appeared.

(a)   Soodiya Bridge from Abu Dhabi
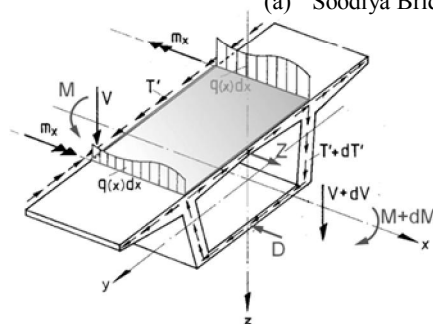
(b) Box beam element
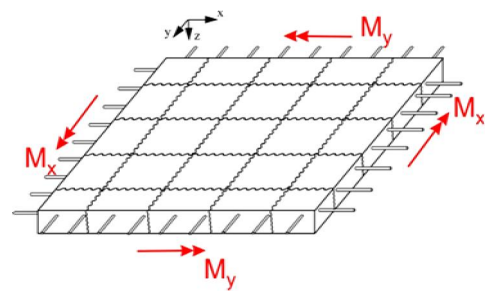
(c) Stresses on the plane element

Figure 1-1 Application for a combined stress in bridge construction

Investigations of orthogonal reinforcement net affecting two-way RC-slabs were also conducted by researches. The major work was performed in the United States by Nawy etal.[12, 13] and Clark[14]. Nawy etal.[12, 13] have reported tests results of two-way concrete slabs reinforced by high-strength welded mesh reinforcement. Two types of cracking were observed: one is an orthogonal crack pattern followed the reinforcement lines, and the other is a diagonal crack pattern, which further developed to the yield line pattern under higher loading. Moreover, a grid index factor was introduced to determine the influence of reinforcing steel spacing, diameter and content, and concrete cover thickness on crack width. However, the influence of orthogonal reinforcement direction on crack pattern was not considered. Clark [14] has reported results of theoretical and experimental studies of one-way spanning slabs with bars at various angles to the direction of moment. Thus, one-way slab specimens simulate regions of two-way slabs with bending predominantly in one direction.

In order to investigate the influence of orthogonal reinforcement on cracking behaviors for two-way slabs subjected to biaxial tension and bending, many experimental and numerical analysis have been carried out at the Institute for Structure Engineering of University of German Armed Forces since 2001 sponsored by DFG (Deutschen Forschungsgesellschaft).

(a) Uniaxial stress situation

(b) Biaxial stress situation
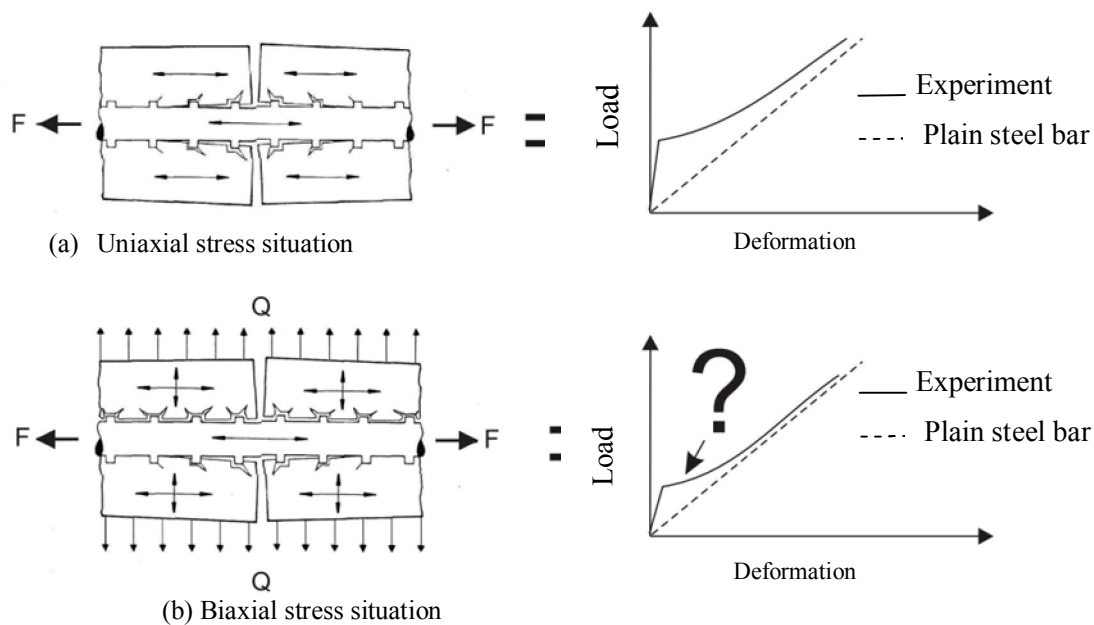
Figure 1-2 Influence of Stress on load-deformation behavior

Purainae [15, 16] conducted experimental and theoretical investigations on load-deformation behavior of RC-plane under biaxial tension. He supposed a reduction of cracking load and thus the load-deformation relationship was changed (Figure 1-2), and crack and load-deformation behavior significantly affected by the orthogonal reinforcement net was appeared. Based on interrelated experiments, the transverse reinforcement mechanism affects on crack behavior was investigated thoroughly and a corresponding theoretical model to predict crack spacing was presented.

Due to different stresses of RC element under tension and bending, further experimental investigations on load-deformation-behavior of RC-slab subjected to biaxial bending were performed by Rüdiger [17] during 2005-2008. The experiment and simulation analysis were conducted based on 15 concrete slabs with different directions of reinforcement net (with the angle of 0°, 22.5° and 45° between rebar net and the bending direction), which subjected to biaxial bending. Test results indicates that crack pattern and spacing was affected by the angle between reinforcement net and bending and their concrete types. Moreover, curves of load-deformation show different behaviors at different angles of 0°, 22.5° and 45°.

According to the previous investigation，it can be observed that the influence of TR on crack behavior was probably affected by parameters of concrete cover (TR-cover), spacing (TR-spacing), direction (TR-direction to bending stress), position (TR-position switches from outside of LR to the inside) and concrete types (normal concrete, high-strength concrete and light-weight concrete).

However, insufficient investigations of the influence of numerous TR parameters on cracking behavior restricted the development of theoretical models. In other words, due to rare investigations studied on inclined TR, which appeared mostly in concrete slabs under

4

biaxial bending, it is difficult to develop theoretical models of crack width for RC slabs under biaxial bending.

Thus, under continuous support of DFG, a number of RC slabs under uniaxial and biaxial bending were tested. In this investigation, four TR parameters and three concrete types were considered to quantitatively study the influence of TR on the crack behavior.

1.2 Objectives

1. Collecting extensive test data during experimental tests of slabs specimens under uniaxial and biaxial bending.

2. Analyzing the mechanism of interaction between TR and intersected cracks and experimentally verifying the influence of TR-parameters on crack behavior.

3. Attempting to establish a numerical model to describe the influence of TR-parameters on crack behavior.

4. Comparing the influence of TR on crack behavior between one-way slab-strips and two-way slabs in order to find the consistency and difference.

5. Modifying the average crack spacing and maximum crack width model of DIN EN 1992-1-2011 and presenting the crack design model of RC slabs under uniaxial bending, based on the test results and the mechanism of interaction between TR and cracks.

6. Verifying the direct correlation between curvature and crack width based on the experimental results.

7. Establishing a new crack design model to calculate maximum crack width by using the direct correlation between curvature and crack width. Steel stress is not involved in this model, but bending stiffness, inertia moment and average concrete strain are involved to calculate the maximum crack width.

8. Comparing test results with predicted values according to two new crack models and other formulas in current codes, such as FIB Model Code 2010 (draft), EN DIN 1992-1-2011, DIN1045-2008 and ACI 318-2008.

1.3 Scope of the thesis

The values of physics related to TR-parameters and crack behavior were recorded, such as the position of TR and its distance to the nearest crack, the angle between TR and intersected cracks, every crack spacing and width at each load step. The total measurement times were more than 10000 times. Moreover, Laserscanner were used to measure the surface deformation with distance of 1cmx1cm.

By using the graphing method, line regression analysis and correlation analysis, the relationship between factors are analyzed to obtain the most effective TR-parameter and

verify the influence mechanism of TR on intersected cracks.

Utilizing the mechanical analysis method, the restrained influence of TR on crack width is representing and the crack restraint model is developed.

Based on the crack spacing and width calculation model of current design codes and the relationship between TR and surrounding concrete, adding the influence of TR on cracks into the current design model to calculate the average crack spacing and maximum width with consideration of TR-parameters

Attempting to experimentally investigate the relationship between crack width and average curvature. Utilizing the physical, geometric and mechanical equilibrium equations to develop a correlation between maximum crack width and effective flexural stiffness and establish a new flexural crack model.

The work was illuminated in Figure 1-3
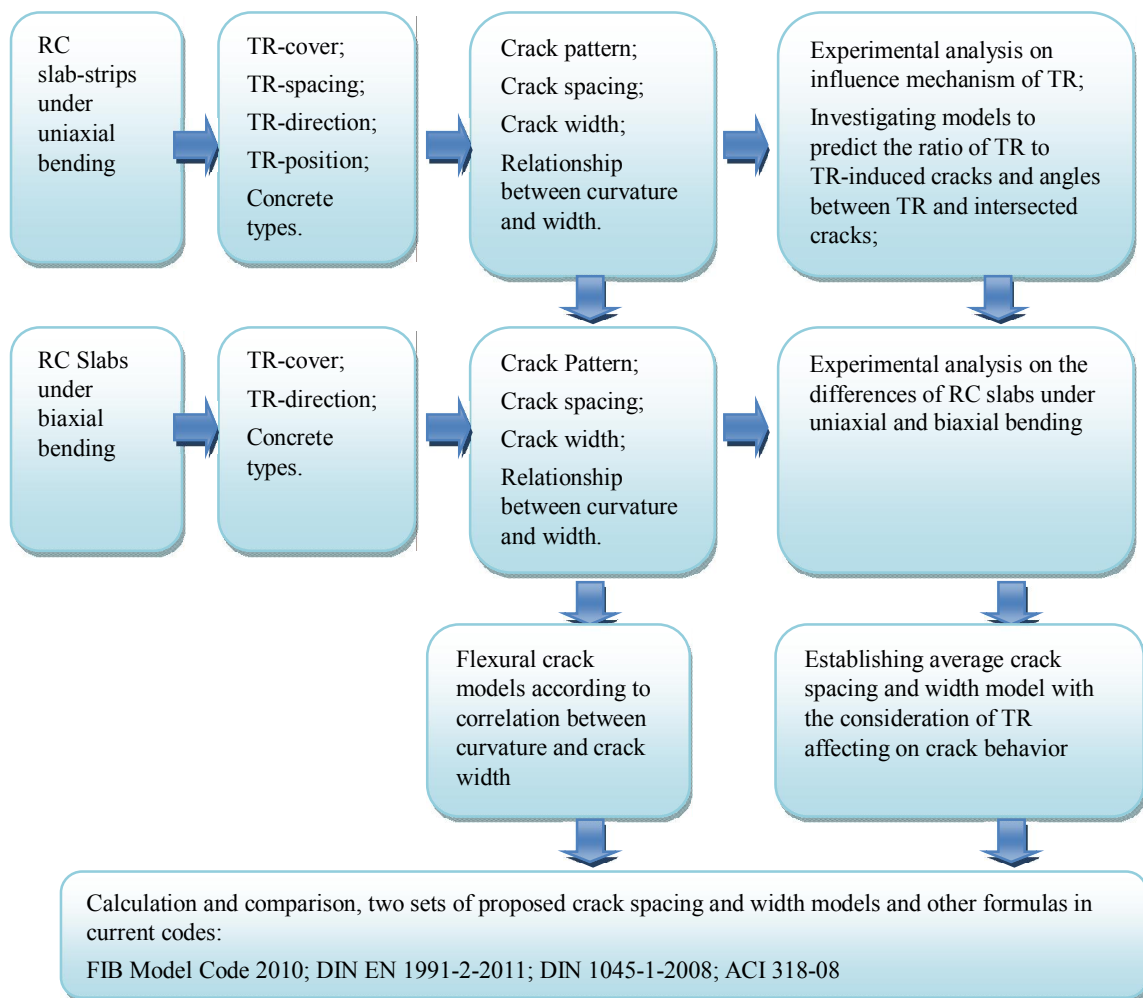
Figure 1-3 Illustration of study work in this dissertation

1.4 Organization

Following Chapter 1, Chapter 2 provides a literature review of investigation carried out by various [18-20] researchers aimed to develop crack spacing and width models considered different variables. It also includes a review of different classical experiments on crack behavior. The experimental results will be adopted in the next chapter to carry out a comparison between test results in this thesis and in pervious tests.

In Chapter 3, three series of slab-strips tests are described. The influence of TR-parameters, TR-cover, -spacing, -direction and –position are investigated. Influence range of TR parameters on cracking behavior is analyzed. Based on this analysis, the calculation model is presented to calculate the ratio of TR-induced cracks to all cracks and the angle between TR and TR-intersected cracks.

Chapter 4 describes test procedure and slab test results, which incorporating TR parameters of one-way slab-strips in Chapter 3, especially the parameters of TR-cover, TR-direction and concrete types. By using unit average crack width values, which are obtained by the average crack width values divided respective value of LR-cover, the influence of OR-direction and concrete types on crack spacing and width are analyzed. Based on the test results, the calculation model of one-way slab-strips is examined. Then the influence of orthogonal reinforcement cover (OR-cover), OR-direction and concrete types, as well as the influence of biaxial bending stress were investigated. Moreover, the correlation between curvature and flexural average crack width in two orthogonal directions is plotted and analyzed in this chapter.

In Chapter 5, a series of theoretical analysis is performed and the influence coefficient is presented to consider the influence of TR-parameters. According to the mechanism of interaction between TR and surrounding concrete, the concrete strain model of the restraint influence of TR between adjacent cracks are presented. And hence, the average crack spacing and maximum crack width formulas are modified to consider the influence of TR-parameters on crack behavior.

In Chapter 6, the forces acted on the cracked and uncracked section are analyzed and then expressions of the height of compressive zone are derived. Furthermore, the physics, geometric and mechanics relationship between crack width and curvature are analyzed. Based on the analysis, a flexural crack design model is developed to evaluate the crack width by incorporating the average concrete tensile stress and strain caused by bond strength.

Finally, in Chapter 7, examples of one slab-strip and one slab are calculated by using the new models in Chapter 5 and Chapter 6 to present the calculation procedure. The predicted values of two proposed crack models and formulas of current codes, including FIB Mode Code 2011, DIN EN 1992-1-2011, DIN 1045-1-2008 and ACI 318-2008, are verified by a comparison of the predicted average crack spacing and maximum crack width.

2 State of the art

2.1 Introduction

This Chapter reviews the most relevant literature on cracking of RC flexural members. The first part introduces the properties of material, such as steel bar, concrete and the interaction between the steel and the concrete. The second part classifies causes of cracking including classical and current parameters. The third part introduces previous researches aimed to develop crack spacing and crack width calculation models. The crack spacing and width prediction formulas according to the current codes, such as FIB Model Code 1990, DIN EN 1992-1-2011, DIN 1045-2008 and ACI 318-2008. Finally, the experimental investigation concerning the performance and results of the RC element subjected to biaxial bending is introduced. Equation Chapter (Next) Section 1

2.2 Material properties

2.2.1 General considerations

In general, due to the complex mechanical behavior of RC structures, many experimental investigations carried out to study the concrete modes of material failure. Such investigations are often quite complicated due to concrete behaves completely different under tension and compression. If tensile stresses are dominating, concrete will fail by cracking. In this case concrete behaves like a fragile material. If compressive stresses are predominate, the failure of concrete will be caused by crushing. In this case, concrete behaves like a tensile material. In contrast to concrete, the mechanical behavior of reinforcing steel bar is characterized by uniaxial tension stress. Compared to concrete behavior, the mechanical properties of steel, as a ductile material, are not very strongly.

In this chapter, the properties of concrete and steel of RC-element subjected to uniaxial bending are examined. Existing models for the compressive and tensile behavior of concrete are introduced.

2.2.2 Uniaxial compressive behavior of Concrete

Concrete is made up of hardened cement paste in which aggregates are mixed and embedded. Hence, it is a heterogeneous material [21, 22]. The concrete behavior in uniaxial compression is usually obtained from testing a cylinders with a height to diameter ratio of 2. Figure 2-1 (a) [23-25] illustrates that the standard cylinder is with a height of 300mm by a diameter of 150mm, and the compressive cylinder strength is f_c'. Smaller size cylinder and cubes illustrated in Figure 2-1 (b) are often used for controlling the production in actual construction. From this test, the stress-strain curve can be measured, as shown in Figure 2-1 (c).
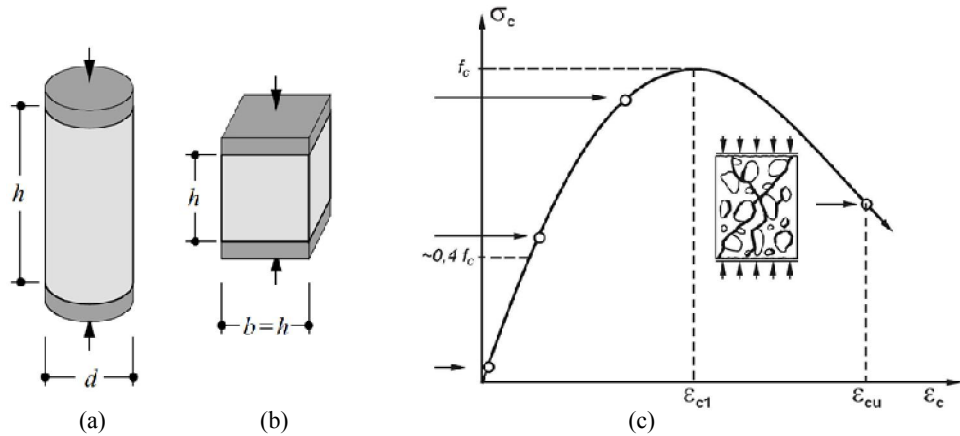
Figure 2-1: Concrete compressive test and bearing capacity model of normal-strength concrete. (a) Cylinder test; (b) cube test; (c) the stress-strain relationship [23-25]

The stress-strain curves are similar to run to its peak point and then show the failure branch on a test specimen. Thus, the higher strength concrete exhibits a significant more brittleness[26]. In FIB Model Code 2010 (draft) [6], the stress-strain relationship for the area of $|\varepsilon_c| < |\varepsilon_{cu}|$ is described by a probable equation of Eq.(2-1),

$$\sigma_c = -\frac{\dfrac{E_{ci}}{E_{cl}} \cdot \dfrac{\varepsilon_c}{\varepsilon_{c1}} - \left(\dfrac{\varepsilon_c}{\varepsilon_{c1}}\right)^2}{1 + \left(\dfrac{E_{ci}}{E_{cl}} - 2\right)\dfrac{\varepsilon_c}{\varepsilon_{c1}}} \cdot f_{cm} \tag{2-1}$$

The value of ε_{c1} is the tangent modulus. ε_{c1} describes the slope of the curve at the origin. ε_{c1} is the secant modulus, which describes the relationship between concrete strength f_{ctm} and associated concrete compression ε_{c1}. The maximum concrete compression strength concrete ε_{c1} in the FIB Model Code 2010 (draft) [6] is defined at constant ε_{c1}=-2.2 ‰. This is contrary to the observation from Rüsch [27] that the compressive strain at maximum concrete strength increases at higher concrete strength classes[18-20]. This effect is considered in the DIN 1045-1-2008. If some of the stress-strain curves of different strength classes in the diagram obtained from the stress-strain relationship of Eq. (2-1), this strength effect can be clearly visible in Figure 2.7.
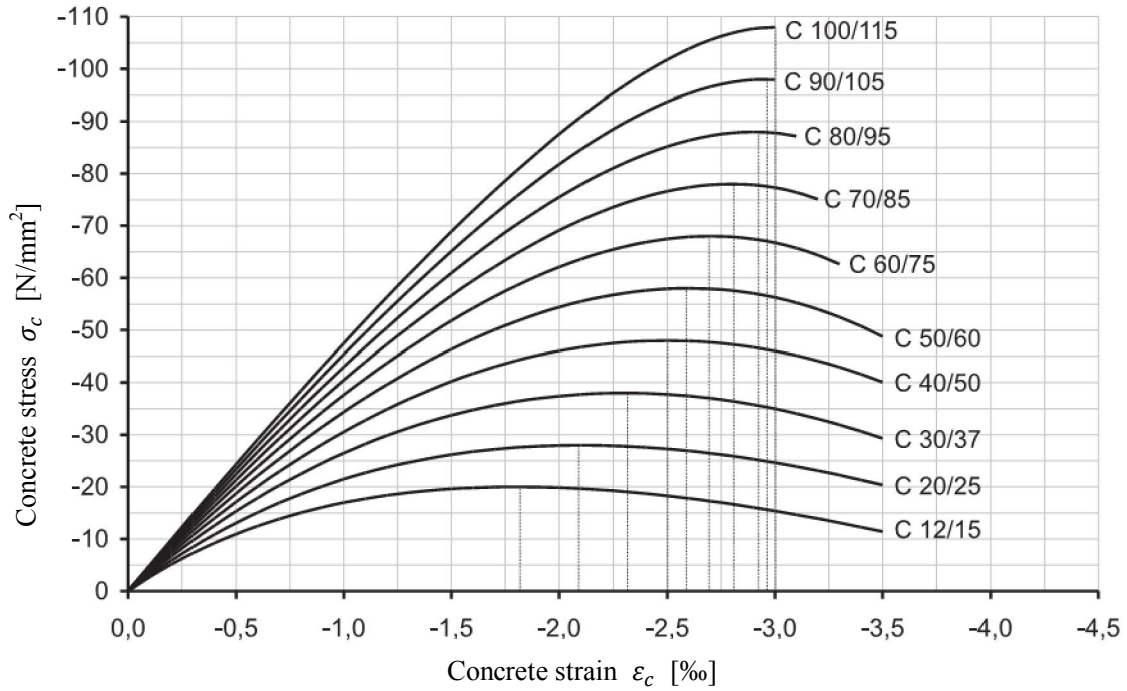
Figure 2-2: Stress-strain relationship for concrete with different strengths from Eq. (2-32)

$$\sigma_c = -\frac{k \cdot \eta - \eta^2}{1 - (k - 2)\eta} \cdot f_{cm} \qquad (2\text{-}2)$$

where $\eta = \frac{\varepsilon_c}{\varepsilon_{c1}}$ and $k = E_{c0m} \cdot \varepsilon_{c1}/f_{cm}$.

Here E_{c0m} is the average value of tangent modulus and is similar to the module for quickly relief from a load level $|\sigma_c| \approx 0.4 f_{ctm}$ [28]. It is calculated according to DIN 1045-1-2008 [29]

$$E_{c0m} = 9500(f_{ck,cyl} + 8)^{\frac{1}{3}} \qquad (2\text{-}3)$$

According to Heft 525 DAfStb [28], the average value of elastic modulus with E_{c0m} from Eq.(2-3)

$$E_{cm} = \alpha_i \cdot E_{c0m} \qquad (2\text{-}4)$$

where $\alpha_i = 0.8 + 0.2 \cdot \frac{f_{cm}}{88} \leq 1.0$ and f_{cm} in N/mm^2.

Here E_{cm} is the secant modulus by $|\sigma_c| \approx 0.4 f_{ctm}$ and describes the stiffness of the uncracked concrete in the serviceability for short term load taking into account of initial plastic strains $\Delta\varepsilon_{c,p}$ [28]. The results of the elastic modulus according to the Eq. (2-3) and (2-4) apply for concrete with quartzitic aggregates. The influence of

aggregate expressed to the effect that the values for the modulus at other aggregates in the range of 20% and 30% [30]. This influence is a multiplicative modification of the E-module in view of factors in Eq. (2-5) from Heft 525 DAfStb [28] and Eq. (2-6) from FIB Mode Code 2011 (draft) [6]. The factors summarized in Table 2-1.

Table 2-1 The values of α_E according to Heft 525 DAfStb [28] and FIB Model Code [6]

Type of aggregate	α_E according to FIB	α_E according to Heft 525
Basalt, density limestone	1.20	1.05/1.45
Quartz	1.00	0.80/1.20
limestone	0.90	0.70/1.10
sandstone	0.70	0.55/0.85

The values of α_E according to [28] are indicated a scatter and it is difficult to calculate a determination. The information provided in FIB Model Code [6] is fixed and easier to calculate.

$$E_{c0m,mod} = \alpha_E \cdot E_{c0m} \tag{2-5}$$

$$E_{c0m,mod} = E_{c0} \cdot \alpha_E \left(\frac{f_{cm}}{f_{cm0}}\right)^{\frac{1}{3}} \tag{2-6}$$

Where f_{cm} is the average concrete strength in N/mm², f_{cm0}=10N/mm², α_E is the stone coeffiencent from Table 2-1. And E_{c0}=21500 N/mm².

To make a consistent and comparable classification of the concrete strength, experiments according to DIN EN 12390 [31] are tested and standardized specimen strength classes are assigned. These cylinders have a height of 30 cm and a diameter of 15cm, and the cube has an edge length of 15 cm. The basic consideration in this type of test and following classification is that there is a possible crack in the high stress area. Therefore, the tensile strength class of a concrete f_{cm} is not the mean value of concrete compressive strength, but a characteristic compressive strength f_{ck} corresponds to the 5% quantile of the population [26]. Thus, the relationship between f_{cm} and f_{ck} is described by:

$$f_{ck} = f_{cm} - 1.64 \cdot \sigma \tag{2-7}$$

where

σ is the standard deviation of samples. The evaluation of many experiments shows that the standard deviation is independent with the strength classes and is about 5N/mm². Therefore, according to DIN 1045-1-2008, Eq. (2-8) is given to calculate the characteristic compressive strength.

$$f_{ck} = f_{cm} - 8 \quad [\text{N/mm}^2] \tag{2-8}$$

2.2.3 Uniaxial tensile behavior

Although concrete is primarily designed to withstand compression, its tensile properties are important to completely describe its material behavior. The tensile strength of concrete

depends on load, subjected rather scatter and may be affected by additional factors such as restrained shrinkage stress. Therefore, it is common to neglect the tensile strength in strength calculation. However, it is not possible in some cases that the bond strength between concrete and reinforcement is independent with tensile stress of concrete. Thus it is a key factor to assess crack spacing and width, concrete and reinforcement stress, deformation and curvature in serviceability limit load[32, 33].

The uniaxial tensile strength can be determined by several direct or indirect methods, such as the method of direct tension test as shown in Figure 2-3 (a). However, these methods are only rarely applied, since it is difficult to achieve truly axial tension without secondary stresses induced by the holding equipment. Commonly, the concrete tensile strength is evaluated by means of indirect tests, such as the four points bending test as shown in Figure 2-3(b), the split cylinder test as shown in Figure 2-3(c), and the double punch test as shown in Figure 2-3(d). Obviously, indirect tests can be much easier performed than direct tests. However, indirect tests require assumptions of the stress in order to calculate the tensile strength by failure load. In most cases, an estimate of the tensile strength according to the uniaxial compressive strength is sufficient. According to DIN 1045-1-2008, $f_{ctm} = 0.3(f_c')^{2/3}$ (Mpa) may be assumed as the average value of tensile strength for normal concrete. And for lightweight concrete, the average value of tensile strength is multiplied by the factor of $\eta = 0.40 + 0.60\varrho/220$. For high-strength concrete (since the class C55/67), $f_{ctm} = 2.12 \cdot \ln(1 + f_{cm}/10)$ (Mpa). Where f_c' is the cylinder compressive strength of concrete, ϱ is the density of lightweight concrete (kg/m^3).
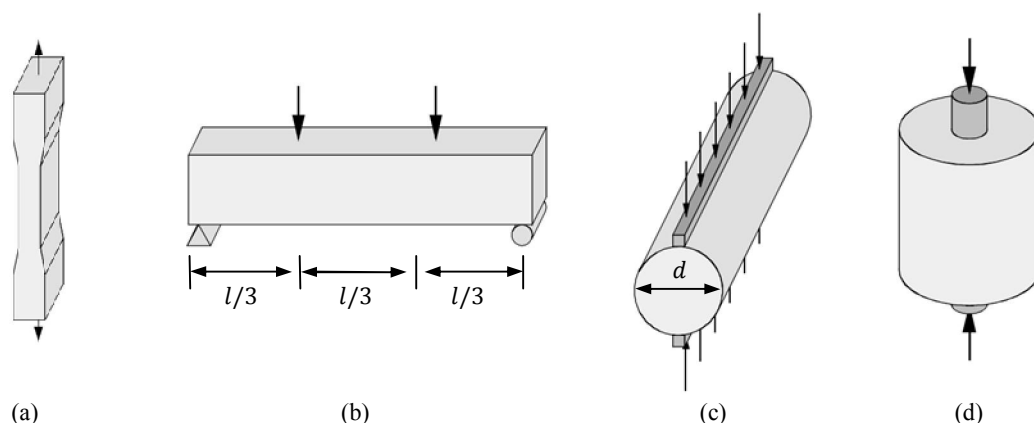
Figure 2-3: Tension test: (a) direct tension test, (b) four points bending test, (c) bending test, (d) double punch test [34]

2.2.4 Creep and shrinkage

The time-dependent deformation of RC element under sustained loads can be divided into research on the long-term and the short-term creep [35-38]. The mechanical behavior of long-term creep is described as a stress-induced redistribution of capillary water within the hardened cement paste of RC structures. In other ways, short-term creep is caused by deformation of the hardened cement paste RC element, according to Wittmann [39]. According to the experimental results of Bazant [40], the creep deformation reached

maybe up to 20-25% under loading after one day. These effects may be influenced by concrete properties summarized as:

$$\varepsilon_c(t) = \varepsilon_{c,el}(t) + \varepsilon_{c,K}(t) + \varepsilon_{c,S}(t) \qquad (2\text{-}9)$$

where

$\varepsilon_{c,el}(t)$ is the proportion of elastic deformation, which depends heavily on the composition, especially on the aggregates [41].

The creep of concrete is the time-dependent deformation under load and is calculated by following equation according to DIN EN 1992-1-2011 [41],

$$\varepsilon_{c,K}(t) = \varepsilon_{cc}(\infty, t_0) = \varphi(\infty, t_0) \cdot \frac{\sigma_c}{E_{c0}} \qquad (2\text{-}10)$$

where

$\varphi(\infty, t_0)$ is the final number of creep, when there is no particular accuracy, it must be set according to [41], provided that the compressive stress in concrete is under beginning load $t = t_0$ is less than $0, 45f_{ck}$,

σ_c is the constant creep caused by concrete stress and E_{c0} is the elastic modulus.

The relaxation is a special case of creep under a constant concrete strain. The expressions of calculating the relaxation of reinforced concrete can be found in [42].

The other concept of shrinkage is the time-dependent volume decrease of concrete constant relative environmental humidity and temperature without the external loads[43, 44].

The opposite is the source where the concrete absorbs the water or moisture in humid environments and thereby increases its volume. The shrinking process takes a long time, after 28 days the concrete has reached about a third of its total consumption level. After 3 years, the process is almost complete.

This phenomenon is caused by many reasons, such as chemical, thermal and hydration process. The decreasing volume in consequence of hydration is named as termedas chemical shrinkage. The drying shrinkage, the drying up to the cement paste and the carbonation dwindling, the carbonation of cement paste are additional shares. Building relates to the termedas chemical shrinkage and drying shrinkage, which can be calculated with following equation from [41].

$$\varepsilon_{c,S}(t) = \varepsilon_{cd}(t) + \varepsilon_{ca}(t) \qquad (2\text{-}11)$$

where

ε_{cd} is the drying shrinkage strain;

ε_{ca} is the autogenous shrinkage strain.

It should be distinguished that a condition of internal stress is caused by shrinkage. It is independent with the level of consumption by the disability from a reduction of shrinkage, which is induced by tensile stresses in the concrete. If all surfaces of the component are

ruled by similar environmental conditions, the shrinkage internal stresses are of minor influence. In this thesis, the time-dependent processes of creep and shrinkage of concrete are not considered since it is only a description of the short-term behavior.

2.2.5 Behavior of reinforcement

The material behavior of reinforcing steel [45, 46]is linear-elastic almost up to the yield stress f_y. The material behavior of reinforcing steel in tension are described as the characteristics of the tensile strength (f_t), the Young's modulus (E_s) and the corresponding uniform strain to the tensile strength (ε_{su}). Furthermore, with the ratio of tensile strength and yield strength (f_y/f_t) or with the value of fracture, the deformation of reinforcing steel can be commonly described as the ductility. In DIN 1045-1-2008 [29], the following ductility limits are specified as: (a) Normal ductility, ε_{su}>2.5% when $f_t/f_y \geq 1.05$; (b) High ductility, ε_{su}>5% when $f_t/f_y \geq 1.08$.

The reinforcing steel can be divided into different types, depending on the production processes, such as: (a) hot rolled, without treatment (natural hard); (b) hot rolled and treated from the rolling heat; (c) cold-deformed.

The structure design according to DIN EN 1992-1-2011 is shown in Figure 2-4 and the simplified stress-strain relationship is given.
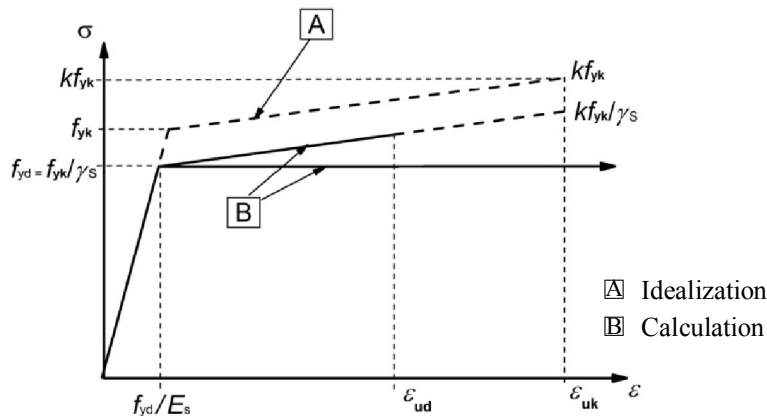
Figure 2-4: Calculation of stress-strain-line of reinforcing steel under tension and compression

This figure illustrates two types of steel tension curves. Type A corresponds to the idealized curve with characteristic material properties. Two curves of Type B explain the partial factors of reinforcing steel with reduced gradients γ_s. Here, one curve shows a linear elastic-plastic material behavior with hardening behaivor of steel bar, the other linear curve illustrates perfectly elastic and plastic behavior. The magnitude of the elastic modulus varies in the range from 195 000 to 210 000 N/mm^2 due to the slight homogeneity[47].

Reinforced concrete structures manufactured today use almost entirely concrete with a characteristic yield strength steel (95% fractile) of 500 N/mm^2 [59]. The reinforcing steel is manufactured in the following cable assemblies: (a) Reinforcing steel bars BSt 500S； (b) welded wire mesh BSt 500M; (c) Reinforcing steel coils BSt 500K.

Type (a) was adopted to present tests in this thesis.

2.2.6 Interaction between concrete and reinforcement

Bond stress strength develops at the steel-concrete interface due to the displacements between concrete and reinforcement[48]. The bond stress acting at the interface of steel bars and surrounding concrete has a significant influence on the formation and propagation of flexural crack in reinforced concrete members. Moreover, the bond stress mostly contributes to the tension stiffening of RC structures[49].

If a flexural crack appeared under tension stress in a RC-member, the concrete strain becomes zero at a cracked section[50]. Subsequently, the concrete near the cracked section will attempt to regain its original stress and will lead to a bond-slip stress between concrete and reinforcing bar[51]. Thus the bond stress formed. The bond stress is formed primarily due to the interlocking of ribs on the deformed reinforcing steel and the surrounding concrete. Forces are primarily transferred to the surrounding concrete by inclined compressive forces radiating out from the bars[52]. Therefore, for large slip values, the chemical adhesion is destroyed and the bond stress is provided by the bearing stress acting on the interface of the rib on deformed bars and concrete. For small slip values, the bond stress is entirely dependent on the chemical adhesion of concrete and steel bars [53].

The stress differences between tensile reinforcing bar and surrounding concrete shaped the bond stress, which is affected by the parameter of the reinforcement U_s and bond strength τ_b. According to DIN EN 1992-1-2011[41], the bond strength equation should take into account of the bond condition between reinforcement and surrounding concrete, as shown in Figure 2-5. The bond strength value of ribbed bars f_{bd} can be determined as:

$$f_{bd} = 2.25 \cdot \mu_1 \cdot \mu_2 \cdot f_{ctd} \tag{2-12}$$

where

f_{ctd} is the design value of concrete tensile strength in accordance with (2-13).

Because of the increasing brittleness of high strength concrete, $f_{ctk,0.05}$ usually limit to concrete class of C60/75.

μ_1 is the coefficient considered the performance of bond conditions and the location of reinforcing bars (see Figure 2-5).

μ_1=1.0 is the coefficient of perfect bond condition;

μ_1=0.7 is the coefficient of other performance of bond conditions, unless it regards as a "good" bond conditions. Rids in components are considered in this equation;

μ_2 is a coefficient of the rid diameter.

The measured value of concrete tensile strength f_{ctd} is defined as

$$f_{ctm} = \mu_{ct} \cdot f_{ctk;0.05}/\gamma_c \tag{2-13}$$

where

γ_c is partial safety factor, γ_c=1.5 for steadily and temporary structures, γ_c=1.2 for

15

extreme structures.

μ_{ct} is the coefficient considered long-term load on the concrete tensile strength.

$f_{ctk;0.05}$ is the concrete tensile stress at 5% fractile.

$$f_{ctk;0.05} = 0.7 f_{ctm} \qquad (2\text{-}14)$$

f_{ctm} is tensile concrete strength, as given in Section 2.6.3.

(a) $45° \leq \alpha \leq 90°$ (b) $h \leq 600$mm

(c) $h \geq 250$mm   (d) $h \geq 600$mm
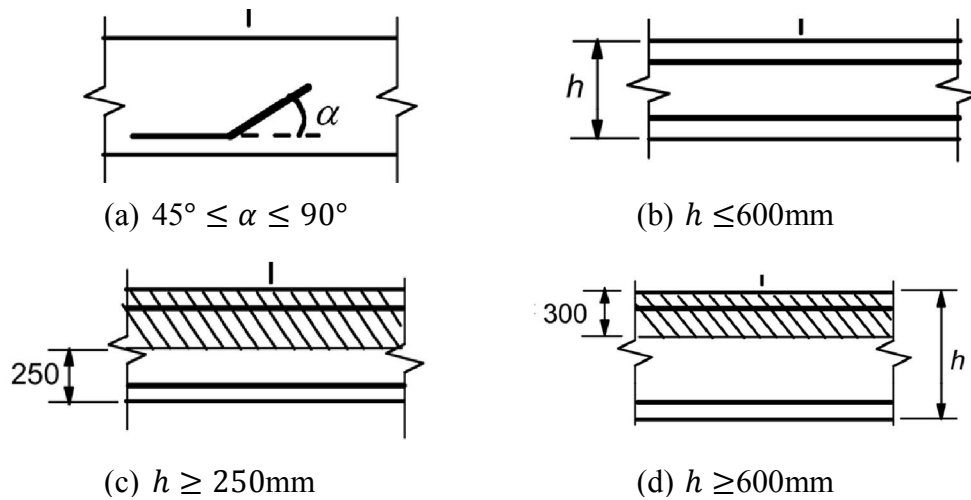
Figure 2-5 Bond strength condition. (a) and (b) are perfect bond condition; unshaded area in (c) and (d) are under perfect bond conditions and shaded area are under light bond conditions[29]

2.3 Flexural crack behavior in RC-elements

2.3.1 Propagation of flexural cracks

Segment AB as a free body subjected to pure bending (Figure 2-7) to study the propagation of flexural cracks. Here, M is bending load, M_{cr} is cracking bending of the member and M_k is the bending moment under service load[54].

- When $M < M_{cr}$ (Figure 2-8)

At moment, there is no crack under this load. Tensile stress of concrete in tension zone is less than concrete tensile strength ($\sigma_{ct} < f_t$). Steel stress, σ_{s1} is a low stress at uncracked stage[55-57].

- When $M = M_{cr}$ (Figure 2-8)

When concrete tensile stress reached f_t and steel stress reached σ_{s1a}, cracking is occurring with all cross sections under limit state of concrete. Some concrete failed to resist tensile stresses leads to the appearance of cracks where micro cracks in concrete are already formed. Concrete tensile stress between cracks transferred through bond stress τ to the steel, results in steel stress increased from σ_{s1a} to σ_{s2} as shown in Figure 2-8 (c). Bond forces τ reduce the steel tension stress from σ_{s2} to σ_{s1a} near the cracked section, as shown in Figure 2-8(d). At this moment, steel stress at the cracked section reaches to

f_t. Neutral axis looks like a wave as shown in Figure 2-8 (a).
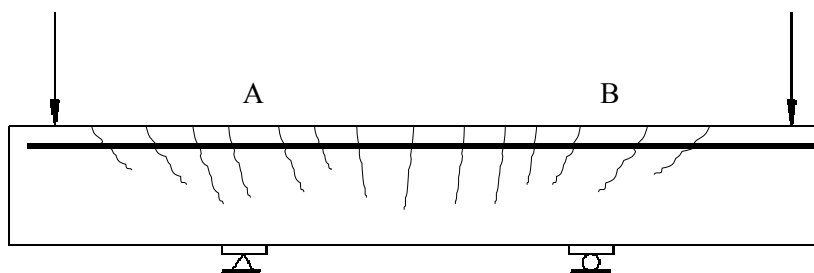
Figure 2-6: RC element subjected to pure bending
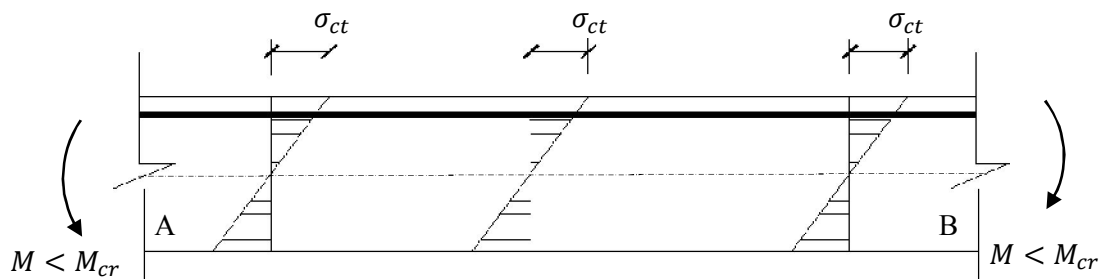
Figure 2-7: Stress distribution of RC element before cracking
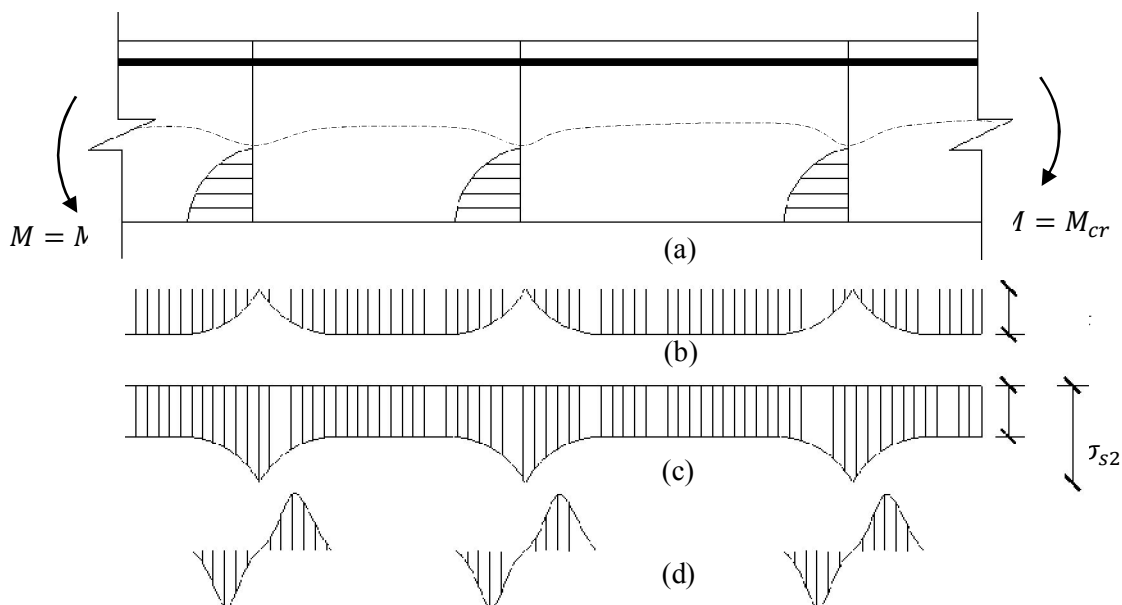
Figure 2-8: Stress distribution after first generation of cracks

- When $M = M_{cr} + \Delta M$ (Figure 2-9)

The second generation of cracks appeared with slightly increased moment ΔM, as illustrated by Figure 2-9 (c). However, due to deformed bars are dominating, bond stress transferred from the steel bars to the concrete at the front surfaces of lugs, cone-shaped exiguous cracks are induced. These cracks normally do not lead to primary cracks[47, 56].

17

- When M increasing from M_{cr} to M_k

Due to bond stress between steel and concrete reduced, concrete tension stress at the position of reinforcement reduces as well at segment AB. A set of phenomena appear in this stage such as slipping between steel and concrete at crack section, wider crack width and higher steel stress[20, 32].
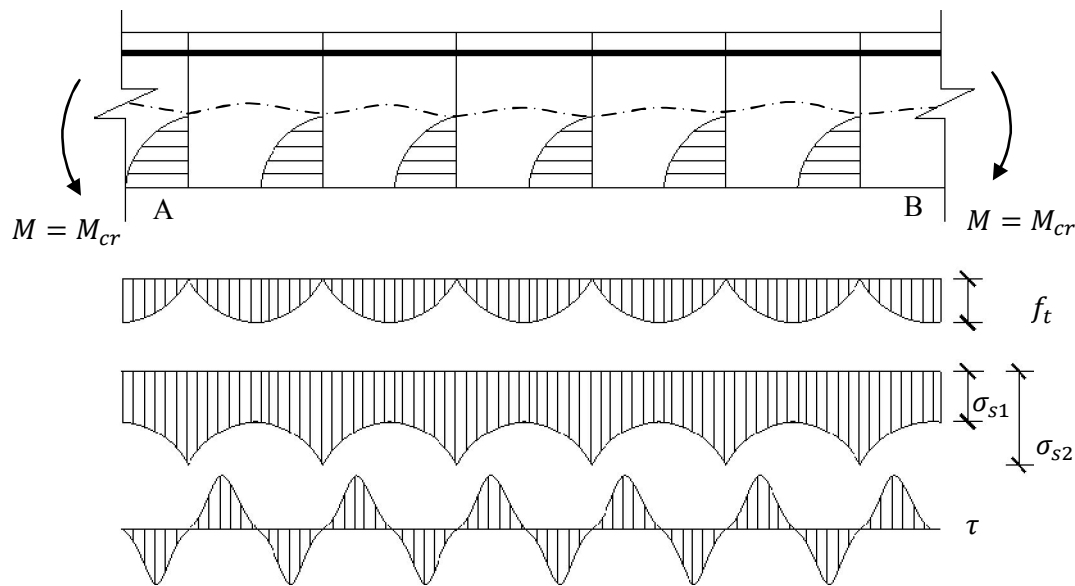
Figure 2-9: Stress distribution after second generation of cracks

2.3.2   Behavior of flexural cracks in RC-elements

Cracks in RC element, are generally formed under loads before service state and even formed prior to practice loading due to shrinkage. Flexural cracks are not only inevitable due to the low concrete tensile strength, but also necessary for the effective usage of reinforcing bars. However, wider cracks may not only destroy the aesthetics of the structure, but also expose steel bar to the surrounding environment leading to corrosion. In some cases no crack is visible because slabs are not subjected to their full service load and the concrete has some tensile strength [57-59]. However, in many other cases, RC slabs subjected to high-service-load steel stresses lead to the formation of many visible cracks.

The causes of cracks in concrete are numerous, but in most cases cracks formed in RC element due to volumetric change and flexural stresses resulting from applied load or reactions. Volumetric changes caused by drying shrinkage and thermal stresses will introduce tensile stresses in the concrete if restrained, and therefore can lead to cracking. In thin RC members, such as floor slabs, the formed cracks may extend to the entire cross section and usually have an approximately same width [60]. If the width of these cracks is not properly controlled, they may disrupt the integrity of structures and considerably reduce the bending stiffness, thus result in large deflections[61, 62].

Flexural crack is one of the main types of cracks caused by external loads. Cracking will

occur in the tension zone of slabs subject to flexure arising from external loads or reactions once the modulus of rupture of the concrete is exceeded. The cracks may form perpendicular to the plane of the slab, as in the case of flexure without significant shear force; or when the shear force is significant, they may form inclined to the plane of the slab.

2.3.3   Dowel action

Dowel action is a local phenomenon characterized by local bending and shearing of the bars on the adjacent concrete[63]. There are also tensile stresses which in turn lead to cracking, as shown in Figure 2-10.
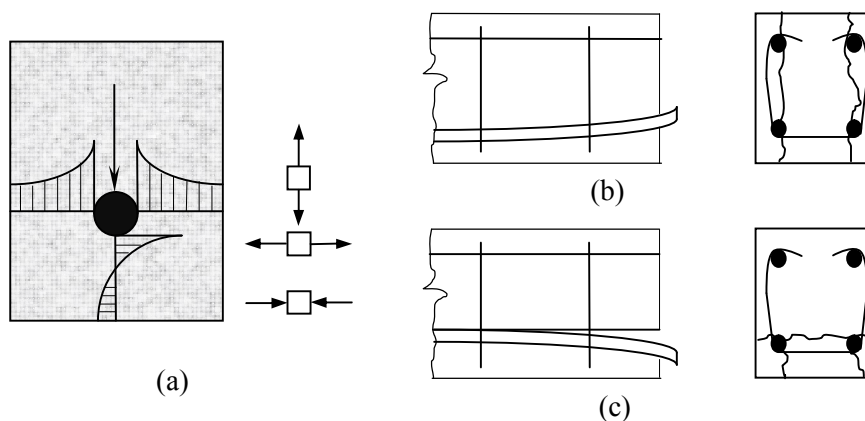
Figure 2-10: Dowel action: (a) local stresses, (b) bar acting against the concrete core, (c)bar acting against the concrete cover

Dowel action depends on whether the bar is acting against the concrete core or the concrete cover. In the first case, the reinforcing bar is acting like a beam on elastic foundation[64]. Failure usually occurs by splitting of concrete under the bar in the plane induced by the dowel load and the dowel bar Figure 2-10(b) [65]. The ultimate resistance depends on the bearing strength of concrete, i.e., on the compressive strength of confined concrete adjacent to the bar. It can be as large as three times the compressive strength of concrete[66]. In the second case, the reinforcing bar may be viewed as a bar on elastic foundation until cracks are induced in the concrete cover, separating the cover from the core. As the bar tends to slip longitudinally through the concrete, it acts like a wedge. This action contributes to the splitting of concrete.

2.4   Parameters influencing crack width

The most important parameter controlling flexural crack width under a given load is the tensile steel strain in the reinforcing steel. This opinion is agreed by all investigators. It can be seen by examining the prediction formulas of crack width, which will be discussed in subsequent sections. It is also commonly accepted that the concrete strength is of minor influence on the cracks width. However, there is no general agreement among various

investigators on the relative significance of other parameters influencing the crack width.

2.4.1 Influence of concrete cover

Experiments by Broms [4] and others[59, 67-69] have shown that both crack spacing and crack width are related to concrete cover, which is the distance between the center of the bar and the surface of the concrete. According to all prediction formulas, an increase of concrete cover will result in an increase of crack width. In spite of this fact, concrete cover with high thickness in provision is considered as the most practical means of protecting reinforcement from corrosion. In order to study the influence of an increase of concrete cover on the maximum crack width, Makhlouf and Malhas [70] carried out rectangular beams tests on 24 beams, which examined the influence of concrete cover with doubled thickness on the maximum crack width and further examined the accuracy of prediction formulas.

Furthermore, as reported by Frosch [71], concrete cover considered in prediction formulas was developed up to 65mm on the basis of experimental results from Gergely and Lutz [2]. As a result, the applicability of ACI 318-2008 is questionable in the case that concrete cover exceeds 65mm.

2.4.2 Influence of reinforcement diameter and distribution in tension zone

Reinforcement distribution in the tension zone includes reinforcement ratio and bar diameter. Individual influences of bar diameter[72] and reinforcement ratio on the crack width have not been investigated respectively due to the interdependency of the two variables. Generally, in order to control cracking, it is suggested to use more bars with small diameter rather than to use bars with large diameter, and these bars should be well distributed in the concrete tension zone.

According to the beam test results, Makhlouf and Malhas [70] further concluded that different reinforcement ratios (0.0031, 0.0056, 0.0087 and 0.0138) had no tangible influence on the measured crack widths. It is noted that different bar diameters (12, 16, 20 and 25mm, respectively) were associated with the above-mentioned reinforcement ratios. One may argue that a decrease of the crack width caused by using higher reinforcement ratios has been compensated by an increase of the crack width resulted from using larger diameter bars, leading to the net change becoming unnoticeable. This shows the possibility of producing ambiguous results due to indirect influences of some variables, leading to inconsistent conclusions.

2.4.3 Influence of beam height

Beam height has not been considered by most investigators as a major variable affecting the spacing and width of cracks; only Clark [73] has included the beam height and effective depth as factors in the crack width prediction formula. In all other analytical investigations, concrete tensile stress blocked between adjacent cracks has been determined considering only the bond force, while neglecting the compressive force acting above the neutral axis at the cracked section. However, ACI Code (ACI 318-05) [74] considers concrete cover of the reinforcing bars and at the cross-sectional area as an

important geometric variable. In order to consider this major factor affecting crack width, a coefficient β contained in the code, is a ratio of the distance between neutral axis and tension surface to the distance between neutral axis and centroid of reinforcing steel.

2.4.4 Influence of transverse reinforcement

2.4.4.1 The action of stress concentration caused by TR (Action-1)

The influence of TR on crack behavior were investigated by some researchers [15, 75-78]. The influence represents a kind of action, which indicates that steel bars reduce the generation of cracks. This action is caused by the TR weakened cross-section. Figure 2-11 shows the increased stress caused by the weakened concrete bond stress by a hole between LR and surrounding concrete. The stress curve of tension σ depends on many geometrical parameters and can be described by the stress gradient[79]. These tensions induced by the hole overlap with the external stress σ_{hom}. A crack near the edge can be expected, when concrete tension stress reached $\sigma_{hom} + \sigma_{het} = f_{ct}$.

Similar to the approach of Petersen [80], Purainer [15] carried out a FE study on a functional relationship between holes with different diameters and stress variation. The investigation found out that the functional relationship depends on the total width b and the TR diameter d:

$$\alpha_{k1} = 1 + 1.94 \cdot \ln\left(\frac{b}{d_{sc}}\right) \tag{2-15}$$

A total factor combined an increased stress due to dowel action of TR and a stress concentration caused by TR, expressed as $\alpha_k = \alpha_{k1} + \alpha_{k2}$.

$$\alpha_k = \left[1 + 1.94 \cdot \ln\left(\frac{b}{d_{sc}}\right)\right] \cdot 2.0 \tag{2-16}$$
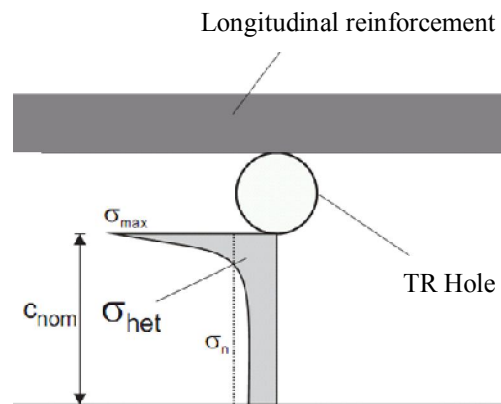
Figure 2-11: The increased stress induced by the weakened concrete bond stress by a TR hole between LR and surrounding concrete

2.4.4.2 Dowel action (Action-2)

TR has not been considered as a major parameter by many investigators and codes. According to the experimental and theoretical analysis from [11, 81] If a tight relationship between LR and TR is observed, based on the introduction in section 2.3.3, a TR is elastically pulled and hence dowel action between TR and the concrete in front of TR is appeared, as shown in Figure 2-12.
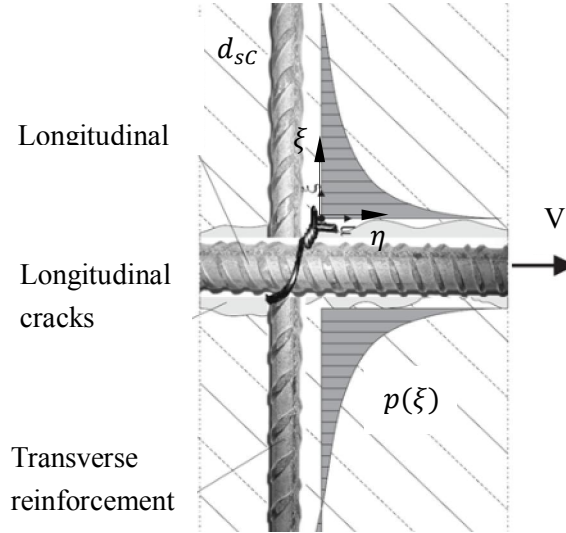
Figure 2-12: Shear stress on TR under LR tension

$$p(\xi) = G \cdot \eta = \frac{1}{d_{sc}} \cdot EI \cdot \frac{\partial^4 \eta}{\partial \xi^4} \qquad (2\text{-}17)$$

p = contact pressure between rebar and concrete;

η = depression of the rebar in the concrete;

G = coefficient of subgrade reaction of the concrete under the reinforcing bar;

ξ = distance from the crack faces;

d_{sc} = diameter of the transverse reinforcing bar;

EI = bending stiffness of the transverse reinforcing bar;

The tension $p(\xi)$ shows that for LR below TR, which revealed substantial steel bar binding. Figure 2-12 can be expected as a solution of Eq.(2-17).

The variation of concrete elastic modulus and the steel diameter at a cross-section results in an increase of steel stress as shows in [80]. This relationship is induced by TR and it represents a factor of α_{k1}=2.

2.5 Calculation model of flexural cracks spacing and width

Above-mentioned factors present that many variables affect flexural cracks spacing and width of RC beams and one-way slabs. Due to the complexity of the problem, a number of theoretical, semi-theoretical, and empirical approaches have been developed to predict the flexural crack width. Each approach contains a set of the variables. The following sections in this chapter will introduce widely accepted the calculation model of flexural cracks spacing and width for beams, one-way slabs and two-way slabs.

2.5.1 Bond-slip mechanism

Bond-slip model was proposed by R. Saliger in 1936 according to the bond-slip relationship between tension steel bar and surrounding concrete. It considers that the stress transfers from steel to concrete in order to predict crack width and spacing (see Hughes and Cifuentes [82], or Beeby [7] for further details on this mechanism). Figure 2-13 and Figure 2-15(a) illustrate the concrete tensile zone of a single reinforcing bar beam and further explain crack spacing formulas in CEB/FIP [83], FIB Model Code 2010 (draft)[6] and DIN1045-1-2008 [29].

Bond-slip mechanism points out that prior to cracking, tensile load applied to the beam causes equal strains in the concrete and the steel. Concrete tensile strains increase along with increasing load until the concrete tensile strain capacity has reached, and cracks developed at this point in concrete. At the crack locations, concrete tensile stress is 0. Between two adjacent cracks, concrete tensile stress increases and reaches to concrete strength, f_{ctm} induced by bond stress. The transfer distance of the bond l_t is presented in Figure 2-13 and Figure 2-15 (a). Hence, the second crack must appear in the range of $l_t \sim 2l_t$. The average crack spacing is $S_m = 1.5\,l_t$. Thus, at l_t cross-section, the equilibrium equation is expressed as:

$$f_{ctm} \cdot A_{c,eff} = f_b \cdot u \cdot l_t \qquad (2\text{-}18)$$

The slip between steel and surrounding concrete is a fundamental factor to control crack width. This slip causes the force transmission from steel to concrete by means of interfacial stress acting on the perimeter of the bar. The bond-slip mechanism is caused by the strains in the concrete and the steel to have a periodical variation along the RC member, as shown in Figure 2-13 (CEB1990 [83], König and Tue 1992). Therefore, crack width depends on the distance over which slip occurs and on the difference between the steel and concrete strain of two adjacent cracks [84-86]. The stress in the steel caused by steel strain will be reduced due to the bond strength f_b between the steel and surrounding tensile concrete.

2.5.2 No-slip Mechanism

Bond-Slip mechanism as an essential hypothesis points out that a crack cross-section is still a plane after concrete cracking and shrinkage. Tests and construction are shown that a cross-section of drying shrinkage concrete is not a plane, but is a gradient on the section

of cracked concrete. Crack width near steel is much smaller than near surface of concrete. This phenomenon illuminates that steel restricts surrounding concrete in an effective restriction area of steel.
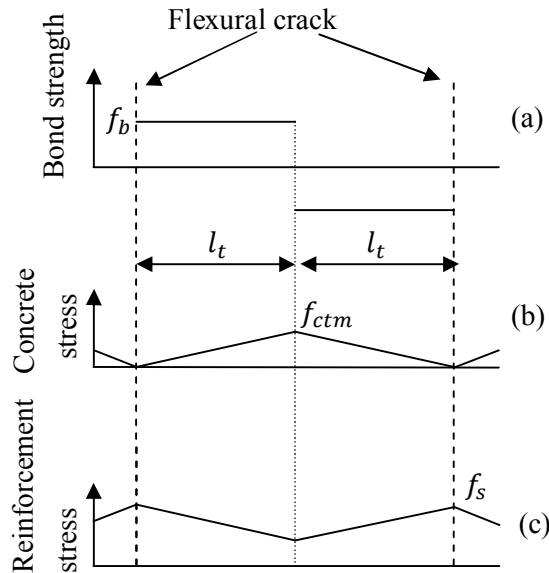
Figure 2-13: Variation of bond strength surrounding reinforcement (a); concrete tensile stress (b) and reinforcement tensile stress(c) adjacent flexural cracks

Moreover, the relative slip between reinforcing steel and concrete is of minor influence under service load that can be neglected, as shown in Figure 2-15 (b)[87].

According to experimental results, Broms and Base [4] found out that a new crack will be appeared at mid cross-section between adjacent cracks only if the crack spacing larger than twice thickness of concrete cover. This argument was used to predict the maximum crack spacing S_{max} equals to twice of the concrete cover ($S_{max} = 2c$) in a beam reinforced with a single bar. The minimum crack spacing S_{min} is half of S_{max} and hence equals to the concrete cover ($S_{min} = c$). The theoretical average crack spacing S_{ave} is predicted as 1.5 times of the concrete cover $S_{ave} = 1.5c$.

However, test results of 10 beams by Broms and Base [4] have shown that for steel stresses ranging from 140 to 205 MPa, the average crack spacing was close to twice of the concrete cover ($S_{ave} = 2c$). The average crack spacing ($S_{ave} = 2c$) was multiplied by the average strain of steel bar $\varepsilon_{s,ave}$ to predict the average crack width. Thus, for steel stresses ranging from 140 to 205 Mpa, the average crack width at the tension surface of a RC element reinforced with a single bar is expressed as

$$w_{t,ave} = 2c\varepsilon_{s,ave} \tag{2-19}$$

2.5.3 Combination model

With an assumption of no slip on the interface of reinforcement and concrete, no-slip mechanism considers concrete cover as the unique parameter to predict crack spacing is obviously oversimplified[88].

The work of Beeby [89] at the Cement and Concrete Association has a clear understanding of the cracking mechanism. Beeby measured crack width and spacing at various points across bottoms of one-way RC slab specimens with various concrete cover c as shown in Figure 2-14 (a). It was found out that crack an increase of spacing and width along with an increase of the distance between bars and measured crack points. However, at certain distances between bars and those points, crack width keeps a constant value, which depends on the height of crack rather than the distance from the bar.

Cracking at a point with a distance to a reinforced bar is illustrated in Figure 2-14 (b). The crack pattern in this case is controlled by crack height h_0. The crack will penetrate nearly to the neutral axis, and its height can be calculated by standard elastic theory using the modular ratio of the steel to concrete. According to St. –Venant's principle, it is evident that concrete tensile stresses between adjacent cracks are substantially unaffected by the crack at distances greater than h_0. Hence, the next crack will be generated at a distance approximately equal to or greater than h_0. If the spacing between two cracks is $2h_0$ or larger, a new crack can be formed between them, and vice versa. Therefore, given a mean crack spacing of $1.5h_0$, the minimum and maximum crack spacing is h_0 and $2h_0$, respectively. However, a mean value of $1.33h_0$ was actually measured by Beeby in the tests. Crack width and spacing were found to be directly proportional to the initial crack height h_0.

A crack below a reinforced bar is illustrated in Figure 2-14(c). According to the No-slip Mechanism mentioned in Section 2.5.2, if there is no bond stress between concrete and steel, the crack pattern will be controlled by the initial crack height h_0. Thus, the influence of slip and internal deformations is to modify the c_0 controlled crack pattern towards the h_0 controlled crack pattern. Crack width in this general case is considered as a function of c_0 and c_0/h_0. The following equation is considered the best expression of Beeby's experimental data:

$$\frac{w_{max0}}{\varepsilon} = K_1 c_0 + K_2 \frac{A}{\phi} e^{-K_3(c_0 h_0)} \tag{2-20}$$

The maximum crack width at a distance between a bar and the crack:

$$\frac{w_{max1}}{\varepsilon_m} = K_1 h_0 \tag{2-21}$$

The maximum crack width at intermediate positions:

$$w_{max} = \frac{c w_{max1} w_{max0}}{c_0 w_{max1} + (c - c_0) w_{max0}} \tag{2-22}$$

where

ε_m is the average longitudinal strain at the level where cracking is being considered;

K_1, K_2 and K_3 are constants that depend on the probability of the crack width being exceeded;

c_0 is the minimum cover to steel;

A is the effective area of concrete in tension surrounding one bar;

ϕ is the bar diameter;

c is the distance from the point of measurement of the crack to the surface of the nearest bar.

Eq.(2-20) and Eq.(2-22) are considered to be too complex for practical use. These two equations can be simplified as Beeby's version [90], which provides a prediction of crack width with an excess of approximately 20% compared to experimental results as given:

$$w_{max} = \frac{3c}{1 + 2[(c - c_0)/(h - kd)]}$$

(2-23)

where

h is the overall depth of the section, kd is the neutral axis depth, and

$$\varepsilon_m = \left[\varepsilon_s - \left(\frac{2.5bh}{A_s} \cdot 10^{-6}\right)\right] \cdot \frac{h - kd}{d - kd}$$

(2-24)

where ε_s is the strain in the steel at a crack; d is the effective depth. Eq.(2-24) for ε_m is the steel streain at a crack less an empirical term due to the stiffening effect of concrete tension between cracks, modified by the strain gradient term to obtain the average strain at the tension fiber of RC member.

This method was approved by other researchers [90]. The real crack width considered the influence of concrete cover on crack spacing and width[7, 89], is likely according to a combination of these two mechanisms, which based on Bond-slip mechanism. Simplified model was expressed as:

$$l_m = K_1 d_c + K_2 \frac{\phi_s}{\rho_{te}}$$

(2-25)

$$w_m = \left(K_1 d_c + K_2 \frac{\phi_s}{\rho_{te}}\right) \varepsilon_m$$

(2-26)

Where w_m is the average crack width, mm; c is concrete cover, mm; K_1, K_2 is empirical constants; is average strain at level where cracking is considered. Some design codes such as Chinese Code for Design of Concrete Structures GB50010-2002 [91] and Indian Standard [92] , tried to accommodate this model to predict average crack spacing and width.

The above discussion has been focused on cracks of a RC member under tension force. For a flexural RC member, the location of the neutral axis as an another factor affects crack width of RC element surface [89].

The above mentioned methods are adopted by Newest European code, EN DIN 1991-1-2011[41] to calculate crack spacing and crack width. The prediction formulas will be introduced in Section 2.6.2.
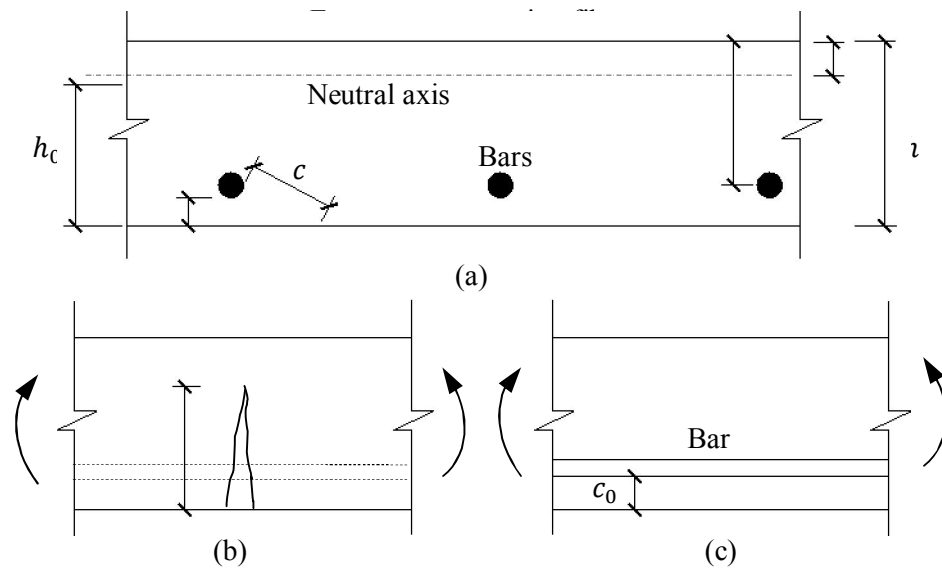
Figure 2-14 Influence of bar proximity on cracking in one-way slabs: (a) cross-section; (b) crack at distance from a bar, (c) crack at a bar.

Bond-slip model

$w \approx c$

Cover= c

(b) No-slip model

ϕ

(c) Combination model
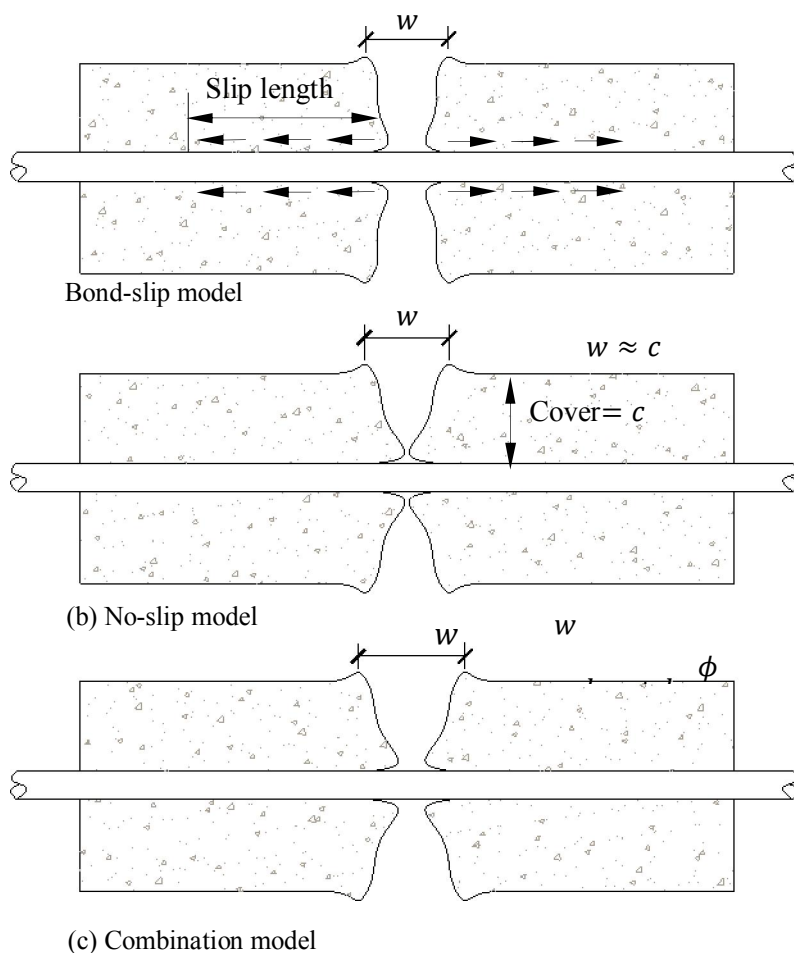
Figure 2-15: Comparison of crack models

2.5.4 Empirical equations - Statistical Approach by Gergely and Lutz

Various parameters are considered to calculate crack spacing and width in different codes. Actually，the interaction between concrete and steel is very complex and cracking is a semi-random process. Several parameters can only be used under certain conditions. The most accepted crack width prediction formulas for beams and one-way slabs in the United States is according to the research results from Gergely and Lutz [2]. Statistical analysis based on experimental data to determine the importance of the considered variables, such as the effective area of concrete in tension, the number of bars, the side or bottom cover, the strain gradient from the steel layer to the tension surface and the steel stress. Then, based on statistical data of bottom cracks (Eq.(2-27)) and lateral cracks, two equations (Eq.(2-28)) are presented for concrete cover up to 63 mm. In 1999, Frosch [71] modified these two equations into a new formula that was adopted by ACI 318-08 [93].

$$w_{max} = 1.1 \cdot \frac{h_2}{h_1} \cdot f_s \cdot \sqrt[3]{d_c A} \cdot 10^{-5} \text{ [mm]} \tag{2-27}$$

$$w_{max} = \frac{1.1 \cdot \sqrt[3]{d_c A}}{1 + \frac{2}{3}(d_s/h_1)} f_s \cdot 10^{-5} \text{ [mm]} \tag{2-28}$$

$$w_{max} = 2000 \cdot \frac{f_s}{E_s} \cdot \frac{h_2}{h_1} \sqrt{d_c^2 + \left(\frac{s}{2}\right)^2} \text{ [mm]} \tag{2-29}$$

where

d_c is the thickness of concrete cover from tension face to center of closest bar [mm];

d_s is the distance from the side of the beam to the center of the adjacent bar [mm];

A is the average effective area of concrete in tension around each reinforcing bar [$A = A_e/n$, and A_e is the rectangular concrete area of width b and with same centroid as steel;

b the beam width ,and n the number of bars;

f_s is the steel stress [N/mm^2];

h_1 the distance from centric of steel to the neutral axis,

and h_2 the distance from the extreme tension fiber to the neutral axis.

Some of the notation shown in Figure 2-16.
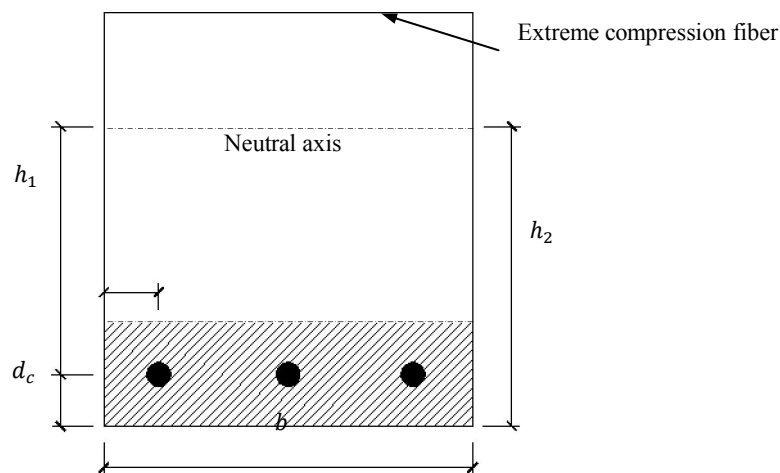
Figure 2-16: Notation for Gergely-Lutz crack width equation [2] [mm]

2.5.5 Other approaches by previous researchers

(a) Venkateswarlu & Gesund method [94]

Venkateswarlu & Gesund [94] analyzed a certain part of beam between two adjacent cracks by using a two-dimensional finite element method to evaluate the influence of bond force. The analysis results have shown that the maximum concrete tensile stress across the cross-section appears at the reinforcement layer. When concrete stress varies

along with the bar, the maximum concrete stress appears at the mid-section between the two cracks.

An analysis of maximum crack spacing was conducted by comparing the predicted maximum tensile stress with concrete tensile strength. The maximum crack width at reinforcement layer was calculated based on the tension stress difference between steel and concrete. Crack spacing and width were expressed by the slip modulus, which relates to the variation of bond strength. The slip modulus was indirectly evaluated by comparing the predicted crack widths with those measured values by other investigators:

$$S_{max} = \frac{14.5\phi}{1 + n\rho_m} \text{ [mm]} \tag{2-30}$$

$$w_{t,max} = \frac{2.4 \cdot 10^{-5}\phi(1462 - f_s)f_s}{(1 - n\rho_m)(662 - f_s)} \tag{2-31}$$

where

S_{max} is maximum crack spacing;

$n = \frac{E_s}{E_c}$ is modular ratio in which E_s and E_c are the elastic modulus of steel and concrete respectively;

ρ_m is modified reinforcement ratio, which relates to the concrete cover.

(b) Bazant & Oh method

Bazant & Oh (1983) [95] carried out a theoretical study on crack spacing and width by using the energy criterion of fracture mechanics as well as the strength criterion. The energy criterion indicates that crack spacing is a function of the axial strain of the bars and also depends on the bar spacing, bar diameter, fracture energy of concrete and its elastic modulus. Both the energy and strength criteria yield a minimum strain necessary to form any cracks. Based on the study, Bazant & Oh (1983) [95] proposed the following equations to predict average crack spacing and maximum crack width in reinforced concrete members.

$$\frac{S_{ave}}{\phi} = 25.7(\phi_1)^{4.5} + 1.66(\phi_2)^{\frac{1}{3}} + \frac{0.236 \cdot 10^{-6}}{\varepsilon_s^2} \tag{2-32}$$

$$\frac{w_{t,max}}{\phi} = \left[159(\phi_1)^{4.5} + 2.83(\phi_2)^{\frac{1}{3}}\right](\varepsilon_s - 0.0002)\phi_3 \tag{2-33}$$

where

ε_s is steel strain;

ϕ_1 is ratio between concrete cover and distance from neutral axis to tension face;

ϕ_2 is ratio between average effective concrete area around steel bar and the area of steel bar;

ϕ_3 is ratio between distances from neutral axis to tension face and steel bars.

A comparison of test results has shown that crack spacing and width predicted by the above formulas are in good agreement with test data.

2.6 Current methods of crack control in codes

2.6.1 FIB Model code 2010 (draft)

Crack-control methods for concrete structures applied to RC element are proposed in the European Model Code. FIB 2010-1992-1-2010 (draft)[6], as a new model code is still under review. Compared to the old CEB-1990 [83], most formulas and factors in the new codes were slightly modified. The new FIB 2010-1992-1-2010 provides Eq. (2-34) to calculate the characteristic crack width w_d of beams and one-way slabs. This formula is based on the strain difference between steel and surrounding concrete.

$$w_d = 2 \cdot l_{s,max}(\varepsilon_{sm} - \varepsilon_{cm} - \varepsilon_{cs}) \tag{2-34}$$

where

$l_{s,max}$ is the maximum crack spacing;

ε_{sm} is the average reinforcement strain over the length, $l_{s,max}$;

ε_{cm} is the average concrete strain over the length, $l_{s,max}$;

ε_{cs} denotes the strain of the concrete due to shrinkage;

The average difference strain in Eq.(2-34) can be obtained from:

$$\varepsilon_{sm} - \varepsilon_{cm} = (\varepsilon_{s2} - \beta\Delta\varepsilon_{sr}) - \beta\varepsilon_{sr1} = \varepsilon_{s2} - \beta\varepsilon_{sr2} \tag{2-35}$$

with

$$\varepsilon_{sr2} = \frac{f_{ctm}}{\rho_{s,eff}E_s}(1 + \alpha_e\rho_{s,eff}) \tag{2-36}$$

where: $\Delta\varepsilon_{sr} = \varepsilon_{sr2} - \varepsilon_{sr1}$

ε_{s2} is the steel strain at the crack;

ε_{sr2} is the steel strain at the crack, under forces causing f_{ctm} in the area of $A_{c,eff}$;

A_{eff} is a sectional area of zone of reinforcement of concrete section in which reinforcement is effective, mm^2. The value of $A_{c,eff}$ refers to Figure 2-17;

ε_{sr1} is the steel strain at the point of zero slip under cracking forces reaching f_{ctm};

β an empirical factor to asses averaged strain within $l_{s,max}$;

f_{ctm} is the average value of concrete tensile strength;

Table 2-2 Values of τ_{bm}, β and η_r for deformed reinforcement

Item	Crack formation stage	Stabilized cracking stage
Short term,	$\tau_{bm} = 1.8f_{ctm}(t)$	$\tau_{bm} = 1.8f_{ctm}(t)$
Instantaneous	$\beta = 0.6$	$\beta = 0.6$

Loading	$\alpha = 0$	$\alpha = 0$
Long term,	$\tau_{bm} = 1.35 f_{ctm}(t)$	$\tau_{bm} = 1.35 f_{ctm}(t)$
Repeated	$\beta = 0.6$	$\beta = 0.4$
Loading	$\eta_x = 0$	$\eta_x = 1$

According to FIB 2010-1992-1-2010 (draft), values of τ_{bm}, β and η_r can be obtained from Table 2-2.

The length $l_{s,\max}$ in Eq. (2-34) can be defined as,

$$l_{s,max} = \frac{1}{4} \cdot \frac{f_{ctm}}{\tau_{bm}} \cdot \frac{\phi_s}{\rho_s} \tag{2-37}$$

where

ϕ_s is reinforcing bar diameter;

τ_{bm} is lower fractal value of the average bond strength, Mpa;
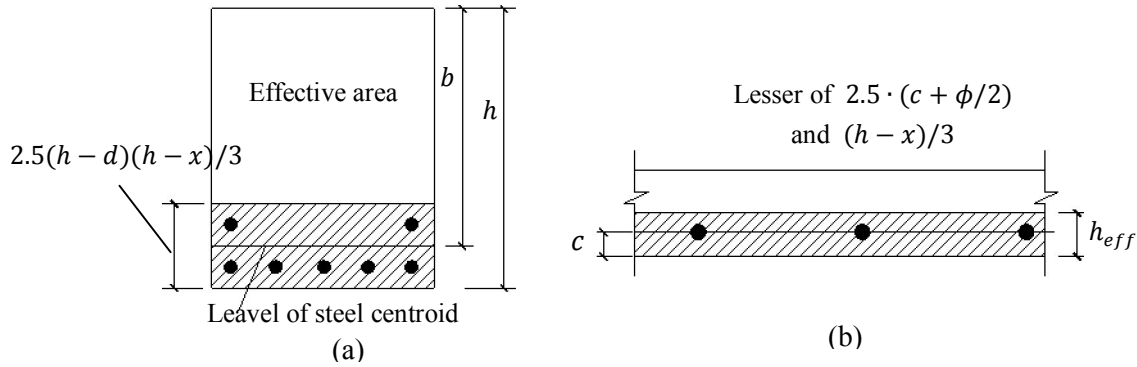
Figure 2-17: Effective tension area of FIB Model code 2010 draft and DIN EN 1992-1-2011: (a) beam; (b) slab

When cracks occur at an angle larger than 15° to the tensile stress direction of reinforcement net of RC slab reinforced in two orthogonal directions, the crack spacing can be calculated by:

$$l_{r,max} = \frac{1}{\dfrac{\cos\theta}{l_{r,max,x}} + \dfrac{\sin\theta}{l_{r,max,y}}} \tag{2-38}$$

where

θ is the angle between the reinforcement along the x-axis and in the direction of the principal tensile stress;

$l_{r,max,x}$ and $l_{r,max,y}$ are the maximum final crack spacings along the x and y axes, respectively, obtained by the mean of equation Eq. (2-37)

2.6.2 EN DIN 1992-1-2011

DIN EN 1992-1-2011 requires that cracking should be limited to a level that does not impair the proper structure or cause an unacceptable appearance. The maximum design crack width is limited to 0.30 mm with sustained load under normal environmental conditions. The characteristic crack width w_k is calculated as:

$$w_k = S_{r,max} \cdot (\varepsilon_{sm} - \varepsilon_{cm}) \tag{2-39}$$

where

$S_{rm,max}$ is maximum stabilized crack spacing;

ε_{sm} is the average strain of the reinforcement under the relevant combination of actions;

ε_{cm} is the average strain of concrete between adjacent cracks;

The value of $\varepsilon_{sm} - \varepsilon_{cm}$ is obtained from the following expression:

$$\varepsilon_{sm} - \varepsilon_{cm} = \frac{\sigma_s - k_t \cdot \dfrac{f_{ct,eff}}{\rho_{eff}}(1 + \alpha_e \cdot \rho_{s,eff})}{E_s} \geq 0.6 \cdot \frac{\sigma_s}{E_s} \tag{2-40}$$

where

σ_s is stress in the tension reinforcement computed on the basis of a cracked section, MPa;

α_e is the elastic modulus ratio of concrete to steel;

$\rho_{s,eff}$ is the reinforcement ratio in effective tensile concrete zone, $\rho_{s,eff} = A_s/A_{eff}$, refer to Figure 2-17;

k_t is the factor of load term, k_t=0.6 for short term load, and k_t=0.4 for long term load.

In fact, Eq. (2-40) is the combination of Eq. (2-35) and (2-36) according to FIB Model Code 2010 (draft).

According to DIN EN 1992-1-2011, when the height of tension zone h_{eff} is smaller than $5 \cdot (c + \phi/2)$, the average stabilized crack spacing, $S_{r,max}$ is calculated by:

$$S_{r,max} = k_3 \cdot c + k_1 \cdot k_2 \cdot k_4 \cdot \phi/\rho_{s,eff} \tag{2-41}$$

c is the concrete cover of LR;

k_1 is 0.8 for deformed bars and 1.6 for plain bars;

k_2 is 0.5 for bending and 1.0 for pure tension;

ϕ_s and $\rho_{c,eff} = A_s/A_{c,eff}$ are the same with above equations. The calculation of $A_{c,eff}$ refers to Figure 2-17.

In order to consider the slab with large concrete cover, when the height of effective concrete tension zone is larger than $5 \cdot (c + \phi/2)$, the maximum crack spacing can be obtained from:

$$S_{r,max} = 1.3(h - x) \tag{2-42}$$

2.6.3 DIN1045-1 2008

DIN1045-2008 adopts a "Bond-slip mechanism" similar with that used in FIB Model

Code 2010 (Draft). Thus, crack spacing prediction formula equals to Eq.(2-37). The design crack width, w_k is obtained from Eq.(2-39) according to DIN EN 1992-1-2011.

The difference between DIN EN 1992-1-2011 and DIN1045-1-2008 is the average strain difference between concrete and steel. This average strain difference can be calculated by using Eq.(2-40), but the coefficient k_t in Eq. (2-40) is constant at 0.4 in DIN1045-2008. DIN1045-1-2008 and FIB Model Code 2010 (Draft) have a similar factor of the effective area in tensile zone $A_{c,eff}$. However, DIN1045-1-2008 is modified to take into account of the height of cross section (refer to Figure 2-18).

(a)   (b)

(c)

In figures

1 effective area of tensile concrete

2 centroidal axis of reinforcement

3 centroidal tension

4 bending
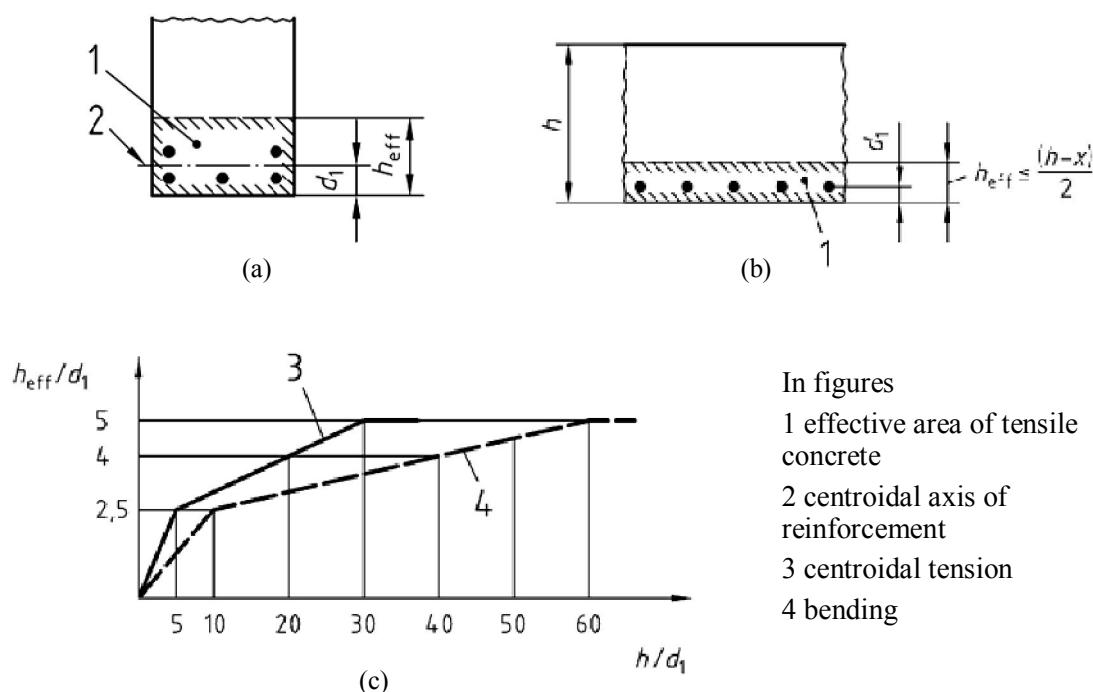
Figure 2-18: Effective tension area of DIN1045-1-2008: (a) beam, (b) slab, (c) effective height h_{eff} depends on concrete cover

The maximum final crack spacing is refered by bond-slip mechanism and FIB Model Code 2010 (draft) Eq.*equation reference goes here* , but may be limited as follows:

$$S_{r,max} = \frac{\phi_s}{3.6\rho_{eff}} \le \frac{\sigma_s \phi_s}{3.6 f_{ct,eff}} \tag{2-43}$$

2.6.4   The American Concrete Institute (ACI 318-2011) approach

Requirements for flexural crack control in beams and thick one-way slabs (span-depth ratio in the range of 4.5m-6m) are based on the statistical analysis [2] of maximum crack width data. Gergely and Lutz[2] proposes a new equation based on the statistic data of 612 bottom cracks and 355 lateral cracks. This equation is adopted by ACI318-95[96]. This study also shows that previous crack width equation is only valid for a relatively narrow range of concrete cover (up to 63 mm [2.5 in.]). Frosch [97] developed a new

formula for a thicker concrete cover, which was adopted by ACI 318-99.

ACI 318-08 [93] has not made a distinction between interior and exterior exposure. It requires that for crack control in beams and one-way slabs, reinforcement spacing closest to a surface in tension shall not only exceed that given by

$$s = \frac{95000}{540 f_s} - 2.5 d_c \quad [\text{mm}] \qquad (2\text{-}44)$$

but also not greater than 300 (252/f_s) mm,

where

d_c is the clear cover from the surface in tension to the flexural tension reinforcement(mm);

f_s is the calculated stress in reinforcement at service load, which equal to unfactored moment divided by the product of steel area and internal moment arm. Normally, f_s can be taken as 0.60f_y (MPa);

2.7 Experiments of RC element subjected to bending

Minor attention has been given to the previous research on flexural crack width for RC slabs under biaxial bending. Major research work performed in the United States is by Nawy et., [12, 13], whereas in the United Kingdom is by Clark [14, 98].

2.7.1 The test of MacGregor, J. G. [99]

In order to calculate the load-deformation behavior under combined stress and to simulate slabs subjected to in-plane tension and bending, MacGregor [99] conducted a model calculation. The slab dimensions, coordinate axis and strain are shown in Figure 2-19. The iterative method is adopted in his paper. This method take into account of the reinforcement direction under compressive forces N_x and N_y. A vertical uniform load q is set on the slab surface. The calculation process can be summarized to seven steps: (a) establishing a $M - \kappa$ relationship between compressive forces N_x and N_y in the x-and y-axis for different slabs;

(b) Using an initial curvature $\kappa_x = 1/r_{x0}$;

(c) Calculating the associated curvature $\kappa_y = (b \cdot \kappa_x)/l$;

(d) Determining the bending moments m_x and m_y according to $M - \kappa$ relationship;

(e) Determining the allowable vertical load q;

(f) Rising the initial curvature κ_x;

(g) Repeating steps of (a)-(e) to reach the maximum deflection.
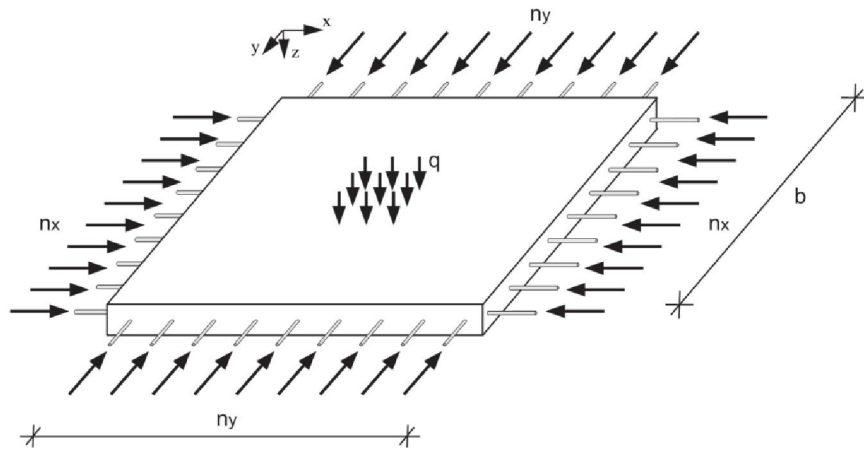
Figure 2-19 Stress in the plate from [99]

2.7.2 The test of Nawy et al. [12, 13]

Normally, crack-control equation of beams underestimates crack widths of two-way slabs and plates [12, 13]. Nawy et. [12, 13] have reported experimental results of 90 two-way slabs with rectangular and square shapes. Under various boundary conditions, these slabs are reinforced by high-strength welded mesh reinforcement. Nawy et. found that crack widths of two-way slabs and plates are primarily controlled by:

(a) The steel stress layer;

(b) Reinforcement spacing in two perpendicular directions;

(c) Clear concrete cover of two-way slabs and plates (It is nearly constant at 20mm for most interior structural slabs, whereas it is a major variable in the crack-control equation for beams).

The experimental results of two distinct types of cracks are summarized as: an orthogonal pattern of cracks followed the reinforcement lines and a diagonal pattern of cracks developed along the yield line pattern at higher loads. Nawy et al. explained this behavior by assuming that the steel force was transferred mainly to the concrete at the node points of crossing steel. The orthogonal pattern of crack is induced by using closely spaced small-diameter wires, whereas the diagonal crack pattern is caused by using widely spaced large-diameter wires. Crack widths in the orthogonal pattern are found to be smaller than those in the diagonal pattern, and hence the orthogonal pattern of cracks are preferred.

2.7.3 The test of Clark [14, 98]

Clark [14, 98] has reported results of theoretical and experimental studies of one-way spanning slabs with bars at various angles to the direction of moment. In his experiments, one-way slabs are used to simulate two-way slabs in one direction.

The presented test showed that the perpendicular transverse reinforcement has minor influence on crack control properties of bars, which located nearest the tension surface. Clark found out a same experimental result of the inclined orthogonal reinforcement net

with different reinforcement spacing. This result indicates that the calculating method of crack widths and the crack pattern formed at an angle to the steel is adequate.

2.7.4   The test of Rizk and Marzouk[100]

Rizk and Marzouk [100] give special attention to thick concrete plates used for offshore and nuclear containment structures. Eight full-scale two-way slabs were designed and tested to examine the influence of concrete cover and bar spacing on crack spacing. Five normal-strength concrete slabs and three high-strength concrete slabs were selected to investigate crack spacing and width behavior. The test results showed that the behaviors of reinforced concrete plates and two-way slabs are different from the behaviors of one-way beams. Flexural yield lines were well developed in all slabs. This failure can be classified as flexure failure. For the slabs failing by flexural punching, the crack pattern is observed prior to punching consisted of almost no tangential crack; the failure patterns of the test slab were shown in Figure 2-20.
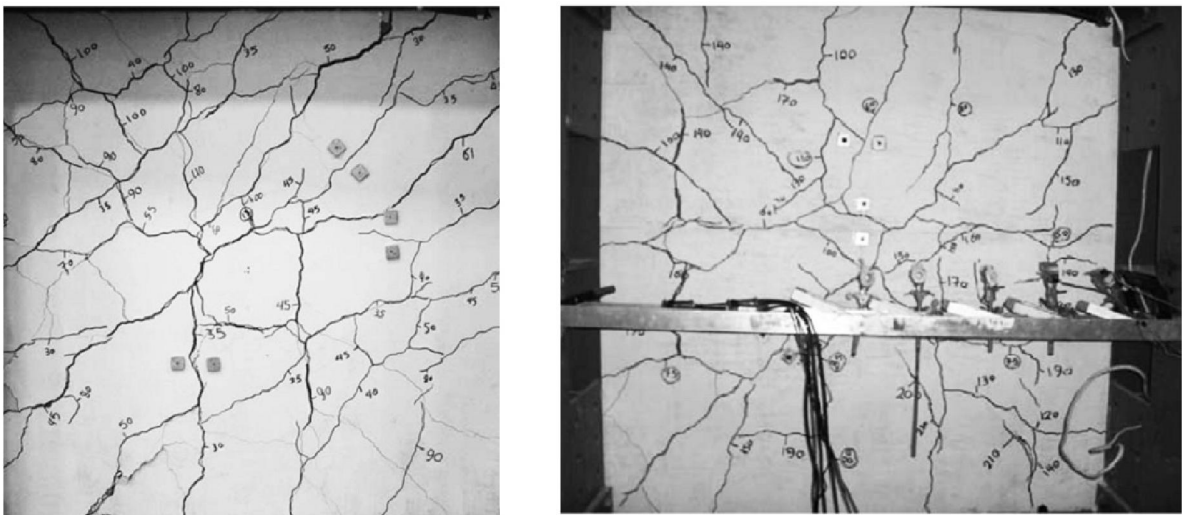
Figure 2-20 Crack patterns of test by Rizk and Marzouk[100]

2.7.5   The test of Lars Ruediger [81]

Under the support of DFG project KE 868/1-1, the load-displacement and cracking behavior of slabs under uniaxial and biaxial bending were tested based on designed RC slab specimens. The following parameters are investigated in test programs:

• Influence of the reinforcement direction α;

• Influence of concrete strength f_{ck};

• Influence of transverse reinforcement spacing s_C.
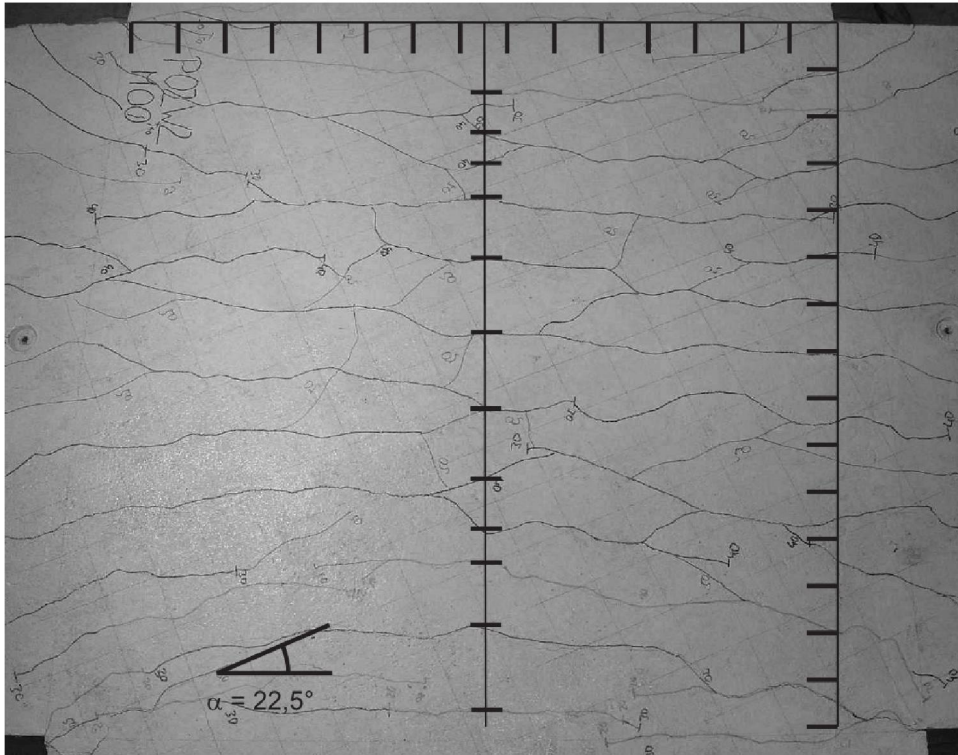
Figure 2-21: crack pattern of slab specimens with 22.5° reinforcement net [81]

This section describes the main test results obtained from experimental programs. Overall, the experiment involved 16 RC slab specimens under uniaxial and biaxial bending aims to investigate the influence of reinforcement net on crack behaviors; 12 RC specimens under tension and 12 RC slab-strips specimens under uniaxial bending are tested to study the individual parameters, such as reinforcement direction, TR spacing and concrete types. The load-deformation and crack behavior were recorded in experimental programs. Ruediger concluded that cracks inclined to the direction of reinforcement in two-way slabs as shown in Figure 2-20. Furthermore, Figure 2-22 illustrates cracking and ultimate loads of 9 tested slab specimens with various reinforcement direction and concrete types. It can be seen from the figure that the slabs made of high-strength concrete have higher ultimate load than that of normal-strength concrete. With the same concrete type, the ultimate load of the slab specimens with reinforcement net in the direction $\alpha = 0°$ is larger than that of reinforcement direction $\alpha = 22.5°$ and 45°. These phenomena indicate that the reinforcement controls crack width under different load situations. Such control behavior relates to the direction of reinforcement and the bond strength between steel and concrete.
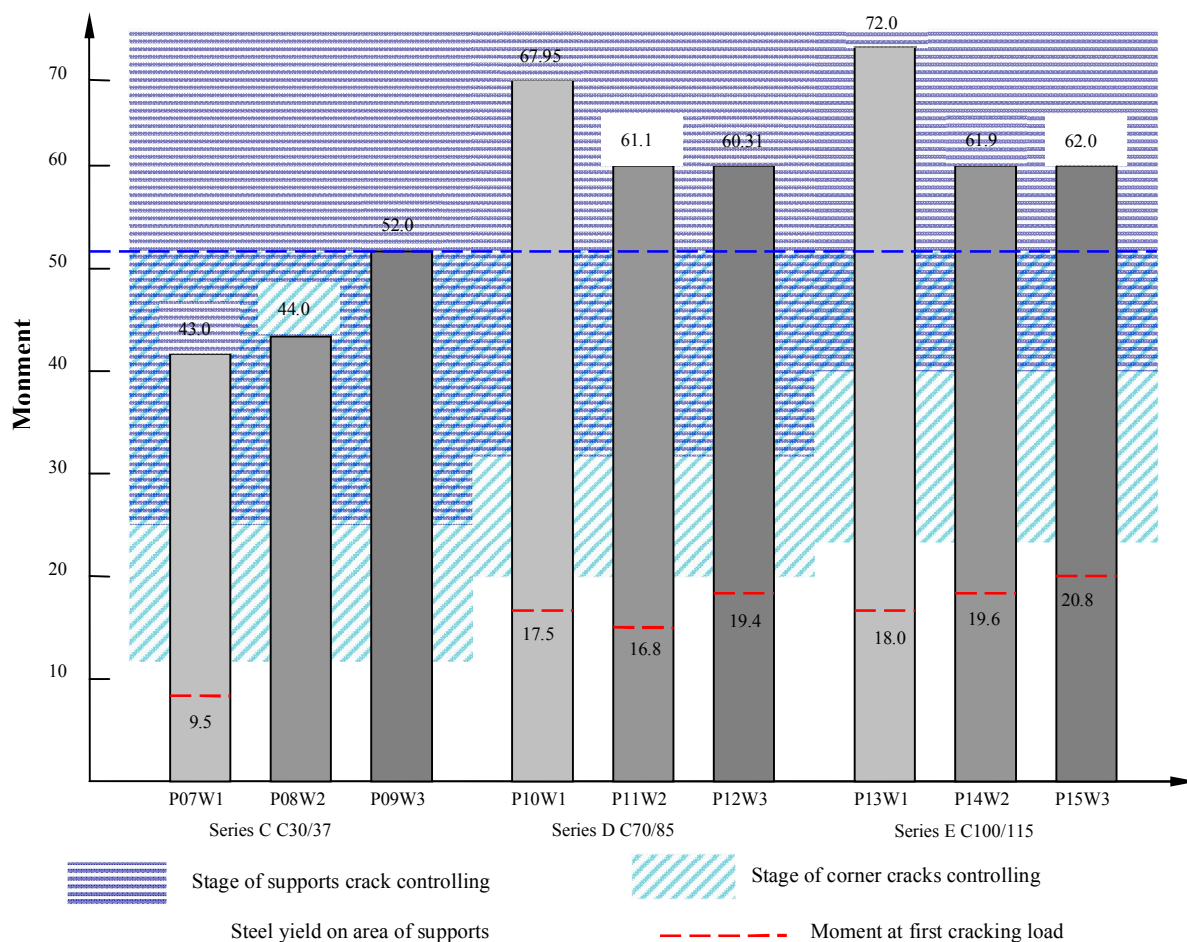
Figure 2-22 Test slabs under the controlling of steel on area of corner area and support area

3 Influence of transverse reinforcement on crack behavior of RC slab-strips subjected to uniaxial moments

3.1 Introduction

As discussed in sections 2.3.4.1 through 2.3.4.3, TR affects principally the crack formation and propagation in terms of three actions, however, the factor of TR is not taken into account in classic theories and formulae in current codes (see Section 2.4 and 2.5). This chapter attempts to investigate the effect of transverse reinforcement (TR) on crack formation and propagation by means of a series of four points bending test for RC slab-strips. Equation Chapter (Next) Section 3

Accordingly, various variables of TR, such as concrete cover of TR (TR-cover), the spacing between TR (TR-spacing), angles of TR to normal direction of bending (TR-direction), the different positions of TR to longitudinal reinforcement (TR-position)

and concrete types were considered in order to quantitatively study the effect of TR on the crack behavior. Furthermore, a new concept of crack behavior named as Cracking Rate was defined to quantify crack propagation.

A total of 33 slab-strips specimens, including 21 NC, 6 HC and 6 LC slab-strips specimens which were selected from 67 RC slab-strips in order to experimentally investigate the crack behavior including factors, such as crack pattern, average crack spacing, maximum and average crack width and crack width propagation. The test results are presented and analyzed as follows:

- Section 3.3 investigates the effect of TR-cover and TR-spacing on crack behavior in a light of linear regression analysis.

- Section 3.4 studies the effect of the angle between TR and normal direction of moment and concrete types on crack behavior.

- Section 3.5 analyzes the effect of TR on crack behavior when the position of TR was switched from the outside of longitudinal reinforcement (LR) to the inside.

It is evident from the mechanics of the flexural RC element that the curvature is the physical quantity to judge the displacement of RC element subjected to bending, and its bending stiffness is greatly affected by flexural cracking. However, there is a noticeable lack of experimental data which indicates the correlation between curvature and flexural crack width. Therefore, in Section 3.6, test specimens of RC-slab strips were tested to analyze the correlation between curvature and flexural crack width.

3.2 Experimental Details

3.2.1 Test specimens

All test specimens of slab-strips were 3300 mm long and 300 mm wide, The LR ratio was 6.54%. The variables and material properties of slab-strips are presented in Table 3-1 (for more details refer to Table A-D of Appendix D3). The position of embedded TR and thickness of reinforcement concrete cover were detected by Ferroscann (the details of HILTI PS 200 S are presented in Appendix C). In order to obtain reliable data from the laser sensors, the upper surface of test specimens was placed flatly. The upper and downside of test specimens was reversed before the loading was performed. The parameters of test specimens in Series 1- 3 are presented in Table 3-2.

The test specimens were classified into three series. Series 1 was designed for investigation of the TR-spacing and -cover on effect crack behavior. Figure 3-1 presents reinforcement layout of Series 1. The three reinforcement plan undertook a fixed effective depth of 157mm and various TR-cover ranging from 10mm to 40mm. This series was comprised of 14 slab-strips designated as Group A (TR-spacing=100mm), Group B (TR-spacing=200mm), and Group C (TR-spacing=300mm). Group A included 6

40

slab-strips with Ac1 (A1c1 and A2c1) (h=180mm, TR-cover of 10mm), Ac2 (A3c2 and A4c2) (h =200mm, TR-cover of 30mm), and Ac3 (A5c3 and A6c3) (h =220mm, TR-cover of 40mm). Group B was made of 6 slab-strips with BC1 (B1c1 and B2c1) (h=180mm), BC2 (B3c2 and B4c2) (h=200mm), and Bc3 (B5c3 and B6c3) (h=220mm). Group C included 2 slab-strips with Cc2 (C1c2 and C2c2) (h=200mm).

Figure 3-2 illustrates reinforcement layout of test specimens for Series 2. Series 2 was designed for invesgation of the TR-direction and concrete types on effect of crack behavior. This serie was made of 6 NC slab-strips (N as first letter), 6 HC slab-strips (H as first letter) and 6 LC slab-strips (L as first letter). The slab-strips of this series had different TR-directions, in which Nw1 (N1w1 and N2w1) (w=0°), Nw2 (N3w2 and N4w2) (w=22.5°) and Nw3 (N5w3 and N6w3) (w=45°). The slab-strips of HC and LC were tested in the same way as NC.

Figure 3-3 illustrates reinforcement layout of test specimen for Serie 3. This serie was designed for investigation of the effect of TR-position on effect of crack behavior. Which consisted 3 NC slab-strips designated as NA (Type A, TR is outside of LR), NB (Type B, TR is inside of LR) and NC (Type C, there is no LR). The slab-strips of NA and NB had a TR-spacing of 100 mm. TR of Type C was set inside of LR with a spacing of 600mm.
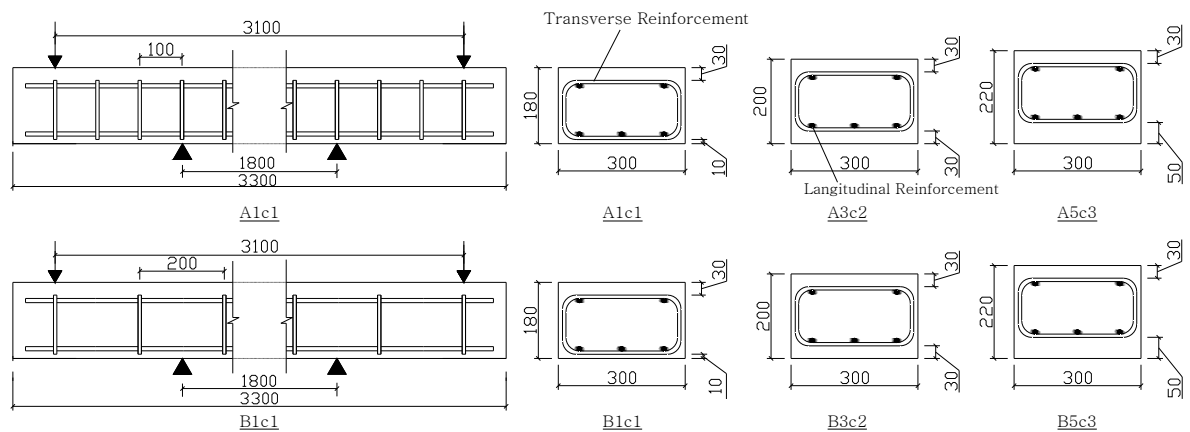
Figure 3-1 Reinforcement layout Series-1
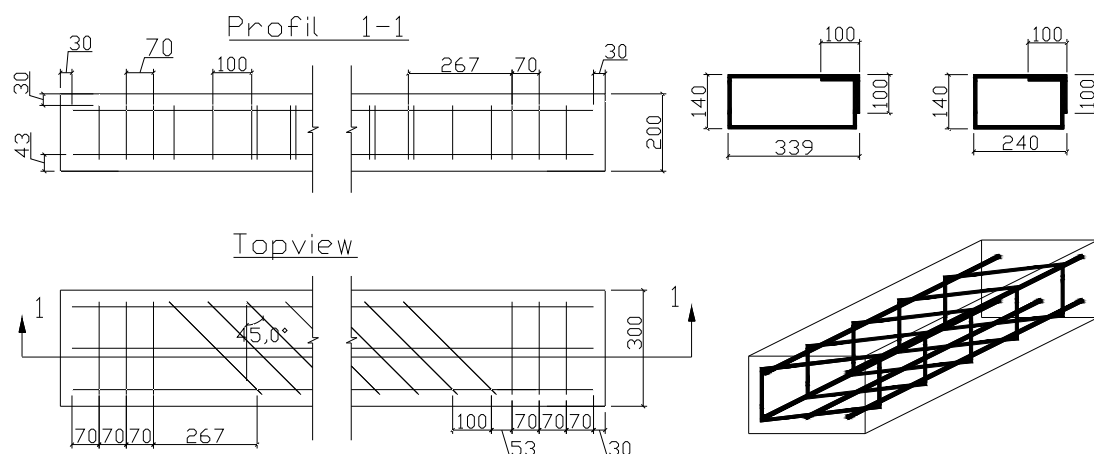
Figure 3-2 Reinforcement layout of Series-2
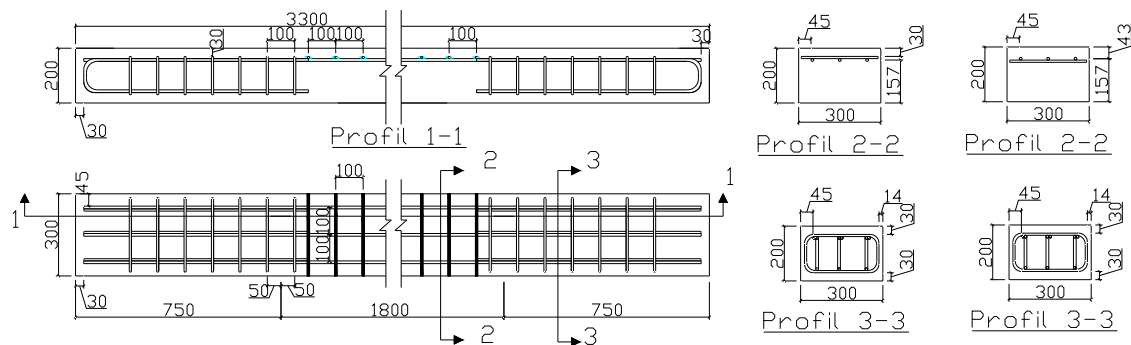
Figure 3-3 Reinforcement layout of Series-3

3.2.2 Material properties

This section describes the production of the test specimens. The properties of concrete and steel reinforcement are shown in Appendix D.

Timber forms were cured the molds for 2 days in a damp condition. This method met the requirements of DIN 1045-3 (DIN 1045-1 2008), and the specimens were stored under room temperature (about 20℃). Three cube (150×150×150mm) were cast for each series and remained under the same conditions as the specimens to determine the compressive strength of the concrete. The average cylinder compressive strength $f_{cm,cube}$, was determined by tested cubes, while the axial tensile strength (f_{ctm}) was calculated according to DIN 1048 [101]. Most of the properties are listed in Sections 3.3 to 3.6. All measured data of specimens is summarized in Tables A to D in Appendix D 3.

3.2.3 Test setup and test procedure

It is essential that the test setup should simulates the bridge slabs situation in construction (see Chatper 1) of slabs subjected to biaxial bending. Thus, it is necessary to simulate a pure biaxial bending through a four point biaxial bending method. In the test series of one-way slab-strips, a four point uniaxial bending test method was adopted.

Figure 3-4 and Figure 3-5 illustrate that the reverse loading method was applied in order to easily observe cracking. This loading method involved two cylinders fixed at both ends of a specimen. Cracks were observed in the area corresponding to 1800 mm between two free supports. The load increment was selected at 4kN up to the formation of the first crack and then the load increment increased to 5kN. Each load step was held for 5 minutes. The loading was continued until the ultimate load.
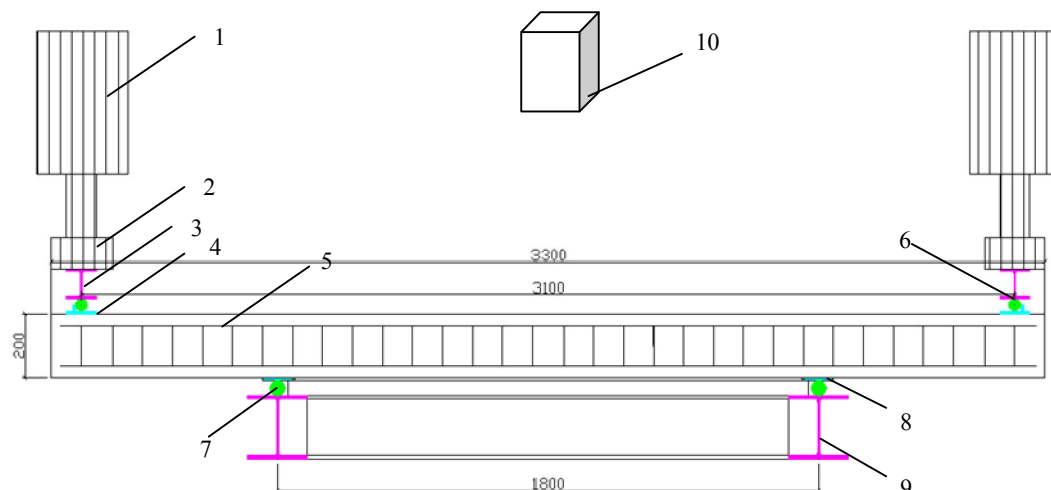
Figure 3-4: Introduction of test setup. 1. Hydraulic jack; 2. Force sensors; 3. HEB 200 I-steel; 4.Steel plate of 5mm; 5. Test specimen; 6. Steel tube (Diameter: 5mm); 7. Steel tube (Diameter: 5mm); 8.Steel plate of 5mm; 9. I-steel frame (HEB 200); 10. Laserscanner.

The tested slab-strips were carefully inspected at each load step. The load and the deformation were measured by force sensors and laser displacement sensors. The arrangement of displacement sensors is shown in Figure 3-6. The all cracks on the upper surface of specimens were marked by different colors The crack pattern of each specimen was recorded by means of photographs at each loading stage throughout the experiment. These photographs were inserted in AutoCAD software on a two-dimensional grid with a scale of one to one. The crack spacing was measured and saved in the Microsoft Excel

Table 3-1: Parameter of test specimens in Chapter 3

	Slab-strips designation	Concrete type	Clear concrete cover	Effective depth	Average TR-cover	TR-spacing	TR-direction	TR Type
	A1C1	NC	19.0	156.0	7.0	100	0	A
	A2C1	NC	19.9	155.1	7.6	100	0	A
	A3C2	NC	38.5	156.5	29.0	100	0	A
	A4C2	NC	39.1	155.9	31.0	100	0	A
	A5C3	NC	56.4	158.6	38.1	100	0	A
	A6C3	NC	55.7	159.3	41.1	100	0	A
Serie 1	B1C1	NC	17.9	157.1	6.6	200	0	A
	B2C1	NC	19.8	155.2	10.6	200	0	A
	B3C2	NC	39.3	155.7	32.3	200	0	A
	B4C2	NC	38.7	156.3	31.1	200	0	A
	B5C3	NC	54.5	160.5	41.5	200	0	A
	B6C3	NC	53.2	161.8	36.7	200	0	A
	C1C2	NC	45.7	149.3	32.8	300	0	A
	C2C2	NC	43.6	151.4	31.2	300	0	A
	N1w1	NC	46.3	148.7	29.0	100	0	A
	N2w1	NC	45.5	149.5	31.0	100	0	A
	N3w2	NC	45.1	149.9	31.0	100	22	A
	N4w2	NC	46.6	148.4	33.0	100	22	A
	N5w3	NC	48.7	146.3	42.0	100	45	A
	N6w3	NC	43.7	151.3	42.0	100	45	A
	H1w1	HSC	47.4	147.6	31.0	100	0	A
	H2w1	HSC	46.8	148.2	32.0	100	0	A
Serie 2	H3w2	HSC	49.1	145.9	32.0	100	22	A
	H4w2	HSC	51.2	143.8	32.0	100	22	A
	H5w3	HSC	53.4	141.6	42.0	100	45	A
	H6w3	HSC	52.6	142.4	44.0	100	45	A
	L3S2	LWC	43.1	151.9	30.0	200	0	A
	L4S2	LWC	45.3	149.7	34.2	200	0	A
	L3w2	LWC	40.4	154.6	36.0	100	22	A
	L4w2	LWC	50.0	145.0	40.0	100	22	A
	L5w2	LWC	45.0	150.0	34.0	100	45	A
	L6w2	LWC	46.4	148.6	35.0	100	45	A
	NA	NA	32.2	162.8	21.5	100	0	A
Serie 3	NB	NB	30.3	164.7	47.3	100	0	B
	NC	NC	34.7	160.3	49.0	100	0	C

software. The crack width was measured by using a crack width measurement instrument (with 2 mm range and 0.01 mm accuracy see Appendix C). In the present work, a new method utilizing a laser scanner, which (see Figure 3-5) obtains 3D Point Clouds, was developed to measure the crack spacing and deformation (see Appendix C). Utilizing this

44

new experimental measurement approach, deformation points cloudy on the overall surface can be obtained with higher accuracy and density than original measurement.
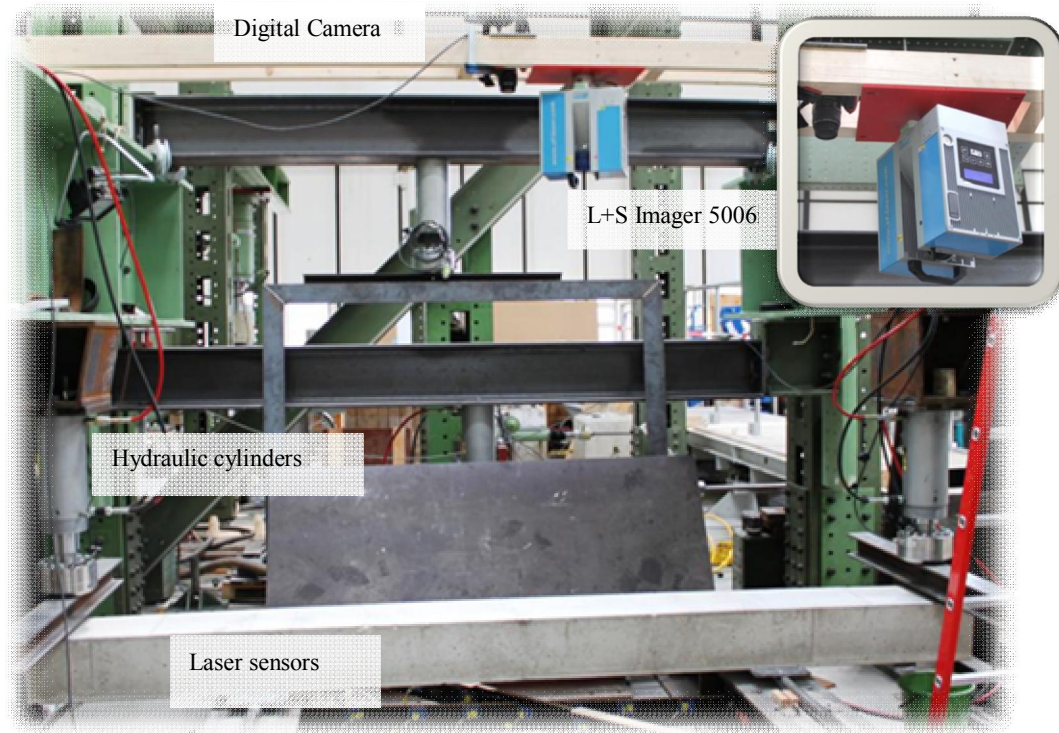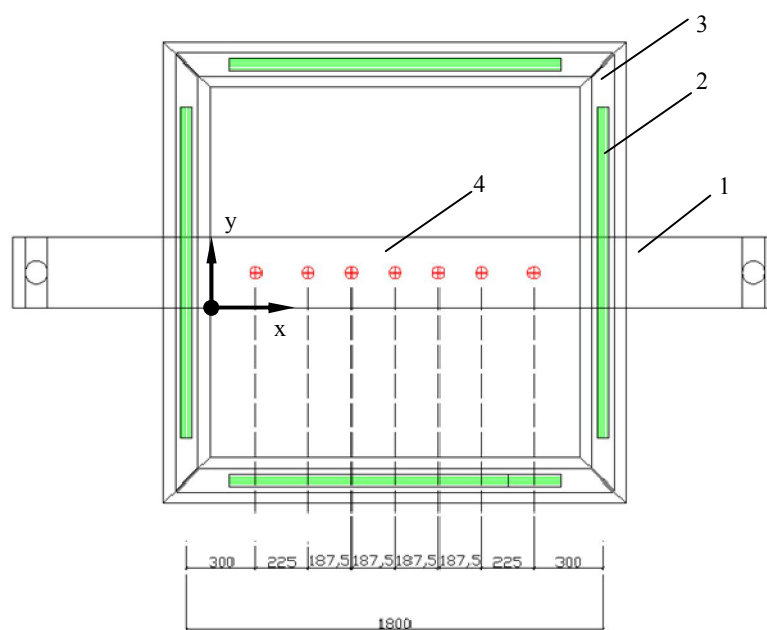

Figure 3-5: Test arrangement

Figure 3-6: Arrangement of laser displacement sensors. 1. Specimen; 2. Solid steel pipe；3. I- Support steel ring; 4. Laser displacement sensors (Total: 7)

3.3 Transverse reinforcement concrete cover and spacing

The experimental results of the tested 14 slab-strips (TR-cover of 10mm, 30mm and 40mm) were compared to find out the influence of TR-cover on crack behavior. Moreover, another two new crack parameters, cracking rate and the correlation between curvature and crack width are presented and investigated. The crack width values were measured at 62.5% yield stress level (upper limit at service limit state).

3.3.1 Crack patterns

Figure 3-7 shows that the tested slab-strips, including HS, NC and LC with 22.5° TR-direction. ruptured along the cross-section of a TR-induced crack. Although concrete material is heterogeneous and cracks occur randomly, it can be observed from the same figure that cracks appeared right along the TR and indicated that certain cracks were induced at TR under certain TR-cover. Figure 3-8 shows the crack pattern of certain tested slab-strips at serviceability state. By using HILTI PS200 S Ferro scan and the photogrammetry method the position of TR can be detected. Red marks refer to the formation of first cracks at the first cracking load. For the case of the slab-strips with TR-cover ranging of 10mm to 30mm (see AC1, BC1 and AC2 in Figure 3-8) cracks induced roughly in the region of a TR. This phenomena is aggremen with Beeby investigation [90]. With increased TR-cover to 40mm fewer crack-forming influence. This indicates that TR-cover is one of major parameter to influence the crack-forming so strong.

In addition, a crack appeared in the region between the two adjacent TR bars were observed. The reason is that the TR-spacing of 200mm was close to or exceeded the maximum crack-spacing calculated with the formulae of bond-slip mechanism (Eq. (2-37)) (for 10mm TR-spacing is 182mm; for 30mm TR-spacing is 206mm; for 40 mm TR-spacing is 229mm). The picture of this phenomenon discussed above is shown in BC1 of Figure 3-8.

In order to describe the formation of cracks caused by TR quantitatively, the radius of TR influence range needs to be evaluated, from Eq. 3-1[9] , as follows:

$$r_t = \frac{r_s}{2} + d_a \qquad (3\text{-}1)$$

where

r_s is diameter of TR;

d_a is maximum aggregate size.

For a maximum aggregate size of 17 mm, the radius TR influence range is 21 mm from both sides of TR. To identify whether cracks are affected by TR or not, the distances between TR and the nearest cracks were measured using AutoCAD software. The average distances between TR and cracks are given in Table 3-2. Furthermore, this table presents the calculated percentage ratios of cracks affected by TR in relation to all appeared cracks,

named η_c. In view of this, for the test specimens of AC1 and AC2 with TR-cover of 10mm, all cracks appeared in the influence range of TR can be presented as η_c=100%. Figure 3-9 illustrates that an increase of TR-cover from 10mm to 40mm for Group A (TR-spacing of 100mm) and Group B (TR-spacing of 200mm) resulted in a decrease of η_c from 100% to 55% and 63% to 26%, respectively, in nearly linear manner. Therefore, TR-cover plays a key role in the formation of cracks affected by TR. The relation can be obtained through linear regression between η_c and TR-cover (c_{TR}) as follows:

$$\eta_{c-\text{cover}} = -0.012 \cdot c_{TR} + 1.085 \tag{3-2}$$

However, it is necessary to note that η_c decreased significantly as TR-spacing increased from 100 mm to 200mm, which was larger than the maximum predicted crack spacing. In order to study the effect of TR-spacing on η_c, Figure 3-10 illustrates the variation of η_c with TR-spacing for a TR-cover of 30mm. As shown in this figure, η_c decreased nearly linearly to 39% (R^2=0.838), when TR-spacing increased from 100mm to 300mm,. Therefore, the discussion above indicates that for the specimens with a thick TR-cover of 30mm, an increase of TR-spacing, s_{TR} results in a decrease of the number of TR-induced cracks, $\eta_{c-spacing}$. Such a relationship can be expressed by the Eq.(3-3) as,

$$\eta_{c-spacing} = -0.0017 \cdot s_{TR} + 0.8477 \quad (100 \le s_{TR} \le 300)[mm] \tag{3-3}$$

Table 3-2 Variables of test specimens in Series 1

Group	Slab Strips no.	TR spacing [mm]	Average TR-cover* [mm]	LR-cover* [mm]	Average Distance between cracks and TR	η_c	Average value of α_{TR}***	Standard diviation	f_c' [MPa]	f_{ctm} [MPa]
Group A	A1c1	100	7	19	6.1	100.0%	2.6	1.0	30.01	2.07
	A2c1	100	7.6	19.9	6.8	100.0%	3.2	2.0	30.01	2.07
	A3c2	100	29	37	30.5	60.0%	3.8	3.4	26,01	2,63
	A4c2	100	31	40	17.6	78.0%	4.2	2.4	26,01	2,63
	A5c3	100	38.1	49.4	18.0	63.6%	5.9	3.6	30.01	2.28
	A6c3	100	41.1	50.8	15.6	55.0%	7.1	6.2	30.01	2.28
Group B	B1c1	200	6.6	17.9	47.4	63.0%	2.4	2.2	30.01	2.28
	B2c1	200	10.6	21.8	47.2	44.4%	2.3	1.4	30.01	2.28
	B3c2	200	32.3	47.1	51.4	45.0%	10.0	5.7	30.01	2.28
	B4c2	200	31.1	44.2	42.9	50.0%	3.5	4.2	30.01	2.28
	B5c3	200	41.5	54.5	26.9	26.7%	4.7	3.4	30.01	2.28
	B6c3	200	36.7	53.1	35.2	30.7%	8.0	3.0	30.01	2.28
Group C	C1c2	300	32.8	45.7	69.8	38.4%	5.9	3.4	30.01	2.28
	C2c2	300	31.2	43.6	75.2	30.8%	6.8	6.0	30.01	2.28

Notes: *Concrete cover of each TR and LR were measured by PS200 HILTI scanner, the average cover were listed in the table.

**Steel reinforcement upper limit yield is 579.5 N/mm2 , lower limit yield is 599.6 N/mm2 and Maximum stress is 696.1 N/mm^2

*** Average angle between cracks and TR. the angle of TR to cracks which appeared in the controlled area of TR

NC Specimen with 30mm TR-cover and 0° TR-direction

HC Specimen with 30mm TR-cover and 0° TR-direction

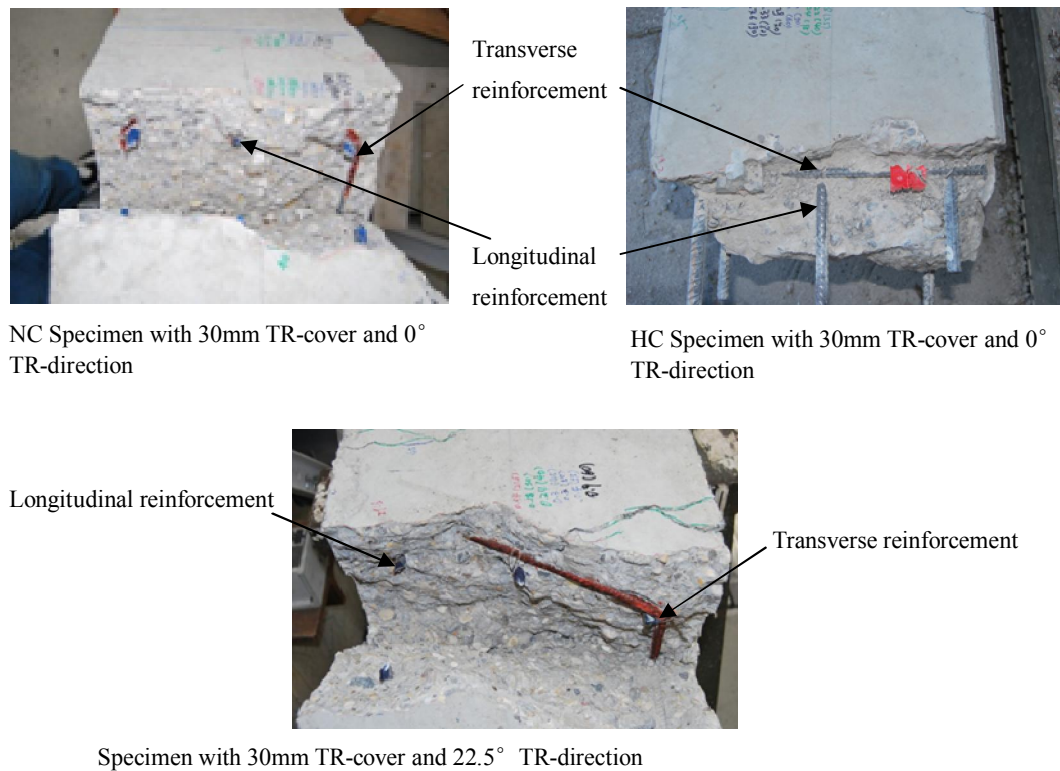Specimen with 30mm TR-cover and 22.5° TR-direction

Figure 3-7: TR-induced cracks

It is indicated in Section 2.3.5 that when TR-induced cracks, then the TR theoretically restrains these cracks from forming and this restraining behavior is assumed to have a close relationship with the angle between TR and cracks. Figure 3-8 illustrates that certain amount of cracks inclined for TR-cover of 40mm. In order to verify the restraining effect of TR on cracks for flexural TR-element, TR-formed cracks and their corresponding angles named as α_{TR} were measured individually in the test. The average values of α_{TR} were calculated and are listed in Table 3-2. From this table it can be observed that when the thickness of TR-cover is 10mm, 30mm and 40mm, the average value of α_{TR} yields 2.62°, 5.37° and 6.43°, respectively. The values of α_{TR} of exceptional cracks were larger than 15° and the standard deviation increased as well. Figure 3-11 schematically shows the variation of α_{TR} with TR-cover in Group A and Group B. For Group A, α_{TR} increaseing in a linear manner with TR-cover and Group B has a very similar trend to Group A. The reason of this linear relationship is that concrete material is heterogeneous and cracks occur at random, the larger the thickness of concrete cover, the higher randomness of cracking direction and the larger the angle between certain cracks and TR (see Figure 3-8). Figure 3-12 illustrates the variation of α_{TR} varies with TR-spacing. It is clearly shown that TR-spacing has no obvious effect on α_{TR}, which indicates that the increase of TR-spacing does not result in an increase of the angle between the crack and TR.

The test results above indicate that the increase of TR-cover results in an increase of the

angle between certain crack and TR. It could be possible to further indicate that TR restrains the opening of flexural TR-induced crack, which will be explained thoroughly in Section 3.3.3 and 3.3.4.

Ac1, load 60kN, 79.1% of Ultimate load

Longitudinal reinforcement
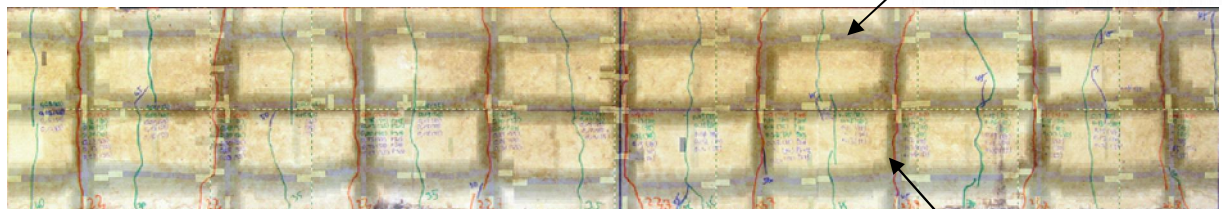
Bc1, load 60kN, 81% of Ultimate load

Transverse reinforcement
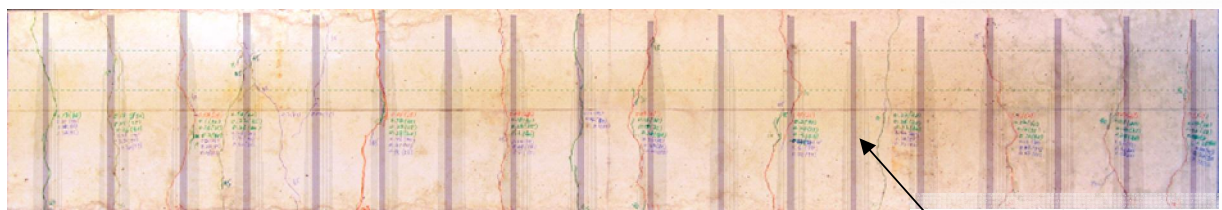
Ahc2, load 55kN, 78.9% of Ultimate load

Transverse reinforcement
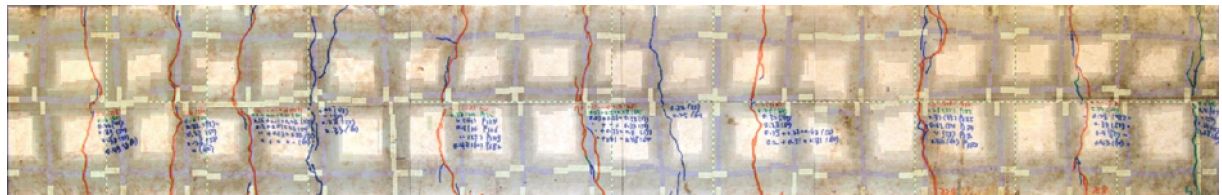
Ac3, load 60kN, 72.4% of Ultimate load
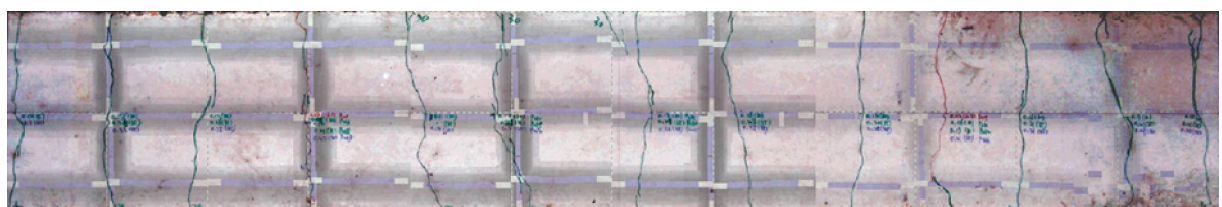
Cc2, load 45kN, 64.3% of Ultimate load

Figure 3-8: Final crack pattern overlapped with the TR layout for test specimens with various concrete covers
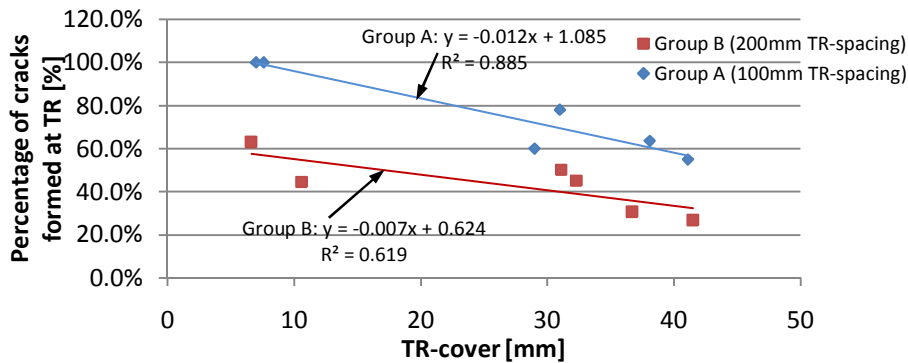
Figure 3-9 The relationship between η_c and TR-cover
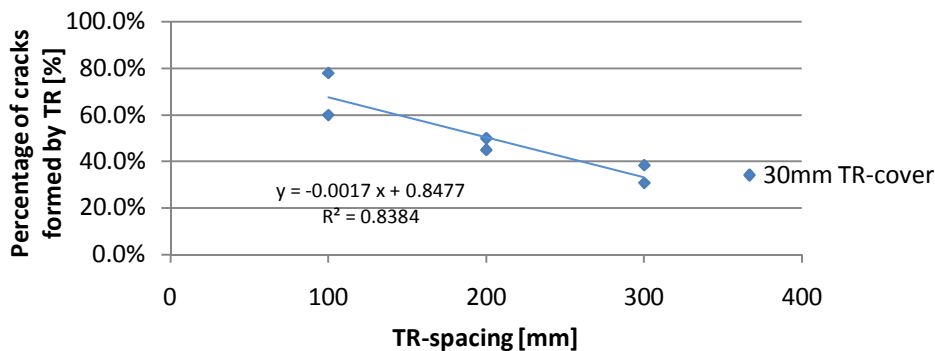
Figure 3-10 The relationship between η_c and TR-spacing
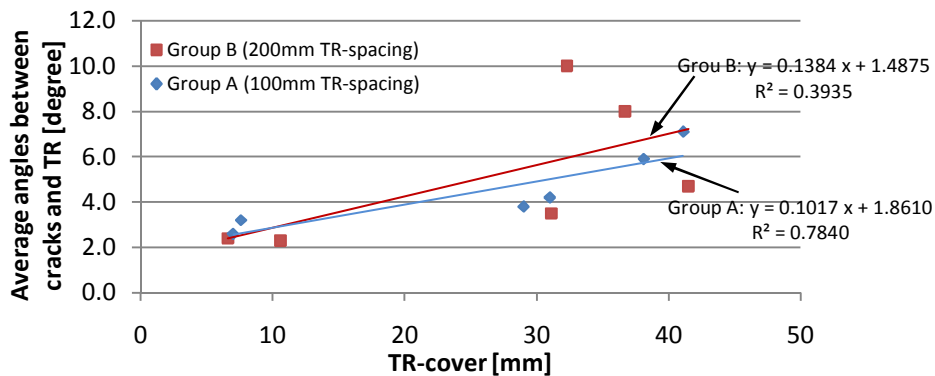
Figure 3-11 The relationship between α_{TR} and TR-cover
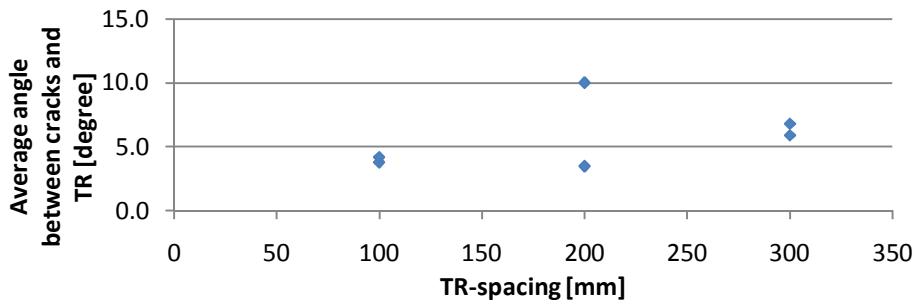
Figure 3-12 The relationship between α_{TR} and TR-spacing

3.3.2 Crack spacing

The effect of TR-cover and TR-spacing on crack spacing is investigated in this section.

Table 3-3 summarizes the average crack spacing of crack pattern for Group A and Group B. It can be observed from this table that the increase of TR-cover from 10mm to 40mm for Group A and Group B resulted in an increase of the average crack spacing by 67% (ranging from 100mm to 167mm for Group A) and 58% (ranging from 100mm to 158mm for Group B)
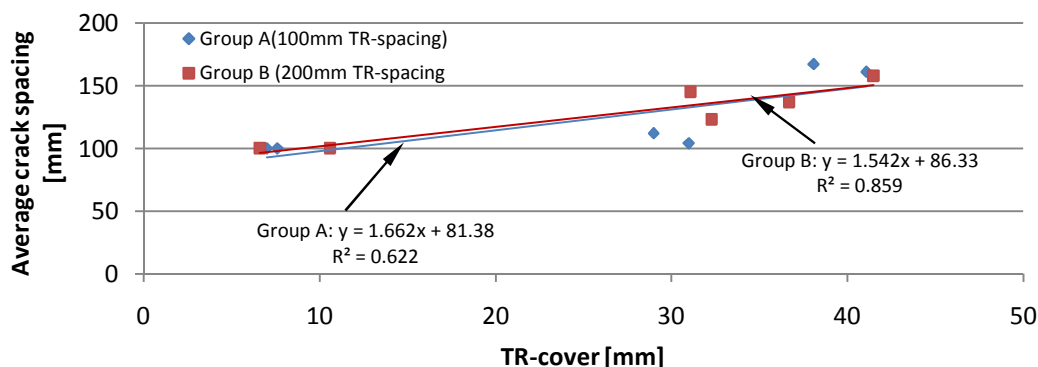
Figure 3-13 Average crack spacing versus variation of TR-cover

The test results of the average crack spacing are presented graphically in Figure 3-13, in which the average crack spacing versus TR-cover was plotted and a regression linear relationship between crack spacing and TR-cover for Group A (coefficient determinations R^2=0.622) and Group B (R^2=0.859) was found. Such linear relationship provides a satisfactory agreement with formulas found in current codes, such as FIB Model Code 2010 (draft) (Eq. (2-37)) and EN DIN 1992-1-2011 (Eq. (2-41)).

However, it could be noted that for TR-cover of 40mm, 100% increase of the TR-spacing of 200mm resulted in a slight, 10%, crack spacing decrease. Two specimens in Group C were tested to study the effect of TR-spacing on crack spacing. The data showed that an increase of TR-spacing by 200% to 300mm resulted in an increase of the average crack spacing by 33% to 144mm. Figure 3-14 illustrates a direct ratio between TR-spacing and crack spacing.

A study of cracks induced in the region near by a TR bar [7], as revealed by Beeby, figured out that crack-forming influence can be so strong that the crack formation and hence the crack spacing are entirely controlled by TR-spacing. Obviously, TR-induced cracks could affect average crack spacing, thus two variables of η_c and average crack spacing were presented in Figure 3-15. From this figure, it can be seen that an increase of η_c results in a linear decrease (R^2=0.691) of the average crack spacing and hence away from the predicted maximum crack spacing, $S_{r,max}$, given by Eq. (2-37) and Eq. (2-41). Therefore, it can be concluded that an increase of TR-cover could result in a decrease of number of TR-induced cracks, and hence decrease the restraining influence of TR. And then, an increase of average crack spacing is observed in Figure 3-15.

$$y = 0.180x + 92.6$$
$$R^2 = 0.641$$
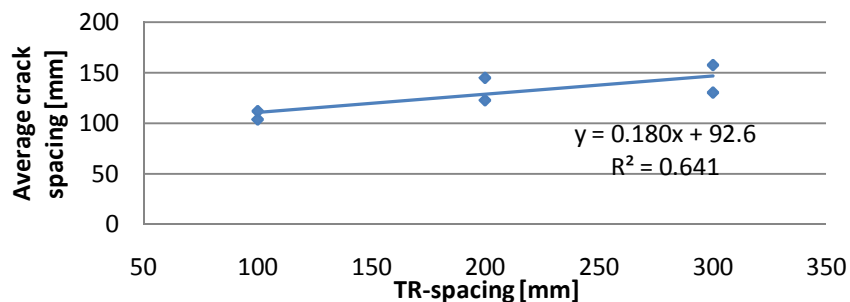
Figure 3-14 The relationship between crack spacing and TR-spacing

Observed spacing: $y = -99.74x + 178.9$
$R^2 = 0.691$
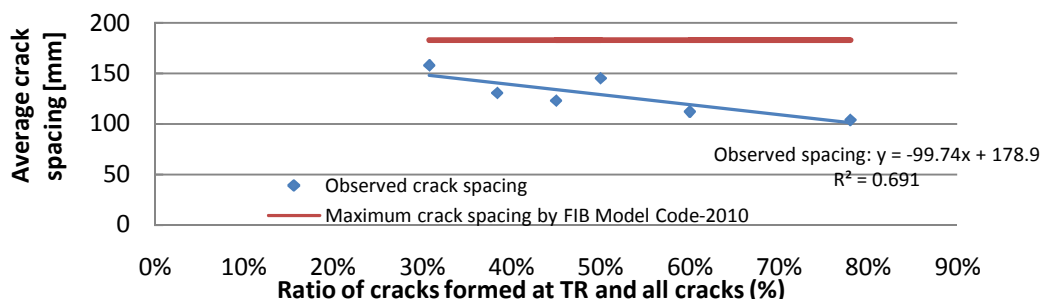
Figure 3-15 relationship between η_c and crack spacing

3.3.3 Crack width

This section attempts to investigate TR-cover and –spacing variation influence on the average and the maximum crack widths.

It is noted in the test procedure in (Section 3.2.3) that the crack widths were measured at each load increment up to the failure. The crack widths measured at the ultimate load (up to 90% of ultimate steel stress) A stress level of 62.5% of the yield strength of steel ($0.625f_y$) is chosen as the upper limit of service limit state in this section. Table 3-3 summarizes the average and maximum crack width of 12 test specimens at the servicability state (at steel stress level of $0.625f_y$ =325MPa). This table illustrates the effect of TR-cover on the crack width, i.e. increasing of TR-cover from 10mm to 40mm for Group A and Group B, resulted in increases of the average and maximum crack widths; for Group A 66% and 36%, and for Group B 128% and 115%, respectively.

Figure 3-16 and Figure 3-17 graphically present the linear correlations between TR-cover and the average and maximum crack width for Group A (R^2=0.621) and Group B (R^2=0.731). From the view points of the current codes (Eq. (2-37)), such a linear relationship was caused by an increase of concrete cover. However, for 40mm TR-cover, when TR-spacing increased from 100mm of Group A to 200mm of Group B, the average crack spacing decreased by 10%, whereas crack width increased by 66%. This phenomenon is discrepancy with crack model in current codes, in which the relationship between crack spacing and width indicates a direct ratio relation. Attention should be paid to this important finding, which indicates an inverse trend between crack spacing and width. This discrepancy is maybe caused by the TR-spacing.

Futhermore, the influence of TR-sapcing on crack width for various TR-cover is presented

in Table 3-3, it indicates that for 10mm TR-cover, a increase of TR-spacing produces nearly no effect on average and maximum crack width; for 30mm TR-cover, the average and maximum crack widths increase 11% and 22%; for 40mm TR-cover they are increase 26% and 66%.

The reason for these phenomenon is the restrain influence of TR on crack width. In fact, it is more reasonable to view the observed results in Section 3.3.2, that when TR-spacing increased from 100mm to 200mm for thick TR-cover of 40mm, the ratio of TR formed cracks decreased from 60% to 30% approximately, which results in a decrease of cracks restrained by TR, and hence results in a increase of crack width. Therefore, it not difficult to accepted that an increase of TR-spacing results in a large increase crack width. Clearly, for the influence of TR on crack width, the crack models in current codes are inapplicable and a different description with consideration of TR is required. However, it needs to be pointed out that a single crack width at serviceability state cannot sufficiently represent the behavior of crack propagation. In order to research the restraining influence of TR, a concept is defined to investigate the crack propagation in the next section.
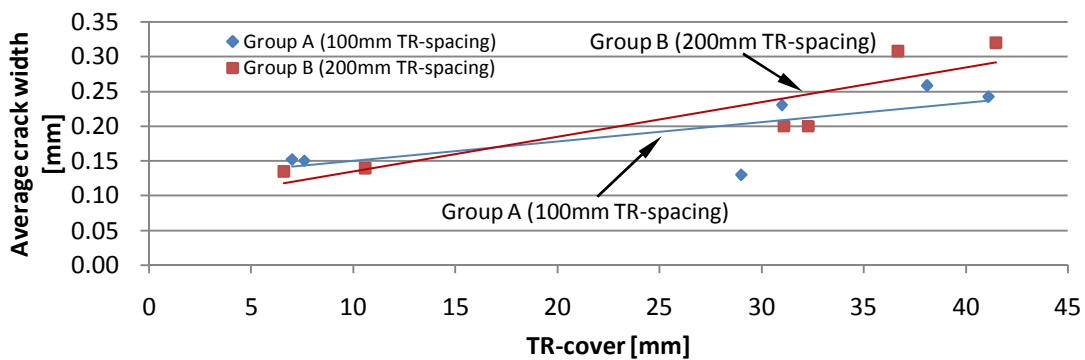

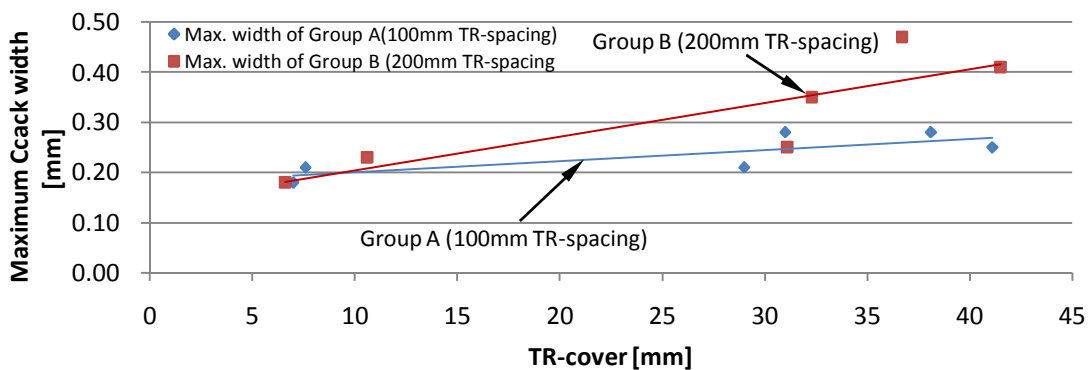**Figure 3-16 TR-cover versus the average crack width at load level of 0.625 f_y**

Figure 3-17 TR-cover versus maximum crack width at load level of 0.625 f_y

Table 3-3 Test results in Series 1

No.	TR-spacing [mm]	Average crack spacing [mm]	Crack Crack width [mm]*		Cracking Rate [mm³/N]**	
			Average values [mm]	Maximum values [mm]*	A-CR	M-CR
A1c1	100	100	0.15	0.18	0.00051	0.00063
A2c1	100	100	0.15	0.21	0.00054	0.00057
A3c2	100	112	0.13	0.21	0.00064	0.00104
A4c2	100	104	0.23	0.28	0.00081	0.00108
A5c3	100	167	0.26	0.28	0.00109	0.00148
A6c3	100	161	0.24	0.25	0.00104	0.00164
B1c1	200	104	0.14	0.18	0.00062	0.00090
B2c1	200	100	0.14	0.23	0.00035	0.00071
B3c2	200	123	0.20	0.44	0.00094	0.00165
B4c2	200	145	0.20	0.25	0.00074	0.00111
B5c3	200	158	0.32	0.41	0.00143	0.00183
B6c3	200	137	0.31	0.47	0.00119	0.00165
C1c2	300	131	0.18	0.25	0.00081	0.00099
C2c2	300	158	0.21	0.27	0.00105	0.00127

* Crack width were measured at level of $0.625f_y$ of servicerbility state;

** A-CR and M-CR were calculated until servicerbility state.

3.3.4 Cracking Rate

In the last section, the discrepancy of an inverse trend between crack spacing and width with the principles in current codes was found. In this section, by using the propagation of crack width as a key for investigation of the reason for this discrepancy, a new variable designated as Cracking Rate was defined as the ratio of incremental steel stress to incremental average crack width (A-CR) and to maximum crack width (M-CR). The ratio obtained by slope of regression line of steel stress against crack width with unit of mm³/N.

Figure 3-18 and Figure 3-19 illustrate variations of average and maximum crack width with the calculated steel stress up to the yield strength. The value of steel stress of each specimen was calculated by a straight-line formula where the steel stress was limited by the yield strength. It can be observed from these two figures that variations in crack widths are positively correlated with those of steel stress in a linear manner. This linear correlation of average and maximum crack width against steel stress has been also proven by other researchers [102, 103]. Therefore, linear regression analysis is adopted to calculate the regression lines and their slopes, in which A-CR and M-CR for 12 test specimens are calculated. Results are listed in Table 3-3. The correlation between TR-cover and A-CR and M-CR is graphically presented in Figure 3-18 and Figure 3-19. In these two figures, A-CR and M-CR of AC1 AC2, AC3 (from Group A with 100mm TR-spacing), and BC1, BC2 and BC3 (from Group B with 200mm TR-spacing) are presented respectively. These 6 specimens are selected from 12 test specimens. Figure

3-18 illustrates that A-CR of AC3 and BC3 with 40mm TR-cover is higher than that of AC2 and BC2 with 200m and AC1 and BC1 with 10mm. Moreover, with increase of TR-spacing from 100mm (Group A) to 30mm (Group B), A-CR of Group A is higher than that of Group B with TR-cover of 10mm, 30mm and 40mm respectively. From the above analysis, it can be concluded that TR-spacing and TR-cover affect A-CR significantly. Figure 3-19 illustrates a similar effect of TR-spacing and TR-cover on M-AT as well as in the former figure.
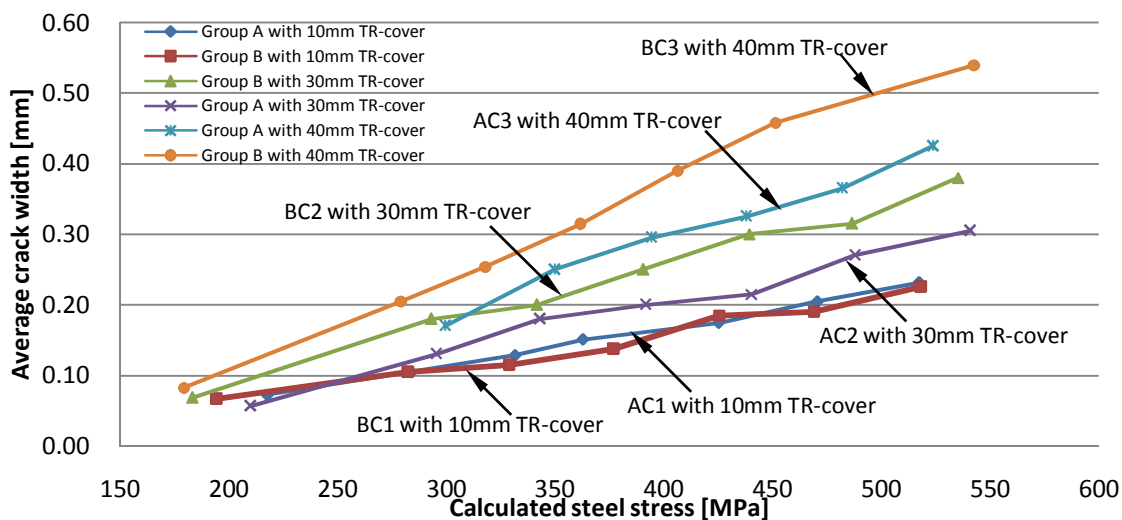
Figure 3-18 Typical plots of the calculated steel stress against the average crack width at load level of 0.625 f_y
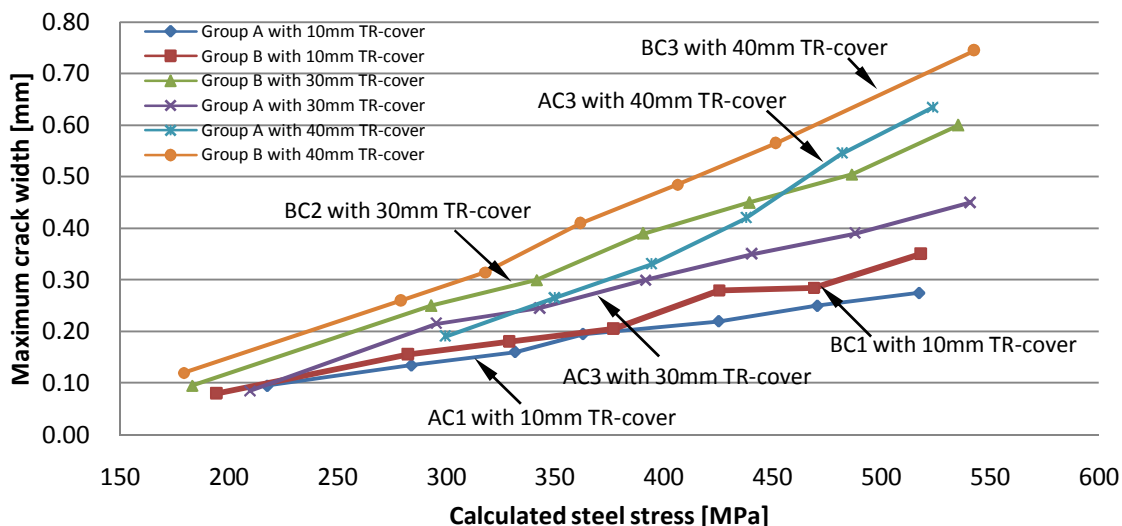
Figure 3-19 Typical plots of the calculated steel stress against the maximum crack width at load level of 0.625 f_y

To investigate the possible influence of TR-cover and -spacing on the Cracking Rate (CR), the calculated A-CR and M-CR are presented graphically in Figure 3-20. This figure illustrates a linear relationship between the TR-cover and A-CR (R^2 are 0.824 for Group A

55

and 0.768 for Group B); and between TR-cover and M-CR (R^2 are 0.931 for Group A and 0.816 for Group B).

At this stage, it is not difficult to accept that the variations in A-CR are direct correlated to the thickness of TR-cover. In the same way, Figure 3-11 indicates that α_{TR} increases along with the increase of TR-cover thickness. Figure 3-22 further indicates the obvious linear relationship between α_{TR} and A-CR (R^2=0.892). Through tests, α_{TR} as the key parameter to restrain the corresponding crack propagation can be found.

In the scope of the experimental test, the influence of TR-spacing on crack propagation can be found in Figure 3-20. Entirely, A-CR and M-CR of Gorup B are higher than Group A. The specific values can be calculated ultimizing the data in Table 3-3. For the specimens with thick TR-cover (40mm), a increae of TR-spacing increased from 100mm to 200mm results in an increase of A-CR by 36%.

In fact, it is more reasonable to view that a decrease of η_c by 30% results in this increase of crack propagation (A-CR), and hence results in the increase of final average crack width by 26%.

Therefore, the discrepancy between test results and crack model of current codes in Section 3.3.3 can be also explained by the restraining influence of TR on crack propagation, which is affected by how many cracks forming in the region of TR and intersecting with these TR. Therefore, TR-cover and TR-spacing play a significant roles on crack spacing and width.
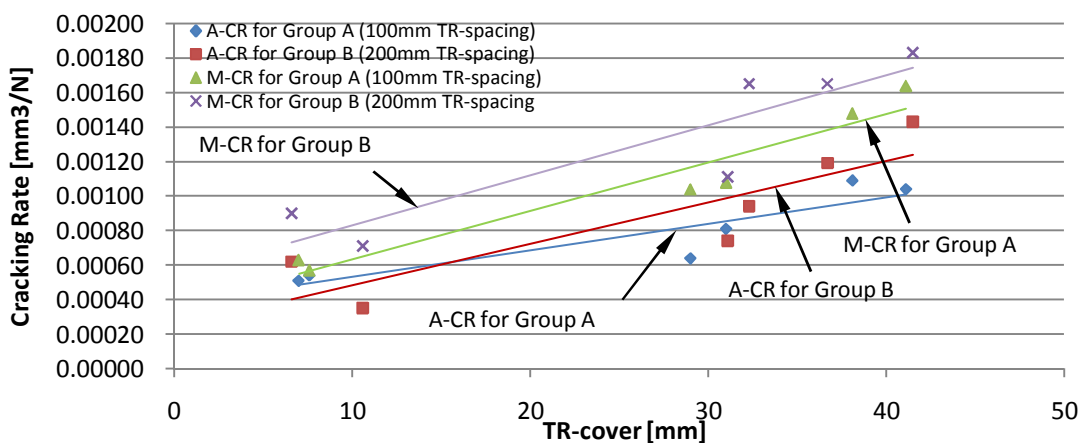
Figure 3-20   A-TR and M-TR versus TR-cover
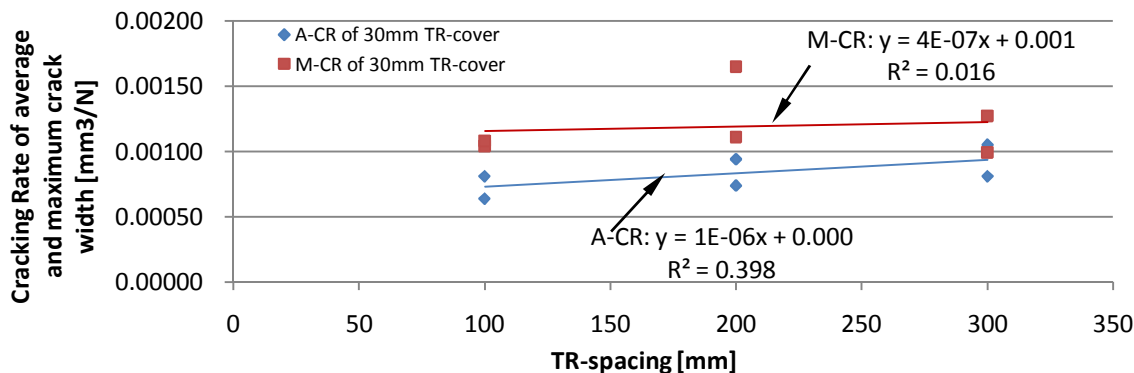
Figure 3-21 A-CR and M-CR versus TR-spacing
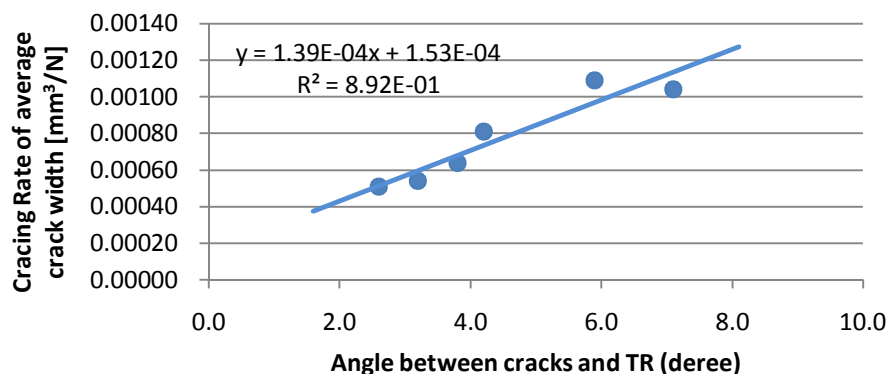
Figure 3-22 Linear regression of Cracking Rate and α_{TR}.

3.3.5   Section Summary

This section investigated the effect of TR-spacing and -cover on crack pattern, spacing, width and rate by means of an analysis of the test results. According to the theory that takes into account the TR restraining behavior on the crack progagation (Chapter 2) the following can be concluded:

1. TR can form certain cracks. Due to the heterogeneous properties of concrete and the random occurrence of cracks, the increase of TR-cover will result in a decrease of the number of TR-induced cracks, named as η_c. The relationship between η_c and thickness of TR-cover (c_{TR}) can be expressed as $\eta_{c-cover} = -0.012 \cdot c_{TR} + 1.085$.

2. The number of TR-induced cracks location is negatively correlated with the variation of TR-spacing (s_{TR}). Such a relationship can be expressed by the equation as $\eta_{c-spacing} = -0.0017 \cdot s_{TR} + 0.8477 \quad (100 \leq s_{TR} \leq 300)[mm]$

3. The test results presented an inverse trend between crack spacing and width, which is discrepancy with crack model in current codes. The reason of this discrepancy is that TR restraining crack propagation and crack width. and the restraining behavior of TR is affected by how many cracks forming in the region of TR and intersecting with these TR. Therefore, Numerical correlation between η_c and TR-cover and TR-spacing can be adopted to calculate the influence of TR on crack spacing and with.

3.4 Transverse reinforcement angle and concrete type

The test results in Section 3.3(see Figure 3-22) shown that TR restrains the crack propagation as to decrease the magnitude of the crack width. Such restraining behavior is directly affected by α_{TR}. In this section, TR-cover and TR-spacing were set at 30mm and 100mm respectively. The variables for TR-direction were selected as 0°，22.5° and 45°. Moreover, in order to study the restraining behavior of TR affected by concrete types i.e., normal strength concrete (NC), high strength concrete (HC) and lightweight concrete (LC), were cast separately.

The experiment involved 6 NC, 6 HC and 6 LC slab-strips specimens, which were mainly designed to study the influence of TR-direction on crack spacing, crack width and Cracking Rate qualitatively. As for Section 3.3, the crack width measured values shown in this section are at load level of $0.625f_y$.

3.4.1 Crack patterns

The relationship between the TR and cracks for all types of concrete is shown in Figure 3-23 Appendix E. In contrast to H1w1 and L1w1, N1w1 shows more evidence of the induced cracks. With the help of HILTI PS200 S Ferro scan, the photogrammetric technology and AutoCAD tool, the angles between cracks and vertical direction were measured and are listed in Table 3-4. To investigate the relations of TR influence, histograms are presented in Figure 3-24, this figure illustrate a comparison of the mean angle between the cracks and the TR-direction for various concrete types and varied TR-direction. With TR-direction of 0°, crack direction has slightly fluctuation. With TR-direction of 22.5°, cracks lean to TR by 6.3° on an average in NC with TR-direction of 22.5°. In contrast, the LC specimens are not affected by TR-direction as shown in the figure. Therefore, the crack pattern of normal strength concrete is affected by TR-direction in an unstable way. Whereas the crack pattern of specimens made of HC and LC affected by the TR-direction is slightly.

Figure 3-23 shows the crack pattern of selected slab-strips at service limit load stage. The load stage and percentage of ultimate load are presented as well. By using the HILTI PS200 S Ferro scan, the positions of TR was detected. Figure 3-7 verifies that exceptionally inclined TR can form the corresponding inclining cracks. In order to study whether inclined TR will form cracks in a common way, the angles between cracks and the direction perpendicular to direction of bending (α_{NB}) were measured using AutoCAD. The degrees of α_{NB} are listed in Table 3-4. It can be observed from this table that degrees of α_{NB} ranged from -2.5° to +7.1°. Figure 3-24 illustrates α_{NB} of all test specimens smaller than 2.2°, except for test specimen of Nw2 (α_{NB}=6.5°). Therefore, for RC element subjected to uniaxial moment，the inclining TR does not affect formation of inclined cracks.

Furthermore，the angle between TR and the corresponding intersecting crack α_{TR} were

measured and are listed in Table 3-4. Figure 3-25 presents the values of α_{TR} and TR-direction for in various concrete types. The Different values between α_{TR} and TR-direction were relatively constant for various concrete types and various TR-direction. These values were close to their corresponding average value of 5.7°. In Section 3.3, for all specimens with thick TR-cover of 30mm, the average value of α_{TR} equaled to 5.7°. Thus, when TR-cover=30mm, 5.7° was regarded as a characteristic value expressed by $\alpha_{TR,k} = 5.7°$.

Therefore, when TR-direction is at random angle θ, α_{TR} can be expressed as follows:

$$\begin{aligned} \text{when } 0° < \theta \leq 5.7°, \qquad \alpha_{TR} &= 5.7°, \\ \text{when } 5.7° < \theta < 90°, \qquad \alpha_{TR} &= \theta - 5.7°, \end{aligned} \tag{3-4}$$

Table 3-4 Test parameter of Series 2

Speci men	TR-dire c-tion (°)*	Average TR-cover* [mm]	Average Clear cover [mm]	α_{NM}**	α_{TR}***	Standard deviation	f'_c [MPa]	f_{ctm}*** * [MPa]
N1w1	0	29	46.3	1.6	3.8	3.4	26.01	2.05
N2w1	0	31	45.5	1.6	4.3	2.4	26.01	2.05
N3w2	22.5	31	45.1	7.1	11.3	5.4	26.01	2.05
N4w2	22.5	33	46.6	5.5	13.9	8.8	26.01	2.05
N5w3	45	32	48.7	1.2	37.8	5.0	26.01	2.05
N6w3	45	32	43.7	3.3	39.6	6.5	26.01	2.05
H1w1	0	31	47.4	0.4	4.3	3.5	73.77	3.48
H2w1	0	32	46.8	-2.5	5.9	4.3	73.77	3.48
H3w2	22.5	32	49.1	0.5	15.8	4.0	73.77	3.48
H4w2	22.5	32	51.2	3.8	16.5	4.6	73.77	3.48
H5w3	45	32	53.4	0.4	40.1	2.4	73.77	3.48
H6w3	45	32	52.6	-0.4	39.0	2.1	73.77	3.48
L1w1	0	30	42	-0.2	6.0	2.6	24.68	2.02
L2w1	0	29	39	1.2	5.6	2.1	24.68	2.02
L3w2	22.5	36	40.4	-1.7	17.2	5.6	21.15	1.81
L4w2	22.5	40	50	1.6	17.8	3.3	21.15	1.81
L5w2	45	34	45	-0.4	40.3	3.7	21.15	1.81
L6w2	45	35	46.4	-1.9	40.4	4.8	21.15	1.81

* Angel between T-and L-reinforcement

**α_{NM} is the angle between cracks with the normal of bending direction, in which the opposite direction of crack to TR is negative value.

***α_{TR} is the angle of cracks with TR

*** *The mean tension strength considers the influence of shrinkage.

According to the analysis results from Section 3.1, when TR-cover=10mm, $\alpha_{TR,k} = 2.6°$; when TR-cover=40mm, $\alpha_{TR,k} = 6.4°$. The results of regression analysis in Figure 3-26 indicate a positive correlation between $\alpha_{TR,k}$ and TR-cover (R^2=0.976). Thus, when TR-cover is at random thickness c_{TR},

$$\alpha_{TR,k} = 0.130 \cdot c_{TR} + 1.435 \ [°] \tag{3-5}$$

where

c_{TR} is the concrete cover of TR $c_{TR} > 10mm$

Substitute the (3-5) to the (3-4),

$$\begin{aligned}
\text{when } 0 \le \theta \le \alpha_{TR,k}, &\qquad \alpha_{TR} = \alpha_{TR,k} \\
\text{when } \alpha_{TR,k} < \theta \le 90°, &\qquad \alpha_{TR} = \theta - \alpha_{TR,k}
\end{aligned} \tag{3-6}$$

According the Eq.(3-5) and Eq.(3-6), the angle of TR and the intersected crack can be given by TR-cover.

$\theta = 0°$ Nw1, loading 45kN, 72% of Ultimate

$\theta = 22.5°$ Nw2, loading 50kN, 76% of Ultimate

$\theta = 45°$ Nw3, loading 45kN, 73% of Ultimate
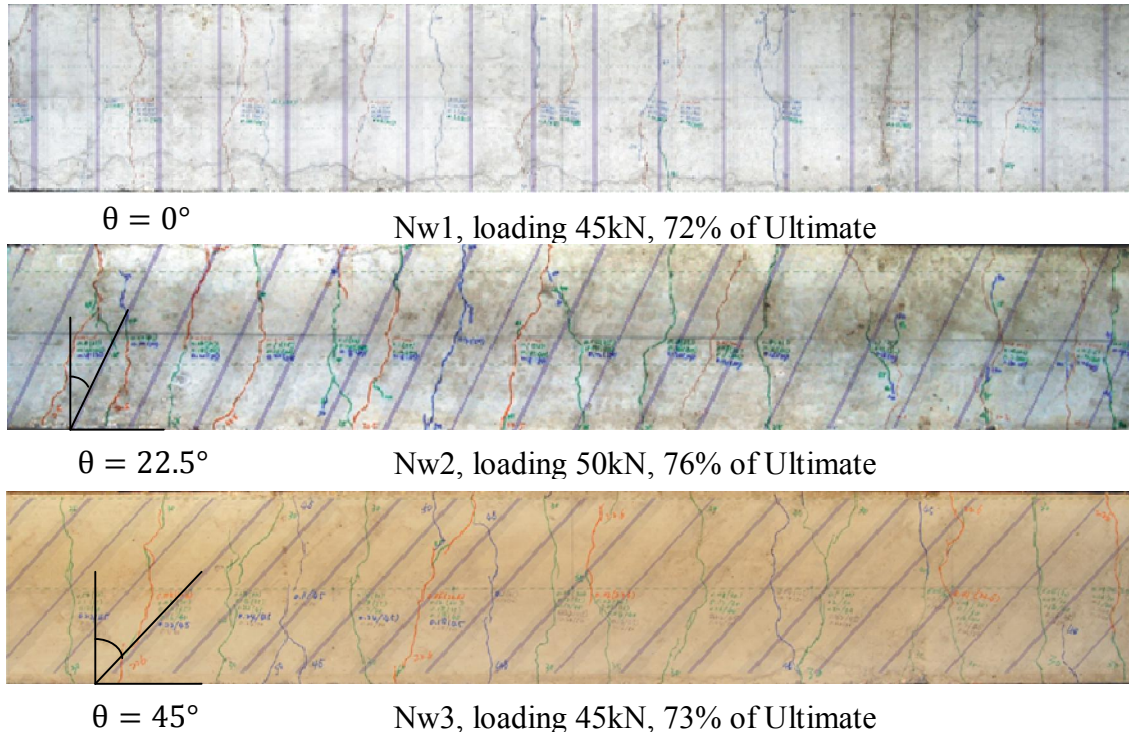
Figure 3-23: Final crack pattern overlapped with TR layout for test specimens with various TR-direction and NC, HC and LC
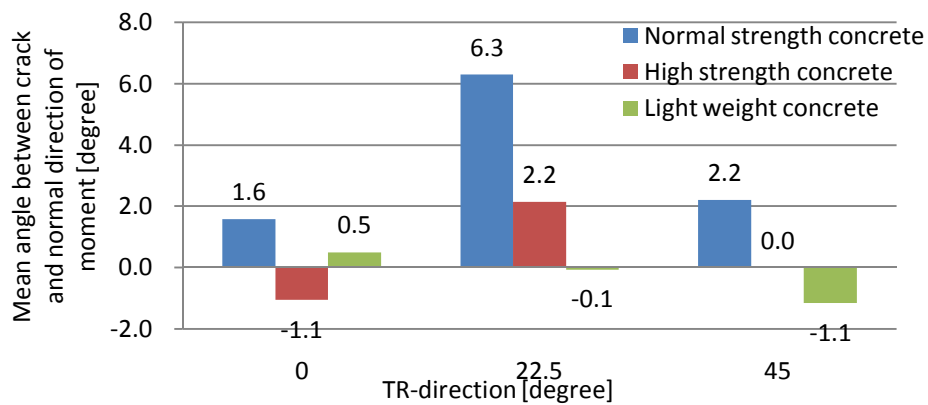
Figure 3-24 Average angles between the crack and normal direction of bending α_{NB}
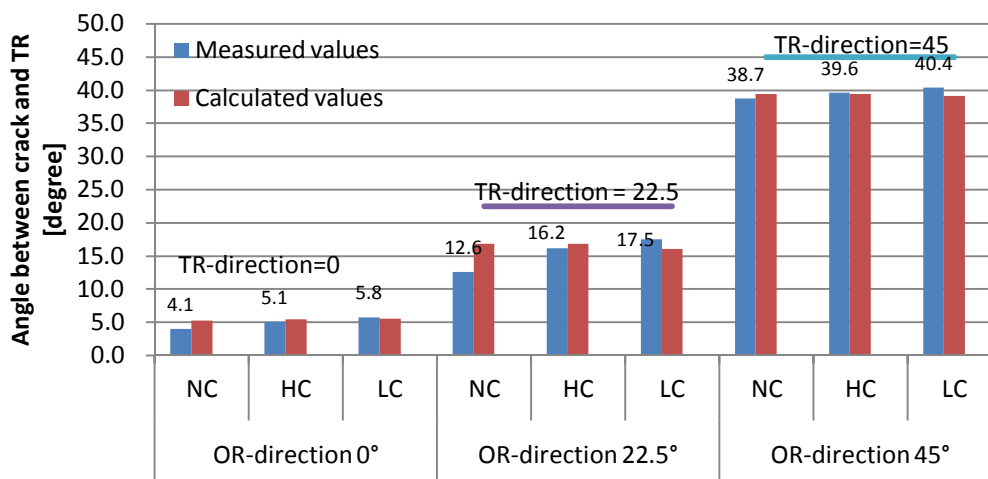
Figure 3-25 Average values of observed angles between crack and normal direction of bending α_{OR} and calculated values of α_{OR} according to Eq.(3-5) Section 3.4.1
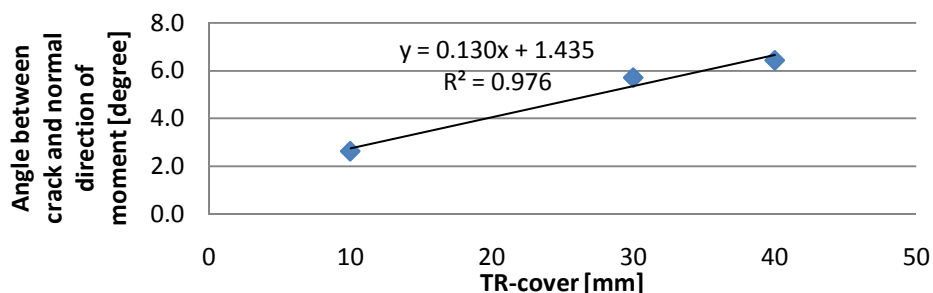
Figure 3-26 Regression analysis of TR-cover and the angle between crack and normal direction of bending

As discussed in Section 3.3.1, the TR restrains the formation of the corresponding intersecting cracks. Figure 3-23 illustrates that as the angle of TR-direction increases from 22.5° to 45°, the number of cracks intersecting TR increases significantly.

From Figure 3-27 (a), it can be seen that the number of cracks intersecting TR depends on TR-direction θ, cross-section width b and TR-spacing s. The geometrical relationship of the TR and intersected cracks can be obtained in Figure 3-27 (b). It is obvious from the figures that the number of cracks intersected TR increases as TR-direction increases. This direct correlation between them will be further discussed in Section 5.4.
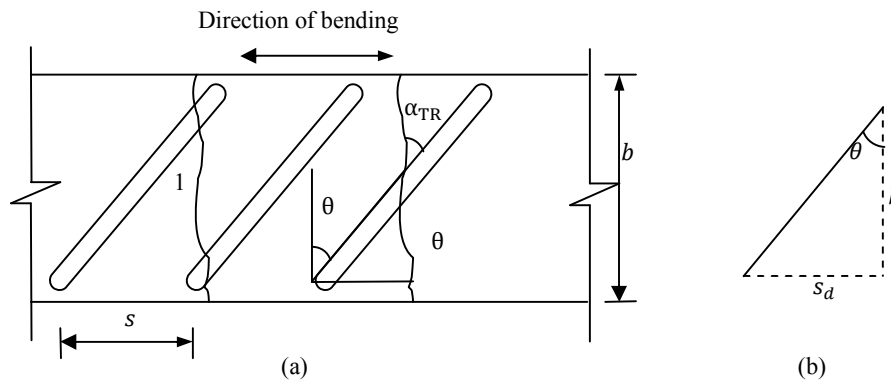
Figure 3-27 Illustration of effect TR-direction on increasing the number of intersected cracks

3.4.2 Crack spacing

Crack spacing was measured at each loading stages by using AutoCAD tools. The stabilized average crack spacing is listed for Table 3-5. From this table, it can be seen that the largest crack spacing was observed for HC specimens, while the smallest crack spacing was observed for LC specimens. It also shows that the largest value of f_{ctm} was obtained in HC specimens and the smallest one in LC specimens. That this values will lead to calculate the concrete strength is in good agreement with the principle of Bond-slip Mechanism approach. This table further indicates that an increase of TR-direction from 0° to 45°results in a decrease of crack spacing of NC, HC and LC by 15%, 29% and 25%, respectively. Figure 3-28 illustrates that the variation of crack spacing of various concrete materials with TR-direction. It indicates that increasing of TR-direction resulted in decreasing of the crack spacing of the three concrete materials. The decrease of crack spacing of NC and HC specimens was observed in a linear manner with a decrease range smaller than 30%. Accordingly, it can be concluded that increasing of TR-direction has limited influence on decreasing of crack spacing.
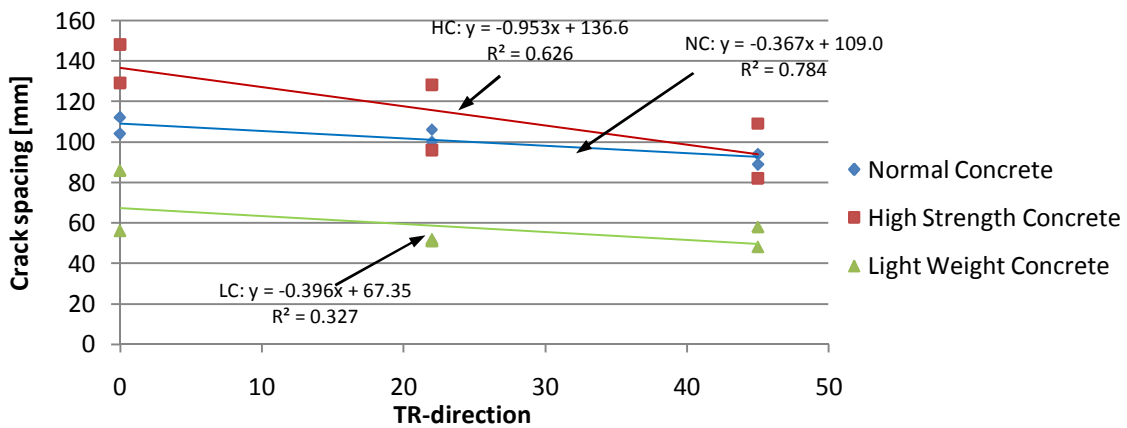
Figure 3-28 Crack spacing versus TR-direction

3.4.3 Crack width

The crack width at the service limit state was recorded for all specimens, the average and maximum crack width are calculated and listed in Table 3-5.This section investigates the influence of TR-direction on the average crack width and attempts to find the reason of this influence. From this table, it can be observed that for TR-direction=0°, HC specimens shows the largest average crack width when compared to those of NC and LC specimens. When is TR-direction=22.5°, a similar value of the average crack width can be observed for the three types of concrete material. However, when is TR-direction=45°, LC specimens show the largest average crack width while HC specimens show the smallest one, One was contrary to the situation when TR-direction=0°. The data shows that an increase of TR-direction from 0° to 45° resulted in a decrease of the average crack width of NC, HC and LC specimens by 53%，84% and 23%, respectively. The average crack width of HC specimens decreased from 0.31mm to 0.03mm, while that of LC specimens decreased the crack width from 0.22mm to 0.13mm. Consequently, the angle inclining TR results in an increasing restraining effect of TR on crack width. Besides, such a restraining effect directly depends on the bonding stress between concrete and reinforcement, and indirectly depends on concrete tensile strength. As a result, it is evident from the above analysis that the effect of TR on crack width needs to be considered in the models in the current codes.

Figure 3-29 presents two variables to investigate the variation of the average crack width of various concrete materials varied with TR-direction. It can be observed that an increase of TR-direction resulted in decrease of the average crack width of various concrete types, The average crack width of HC specimens decreases the most and nearly in a linear manner. It is evident that the larger the absolute value of the slope of regression line, the larger the restraining effect of TR on crack width, and vice versa. Compared to HC specimens, slopes of regression lines of NC and LC specimens increased by 59% and 83%, respectively. Figure 3-31 shows that the variation of the two variables varied in linear manner. Therefore, it can be determined that the restraining effect of TR on the average crack width depends on the bond strength between concrete and TR, which are defined by tension strength of concrete, namely f_{ctm}. Table 3-5 presents the variation of maximum crack width with TR-direction, which indicates a linear relationship between these two variables.
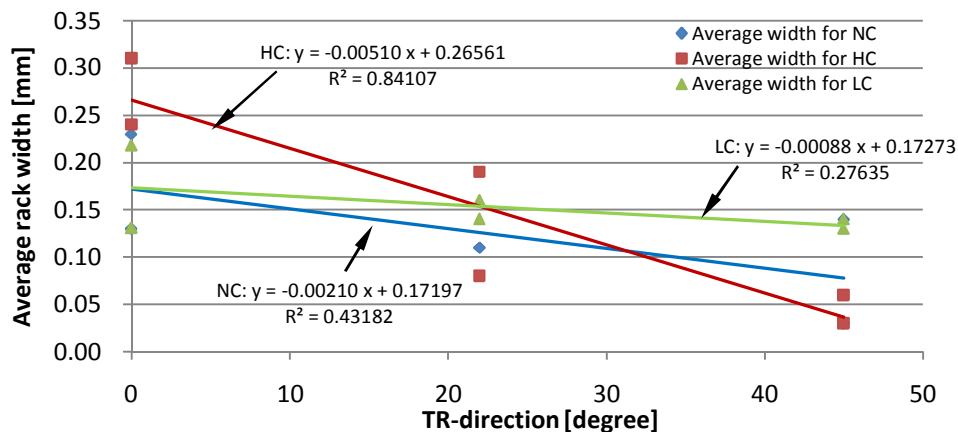
Figure 3-29 The average crack width versus TR-direction at load level of 0.625 f_y
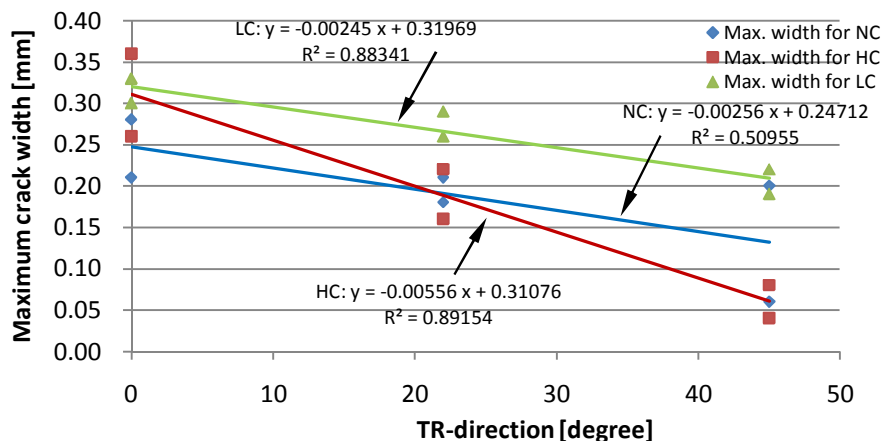
Figure 3-30 Maximum crack width versus TR-direction at load level of 0.625 f_y
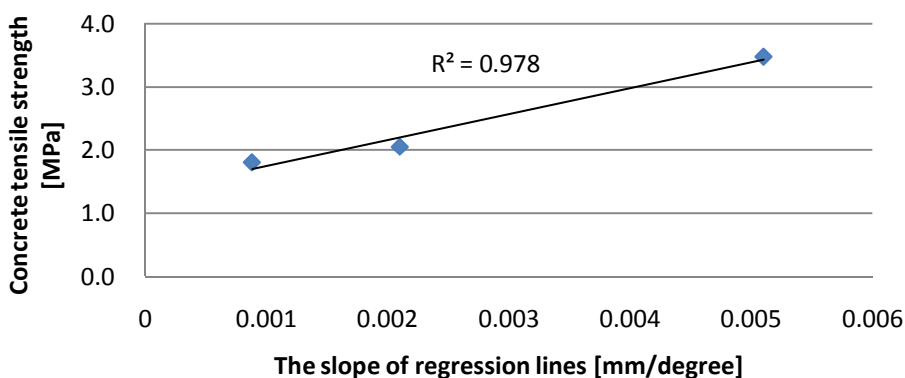
Figure 3-31 Linear regression of concrete tensile strength and cracks restrained by inclined TR

3.4.4 Cracking Rate

According to the definition and calculation method of Cracking Rate in Section 3.3.4, A-CR (Cracking Rate of the average crack width) and M-CR (Cracking Rate of maximum crack width) were calculated and listed in Table 3-5. Figure 3-32 presents two variables to

investigate the variation of A-CR of various concrete types with variable TR-direction. It can be observed that an increase of TR-direction results in a decrease of A-CR of various concrete types, in which A-CR of HC specimens decreased the most and in nearly a linear manner. It is in evidence that the slope of regression line of A-CR represents the magnitude of restraining effect of TR on crack propagation. The bond strength is the probable variables affecting crack propagation, and the tensile strength is the one of the major factor of bond strength. Thus, the relationship between tensile strength and the slop of regression lines are presented in Figure 3-34. The strong direct relationship between them is represented in this figure, it indicate the restraining effect of TR on the average crack width propagation depends on bond strength and thus depends of concrete tensile strength.

Table 3-5 Test results in Series 3

| No.*	TR-direction [°]	Concrete types	Mean crack spacing [mm]	Crack width [mm]		Cracking Rate [mm3/N]	
				Average values	Maximum values	A-CR	M-CR
N1w1	0	NC	112	0.13	0.21	0.00061	0.001043
N2w1	0	NC	104	0.23	0.28	0.00081	0.001076
N3w2	22.5	NC	100	0.11	0.18	0.00062	0.000895
N4w2	22.5	NC	106	0.11	0.21	0.00090	0.001399
N5w3	45	NC	89	0.03	0.06	0.00023	0.000518
N6w3	45	NC	94	0.14	0.20	0.00060	0.000885
H1w1	0	HC	129	0.31	0.36	0.00137	0.001303
H2w1	0	HC	148	0.24	0.26	0.00136	0.001400
H3w2	22.5	HC	128	0.19	0.22	0.00076	0.000978
H4w2	22.5	HC	96	0.08	0.16	0.00072	0.001213
H5w3	45	HC	109	0.06	0.08	0.00031	0.000699
H6w3	45	HC	82	0.03	0.04	0.00033	0.001025
L1w1	0	LC	56	0.13	0.30	0.00048	0.000780
L2w1	0	LC	86	0.22	0.33	0.00079	0.000960
L3w2	22.5	LC	52	0.14	0.26	0.00047	0.000817
L4w2	22.5	LC	51	0.16	0.29	0.00050	0.000912
L5w2	45	LC	58	0.13	0.19	0.00047	0.000729
L6w2	45	LC	48	0.14	0.22	0.00034	0.000947

Note:

* NC, HC and LC stand for Normal concrete, High strength concrete and Lightweight concrete

Figure 3-33 represents an equally appreciable linear relationship between M-CR and TR-direction. Combined with the analysis in Section 3.4.3, it can be concluded that inclining TR will restrain propagation of each crack intersected TR and then greatly decrease the final crack width. Such a restraining effect has a linear correlation with bond strength between concrete and steel. As a result, it is evident from the above analysis that the effect of TR on crack width needs to be considered by the Bond Slip principle adopted in the current codes.
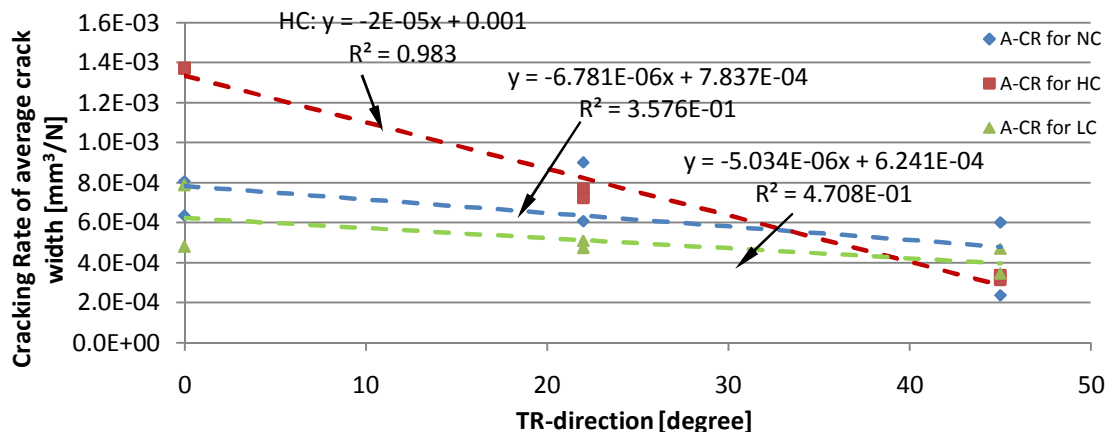
Figure 3-32 A-CR in various concrete types
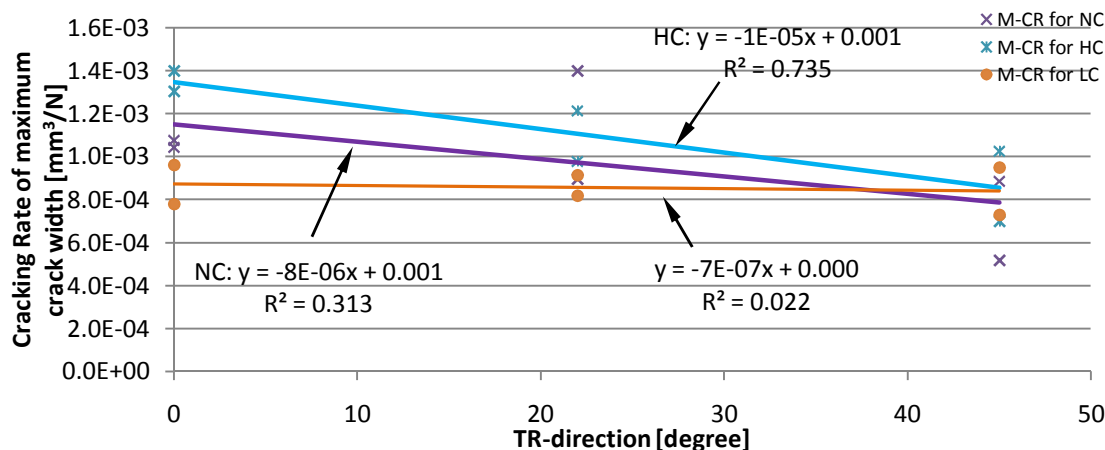
Figure 3-33 M-CR in various concrete types
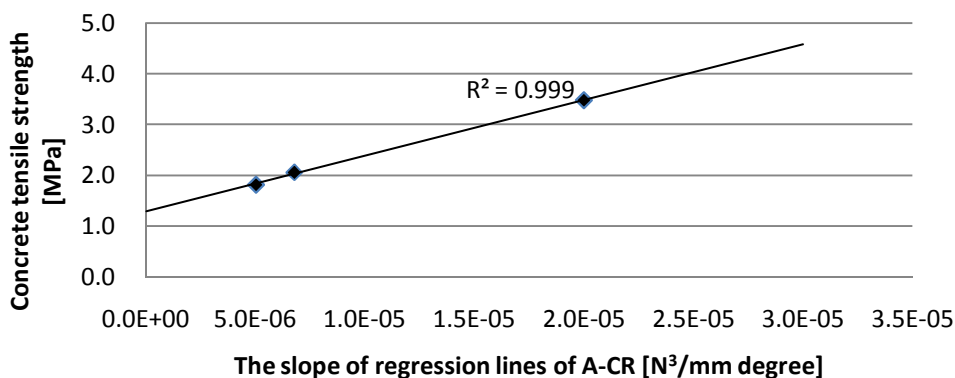
Figure 3-34 Regression analysis between concrete tensile strength and crack width propagation restrained by inclined TR

3.4.5 Section summary

In this section, the TR-direction parameters were varied from 0° to 45°. Moreover, the effect of concrete types on this restrained behavior by TR was investigated.

Conclusions can be made by based on analysis of the test results from this section as

follows:

For the three concrete types, the degree of α_{TR} increases in a linear manner as TR-direction increases.

As concrete material is heterogeneous and cracks appeared at a random position, the angle between TR-direction and α_{TR} remains constant. The test results indicate that as a direct ratio existed between the characteristic value of this angle and TR-cover (c_{TR}), for a given TR-cover and TR-spacing θ, α_{TR} can be expressed as follows:

$$\text{when } 0 \leq \theta \leq \alpha_{TR,k}, \qquad \alpha_{TR} = \alpha_{TR,k}$$

$$\text{when } \alpha_{TR,k} < \theta \leq 90°, \alpha_{TR} = \theta - \alpha_{TR,k}$$

where $\alpha_{TR,k} = 0.130 \cdot c_{TR} + 1.435 \ (c_{TR} \geq 10\text{mm})$

TR restrains the propagation of its corresponding intersecting crack. Such restraining behavior has a direct relationship with α_{TR} and f_{ctm}. Thus, α_{TR} and f_{ctm} are negatively correlated with A-CR and final crack width.

It is recommended that the effect of TR on crack width needs is considered in current codes. Factors α_{TR} and f_{ctm} as two prominent parameters are further discussed in Chapter 5.

3.5 Transverse reinforcement position and concrete type

In Section 3.3 through 3.4, the variables of TR, such as TR-cover, -spacing，and -direction have been investigated.

For the orthogonal direction of two-way RC-slabs subjected biaxial moment, the orthogonal reinforcement nets in different layers is shown in Figure 3-35. The tensile reinforcement named as LR in its bending direction, and the reinforcement along vertical direction named as TR. According to different positions TR (TR-position), Type A (TR is outside of LR) and Type B (TR is inside of LR) were designated in two-way slabs. One-way slab-strips with the different of TR-positions designated as Type A and Type B as well as Type C (TR-spacing of 600mm). Type C is the type of TR-spacing of 600mm to investigate the crack behaviors of specimens with no TR.
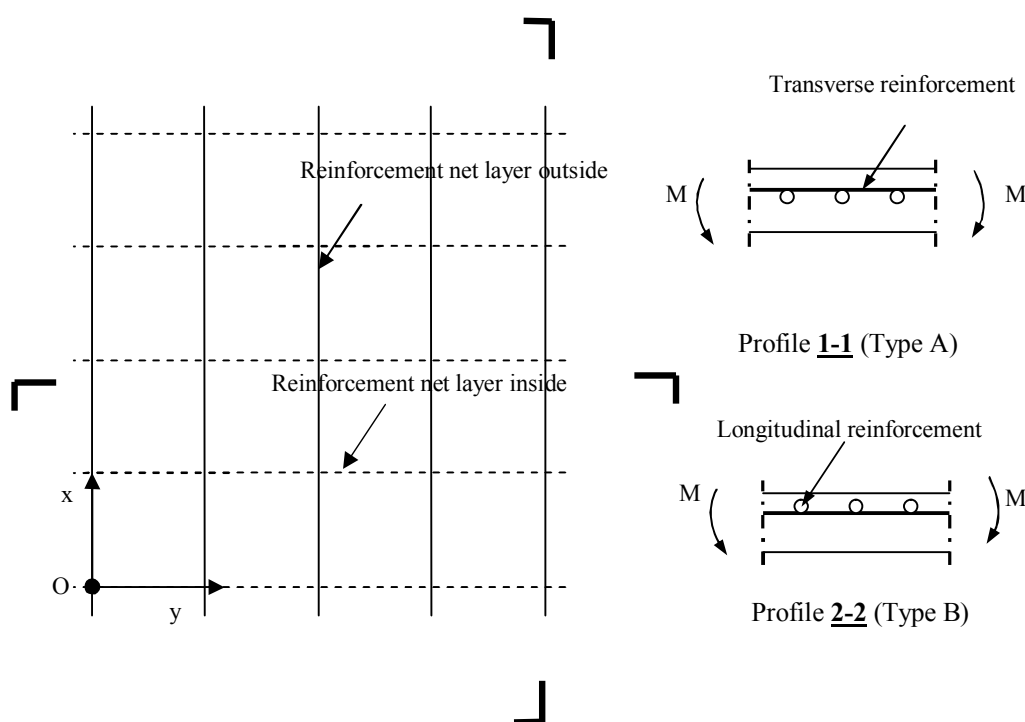
Figure 3-35 Illustration of Type A and Type B for two-way slabs

To investigate the effect of TR-position on crack behavior, LR in compressive zone was not utilized. However, the reinforcement ratio in tensile zone of these three specimens keep constant with all the specimens in last two sections.

3.5.1 Crack patterns

The relationship between TR layout and crack patterns for selected specimens is shown in Figure 3-36. According to the evaluation equation[9], radius of influence of steel bar was 21 mm from both sides of T-reinforcement. η_c was calculated and is given in Table 3-6.

Crack pattern of Type A and Type B in Figure 3-36 indicates that 86.7% and 50% of

TR-induced cracks. According to equation in Section 3.3.1,

$$\eta_c = -0.012 \cdot c_{TR} + 1.085 \quad (\eta_c \leq 1)$$

$\eta_{cA} = 83\%$ for Type A and $\eta_{cB} = 52\%$ for Type B. The predicted values were very close with the measured values of 86.7% and 50%. Therefore, different layers or outside/inside position of TR have no obvious effect on η_c.

Table 3-6 Test variables in Series 3

Speci mens	Type of TR	TR-spacing[mm]	Average TR-cover [mm]	Average LR-cover [mm]	Average value of distance*	Standard divation	η_c**	$f_c^{'}$ [MPa]	f_{ctm} [MPa]
NPS01	Type A	100	21.47	32.23	9.91	9.20	86.7%	23.21	2.44
NPS02	Type B	100	47.33	30.28	20.63	16.00	50%	23.21	2.44
NPS03	Type C*	600	49.00	34.70	-	-	-	23.21	2.44

* Type C is the slab-strip with TR-spacing of 600mm. refer to Appendix F
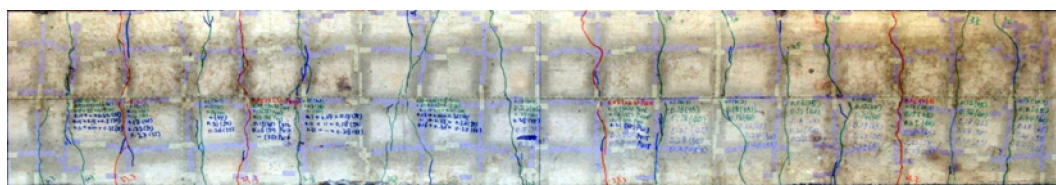
NPS01-Type A
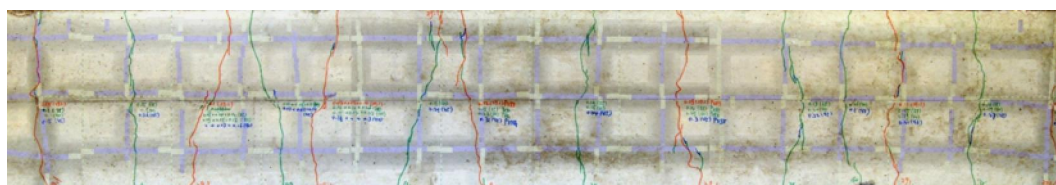
NPS02-Type B
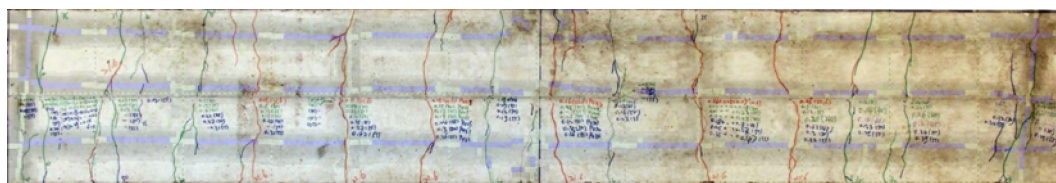
NPS03-Type C

Figure 3-36: Crack pattern of Type A, Type B and Type C

3.5.2 Average crack spacing
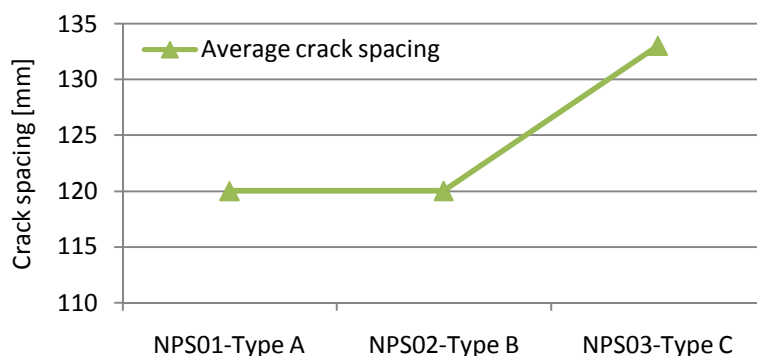
Figure 3-37 The average crack spacing of Type A, Type B and Type C

In Figure 3-37, the average crack width of three type specimens is plotted. It can been seen that crack width remains constant for both Type A and Type B, while for of Type C it increased by 11%. It has to be noted that the specimens with three types of TR-position, Type A, Type B and Type C, have the same concrete cover of longitudinal reinforcement. Therefore, it can be concluded that   the position of TR shifted from outside of LR to inside does not weaken the influence of TR on crack spacing. whereas, the crack spacing increase without the restrained action of TR, as shown in NPS03-Type C in Figure 3-37.

3.5.3 Crack width
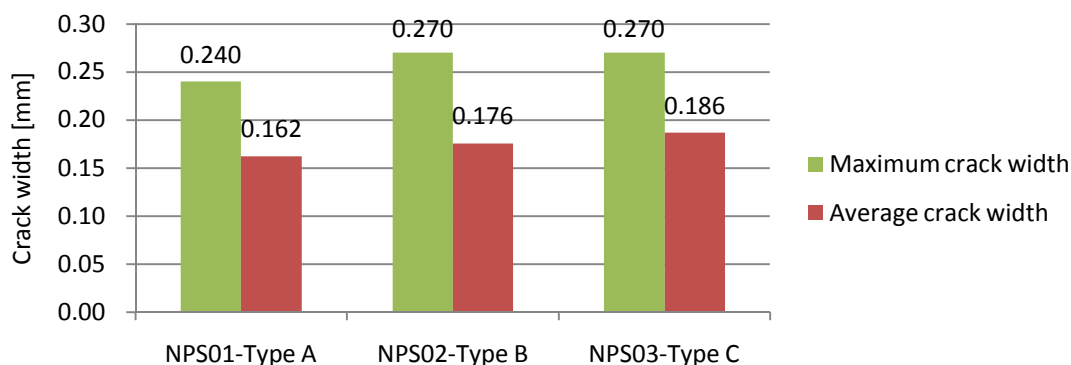
Figure 3-38 Crack width of Type A, Type B and Type C

The average and maximum value of crack width are plotted in Figure 3-38. The average crack width of Type C is the largest one in three Types. The average crack width of Type B is larger than that of Type A. This phenomenon proves that TR affects crack width (see Chapter 3.3). Figure 3-39 indicates that crack width of Type A is slightly lower than those of Type B and Type C. When steel stress at crack width reaches 0.3mm, steel stress of type A is higher than those of Type B and Type C.
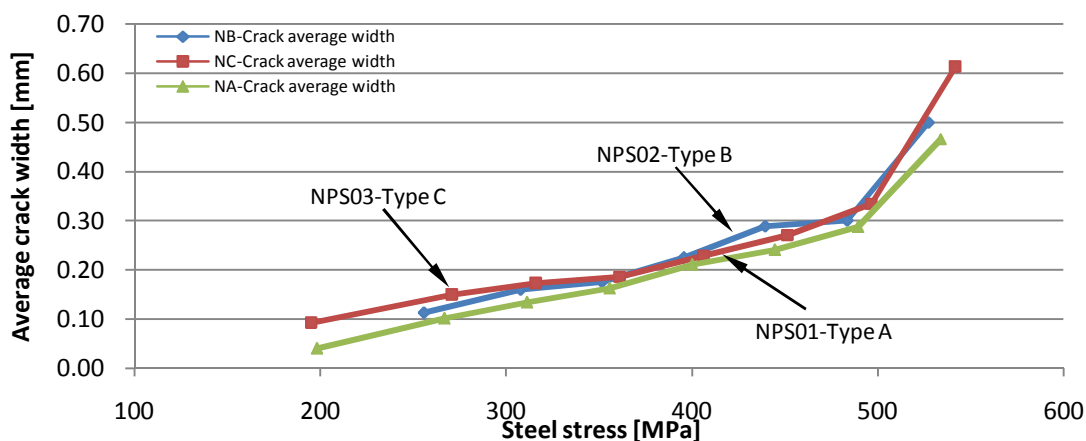
Figure 3-39 Average crack propagation versus steel stress

3.5.4 Cracking Rate

The concept of Cracking Rate was defined and introduced in Chapter 3.3.3. The relationship between TR-position and CR is shown in Figure 3-40. A-CR increased by 5% when changing TR-position from outside to inside. M-CR decreased slightly by 15%.

The decrease of number of cracks from Type A (86%) to Type C (20%) TR-induced cracks reduced the restraining effect of TR on crack propagation. The decrease leads to the increase of A-CR and crack width.
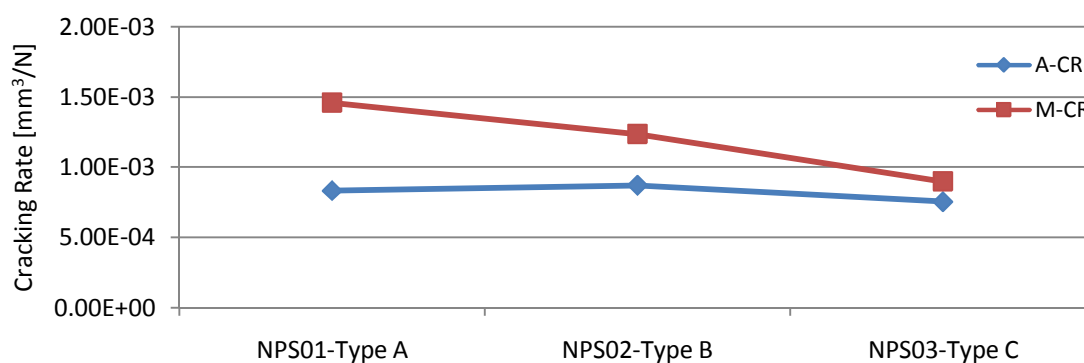
Figure 3-40 Comparison of Cracking Rate between Type A, Type B and Type C

Table 3-7 Test results in Series 3

No.*	TR-posit ion	Crack spac. [mm]	Crack width [mm]						Cracking Rate [mm3/N]
			Avera- ge width [mm]	Max. width [mm]	Computed according to codes				
					FIB Model Code 2010	DIN EN 1992-2011	DIN1045	ACI318	
NPS01	Type A	120	0.162	0.240	0.028(15%)	0.27(12%)	0.32(12%)	0.31(28%)	0.001457
NPS02	Type B	120	0.176	0.270	0.27(0%)	0.26(-2%)	0.32(18%)	0.30(12%)	0.001234
NPS03	Type C	133	0.186	0.270	0.30(12%)	0.29(9%)	0.32(19%)	0.35(29%)	0.000897

3.5.5 Section summary

The comparison results of crack pattern, average crack spacing and the average crack

width indicate that the variation of TR-position has no effect on the restraining behavior of TR. The increase of TR-cover from Type A to Type B leads to the decrease of number of cracks from Type A (86%) to Type B (52%) and further leads to the increase of A-CR and crack width.

Therefore, in the experimental analysis of two-way slabs, the restraining effect of TR on crack propagation of Type A and Type B depends on TR-cover.

3.6 Correlation between curvature and crack width

Formulas in current codes, such as FIB Model Code 2010 (draft), DIN EN 1992-1-2011 and DIN 1045-1-2008, are mostly developed on the basis of Bond-slip Mechanism or empirical equations. Thus, these formulas are more suitable for calculation and analysis of RC element subjected to tension forces.

However, bending is a different load with tension force. Tensile stress on the tensile zone is not only affected by geometrical size and tension steel in cross-section, but also affected by inertial moment and bending moment redistribution. When a RC element is subjected to biaxial bending or triaxial bending, the steel stress become more and more complex.

Strain is the physical quantity to judge the displacement of a RC element subjected to tension, accordingly, curvature is the physical quantity to judge the displacement of RC element subjected to a bending moment. Therefore, in this section, the curvature is calculated based on test data of deformation. Furthermore, the relationship between curvature and crack width will be analyzed.

The analyzed test specimens in this section are selected from Series-1 (see Section 3.3) and Series-2 (see Section 3.4).

3.6.1 Calculation of the curvature of test specimens

According to the illustration of measurement set-up in Section 3.2, deformation of several points was measured by laser sensors. Based on these deformation data, the curvature along the deformation measurement line can be calculated. Figure 3-41 illustrates the geometrical relationship between the curvature and deformation of measurement points.
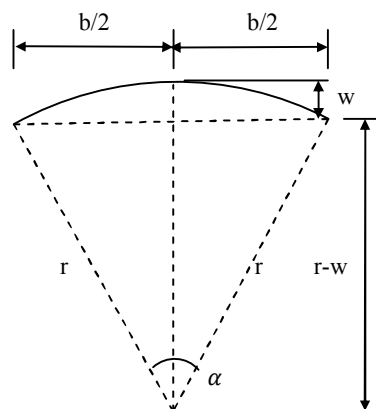
Figure 3-41 Geometrical relationship between deformation w and curvature $\kappa = 1/r$

$$\kappa = \frac{1}{r} = \frac{2w}{\left(\frac{b}{2}\right)^2 + w^2} \tag{3-7}$$

3.6.2 Test results in Series 1

The curvature of test specimens was calculated from the deformation date of each sensor. The relationship between the curvature and maximum crack width is plotted in Figure 3-42 and Figure 3-43. TR-spacing of 100mm and TR-spacing of 200mm are presented respectively in two figures. These two figures show that maximum crack width increased in nearly linear manner as the curvature increased. To verify linear relationship between the curvature and crack width, the slope of regression line of each curve and its determination coefficients (R^2) is calculated and listed in Table 3-8. In this table, the average value of R^2 is over 0.931, which indicates that maximum crack width increases in linear manner. This linear relationship indicates the possibility of developing a new crack model, in which curvature (moment and stiffness) is regarded as a initial factor.
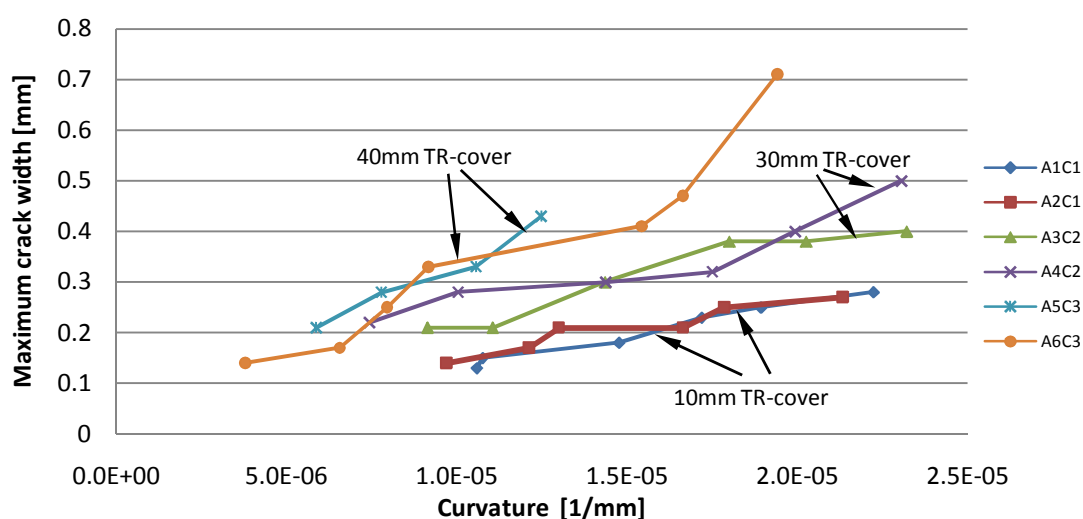
Figure 3-42 Crack propagation versus curvature for TR-spacing of 100mm
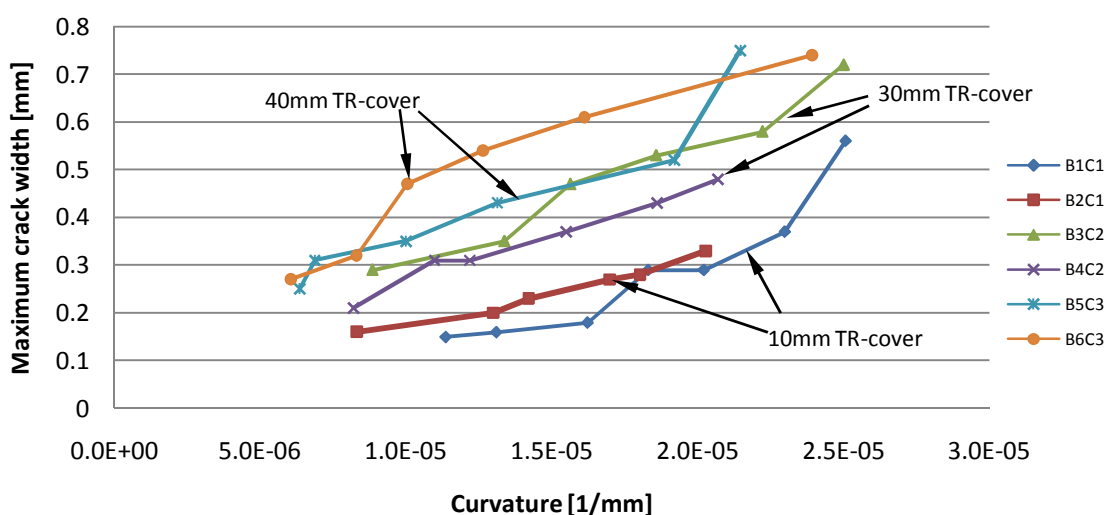
Figure 3-43 Crack propagation versus curvature for TR-spacing of 200mm

Table 3-8 Coefficient of regression line of Series 1

No.	Slope [mm^2]*	R^2**	No.	Slope [mm^2]	R^2
A1C1	12678	0.976	B1C1	26999	0.861
A2C1	10756	0.905	B2C1	14116	0.971
A3C2	15404	0.927	B3C2	25973	0.961
A4C2	15681	0.885	B4C2	19985	0.976
A5C3	38479	0.984	B5C3	27133	0.902
A6C3	32143	0.907	B6C3	26297	0.916
Average	-	0.931	-	-	0.931

* Slope of regression linear;

** R^2 is the determination coefficients.

3.6.3 Test results in Series 2

The linear relationship between the curvature and crack width has been proved in the last section. This relationship exists in various concrete cover from 10mm to 50mm. This relationship with different concrete types will be investigated in this section by means of test analysis of Series 2. According to Eq. (3-7), the curvature is calculated in a same way as in the last section. The curvature and crack widths of specimens of three concrete types are plotted in Figure 3-44.

The results of linear regression analysis in Figure 3-44 indicate that maximum crack width increased in nearly linear manner as the curvature increased with three concrete types. Figure 3-44 also indicates that as test specimens of LC reached plastic state and crack width increased to 1.0 mm, the relationship between crack width and curvature remains in linear manner. Table 3-8 lists the slopes of regression line of each curve and R^2. The average values of R^2 are 0.948 for NC, 0.938 for HC and 0.841 for LC. Therefore, it can be concluded that linear relationship between the curvature and crack width existed in three concrete types.

Table 3-9 Coefficients of regression line for three concrete types

No.	Slop	R^2	No.	Slop	R^2	No.	Slop	R^2
	Normal concrete			High strength concrete			Lightweight concrete	
N1	15681	0.888	H2	68559	0.883	L1	21583	0.776
N2	15404	0.927	H4	12189	0.993	L2	22796	0.864
N3	26644	0.966	-	-	-	L3	4251	0.721
N4	21818	0.986	-	-	-	L4	15522	0.935
N5	19929	0.983	-	-	-	L5	21753	0.868
N6	21608	0.937	-	-	-	L6	19369	0.881
Average	-	0.948	-	-	0.938	-	-	0.841
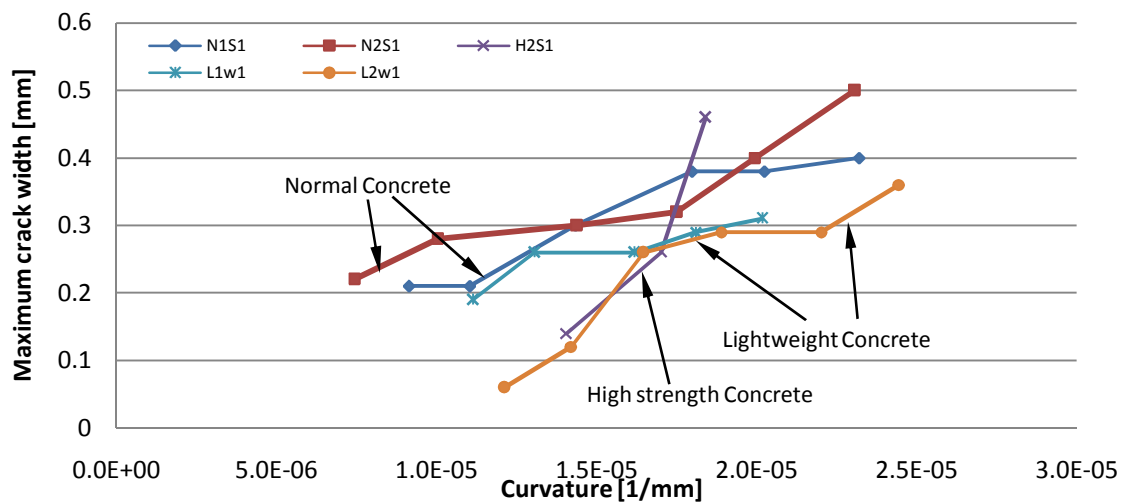
Figure 3-44 Crack propagation versus curvature for three concrete types

3.6.4 Section summary

The direct ratio relationship (linear in manner) between curvature and crack width for slab-strips subjected to uniaxial bending are testified in this section. Furthermore, these linear relationships are not only in elastic state, but also in plastic state. The test results proved the direct ratio of curvature to crack width. This relationship will be proved by slab test results. These test results will regard as a significant experimental foundation to establishing a specific flexural crack model in Chapter 7, which differs from the common tensile crack model.

3.7 Chapter summary

Experimental work of RC slab-strips subjected to uniaxial bending was presented in this Chapter. Variables of TR, such as TR-cover, TR-spacing, TR-direction, TR-position and concrete types, were considered to quantify the effect of each variable of TR on crack behavior. On the basis of analysis results in the above sections, conclusions can be obtained as follows:

1. The test results presented an inverse trend between crack spacing and width, which is discrepancy with crack model in current codes. The reason of this discrepancy is that TR restraining crack propagation and crack width. and the restraining behavior of TR is affected by how many cracks forming in the region of TR and intersecting with these TR. Therefore, Numerical correlation between η_c and TR-cover, TR-spacing and TR-direction, θ, can be adopted to calculate the influence of TR on crack spacing and with, the numerical correlations are as follow:

   (a) Increase of TR-cover will result in decrease of number of TR-induced cracks, named as η_c. The relationship between η_c and thickness of TR-cover (c_{TR}) can be expressed as $\eta_{c-cover} = -0.012 \cdot c_{TR} + 1.085$

   (b) The number of TR-induced cracks is negatively correlated with the variation of TR-spacing (s_{TR}). Such a relationship can be expressed by the equation as $\eta_{c-spacing} = -0.0017 \cdot s_{TR} + 0.8477$ $(100 \leq s_{TR} \leq 300)$[mm]

   (c) As concrete material is heterogeneous and cracks appeared at random, the angle between TR-direction and α_{TR} remains constant. The test results indicate that as a direct ratio existed between the characteristic value of this angle and TR-cover (c_{TR}), for a given TR-cover and TR-spacing θ, α_{TR} can be expressed as follows:

   $$\text{when } 0 \leq \theta \leq \alpha_{TR,k}, \quad \alpha_{TR} = \alpha_{TR,k}$$

   $$\text{when } \alpha_{TR,k} < \theta \leq 90°, \quad \alpha_{TR} = \theta - \alpha_{TR,k}$$

   where $\alpha_{TR,k} = 0.130 \cdot c_{TR} + 1.435$ $(c_{TR} \geq 10\text{mm})$

   (d) TR restrains the propagation of its corresponding intersecting crack. Such restraining behavior has a positive correlation with α_{TR} and f_{ctm}. Thus, α_{TR} and f_{ctm} are negatively correlated with A-CR and final crack width.

2. The above mentioned parameters can be summarized in three major factors (a) TR-cover; (b) angle between TR normal direction of moment; (c) concrete tensile strength.

3. The variation of TR-position has no effect on the restraining behavior of TR. The increase of TR-cover from Type A to Type B leads to the increase of A-CR and crack width. Therefore, in the experimental analysis of two-way slabs, the restraining effect

of TR on crack propagation of Type A and Type B depends on TR-cover.。

4. It is recommended that the effect of TR on crack width needs to be considered in current codes. α_{TR} and f_{ctm} as two prominent parameters will be further discussed in Chapter 5.

5. The direct ratio relationship (linear in manner) between curvature and crack width for slab-strip subjected uniaxial bending moments are testified in this section. Furthermore, these linear relationships were found not only in elastic state, but also in plastic state. This correlation will be applied as an experimental foundation of new flexural crack model in Chapter 6.

4 Influence of orthogonal reinforcement net on crack behavior of RC-slabs subjected to biaxial bending

4.1 Introduction

It can be obtained from the experimental analysis of RC slab-strips subjected to uniaxial bending in the last chapter that the restraining behavior of TR on concrete crack width is affected by the following three prominent factors: (a) TR-cover; (b) angle between TR and normal direction of bending; (c) concrete tensile strength.

In this chapter, the effect of the most important parameters of TR on crack behavior of slabs subjected to biaxial pure bending will be investigated. Such an effect is quite different to that of slabs under uniaxial bending, as TR and LR exchanged over each other in orthogonal direction. Figure 4-1 presents definitions of the major parameters in order to explain symbols of each variable in this chapter. The two-way slab specimens were subjected to pure bending in Y-axis and X-axis. Steel layer of Type A and Type B (see Section 3.5) were distributed in Y-axis and X-axis respectively, thus reinforcements in direction of Type A and Type B have various height of concrete cover. The major tensile reinforcement along Type A and Type B was designated as LR_A and LR_B. Besides, the transverse reinforcement perpendicular to LR_A and LR_B were designated as TR_A and TR_B. OR-direction between LR_A and Y-axis (between LR_B and X-axis) was designated as φ.

In this chapter, the following three key parameters are considered comprehensively in the RC slab test: (a) φ with angles of 0°, 22.5° and 45°; (b) Concrete types, such as NC, HC, LC; (c) TR-cover considered as concrete cover of TR_A and TR_B.

The major objectives of the experimental work of this chapter are:
- investigating the effect of φ，concrete cover of TR_A and TR_B and concrete types on crack patterns, especially the effect of these parameters on the values of α_{TR}, and then analyzing the difference between one-way slab-strips and two-way slabs.
- investigating the effect of φ，concrete cover of TR_A and TR_B and concrete types on the average crack spacing in their respective directions, and then analyzing the difference between one-way slab-strips and two-way slabs.
- investigating the effect of φ，concrete cover of TR_A and TR_B and concrete types on crack propagation and Cracking Rate, and analyzing value variations of each parameter from test results in order to find the correlation between these parameters and crack propagation.

Moreover, same as Section 3.5, correlation between curvature and flexural crack width were analyzed by the test of 9 two-way slabs. Equation Chapter (Next) Section 1

4.2 Experimental equipments and procedures

4.2.1 Test specimens

Figure 4-2 presents the reinforcement layout of typical two-way slabs specimens. In order to conduct a comparison of the performance of two-way slab test with that of one-way slab-strips in the last chapter, test specimens of two-way slabs were set at the length of 3300mm, which was same with that of slab-strip specimens. The slab width was set at 1200 mm, concrete cover of LR_A (TR_B) and LR_B (TR_A)were 40mm and 30mm, and orthogonal reinforcement net (Diameter ϕ=10mm in constant) spacing was constant at 100mm.

The test specimens were classified into three series. Series 1 was designed to investigate the effect of orthogonal reinforcement direction φ on crack behavior for NC. The RC-slabs of this group had different values of φ, in which P01 (φ =0°), P02 (φ =22.5°) and P03 (φ =45°) φ are illustrated in Figure 4-3. More details are summarized in Appendix D.2.

Series 2 and 3 were designed to study the effect of φ on the crack behavior for HC and LC. The values of φ were set as 0°, 22.5° and 45°.

Table 4-1 presents all parameters of test specimens, in which parameters of each specimen along X-axis and Y-axis were studied separately.
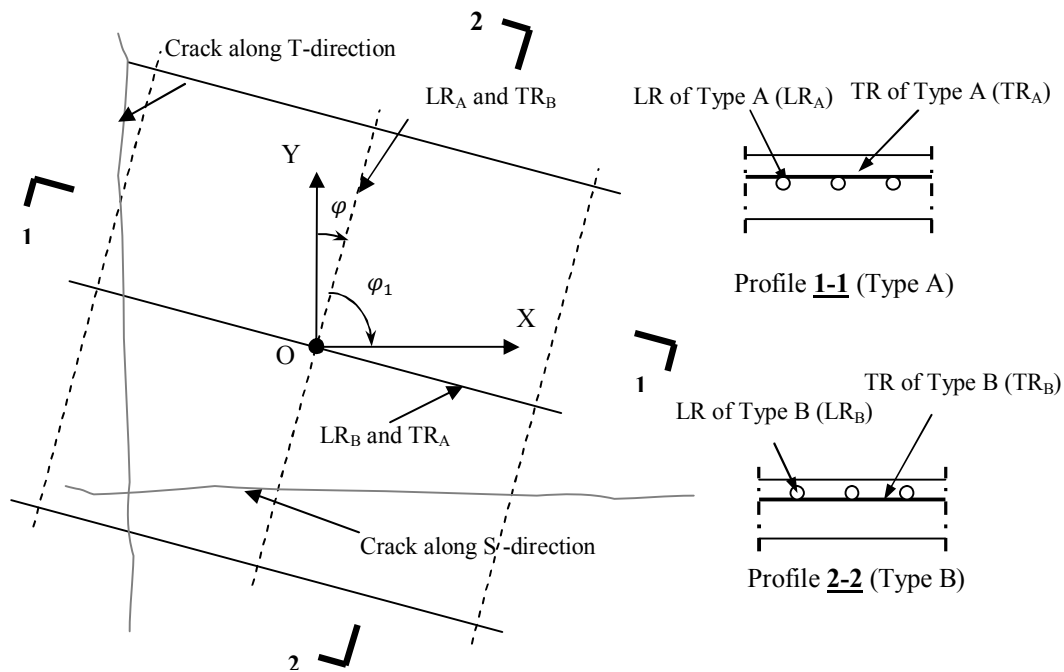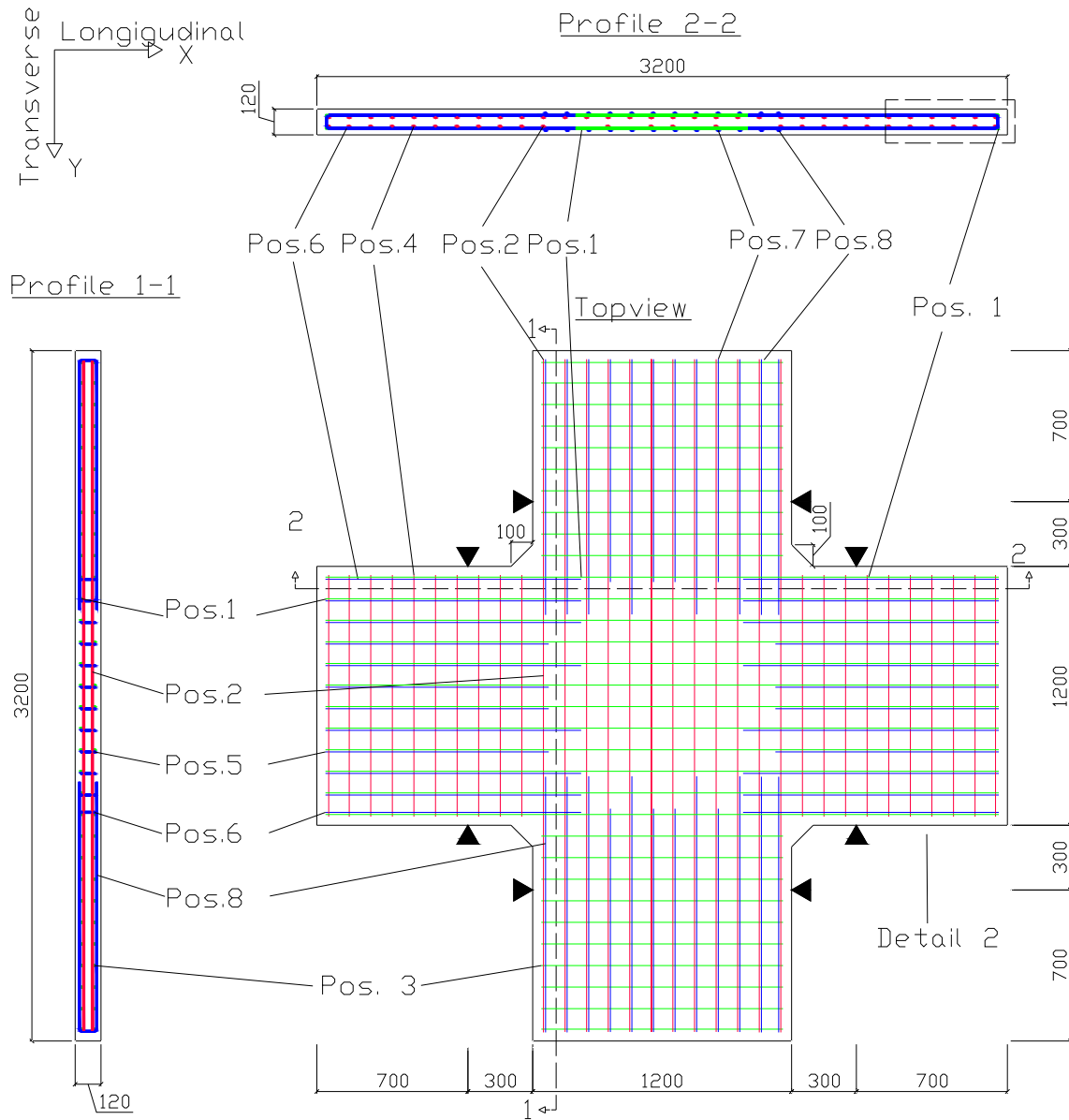

Figure 4-1 Sign convention

Figure 4-2 Illustration of RC slab specimen

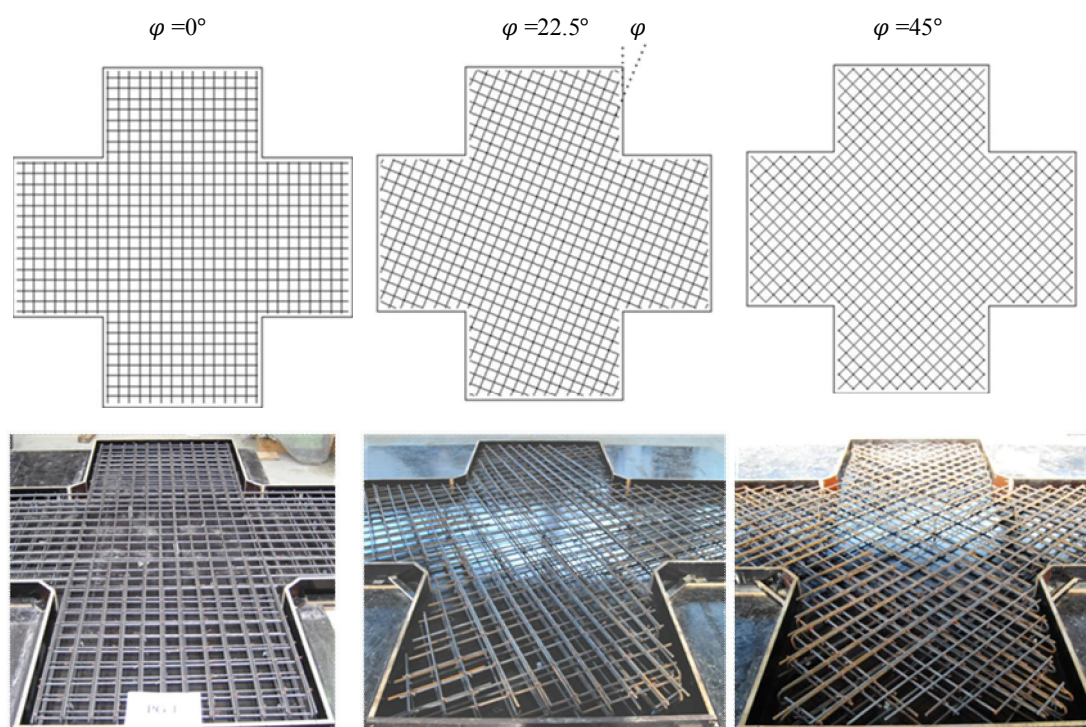$\varphi =0°$ $\varphi =22.5°$ φ $\varphi =45°$

Figure 4-3 Illustration of orthogonal reinforcement net of RC slab

4.2.2 Testing setup and procedure

The concrete casting and curing method of two-way slab test is in accordance with the method of the one-way slab-strips.

To simulate the situation of a two-way slab subjected to a biaxial pure bending in a real construction, a four point biaxial bending method was adopted. The test setup frame was identical with that of one-way slab-strips, and two cylinders with same type were installed additioanlly in the orthogonal direction of original two cylinders, as shown in Figure 4-4.

During performing the test, the load was detected by force sensors fixed on hydraulic cylinders (with an accuracy of 0.1kN). Moreover, deformations were detected by displacement sensors, as shown in Figure 4-7. The detection data from sensors were then recorded by computer.

In order to obtain steady results of crack behavior, loading stages were divided into four stages:

1. Trial loading: before the test, 40% first cracking load is loaded with 3 levels to check the devices. Then all devices adjust back to 0.

2. Formal loading: before crack, loading to 90% of the first cracking load with 3 levels. Then loading to first crack with the level of 5% first cracking load. Holding 5min for each level loading. Observing crack propagation and recording.

3. After final crack patterns, loading to 90% of the ultimate bearing load with 7-8 levels. Then increased the load and destroyed the specimen with the increasing level of 5% of ultimate load. Holding 10min for each level loading. Observing crack propagation and

recording.

4. After failure, uninstall the device and prepare next test.

To obtain a steady and reliable crack width measurement value, each loading level is divided into four steps, from Step A to Step D, as shown in Figure 4-5. Cracks were marked with different colors, crack widths were measured and crack pattern was recorded by digital photos during holding time (Step C). For each of increasing load stages, the colors of green, blue, red and black were used for each two loading stages.
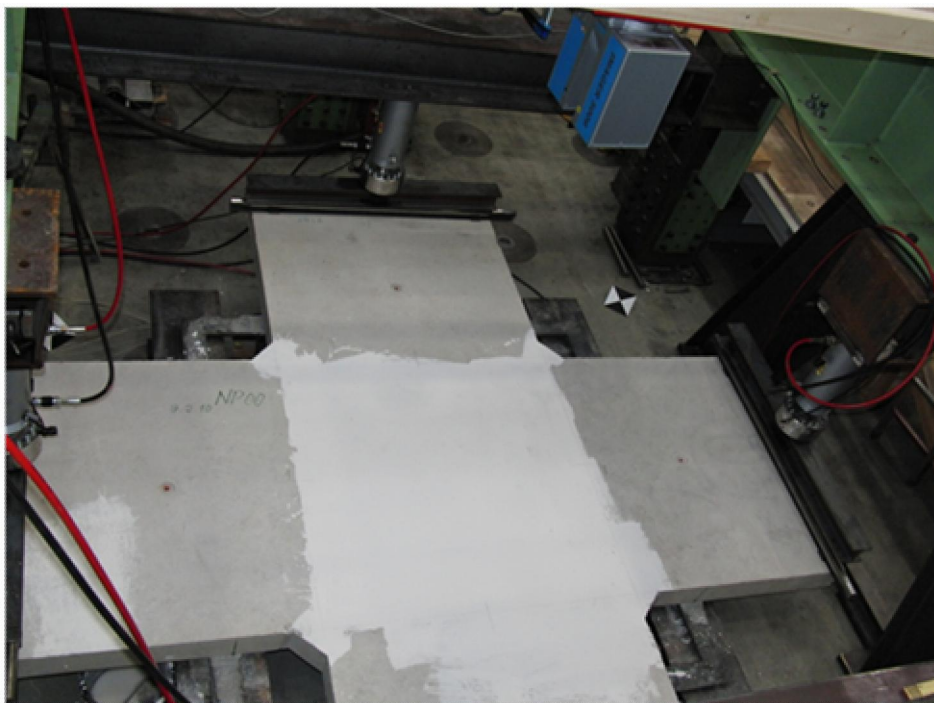
Figure 4-4: Illustration of test setup
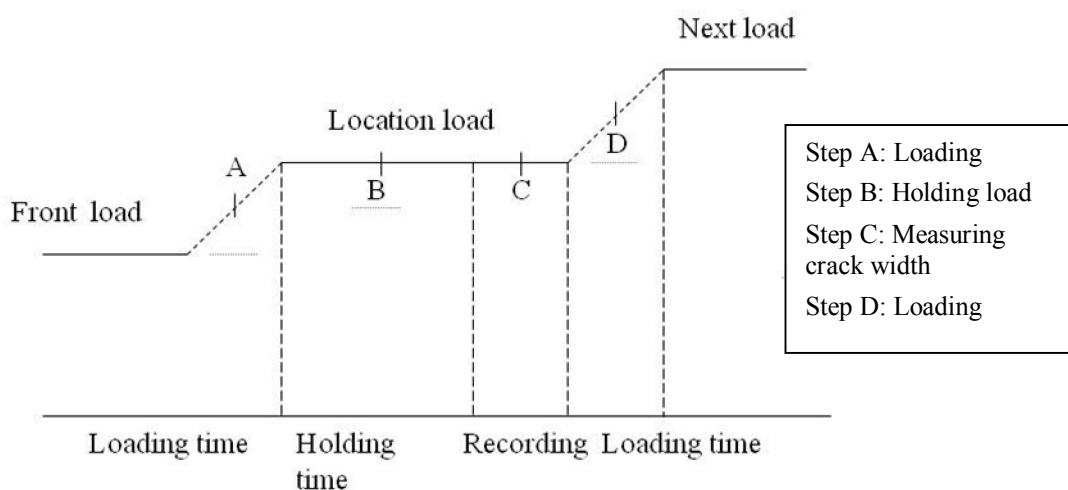
Figure 4-5: Illustration of measurement procedure of various loading steps

4.2.2.1 Detecting reinforcement and measuring deformation

The positions of the embedment of the orthogonal reinforcement (OR) as well as concrete cover of OR were detected by Ferroscann (see Figure 4-6).

Deformation was measured by laser sensors. The distribution of displacement sensors is illustrated in Figure 4-7. This figure also shows that sensors distributed in horizontal and diagonal direction.

Figure 4-6: Illustration of orthogonal reinforcement detected by Reinforcement Scanner
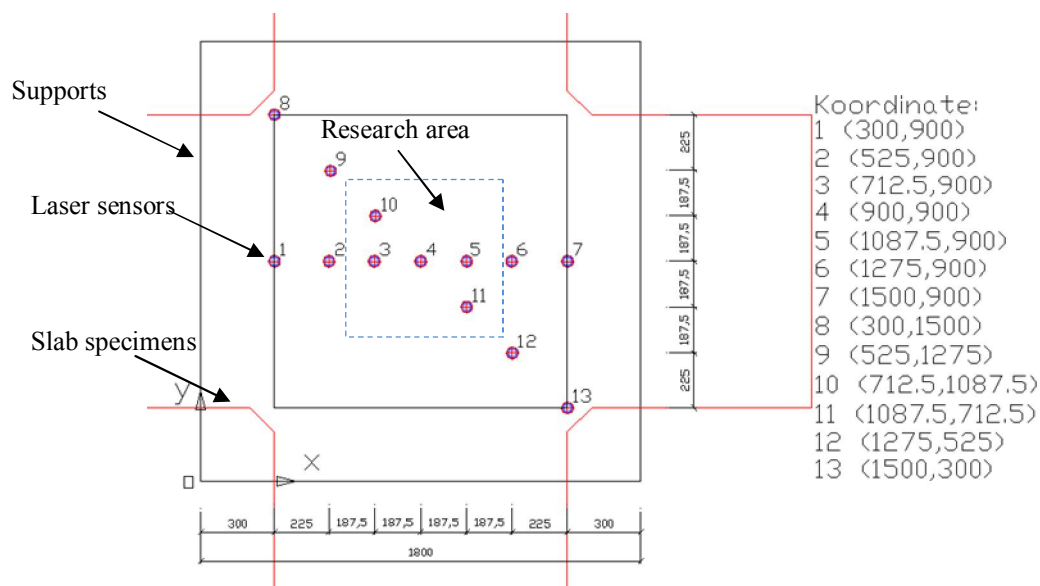
Figure 4-7: Distribution of laser displacement sensors

84

4.2.2.2 Measurement of crack widths

Due to complex inner stress in a RC slab subjected to biaxial moments, the crack widths in the central areas under pure moment (Area-1), supports area (Area-2) and four corner areas (Area-3) were defined as follows:

Area-1: the area is the square by 300mm distance away to supports. Crack widths are detected along two middle lines of Y-axis and X-axis (see Figure 4-8).

Area-2: The areas are in the four areas of 300mm distance to supports (see Figure 4-8). Crack widths are detected along two middle lines of 2 areas in Y-axis and 2 areas in X-axis.

Area-3: Crack widths are measured along the lines, which link to middle points of two near supports.

In this Chapter, the data are adopted and analyzed in the research area of 600×600 mm, as shown in Figure 4-8.
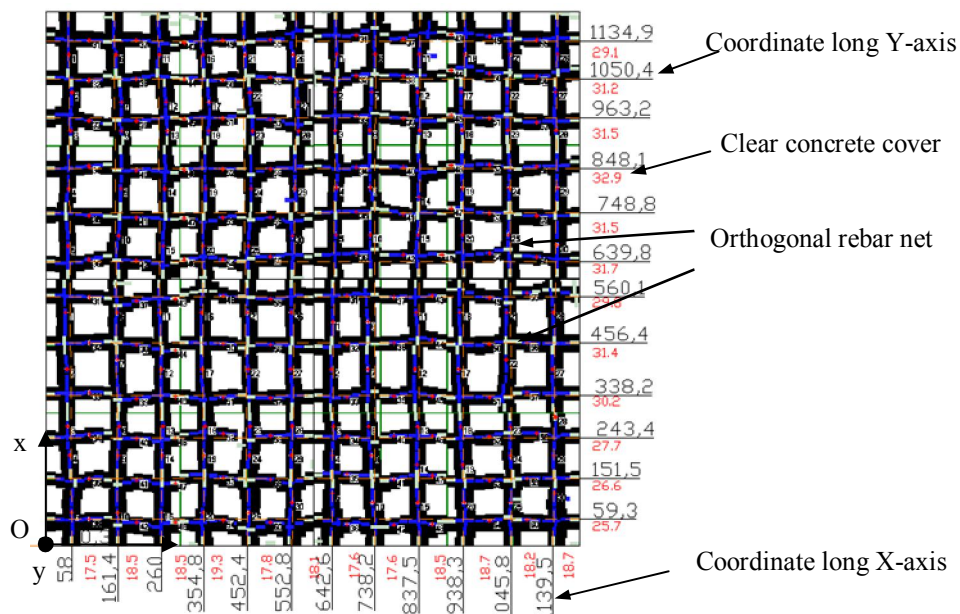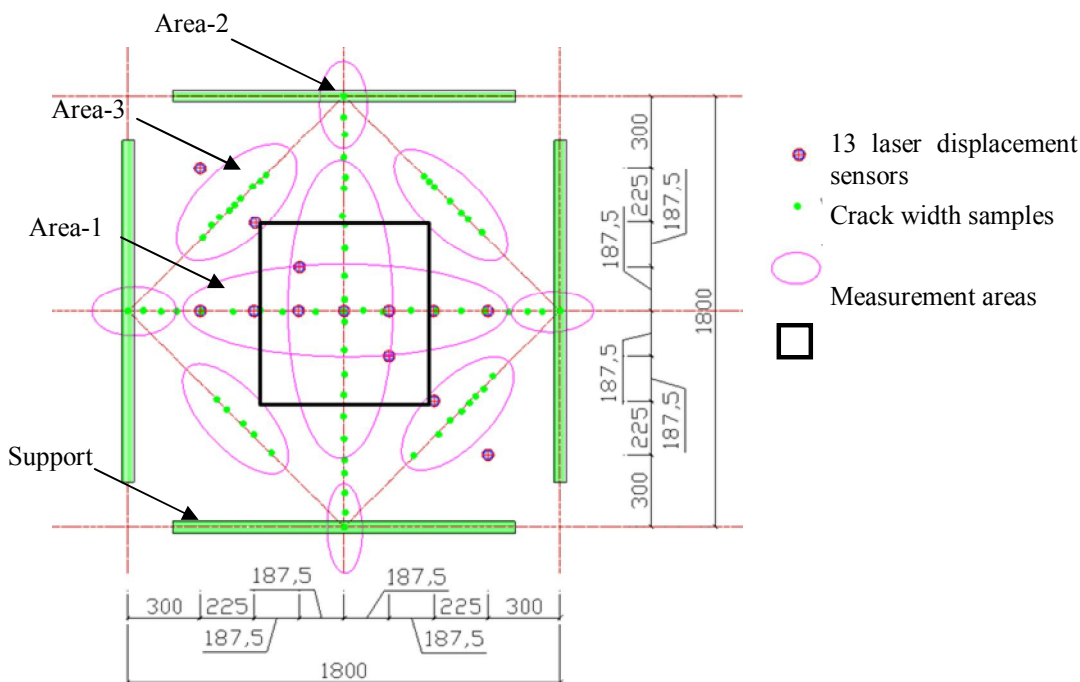

Figure 4-8: Measurement areas of crack widths

4.2.3 Moment redistribution

In the calculation of two-way slabs, FIB Model Code 2010 defines four types of analysis: linear analysis, linear analysis with redistribution, plastic analysis and non-linear analysis with a realistic modeling of the material behavior. In this paper, on one hand, the RC slabs are subjected to biaxial moments; on the other hand, crack behavior is investigated till 90% ultimate load, especially under serviceability load (at the level of $0.625f_y$). Therefore, the test slabs subjected to biaxial moment are analyzed according to the linear elastic analysis method.

Owing to the different lays of reinforcement net and different inertia of moment in two

othorgonal directions, the moment redistribute in the area, which is subjected to biaxial bending. and hence it causes a different bending stress and deformation on the surface in both directions. it have to be note that the deformation at middle intersection point in X-direction (v_X) is equal to Y-direction (v_Y). According to mechanical method, v_X and v_Y are given:

$$v_X = \frac{M_X \cdot l_X^2}{8 \cdot E \cdot I_X} \tag{4-1}$$

$$v_Y = \frac{M_Y \cdot l_Y^2}{8 \cdot E \cdot I_Y} \tag{4-2}$$

where,

M_x and M_y are the moment in x-axis and y-axis directions;

E the modulus of cross section;

I_X and I_Y are the inertia of moment in direction of X-axis and Y-axis;

l_X and l_Y are the clear span in direction of X-axis and Y-axis;

Eq.(4-1) is equal to Eq.(4-2), then the following equation can be given,

$$\frac{M_X \cdot l_X^2}{8 \cdot E \cdot I_{LR_B}} = \frac{M_Y \cdot l_Y^2}{8 \cdot E \cdot I_{LR_A}} \tag{4-3}$$

And then,

$$\frac{M_X}{M_Y} = \frac{I_{LR_B} \cdot l_Y^2}{I_{LR_A} \cdot l_X^2} \tag{4-4}$$

And in this paper, $l_X = l_Y$, Eq.(4-4) can be expressed,

$$\frac{M_X}{M_Y} = \frac{I_{LR_B}}{I_{LR_A}} \tag{4-5}$$

In order to take account of the decrease of the inertial moment I_X and I_Y, the method of Branson and Rangan [104] is adopted here. Subsequently, the steel stress can be calculated by the value of M_X and M_Y

Table 4-1 Slab test specimens in Chapter 4

	Slab No.	φ [grad]	Reinforcement position direction**	Age old [days]	f_{ck} [Mpa]	f_{ctm} [MPa]	LR-cover	TR-cover	η_c***	α_{NB}****	α_{TR}***	Standard deviation
Serie-1	P01	0	Along Y-axis (Type A direction)	167	36.90	3.33	28.13	14.46	78%	7.1	14.3	1.7
Normal concrete			Along X-axis (Type B direction)	167	36.90	3.33	14.46	28.13	66%	14.3	7.1	1.6
	P02	22.5	Along Y-axis (Type A direction)	171	36.90	3.33	43.60	27.30	-	6.3	22.5	5.2
			Along X-axis (Type B direction)	171	36.90	3.33	27.30	43.60	-	0.2	22.5	6.7
	P03	45	Along Y-axis (Type A direction)	175	36.90	3.33	43.70	29.80	-	6.4	40.4	4.2
			Along X-axis (Type B direction)	175	36.90	3.33	29.80	43.70	-	4.6	38.6	5.8
Serie-2	P04	0	Along Y-axis (Type A direction)	53	55.74	4.24	43.31	28.75	67%	2.8	11.3	3.1
High strength concrete			Along X-axis (Type B direction)	53	55.74	4.24	28.75	43.31	50%	11.3	2.8	2.0
	P05	22.5	Along Y-axis (Type A direction)	55	55.74	4.24	44.19	33.80	-	2.4	14.1	7.5
			Along X-axis (Type B direction)	55	55.74	4.24	33.80	44.19	-	8.4	20.1	8.6
	P06	45	Along Y-axis (Type A direction)	51	55.74	4.24	41.29	31.31	-	1.8	38.0	6.3
			Along X-axis (Type B direction)	51	55.74	4.24	31.31	41.29	-	7.0	43.3	6.0
Serie-3	P07	0	Along Y-axis (Type A direction)	135	22.32	1.87	37.38	23.75	67%	0.3	2.3	3.7
Lightweight concrete			Along X-axis (Type B direction)	135	22.32	1.87	23.75	37.38	50%	2.3	0.3	3.1
	P08	22.5	Along Y-axis (Type A direction)	132	22.32	1.87	45.38	30.25	-	0.3	18.1	6.1
			Along X-axis (Type B direction)	132	22.32	1.87	30.25	45.38	-	4.4	22.8	3.0
	P09	45	Along Y-axis (Type A direction)	136	22.32	1.87	45.25	36.81	-	11.2	41.8	4.2
			Along X-axis (Type B direction)	136	22.32	1.87	36.81	45.25	-	3.2	33.8	6.7

*   NC, HC and LC stand for Normal concrete, high strength concrete and lightweight concrete;

** The determination direction refers to Figure 4-1;

*** η_c is the ratio of TR-induced cracks to all cracks in research area;

**** α_{NB} is the angle between crack and bending direction;

***** α_{OR} is the angle between crack and OR.

4.3   Results of RC-slab tests

4.3.1   Crack pattern

In this section, the crack patterns are investigated in two load levels, at first cracking load and serviceability load. In the research area of 600×600mm, the angles between Y-axis and cracks along this axis (α_{NB-Y}) and the angles between X-axis and cracks along this axis were measured (α_{NB-X}) and. Besides, the angles between the TR$_B$ (α_{TR_B}) and TR$_A$ (α_{TR_A}) and intersecting cracks were also measured.

4.3.1.1   Cracking patterns

According to the mechanical analysis, principle stress direction can affect crack direction derived by the reinforcement. According to the equilibrium relationships of Baumann[105], a crack model is established based on longitudinal and transverse principal normal forces, shear forces to calculate cracks in different direction.

These considerations are even today still the basis for the design of orthogonal reinforcement systems in reinforced concrete slabs subjected to bending. In the section, predominantly phenomenological description of the influence of the reinforcement on the crack pattern. In Figure 4-9, the course of principle stress in a slab is shown qualitatively equal load. For this course, which sets up (not down) with a reinforced concrete slab only state-I can possibly estimate the first cracking pattern. However, it cannot exactly be predicted, since the concrete with it inhomogenities and variations in material properties always include uncertainty factors. Despite the uncertainty, the images of the initial plans of the experimental plates P01w0, P04 and P07 in the Appendix E that these are very well predictable. It indicates that the slab is approximately an isotropic slab in state I, and the first crack will appear always perpendicular to the principal tensile stresses.

With the appearance of the first cracks the behavior of a reinforced concrete slab changes significantly. Firstly, the stiffness decreases from the state-I to state-II. The bending stiffness in order for the plate is much softer. Secondly, reinforcement in X-axis and Y-axis begins to bear tensile stress.

Figure 4-10 illustrates the overlapping of deformation field plotting and crack patterns by means of laser scanning and Matlab software. In this figure, various deformation values were represented by different colors. From this figure, it can be seen that after cracking load, changing of deformation (represented as the Curvature) in direction of LR$_B$ was larger than that in direction of LR$_A$. More cracks perpendicular to the direction of LR$_B$ appeared before that to direction of LR$_A$. Then, during load increment, values of the Curvature in these two directions were becoming equal, which is presented by (b) and (c) of this figure. When the load reached 71% of Ultimate load, values in these directions equaled to each other and final crack patterns formed as shown in part (d) of this figure. The reason of this phenomenon is that the effective depth of the compressive zone in direction of LR$_B$ was deeper than that in direction of LR$_A$ and the value of inertia moment

represented as I_{LR_B} was also larger than that of I_{LR_A}. It can be known from Eq.(4-5) that M_Y was larger than M_X. Thus, the more cracks formed in direction of LR$_B$, the lower bending stiffness was in direction of LR$_B$. Final crack patterns were formed when bending stiffness in direction of LR$_A$ and LR$_B$ was identical with each other.

4.3.1.2　Final crack pattern

According to the test results in Section 3.3 and Section 3.5, TR formed certain crack, the ratio η_c of which not depends on TR-position but on TR-cover. Figure 4-13 illustrates the overlapping of reinforcement layoutping and crack patterns. When $\varphi = 0°$, certain cracks appeared along TR. In order to further study the effect of OR-direction and concrete types on crack direction, α_{NB-Y} and α_{NB-X} were measured. Besides, α_{TR_B} and α_{TR_A} were measured. Moreover, as considering the random variation of crack direction caused by the inhomogeneity of concrete, the measurement scope was confined to width area of 100mm along the middle lines of X-axis and Y-axis in the research area of 600×600mm. Table 4-1 showed the measurement results of α_{NB-Y} , α_{NB-X}, α_{TR_B} and α_{TR_A}.

Furthermore, the influence radius of TR can be evaluated by Eq.(3-1). With a maximum aggregate size of 16 mm, the influence radius is 21 mm. Thus, for specimens P01, P04 and P07 with φ=0°, the values of η_c were counted and presented in Table 4-1. From this table, two phenomena can be obtained as follows:

(a) α_{NB-Y} and α_{NB-X} varied in the range of 0-11.3°; for concrete specimens made of NC, HC and LC, average values of α_{NB} with different concrete types and directions closed to overall average value of 5.2°. However, the increase of φ resulted in an increase of the standard deviation and an increase of variation of the crack direction. Thus, increase of φ did not change the overall direction of cracks, which remained perpendicular to bending direction. And this phenomenon was identical with test results of slab-strips in Section 3.4.1.

(b) The value of α_{TR_B} and α_{TR_A} depends not on the concrete types but on the distribution of the steel layer (represented as TR-cover). According to Eq. (3-3) in Section 3.4.1, α_{TR_B} and α_{TR_A} were calculated and presented in Figure 4-11. This figure shows that the predicted value of 6.0° is closing to the measured value of 5.2°. Therefore, this prediction formula of Eq. (3-3) can be also applied to two-way slab specimens. However, by carrying out tests, when OR-direction varied, variation of crack direction can be found experimentally, with the result that overall crack direction kept perpendicular to bending direction, which is in discordance with overall crack direction inclining to reinforcement direction found by Clark [12, 37] and Dr. Ruediger [81].

Besides, the observed values of η_c and the TR-cover were presented in Figure 4-12. It can be seen that an inverse correlation (R^2=0.931) existed between η_c and TR-cover. Comparing with the predicted values calculated by Eq. (3-2), the overall average values of observed values decreased by 15.3%. Therefore, this formula of Eq. (3-2) can be applied
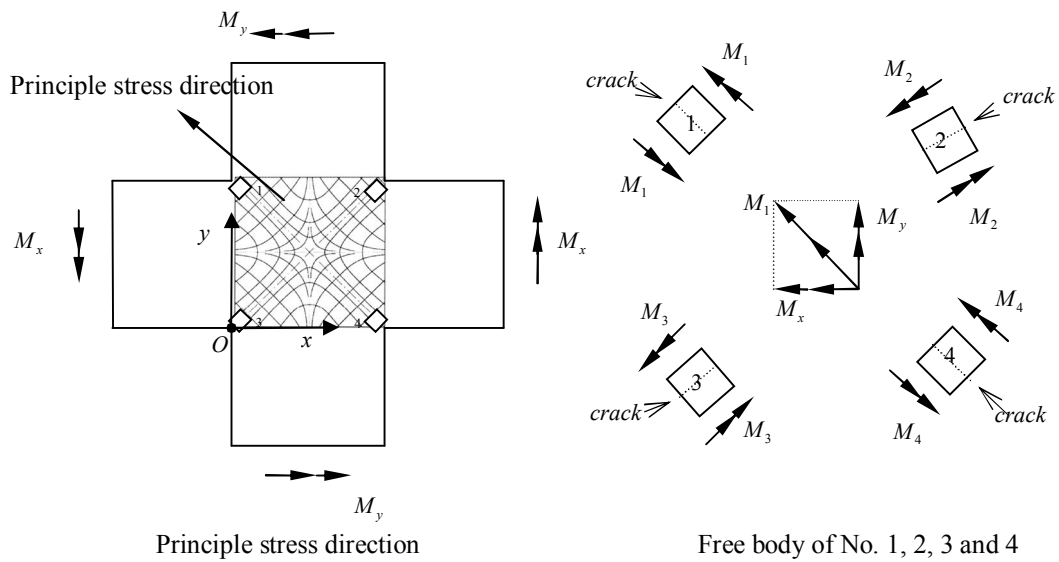
to predict values of η_c in two-way slabs.

Principle stress direction

Free body of No. 1, 2, 3 and 4

Figure 4-9 Principle stress direction of isotropy plane and illumination of free body in the shear areas

(a) first cracking load

(b) 30% Ultimate load
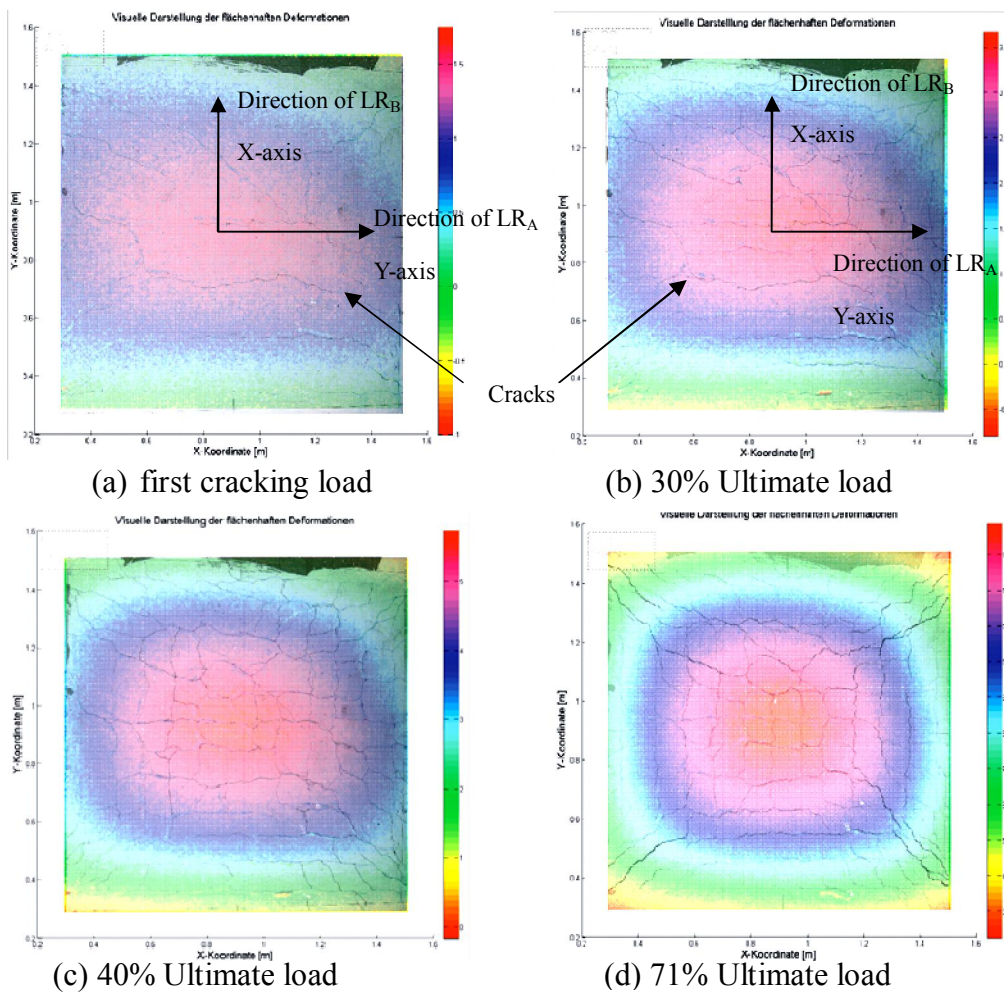

(c) 40% Ultimate load

(d) 71% Ultimate load

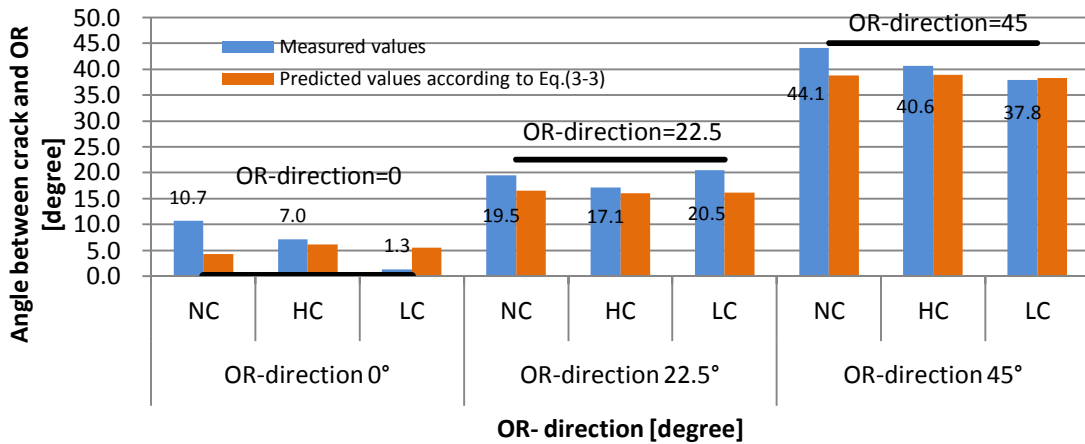**Figure 4-10 Deformation map with increase of load**

Figure 4-11 Average values of observed angles between crack and normal direction of bending α_{TR} and predicted values of α_{TR} according to Eq. (3-3) for slab-strips in Section 3.4.1
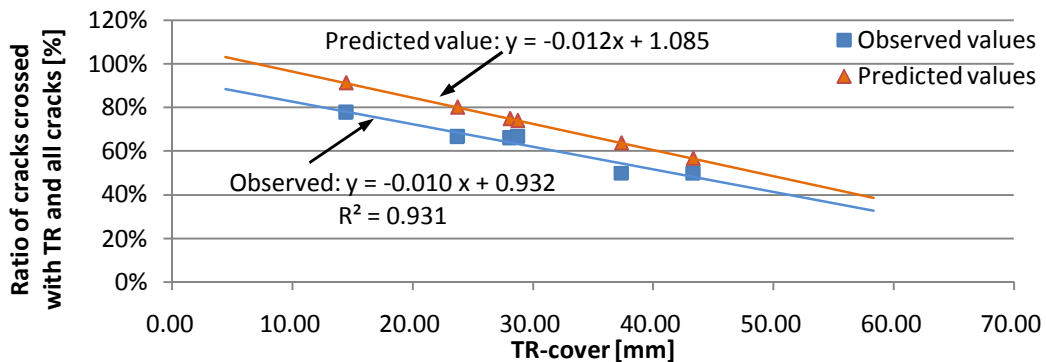

Figure 4-12 The ratio of TR-induced cracks to all cracks (η_c) and its predicted values according to Eq. (3-2) in Section 3.3.1.
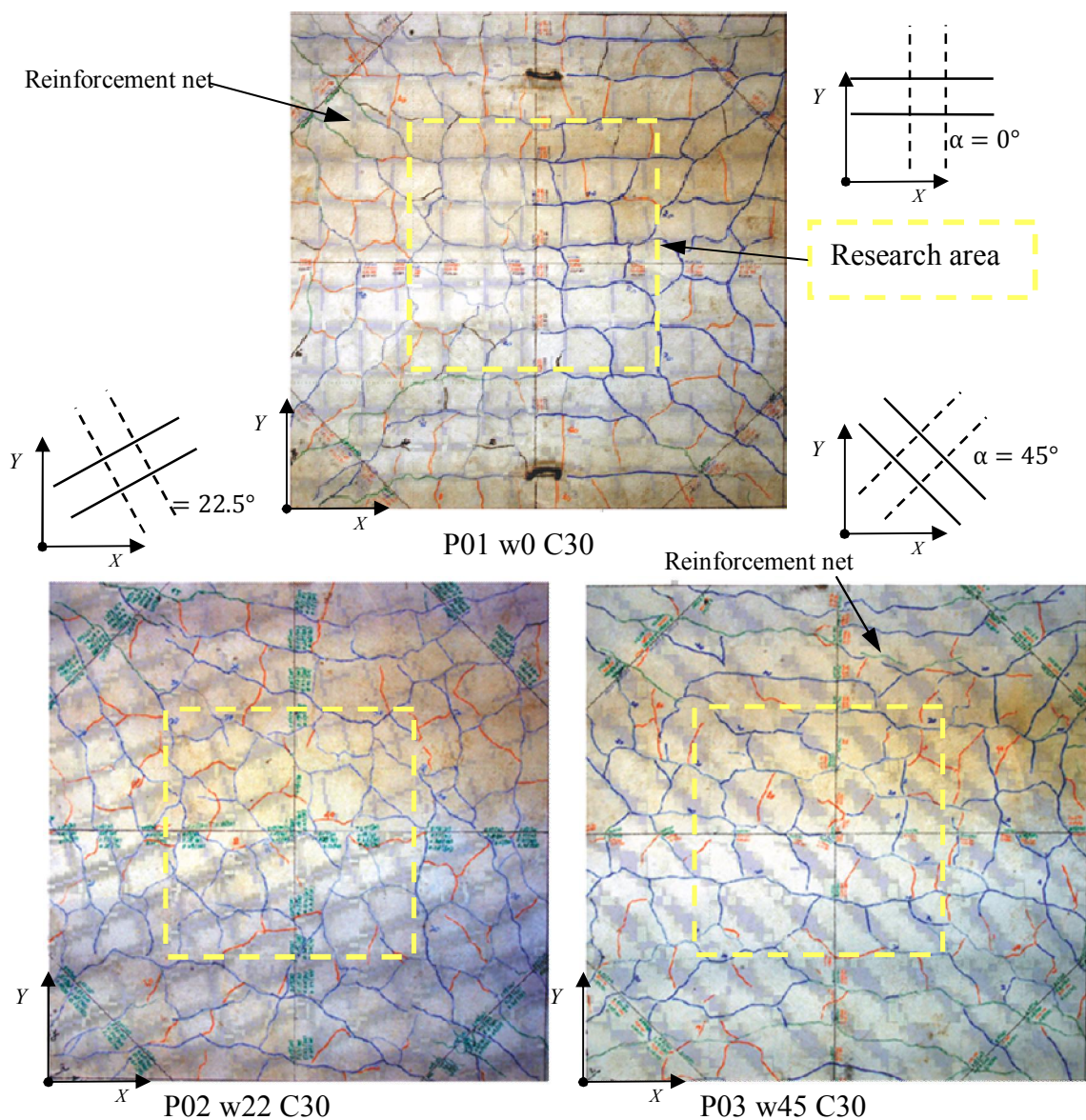
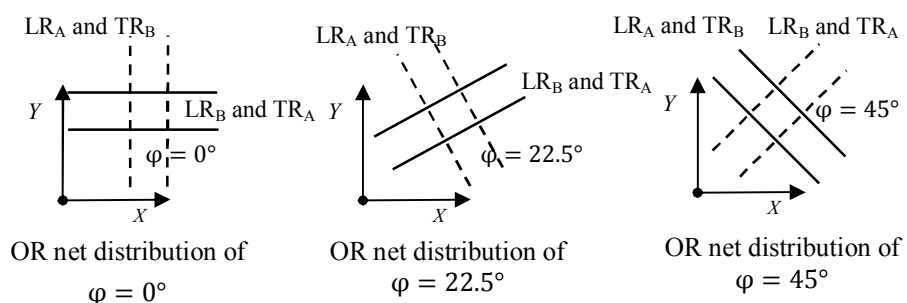**Figure 4-13 Overlapping of reinforcement net mapping and crack pattern**

Figure 4-14 Illustration of Y-axis and X-axis and their corresponding reinforcement layer of Type A and Type B

4.3.2 Crack spacing

Crack spacing was measured at each loading stage along the middle lines of the slabs. The average crack spacing, average and maximum value of crack width in the research area of 600×600mm (see Figure 4-8) were listed in Table 4-2. All measured values of the crack width in this table were taken at the service limit state with a steel stress about 325MPa (equivalent to $0.625f_y$). Besides, all measured values of crack spacing and width at each load stage are presented in Appendix E.2.

The effect of OR-direction on crack spacing was investigated in terms of studying the correlation between average crack spacing in X-axis and Y-axis and corresponding α_{TR_A} and α_{TR_B}. The directions of these two variables should be identical to each other, average crack spacing in X-axis and Y-axis were converted to the direction of LR_A (S_{ro,LR_A}) and TR_B (S_{ro,LR_B}). Figure 4-15 shows that there is an inverse correlation between α_{TR} and S_{r,LR_A}(R^2=0.610) and S_{r,LR_B}(R^2=0.331). This phenomenon is in good agreement with the test results in Section 3.4.2 (see Figure 3-28). Thus, it is not difficult to accept that α_{TR_A} and α_{TR_B} has an influence on the crack spacing and this influence has been appropriately considered by current codes.

Furthermore, the values of the average crack spacing along Y-axis and X-axis can be obtained by predicted values multiplied by 3/4 according to EN DIN 1992-2011 (refer Eq. 2-35). These calculated values were presented in Table 4-2. The correlation between calculated and observed values of average crack spacing against their TR_A -cover and TR_B-cover was presented in Figure 4-16. There is an identical inverse correlation between TR-cover and the observed crack spacing as well as between TR-cover and the predicted crack spacing in code EN DIN 1992-2011. However, the predicted values in direction of Y-axis are underestimated by 18% and those in X-axis by 31%. Such an underestimation is maybe caused by bond-slip stress between steel and concrete which was decreased by perpendicular cracks. According to Bond-slip Mechanism principle, such a decrease will significantly increase value of crack spacing.

A phenomenon was observed in one-way slab-strips that an increase of the number of intersecting crack with TR (η_c) resulted in a decrease of average crack spacing and further away from predicted maximum crack width. It is quite possible to obtain such a phenomenon in two-way slabs if TR also affects crack spacing. The picture of the phenomenon assumed in the discussion above is shown schematically in Figure 4-17, in which predicted values of maximum crack width according to Bond-slip Mechanism crack model were presented. From this figure, it can be seen that an increase of η_c resulted in a trend of decrease of average crack spacing in Y-axis and X-axis and also resulted in an increase of D-values. This correlation can be shown experimentally in Section 3.3.2 that this is in fact the case. Therefore, it can be concluded that a decrease of bond-slip stress on perpendicular direction and η_c of TR will result in an increase of crack spacing. These two variables will interact to affect average crack spacing. This effect should be taken into account in development of equations in current codes.
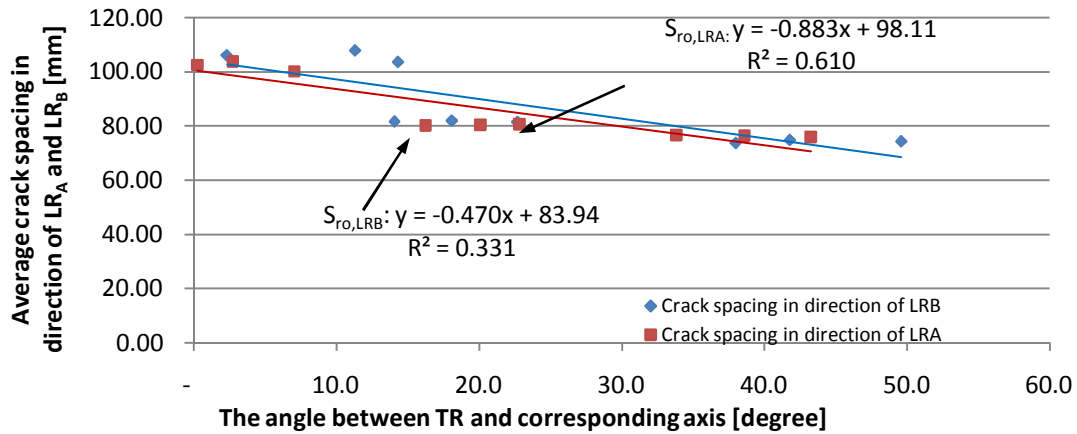
Figure 4-15 Plots of observed crack spacing calculated in direction of LR_A and LR_B against change of α_{TR} in direction of TR_B and TR_B
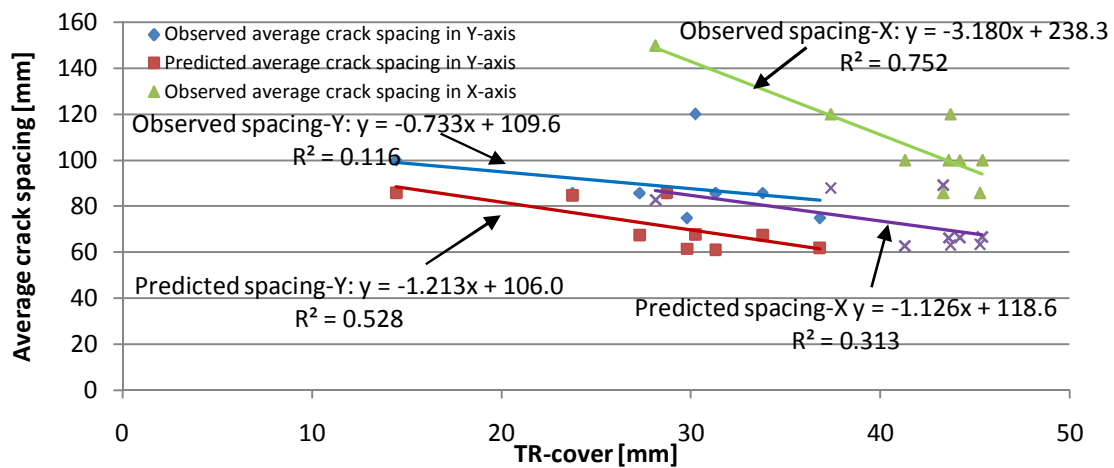

Figure 4-16 Plots of observed and calculated crack spacing in Y-axis and X-axis against change of concrete cover of corresponding TR_A and TR_B (TR_A-cover and TR_B-cover)
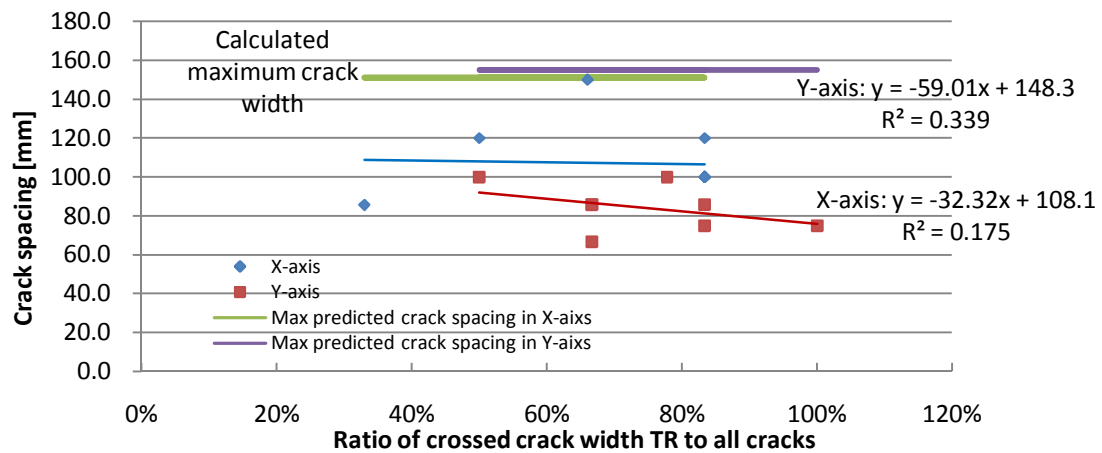

Figure 4-17 Plots of average crack spacing in Y-axis and X-axis against change of η_c in direction of TR_B and TR_A

4.3.3 Crack width

The crack width at each load stage was measured until the ultimate load (up to 90% of ultimate steel stress). Crack widths at serviceability state were measured within the region of 600×600mm. The average crack width values are presented in Table 4-2. It was assumed in the last section that a decrease of magnitude of bond strength due to perpendicular crack resulted in a significant increase of crack spacing. If this correlation is true, an additional assumption is made that the decrease of magnitude of bond strength leads to an increase of crack width. This assumption can be testified by comparison of the average crack width between two-way slabs and one-way slab-strips. Thus, two-way slabs and one-way slab-strips made up of NC in TR-directions of 0°, 22.5° and 45°are shown schematically in Figure 4-18. In this figure, average crack width per unit TR-cover value were obtained by the average crack width values divided respective value of LR-cover. From this figure, it can be seen that overall values of average crack width per unit TR-cover of two-way slabs were larger than those of one-way slab-strips. It needs to be pointed out that an increase of OR-direction from 0° to 45°results in a significant decrease of average crack width per unit TR-cover. Table 4-3 presented the values of average crack width per unit TR-cover and the different percentage between two- and one-way slabs. The crack width increases by 9% from one-way slab-strips to two-way slabs. Thus, it is found that the decrease of magnitude of bond stress due to perpendicular cracks leads to an increase of crack width.

It remains to assess other parameters that are likely to affect the average crack width. Qualitatively, these can be assessed in Figure 4-19. This figure presents an inverse relationship between α_{TR} and average crack width per unit TR-cover. In the same way, Figure 4-20 presents an inverse relationship between η_c and unit average crack width values. The reason of these two phenomena can eventually be expected that TR affects corresponding intersecting crack width in two-way slabs. Such a behavior is similar to that of one-way slab-strips.

Therefore, comparing with the test results of one-way slab-strips, a decrease of bond-slip stress of two-way slabs due to perpendicular cracks will result in a significant increase of the average crack width. This effect is taken into account in the development of equations in Chapter 5. It is observed that the decrease of bond-slip stress affects appreciably on crack width.

So far, the discussion has been confined to specimens made up of NC with in OR-direction of 0°. By means of Cracking Rate, next section will further analyze other specimens made up of HC and LC with in OR-direction of 22.5° and 45°.
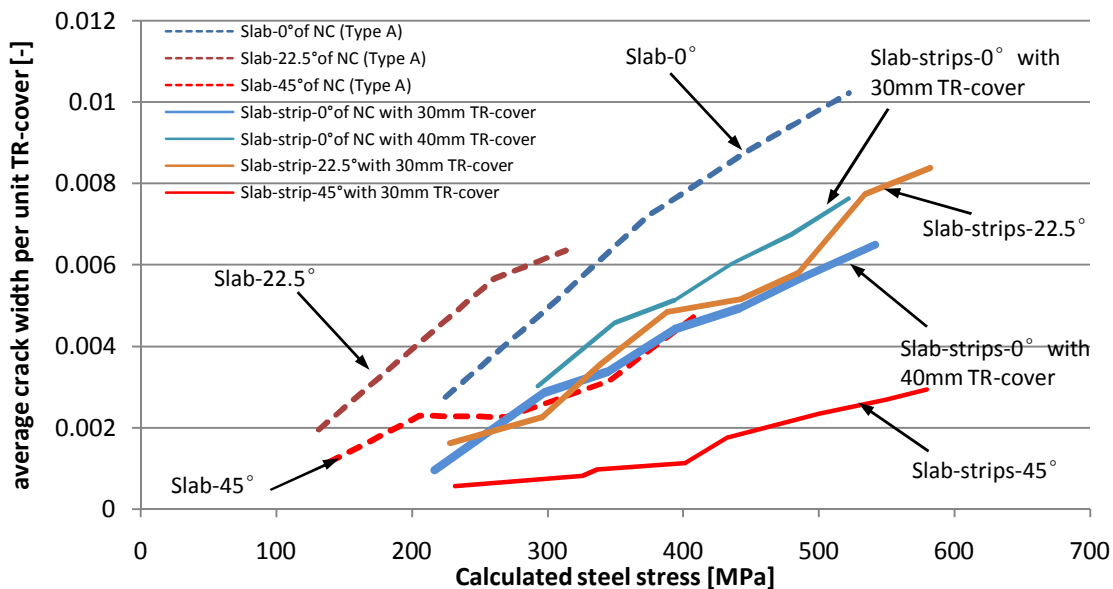
Figure 4-18: Steel stress versus average crack width per unit TR-cover for NC slabs and slab-strips
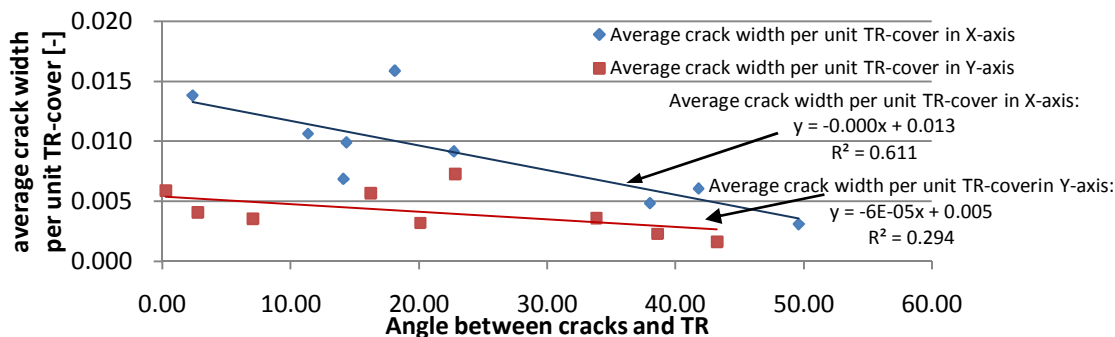

Figure 4-19: Angles between crack and TR (α_{TR}) versus average crack width per unit TR-cover for two-way slabs specimens at load level of 0.625 f_y
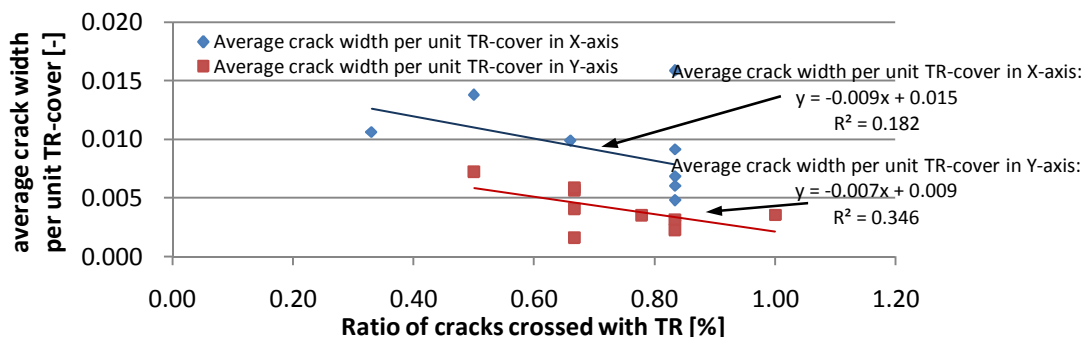

Figure 4-20: The ratio of cracks intersected TR to all crack (η_c) versus average crack width per unit TR-cover for two-way slabs specimens at load level of 0.625 f_y

4.4 Cracking Rate

It is known that for NC specimens with OR-direction of 0°, a decrease of bond-slip between steel and concrete due to perpendicular cracks resulted in an increase of crack width. Figure 4-21 illustrates the Cracking Rate of average crack width per unit TR-cover value (named A-CR-U) of other specimens made up of HC and LC with in OR-direction of 22.5° and 45°. This figure indicates that unit A-CR-U of two-way slabs is larger than that of one-way slab-strips. The increase percentages from one-way slab-strips to two-way slabs of different TR-direction and concrete types are close to overall average value of 32%, as shown in Table 4-3. This value can be used to calculate the increase of crack width, which is caused by two direction bending stress. This increase of 32% is taken into in the new crack width model in Chapter 5.

At this stage, it is not difficult to accept that the Cracking Rate of NC, HC and LC slabs increased under biaxial bending. It can also be explained that a decrease of bond strength resulted in a decrease of restraining influence of TR on concrete surrounding and ultimately resulted in an increase of crack width.

It is more reasonable to view that the decrease of restraining influence will result in an increase of crack propagation subjected to biaxial bending and ultimately resulted in an increase of final crack width. Thus in this case, the current models of crack width for RC-slabs under biaxial bending should be modified to take account of the influence of a decrease of bond strength on crack width.
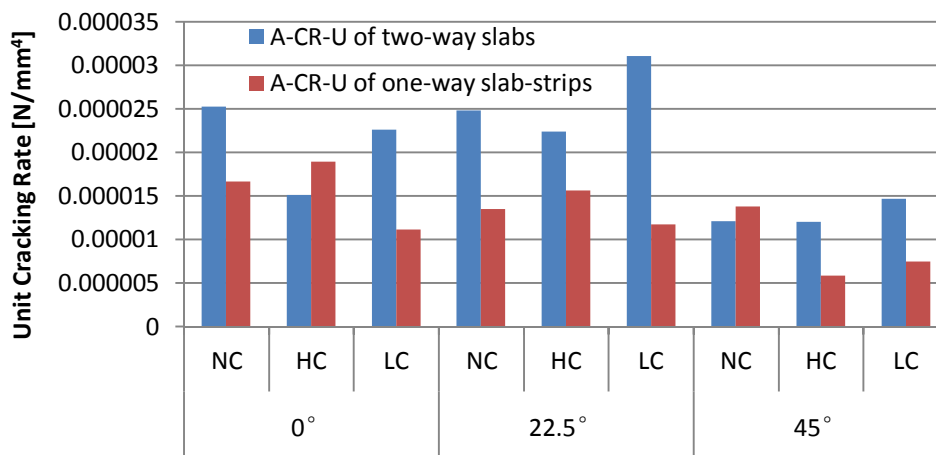
Figure 4-21 Comparison of Cracking Rate of average crack width per unit TR-cover between various OR-direction and concrete types

Table 4-2 Test results of slab specimens

Specimen No.	OR-Types and direction*	σ_s [MPa]**	S_m [mm]***	Predicted crack spacing ****	Average crack width [mm] $w_{r,m}$	Maximum crack width [mm] $w_{r,max}$	Cracking Rate [mm3/N]
P01 W0	Type A(y-axis)	373	100	85.68	0.10	0.18	0.00071

NC	Type B(x-axis)	461	200	82.81	0.14	0.25	0.00068
P02 W22	Type A(y-axis)	260	100	67.45	0.25	0.32	0.00180
NC	Type B(x- axis)	350	85	66.25	0.25	0.40	0.00189
P03 W45	Type A(y- axis)	328	75	62.34	0.10	0.31	0.00154
NC	Type B(x- axis)	244	150	62.34	0.09	0.13	0.00098
P04 W0	Type A(x- axis)	343	75	89.19	0.18	0.31	0.00107
HC	Type B(y- axis)	448	100	85.82	0.31	0.59	0.00103
P05 W22	Type A(x- axis)	294	85	67.60	0.14	0.27	0.00128
HC	Type B(y- axis)	358	100	66.47	0.23	0.27	0.00104
P06 W45	Type A(x- axis)	315.	85	61.89	0.07	0.11	0.00071
HC	Type B(y- axis)	262	100	61.89	0.15	0.21	0.00168
P07 W0	Type A(x- axis)	297	86	87.78	0.22	0.28	0.00099
LC	Type B(y- axis)	375	120	84.72	0.33	0.50	0.00112
P08 W22	Type A(x- axis)	273	120	67.83	0.33	0.40	0.00163
LC	Type B(y- axis)	362	100	66.71	0.48	0.54	0.00123
P09 W45	Type A(x- axis)	286	75	62.68	0.16	0.20	0.00089
LC	Type B(y- axis)	337	86	62.68	0.22	0.34	0.00083

* Orthogonal reinforcement net types and direction is according to Figure 4-4 and 4-9.

** σ_s is steel stress, which is calculated by 40 kN of each cylinder. And the moment redistribution is calculated according to Section 4.2.4;

*** S_m is average crack spacing at stabilization state;

**** The prediction of average crack spacing are calculated by DIN EN 1992-1-2011.

Table 4-3: The comparison of average crack width and A-CR per unit TR-cover between one-way slab-strips and two-way slabs

TR-direction	Concrete types	Average crack width per unit TR-cover*			A-CR per unit TR-cover**		
		two-way slabs	one-way slabs	Percentage errors	two-way slabs	one-way slabs	Percentage errors
0°	NC	0.00352	0.00338	4%	2.53E-05	1.66E-05	34%
	HC	0.00407	0.00654	-61%	1.51E-05	1.90E-05	-26%
	LC	0.00589	0.00304	48%	2.26E-05	1.11E-05	51%
22.5°	NC	0.00566	0.00244	57%	2.48E-05	1.35E-05	46%
	HC	0.00317	0.00387	-22%	2.24E-05	1.57E-05	30%
	LC	0.00727	0.00347	52%	3.10E-05	1.18E-05	62%
45°	NC	0.00226	0.00320	-42%	1.21E-05	1.38E-05	-14%
	HC	0.00159	0.00112	29%	1.20E-05	5.85E-06	51%
	LC	0.00356	0.00302	15%	1.47E-05	7.46E-06	49%
Average values		0.00411	0.00334	9%	2.00E-05	1.27E-05	32%

* Average crack width per unit TR-cover is equal to the ratio of average crack width to TR-cover in corresponding direction;

** A-CR per unit TR-cover is the Cracking Rate of average crack width per unit TR-cover.

4.5 Relationship between curvature and crack width

In Section 3.7, a direct relationship between curvature and crack width for slab-strips subjected uniaxial bending was testified. In this section, the relationship between curvature and crack width for two-way slabs subjected to biaxial bending will be investigated.

As shown in Figure 4-7, displacement laser sensors were arranged in X-axis direction. Sensor-4 was placed at middle line of the slab; Sensor-3 and Sensor-5 were placed respectively in both sides of Sensor-4 by 187.5mm along X-axis. Values of the curvature were calculated by measured deformation values of Sensor 3 through 5. As in the research area of 600×600mm, the curvature was measured along X-axis direction. Average and maximum crack width values and the curvature of slabs with various concrete types are plotted in Figure 4-22 and Figure 4-23, respectively. In these figures, not only the direct relationship between curvature and crack width was presented, but also the influence of OR-direction on the average crack width values with different concrete types can be compared.
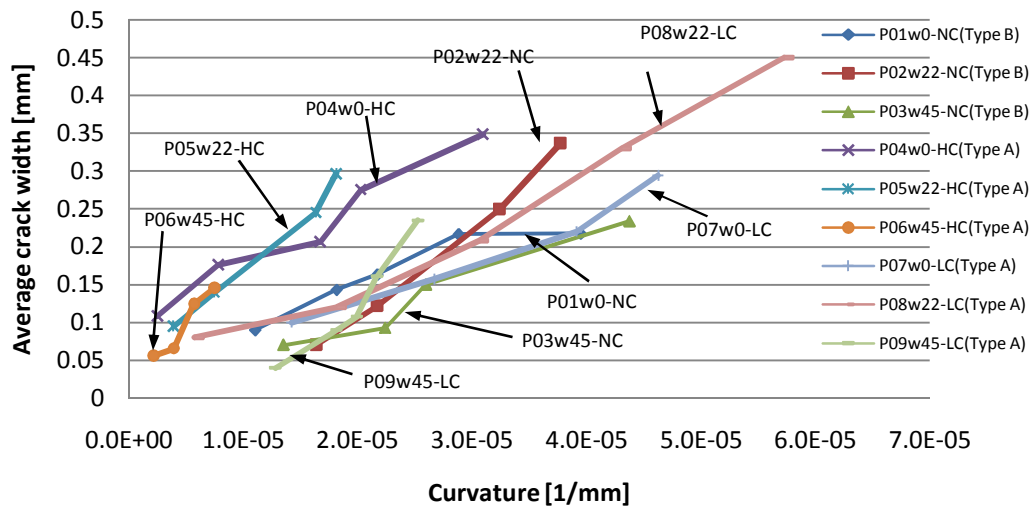

Figure 4-22 The average crack width propagation versus curvature for slabs made up of NC, HC and LC
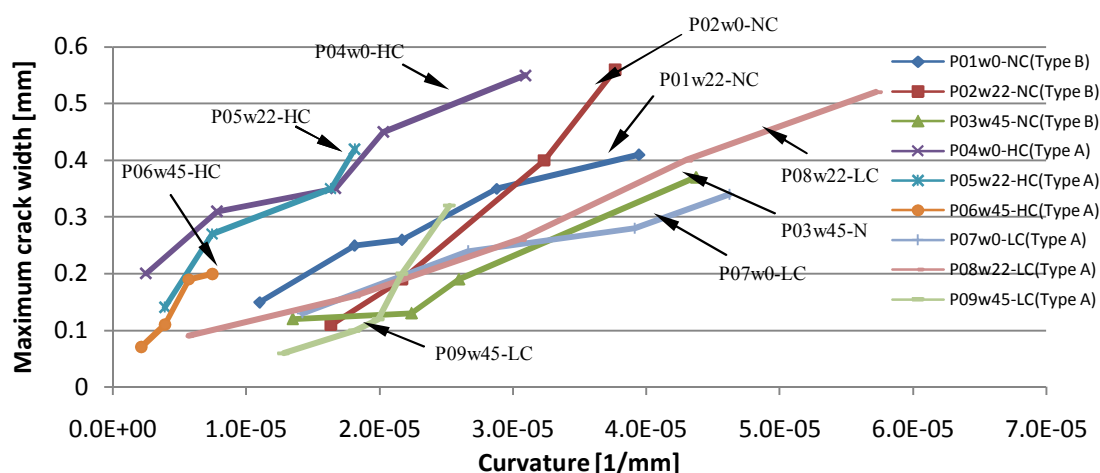
Figure 4-23 Maximum crack width propagation versus curvature for three OR-direction slabs made of NC, HC, and LC

Table 4-4: Coefficient of regression linear for three types of concrete

items	No. of slab	Average crack width		Maximum crack width	
Concrete types		Slop [mm^2]	R^2	Slop[mm^2]	R^2
Normal concrete	P01w0	4604	0.865	9057	0.966
	P02w22	12424	0.992	20813	0.986
	P03w45	5628	0.953	8829	0.934
High strength concrete	P04w0	8204	0.965	11837	0.958
	P05w22	13465	0.985	16781	0.919
	P06w45	18434	0.930	26438	0.93
Lightweight concrete	P07w0	5828	0.968	6161	0.964
	P08w22	7440	0.974	8602	0.988
	P09w45	15595	0.929	20569	0.845
Total	-	-	0.951	-	0.941

*   Slope of regression linear;

** R^2 is the determination coefficients.

4.6 Chapter summary

This chapter was investigated the influence of TR on the crack pattern, crack spacing and width for two-way slabs. Conclusions can be obtained as follows:

(a) by carrying out tests, when OR-direction was varied, a variation of crack direction can be found experimentally, with the result that overall crack direction kept perpendicular to bending direction, which is in discordance with overall crack direction inclining to reinforcement direction found by Clark [12, 37] and Ruediger [81].

(b) When the OR-direction is 0°, the predicted value of η_c of 6.0° is closing to the measured value of 5.2°. Therefore, the prediction formula of Eq. (3-3) can be

applied to two-way slabs as well.

(c) The distribution of steel layers affects on the distribution of their corresponding bending moment. Such an effect results in the sequence of crack formation. Generally, steel on surface layer will share more bending moment and form cracks earlier than on perpendicular steel layer.

(d) A decrease of bond-slip stress on perpendicular direction and η_c of TR will result in an increase of crack spacing. These two variables will interact to affect average crack spacing and crack width. This effect will be taken into account in the development of the equations in Chapter 5 and 6.

(e) In this chapter, experimental results verify that a decrease of bond strength of two-way slabs due to perpendicular cracks will result in a significant increase of the average crack width.

Moreover，the direct relationship between curvature and crack width for two-way slabs subjected biaxial bending was testified. This relationship will be applied as an experimental foundation for development of new flexural crack model in Chapter 6.

5   New crack models to calculate crack spacing and width for one-way and two-way slabs

5.1   Introduction

In the last two chapters, variables of TR-cover, -spacing and -direction affecting the behavior of crack pattern, spacing and width were investigated with consideration of restraining influence of TR on intersected cracks. Equation Chapter (Next) Section 1

In this chapter, values of η_c and α_{TR} are predicted by simulating one-way slab-strips test results and these two variables are combined to regard as an influence coefficient of average crack spacing. Another influence coefficient is adopted to assess the reduced restraining influence of TR on crack propagation due to the decreased bond strength in two-way slabs. With these considerations, a new model to evaluate the TR strain is developed by analyzing the interaction of inner forces between TR and surrounding concrete at the cracked section. The proposed crack spacing model is conducted by a comparison of predicted crack spacing between the proposed model and DIN EN1992-1-2011 with the measured results.

Subsequently, based on the proposed TR strain model at the cracked section, a new crack width model is developed to calculate the maximum crack width with consideration of restraining influence of TR. This proposed crack width model is conducted by a comparison of predicted crack width with the measured experimental results in Chapter 7.

5.2   Estimation of the effect of TR on crack spacing

5.2.1   The ratio of cracks intersect TR to all cracks η

It is known from Section 3.3.1 that an inverse relationship between TR-cover and TR-spacing and η_c can be expressed by

$$\eta_c = -0.012 \cdot c_{TR} + 1.085 \tag{5-1}$$

$$\eta_c = -0.0017 \cdot s_{TR} + 0.8477 \quad (l_e \leq s_{TR} \leq 300)[mm] \tag{5-2}$$

where

c_{TR} is TR-cover

s_{TR} is TR-spacing

l_e is the predicted minimum crack spacing according to Bond-slip Mechanism (See Eq. (2-33)).

When c_{TR}=30mm and s_{TR}=100mm, Eq. (5-1)and Eq. (5-2) have an identical value of η_c,

and thus it can be expected to have an intersection of two straight lines. The theoretical approach derived from spatial geometry modeling and its application in engineering. According to the principle of spatial geometry, two equations of straight lines can determine one equation of a plane in 3D coordinate system. This method is used to determine an equation of a plane by utilizing Eq. (5-1)and Eq. (5-2). it is supported the plane equation formation is

$$y = Ax + Bx + C$$

Eq. (5-1)and Eq. (5-2) and their intersection point c_{TR}=30mm and s_{TR}=100mm can determine factors A, B, C by using the MATLAB software. $A = -\frac{353}{27736}$, $B = \frac{5}{48538}$ and $C = 1.0993$. Thus, the plane equation can be expressed as

$$\eta_c = -\frac{353}{27736}c_{TR} + \frac{5}{48538}s_{TR} + 1.0993 \leq 1 \ (c_{TR} \geq 10\text{mm}) \qquad (5\text{-}3)$$

where

c_{TR} is TR-cover;

s_{TR} is TR-spacing.

Table 5-1 test results of one-way slab-strips in Series 1

No.	TR-cover [mm]	TR-spacing [mm]	η_c [%]*		Average crack spacing [mm]		
			Observed values	Predicted values*	Observed values	Predicted by DIN EN 1992-1-2011	Predicted by proposed model
A1C1	7.00	100.00	100.0%	100%	100	132.4(20%)**	109.74(10%)
A2C1	7.60	100.00	100.0%	100%	100	134.7(21%)	109.79(10%)
A3C2	29.00	100.00	60.0%	74%	112	192.9(38%)	125.09(12%)
A4C2	31.00	100.00	78.0%	72%	104	194.5(49%)	125.53(21%)
A5C3	38.10	100.00	63.6%	62%	167	249.3(18%)	148.50(-11%)
A6C3	41.10	100.00	55.0%	59%	161	247.5(21%)	149.06(-7%)
B1C1	6.60	200.00	63.0%	63%	100	129.5(23%)	101.42(1%)
B2C1	10.60	200.00	44.4%	62%	100	134.5(15%)	102.46(2%)
B3C2	32.30	200.00	45.0%	44%	123	195.0(34%)	127.33(4%)
B4C2	31.10	200.00	50.0%	46%	145	193.4(13%)	126.68(-13%)
B5C3	41.50	200.00	26.7%	38%	158	244.4(33%)	148.03(-6%)
B6C3	36.70	200.00	30.7%	42%	137	241.0(50%)	145.66(6%)
C1c2	32.80	300.00	38.4%	52%	130.50	211.6(32%)	132.63(2%)
C2c2	31.20	300.00	30.8%	53%	157.70	206.2(6%)	130.56(-17%)
Average values of errors						28%	1%

* Values of η_c were calculated by Eq.(5-3) and Eq.(5-4);

** Percentage is the difference between predicted and observed crack spacing.

In a view of the actual circumstances, the effect of TR-spacing and TR-cover on crack forming can be so strong that the crack formation, and hence the crack spacing and width are affected by the TR. According to the test results presented in Chapter 3.3, there is a

relationship between TR-spacing and the predicted minimum crack spacing l_e, which is calculated according to DIN 1045-1-2008. Adding boundary conditions into Eq.(5-3), it can be extended to:

$$\text{when } l_e \leq s_{TR} \leq 1.5l_e \quad \rightarrow \quad \eta = \eta_c$$

$$\text{when } s_{TR} > 1.5l_e \quad \rightarrow \quad \eta = \frac{\eta_c}{1 + j_1} \tag{5-4}$$

where j_1 is the correction coefficient of TR-spacing, $j_1 = \frac{1.5 \cdot l_e}{s_{TR}}$,

This equation, named as Model-1, can be used to predict the ratio of TR-induced crack to all cracks, η_c, with consideration of parameters of TR-cover and TR-spacing. With this proposed Model-1, η_c, can be calculated by a given TR-spacing and TR-cover.

Substituting the values of TR-cover and TR-spacing into Eq.(5-4), the values of η can be predicted and are listed in Table 5-1. A comparison between the observed and the predicted ratio of TR to TR-induced cracks in this table is plotted in Figure 5-1, which indicates that the predicted values of η are in good agreement with those obtained from observation. Thus, it indicates that Eq. (5-4) can be utilized to assess the ratio of TR-induced cracks to all cracks with a given TR-spacing and TR-cover.
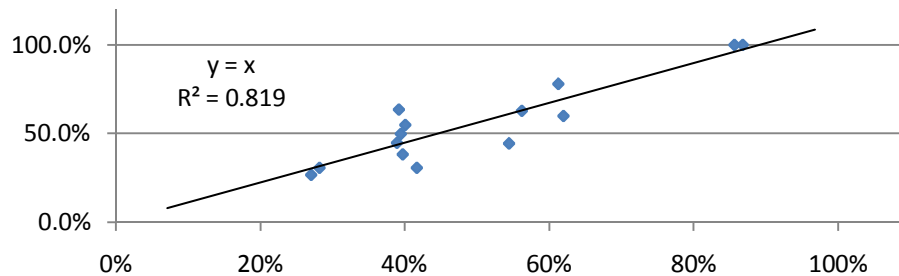

Figure 5-1 Comparison of measured and calculated values of η according to Model-1 (Eq. (5-4))

5.2.2 The effective factor of j

In last section, Model-1 was proposed to calculate the ratio of TR-induced cracks to all cracks, η, with given TR-cover and TR-spacing. According to test results in Section 3.4.2, an increase of TR-inclination results in an increase of the value of η to affect average crack spacing and width. The variable of TR-direction is required to calculate the influence coefficient of j.

According to the geometric relationship between cracks and inclined TR, as shown in Figure 5-2, the higher the ratio of projection of inclined TR, s_d, to TR-spacing the higher the ratio of cracks intersected TR, η, and hence j.

The projection length of inclined TR, s_d, can be expressed as:

$$s_d = \tan \alpha_{TR} \cdot b$$

where

α_{TR} is the angle between TR and its intersected crack, given by Eq. (3-5);

b is the unit width of cross-section, 1000mm;

Furthermore, the percentage of crack intersecting with TR, η_a, can be calculated by the ratio of the projection length of inclined TR to TR-spacing in the following equation:

$$\eta_a = \frac{s_d}{s_{TR}} \qquad (5\text{-}5)$$

where s_{TR} is TR-spacing;

The influence coefficient of TR-direction affecting crack behavior, j, is equal to the product of η (Eq. (5-4)) multiplying η_a (Eq. (5-5)). Thus, j can be expressed as:

$$j = \eta \times \eta_a = \eta \times \frac{s_d}{s_{TR}} = \eta \times \frac{tan\,\alpha_{TR} \cdot b}{s_{TR}} \qquad (5\text{-}6)$$

This equation, named as Model-3, can be used to calculate the percentage of cracks intersecting TR with given parameters of TR-cover, TR-spacing and TR-direction. These cracks appear in the region of TR and hence crack spacing closes to TR-spacing. Thus, the influence coefficient, j, is one of the key parameters of TR affecting crack spacing and width. Model-3 is used to take into account of the influence of TR-parameters on crack spacing and width in the next sections.
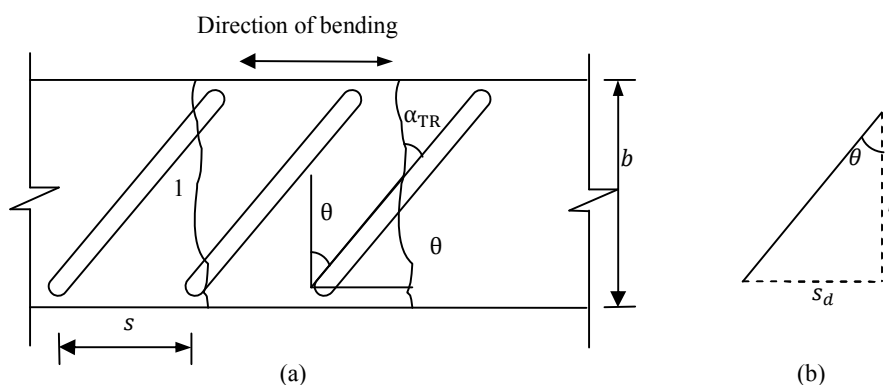
Figure 5-2 Illustration of the influence of increasing TR-inclination on the ratio of TR-intersected cracks to all cracks

5.2.3 New crack spacing model for one-way slabs

According to the test results in Section 3.3 and 3.4, TR parameters, including TR-cover, TR-spacing and TR-direction affect crack pattern and hence the average crack spacing matches TR-spacing. In this section, the crack spacing formula in DIN EN 1992-1-2011 is modified by Model-3 with consideration of the influence of TR on crack spacing. In the limiting case of a one-way slab, with a given TR-spacing (s_{TR}), if the number of TR-induced cracks in the ratio range of j, which predicted by Model-3, cracks in the rest

ratio range (1-j) appeared due to the bond stress between the concrete and the steel. The bond stress produced cracks can be predicted by TR-spacing and average crack spacing formulas in DIN EN 1992-1-2011. Considering the influence of TR on crack spacing, it is more reasonable to view two crack-forming influences of TR as given:

$$S_{r,m} = (1 - \eta) \cdot S_{r,m-EN} + \eta \cdot s_{TR} \cdot j_1 \tag{5-7}$$

where

j_1 is the correction coefficient of TR-spacing;

$S_{r,m-EN}$ is the predicted average crack spacing.

This equation, denominated as Model-4, is used to calculate the average crack spacing of one-way slab considered the influence of TR-induced cracks on crack spacing.

It is worth noting that the predicted maximum crack spacing values were divided by a coefficient of 2 to obtain the average crack spacing values, as given:

$$S_{r,m-EN} = \frac{S_{r,max}}{2} \tag{5-8}$$

Table 5-2 test results of one-way slab-strips of Series 2 according to Model-4 (Eq.(5-7))

No.	TR-cover [mm]	TR-direction [°]	Observed average crack spacing	Predicted crack spacing by DIN EN 1992-1-2011	Predicted crack spacing by Model-4	Error of DIN EN 1992-1-2011	Error of Proposed model
N1w1	30	0	112	211	98.26	88%	-12%
N2w1	31.00	0	104	208	99.35	100%	-4%
N3w2	31.00	22..5	100	207	99.14	107%	-1%
N4w2	33.00	22.5	106	211	101.45	99%	-4%
N5w3	32.00	45	89	217	101.83	143%	14%
N6w3	32.00	45	94	204	99.11	117%	5%
H1w1	31.00	0	129	213	100.35	65%	-22%
H2w1	32.00	0	148	212	100.80	43%	-32%
H3w2	32.00	22.5	128	218	102.05	70%	-20%
H4w2	32.00	22.5	96	223	103.20	132%	7%
H5w3	32.00	45	109	229	104.40	110%	-4%
H6w3	32.00	45	82	227	103.96	176%	27%
L3S2	30.00	0	56	200	141.12	256%	152%
L4S2	34.20	0	86	192	148.75	123%	73%
L3w2	36.00	22..5	52	195	99.82	276%	92%
L4w2	40.00	22.5	51	220	109.21	331%	114%
L5w2	34.00	45	58	207	101.27	257%	75%
L6w2	35.00	45	48	211	102.85	339%	114%
					Average values of errors	158%	32%

Assuming that the average crack spacing in the slab-strips specimen of Series 1 and Series 2 is calculated according to the proposed Model-4 (Eq.(5-7)), values of $S_{r,m}$ can be

obtained and are given in Table 5-1 and Table 5-2 . That these values in good agreement with those obtained experimentally can be seen in Figure 5-3 and Figure 5-4. It indicates that the estimated values of average crack spacing calculated by Model-1 were much closer to the experimental results of Series 1 and 2 with approximately 1% and 32% error, respectively, than the predicted values with DIN EN 1992-1-2011 of approximately 27% and 158% error, respectively. The code's formulas neglect the influence of TR on crack spacing. Thus, it is not difficult to agree that Eq. (5-7) and Eq. (5-8) considered the influence of TR on crack spacing give a better assessment of average crack spacing.
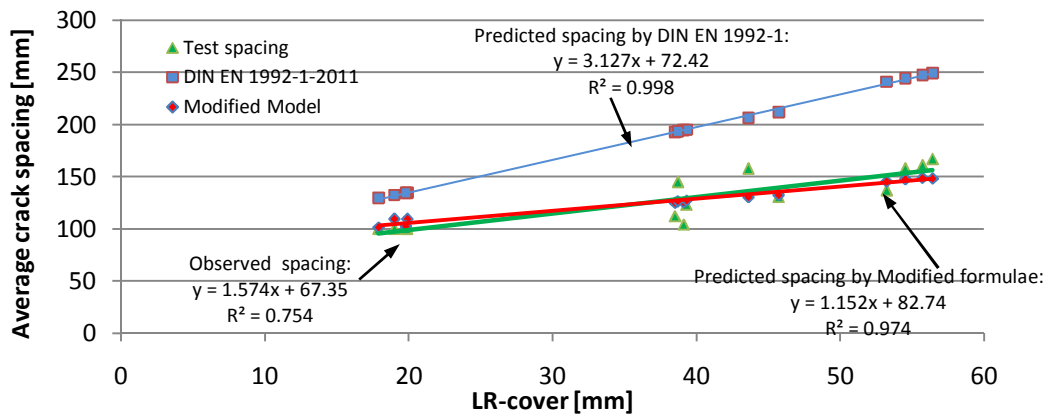
Figure 5-3 Comparison of the predicted average crack spacing in one-way slabs between Model-4 (Eq.(5-7)) and DIN EN 1992-1-2011 with the observed results
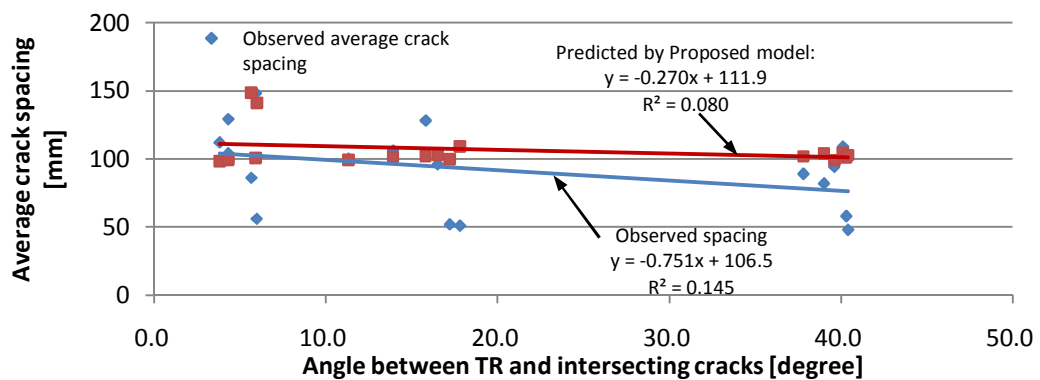
Figure 5-4 Comparison of predicted average crack spacing in one-way slabs between the proposed Model-4 (Eq.(5-7)) and the observed results

5.2.4   New crack spacing model for Two-way slabs

➢ **Influence of TR-cover and -spacing on crack spacing**

It remains to discover the average crack spacing in two-way slabs subjected to biaxial bending in more normal circumstances. Section 4.3.1 proves a similar influence of TR-cover on the ratio of the TR-induced cracks to all cracks for slabs under uniaxial and biaxial bending. Thus, Eq. (5-3) can be used in two-way slabs. In this equation, the concrete cover reinforcement nets are the values of TR-cover in two orthogonal directions.

Hence, η_c in direction of Y-axis (η_{TR_A}) and X-axis (η_{TR_B}) are calculated, respectively.

$$\eta_{TR_A} = -\frac{353}{27736}c_{TR_A} + \frac{5}{48538}S_{TR_A} + 1.0993 \leq 1$$

$$\eta_{TR_B} = -\frac{353}{27736}c_{TR_B} + \frac{5}{48538}S_{TR_B} + 1.0993 \leq 1$$

(5-9)

➢ **The influence of the bending stresses in two orthogonal directions on crack spacing**

According to test results in Section 3.3.2, the bending stresses existed in two orthogonal directions resulted in a decrease of bond strength and thus an increase of crack spacing. The predicted value of crack spacing according to DIN EN 1992-1-2011 (Eq. (2-41)) is increased to consider this influence. The increased value is conducted by utilizing the maximum crack spacing equation (Eq. (2-41)) to calculate average crack spacing in the proposed crack spacing model of two-way slabs.

➢ **The influence of TR-direction on crack spacing**

The influence of TR-direction on crack spacing has been considered by EN DIN 1992-1-2011, whereas the predicted values of average crack spacing have been underestimated. A reason of this underestimation is assumed that the influence of TR on intersected cracks along lines of TR bars is neglected by current codes. Thus, the variable of TR-direction in two-way slabs needs to be considered in current code's Eq. (2-24), and it has been verified from test results in Section 4.3 that this variable can noticeably affect the average crack spacing. It can be observed from Figure 5-5 that such influence behaves in a similar way in the two orthogonal directions. In other words, crack spacing in direction of Y-axis is affected by LR_A and TR_A, as well as in direction of X-axis affected by LR_B and TR_B.

Assuming that the sharp angle between LR and the corresponding crack designated as α_{TR}, the average crack spacing of LR_A and TR_A in direction of Y-axis can be expressed by $S_{rm-Y-LR_A}$ and $S_{rm-Y-TR_A}$ as given:

$$S_{rm-Y-LR_A} = \left(\frac{\cos \alpha_{TR}}{S_{rm-LR_A}} + \frac{\sin \alpha_{TR}}{S_{rm-LR_B}}\right)^{-1}$$

$$S_{rm-Y-TR_A} = \left(\frac{\cos \alpha_{TR}}{S_{rm-TR_A}} + \frac{\sin \alpha_{TR}}{S_{rm-TR_B}}\right)^{-1}$$

(5-10)

where

α_{TR} is the sharp angle between LR and crack given by Eq. (3-4);

S_{rm-LR_A} and S_{rm-LR_B} are the average crack spacing in direction of LR_A and LR_B given by Eq. (2-41).

S_{rm-TR_A} and S_{rm-TR_B} are the average crack spacing in direction of TR_A and TR_B given
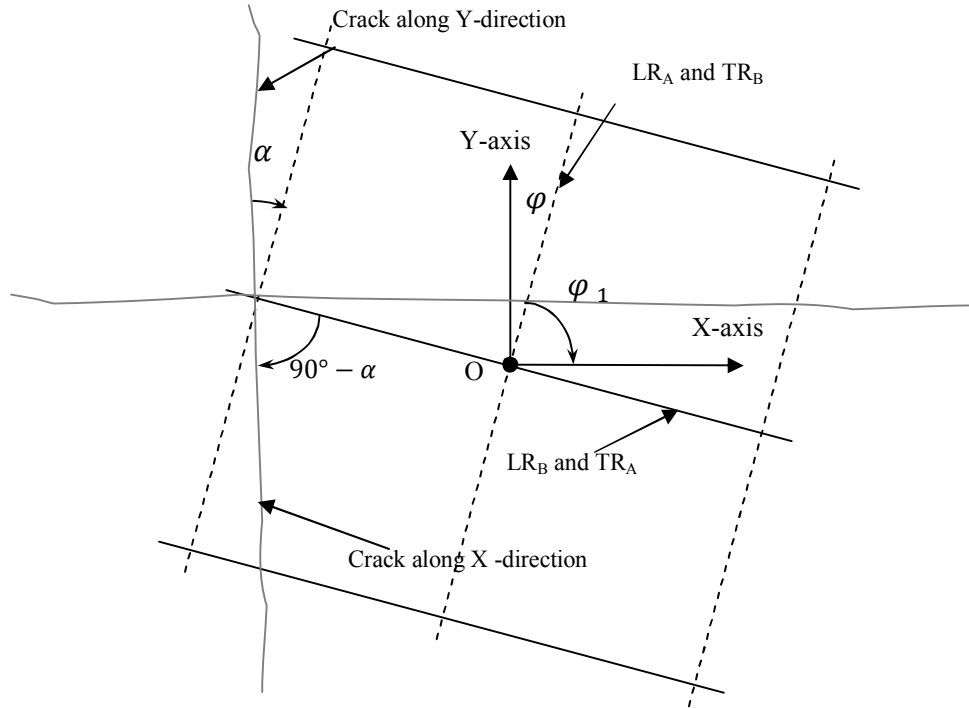
by Eq. (2-41).

Figure 5-5 symbol in formulas. LR$_A$ and LR$_B$ stand for the longitudinal reinforcement in directions of sharp angle with Y-axis and X-axis; TR$_A$ and TR$_B$ stand for the transverse reinforcement in directions of sharp angle with Y-axis and X-axis ; φ stands for the sharp angle between bending direction and reinforcement net; α stands for the sharp angle between cracks and reinforcement, and α_{TR_A} and α_{TR_B} stand for the sharp angle between cracks and TR$_A$ and TR$_B$.

In the same way, the average crack spacing of LR$_B$ and TR$_B$ in direction of X-axis can be expressed by $S_{rm-X-LR_B}$ and $S_{rm-X-TR_B}$ as given:

$$S_{rm-X-LR_B} = \left(\frac{\cos \alpha_{TR}}{S_{rm-LR_B}} + \frac{\sin \alpha_{TR}}{S_{rm-LR_A}} \right)^{-1}$$

$$S_{rm-X-TR_B} = \left(\frac{\cos \alpha_{TR}}{S_{rm-TR_B}} + \frac{\sin \alpha_{TR}}{S_{rm-TR_A}} \right)^{-1}$$

(5-11)

On the basis of crack-forming influences of TR and bond strength of one-way slabs expressed by Eq. (5-7), Eq. (5-8), (5-10) and (5-11) can be used to calculate S_{rm-Y} and S_{rm-X} in two-way slabs as given:

$$S_{rm-Y} = \left(1 - \eta_{TR_A}\right) \cdot S_{rm-Y-LR_A} + \eta_{TR_A} \cdot S_{rm-Y-TR_A}$$

$$(5\text{-}12)$$

$$S_{rm-X} = \left(1 - \eta_{TR_B}\right) \cdot S_{rm-X-LR_B} + \eta_{TR_B} \cdot S_{rm-X-TR_B}$$

Eq. (5-12) is denominated as Model-5 (Eq.(5-12)), and is used to predict average crack spacing for two-way slabs with consideration of TR-parameters.

Assuming that the average crack spacing is calculated by Model-5 (Eq.(5-12)), the predicted values of S_{rm-Y} and S_{rm-X} can be obtained from this model and are given in Table 5-3.

Table 5-3 presents a comparison of average crack spacing between Model-5 (Eq.(5-12)) and DIN EN 1992-1-2011 with the measured experimental values in Section 4.3.2. Results analysis given in Table 5-3 indicates that Model-5 (Eq.(5-12)) provides better estimates for average crack spacing in two-way slabs in different OR-directions.

Table 5-3 test results of two-way slabs

Type	OR-dire ction [°]	Concre te	Observed crack spacing [mm]	A-width [mm]	A-CR [mm³/N]	Average crack spacing [mm]	
						Calculated according to DIN EN 1992-1-2011	Proposed Model-5 (Eq.(5-12))
Type A	0°	NC	100.0	0.09	0.00071	85.68(-14%)	102.7(2%)
		HC	66.7	0.17	0.00065	82.81(34%)	107.0(60%)
		LC	85.7	0.22	0.00085	66.25(2%)	105.4(23%)
	22.5°	NC	150.0	0.14	0.00036	67.44(-45%)	104.0(-30%)
		HC	85.7	0.2	0.00050	62.33(0%)	107.5(26%)
		LC	120.0	0.33	0.00066	62.33(-29%)	106.2(-11%)
	45°	NC	85.7	0.25	0.00108	89.19(-21%)	92.6(29%
		HC	85.7	0.14	0.00099	85.82(-21%)	93.0(30%)
		LC	120.0	0.33	0.00141	66.46(-43%)	93.3(-7%)
Type B	0°	NC	100.0	0.34	0.00113	67.60(-34%)	92.9(12%)
		HC	100.0	0.23	0.00082	61.89(-34%)	93.2(12%)
		LC	100.0	0.48	0.00107	61.89(-33%)	93.5(12%)
	22.5°	NC	75.0	0.1	0.00053	87.78(-17%)	83.4(11%)
		HC	85.7	0.07	0.00050	84.72(-28%)	82.8(-3%)
		LC	75.0	0.16	0.00066	66.70(-16%)	83.9(12%)
	45°	NC	120.0	0.15	0.00066	67.83(-48%)	83.4(-30%)
		HC	100.0	0.15	0.00069	62.68(-38%)	82.9(-17%)
		LC	85.7	0.22	0.00052	62.68(-27%)	83.9(-2%)
	Average values of error					-23%	7%

Figure 5-6 and Figure 5-7 illustrate a comparison of different trend of average crack spacing between Model-5 (Eq.(5-12)) and DIN EN 1992-1-2011 with the measured

experimental results. These two figures indicate that the estimated values of average crack spacing calculated by Model-5 (Eq.(5-12)) are much closer to the experimental results with approximately 7% error than approximately -23% error calculated by a current code. The code's formulas neglect the influence of TR on crack spacing, whereas Model-5 (Eq.(5-12)) is much more rational as it thoroughly considers the influence of TR on crack spacing in two orthogonal directions.
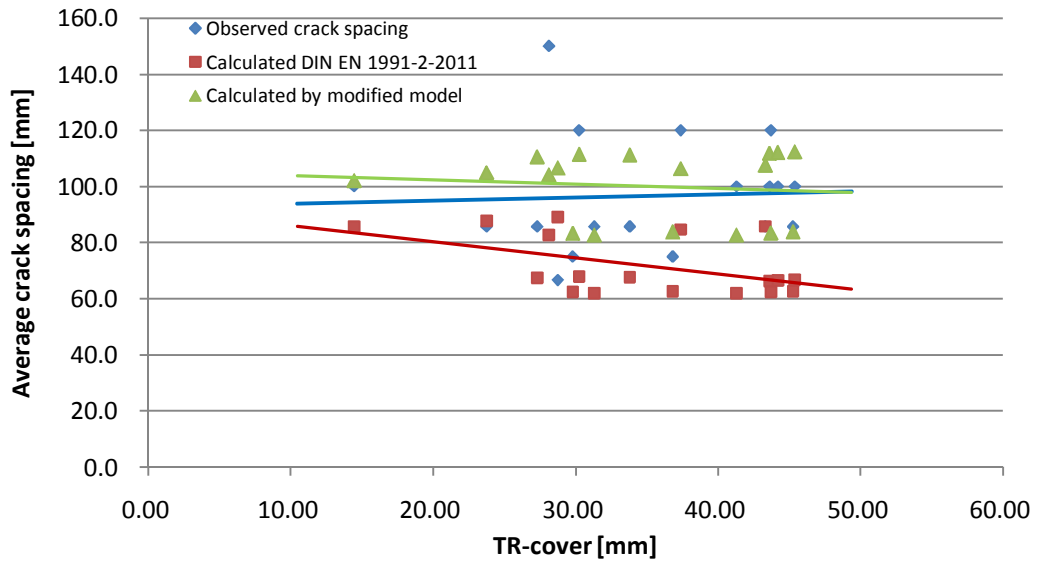

Figure 5-6 Comparison of predicted average crack spacing in two-way slabs between the new proposed model and DIN EN 1991-2-2011 with the measured experimental results
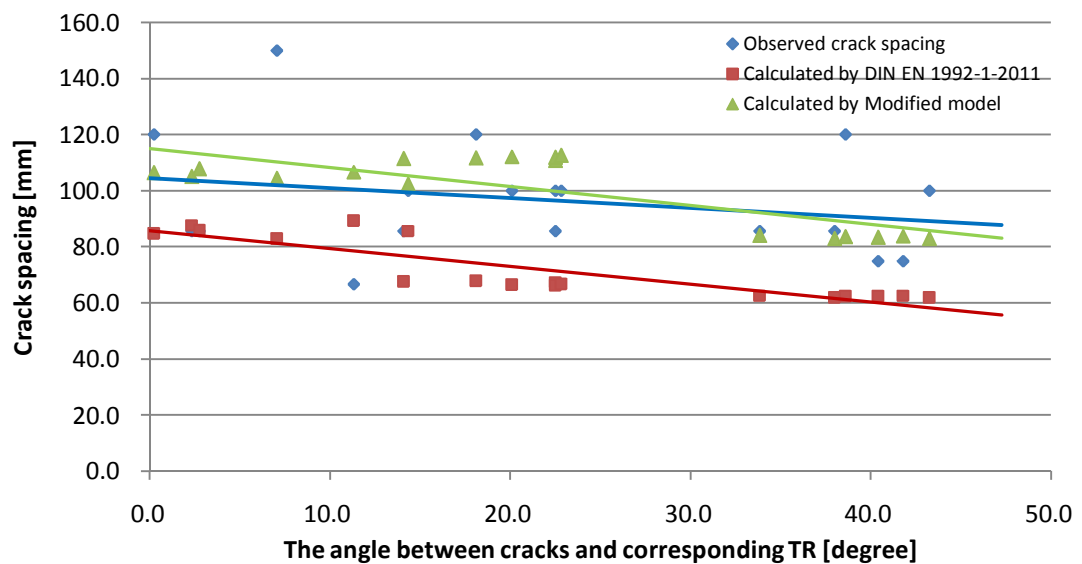
Figure 5-7 Comparison of angle between cracks and corresponding TR (α_{TR}) between the new proposed model and DIN EN 1991-2-2011 with the measured experimental results

5.3 Concrete strain between two adjacent flexural cracks in constant moment region

The average concrete stress calculated between adjacent flexural cracks in constant moment regions is described in this section. According to Hooker's law, the average strain of concrete is equal to the ratio of concrete stress to concrete modulus, as given:

$$\varepsilon_c = \frac{\sigma_c}{E_c} \tag{5-13}$$

where

σ_c is the concrete stress;

E_c is the Young's modulus of concrete.

On the section of tensile zone, the concrete tensile stress equals to the ratio of tensile forces to the effective tension area as given:

$$\sigma_c = \frac{F_c}{A_{c,eff}} \tag{5-14}$$

where

A_{eff} is the effective area of concrete in tension zone, which is calculated according to FIB Model 2010 code (draft).

F_c is the concrete force in tension zone.

According to bond-slip model presented in Section 2.4.1.1, the concrete force generated from the bond stress between the reinforcement and the concrete. Thus, the concrete tensile force equals to the bond stress of concrete around steel bars as

$$F_c = \tau_m \cdot u \cdot S_r \tag{5-15}$$

where

τ_m is the average bond strength between the reinforcement and the surrounding concrete, which is calculated by DIN 1045-1-2008:

$$\tau_m = 2.25 \cdot f_{cm,0.05} \tag{5-16}$$

$$f_{cm,0.05} = 0.7 \cdot f_{cm} \tag{5-17}$$

u is the perimeter of all reinforcement;

$S_{r,max}$ is the crack spacing, such as average or maximum crack spacing.

Substitute Eq. (5-14) and (5-15) to Eq. (5-13):

$$\varepsilon_c = \frac{4 \cdot \tau_m \cdot A_s \cdot S_r}{A_{eff} \cdot E_c \cdot \phi} \tag{5-18}$$

where

ρ_{eff} is the reinforcement ratio in effective tension zone, $\rho_{eff} = \frac{A_s}{A_{eff}}$, and the effective area of concrete tension zone can be simply calculated by $A_{eff} = s_{TR} \cdot c_{TR}$.

ϕ is the diameter of reinforcement.

Eq. (5-18) can be used to calculate the concrete stress, which is induced by bond stress of steel bars between adjacent two cracks. The concrete strain in the crack width equation of DIN EN 1992-1-2011 is substituted by the calculated concrete strain according to Eq. (5-18). This substitution is considered in the following new models to calculate the crack width of slabs under uniaxial and biaxial bending.

5.4 Estimation of the restraining influence of TR on crack width

5.4.1 TR strain model at crack for the slab under uniaxial bending

A study of crack width, as revealed by FIB Model Code 1990, suggests that the value of crack width equaled to strain difference between the tensile steel and the concrete. In other words, as concrete surrounding steel restrained stretched tensile steel, Eq.(2-22) considered the steel strain at the crack under f_{ctm} can be expressed as:

$$\varepsilon_{sr2} = \frac{f_{ctm} \cdot A_{c,eff}}{E_s \cdot A_s} + \frac{f_{ctm}}{E_c} = \varepsilon_{LR} + \varepsilon_c \qquad (5\text{-}19)$$

ε_{sr2} can be also explained by a summation of LR tensile strain on the effective concrete stress area, A_{eff}, and the concrete tensile strain. It indicates that the restraining influence of LR on crack propagation leads to decrease the values of crack width. This relationship is identical with the restraining influence of TR on crack propagation, as shown in Figure 5-8. As the sectional view of (b) indicates that TR behaves in a manner similar with LR, it can be seen from the inner forces of (d) that the equilibrium equation of forces between the TR and the surrounding concrete is described as:

$$F_c = F_{TR} \qquad (5\text{-}20)$$

The equilibrium equation at crack under f_{ctm} is

$$\varepsilon_{TR} \cdot E_s \cdot A_{s-TR,eff} = f_{ctm} \cdot A_{c,eff-TR} \qquad (5\text{-}21)$$

where

ε_{TR} is the strain at crack under f_{ctm};

$A_{s-TR,eff}$ is the effective area of TR in tensile concrete;

$A_{c,eff-TR}$ is the effective concrete area of TR. Because the TR does not bear tension stress from the load, the effective area of TR is limited in TR-cover. In the length of two adjacent TR, s_{TR}, the effective area of tension concrete, $A_{c,eff-TR}$ can be calculated by $A_{c,eff-TR} = s_{TR} \cdot c_{TR}$.

In this case, TR tensile strain ε_{TR} is

$$\varepsilon_{TR} = j \cdot \frac{f_{ctm} \cdot A_{c,eff-TR}}{E_s \cdot A_{s,eff-TR}} \tag{5-22}$$

where

j is the influence coefficient given by Eq.(5-6).

In Figure 5-8, $A_{s,eff-TR}$ is equal to the projection area of A_{s-TR} in bending direction as shown in sectional view (a) and (b), as given by:

$$A_{s,eff-TR} = \eta_a \cdot \frac{A_{s-TR}}{\sin(\alpha_{TR})} \tag{5-23}$$

and α_{TR} is the angle between cracks and the TR, given by Eq. (3-5).

$$\begin{aligned} \text{when } 0 \le \theta \le \alpha_{TR,k}, \qquad \alpha_{TR} = \alpha_{TR,k} \\ \text{when } \alpha_{TR,k} < \theta \le 90°, \qquad \alpha_{TR} = \theta - \alpha_{TR,k} \end{aligned} \tag{5-24}$$

where

θ is the angle between the TR and the normal direction of bending.

Substitute Eq.(5-23) into Eq.(5-24), and solving for ε_{TR}, obtains

$$\varepsilon_{TR} = j \cdot \frac{f_{ctm} \cdot A_{c,eff-TR} \cdot \sin \alpha_{TR}}{E_s \cdot A_{s-TR}} \tag{5-25}$$

where $A_{c,eff-TR}$ is the effective concrete area of TR.

when the effective TR ratio is $\rho_{eff-TR} = \frac{A_{s-TR}}{A_{s,eff-TR}}$,

$$\varepsilon_{TR} = j \cdot \frac{f_{ctm}}{E_s \cdot \rho_{s,eff-TR}} \tag{5-26}$$

With Eq.(5-25), it is convenient to find out the direct relationship between ε_{TR} and $A_{c,eff-TR}$, α_{TR} and f_{ctm}.

The average concrete strain in tensile zone between the adjacent two cracks can be divided into two parts: one is the concrete strain induced by bond stress from steel bar, ε_c; the other is the concrete strain induced by TR in the area of TR-cover, ε_{TR}. Thus the average strain in concrete between adjacent cracks, ε_{cm}, is equal to the summation of ε_c and ε_{TR}:

$$\varepsilon_{cm} = \varepsilon_c + \varepsilon_{TR} = \frac{4 \cdot \tau_m \cdot S_r \cdot A_s}{E_c \cdot A_{eff} \cdot \phi} + j \cdot \frac{f_{ctm}}{E_s \cdot \rho_{s,eff-TR}} \tag{5-27}$$

where ε_c is the average concrete strain between two adjacent flexural cracks, as given by Eq.(5-18).

Thus, it can be obtained from the proposed average strain model that there is a direct relationship between TR strain at crack and TR-cover，α_{TR} and f_{ctm}. This relationship is identical with test results in Section 3.3 and 3.4. So far, the discussion has been confined to one-way slab-strips under uniaxial bending by means of superposition relationship of

114

two-way slabs between two orthogonal directions. The average strain model of two-way slabs subjected to biaxial pure bending will be further analyzed in the next sections.

(a) Top view

(b) Sectional view: 1-1

(c) Sectional view: 2-2

(d) Inner force diagram
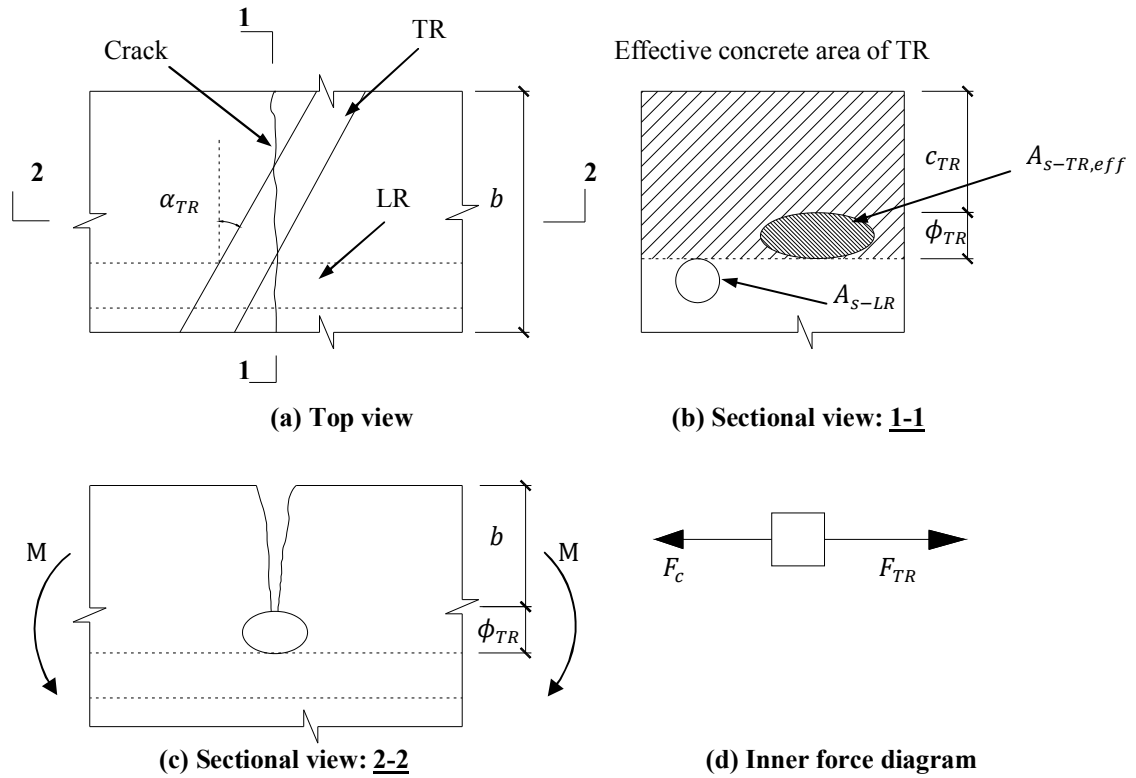
Figure 5-8: Illustration of TR restraining crack width

5.4.2   TR strain model at crack for the slab under biaxial bending

Figure 5-9 illustrates a superposition relationship of two-way slabs subjected to biaxial pure bending between two orthogonal directions. According to the average concrete strain in tensile zone for one-way slabs, which was expressed by Eq.(5-27), the average concrete tensile strain between adjacent cracks along X-axis, ε_{cm-X}, is equal to the summation of the concrete strain induced by the bond stress from LR$_A$, ε_{c-LR_A} and the concrete strain induced by TR$_A$, ε_{TR}. Thus ε_{cm-X} can be expressed as:

$$\varepsilon_{cm-X} = \varepsilon_{c-LR_A} + \varepsilon_{TR_A} \tag{5-28}$$

In the same way, along Y-axis, the equation of ε_{cm-Y} is：

$$\varepsilon_{cm-Y} = \varepsilon_{c-LR_B} + \varepsilon_{TR_B} \tag{5-29}$$

where

ε_{c-LR_A} and ε_{c-LR_B} are the concrete strain between two adjacent flexural cracks of LR$_A$ and LR$_B$ in Y-axis and X-axis, according to Eq. (5-18),

$$\varepsilon_{c-LR_A} = \frac{4 \cdot \tau_m \cdot A_{s,eff-LR_A} \cdot S_{r-LR_A}}{\phi_{s,eff-LR_A} \cdot E_c \cdot A_{c,eff-LR_A}} \tag{5-30}$$

$$\varepsilon_{c-LR_B} = \frac{4 \cdot \tau_m \cdot A_{s,eff-LR_B} \cdot S_{r-LR_B}}{\phi_{s,eff-LR_B} \cdot E_c \cdot A_{c,eff-LR_B}} \tag{5-31}$$

where

$A_{s,eff-LR_A}$ and $A_{s,eff-LR_B}$ are the projection area of LR$_A$ and LR$_B$ in directions of Y-axis and X-axis;

$A_{c,eff-LR_A}$ and $A_{c,eff-LR_B}$ are the effective concrete areas in directions of Y-axis and X-axis, as given by Eq.(5-23).

$\phi_{s,eff-LR_A}$ and $\phi_{s,eff-LR_B}$ are the equivalent diameters of LR$_A$ and LR$_B$ in directions of Y-axis and X-axis, which are calculated by the projection area of LR$_A$ and LR$_B$ in directions of Y-axis and X-axis, as given by:

$$\phi_{s,eff-LR_A} = 2 \cdot \sqrt{\frac{A_{s,eff-LR_A}}{\pi \cdot n}} \tag{5-32}$$

$$\phi_{s,eff-LR_B} = 2 \cdot \sqrt{\frac{A_{s,eff-LR_B}}{\pi \cdot n}} \tag{5-33}$$

According to the equation of TR strain in concrete tension zone in Eq.(5-25), the TR$_A$ and TR$_B$ strain in concrete tension zone (ε_{TR_A} and ε_{TR_B}) along directions of X-axis and Y-axis can be expressed as:

$$\varepsilon_{TR_A} = j_{TR_A} \cdot \frac{f_{ctm} \cdot A_{c,eff-TR_A} \cdot \sin(\alpha_{TR})}{E_s \cdot A_{s-TR_A}} \tag{5-34}$$

$$\varepsilon_{TR_B} = j_{TR_B} \cdot \frac{f_{ctm} \cdot A_{c,eff-TR_B} \cdot \sin(\alpha_{TR})}{E_s \cdot A_{s-TR_B}} \tag{5-35}$$

where

α_{TR} is the sharp angle between crack and TR, as shown in Figure 5-9;

A_{s-TR_A} and A_{s-TR_B} are the reinforcement area of LR$_B$ or TR$_A$;

$A_{c,eff-TR_B}$ or $A_{c,eff-LR_A}$ is the effective concrete area in the direction of Y-axis;

$A_{c,eff-TR_A}$ or $A_{c,eff-LR_B}$ is the effective concrete area in the direction of X-axis;

j_{TR_A} and j_{TR_B} are the influence coefficients of TR-spacing, TR-cover and TR-direction, which were given by Eq. (5-6) and were modified in two-way slabs as:

$$j_{TR_A} = \eta_{TR_A} \cdot \eta_{a-TR_A} = \eta_{c-TR_A} \cdot \frac{\tan(\alpha_{TR}) \cdot b_X}{s_{TR_A}}$$

$$j_{TR_B} = \eta_{TR_B} \cdot \eta_{a-TR_B} = \eta_{c-TR_B} \cdot \frac{\tan(\alpha_{TR}) \cdot b_Y}{s_{TR_B}} \tag{5-36}$$

116
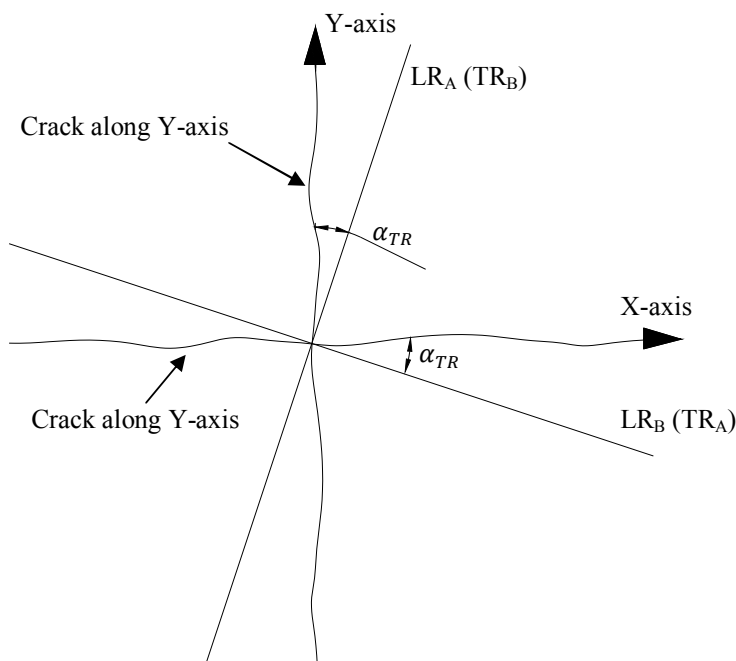
Figure 5-9: Illustration of sign convention in two-way slabs. LR$_A$ and LR$_B$ stand for the longitudinal reinforcement in directions of sharp angle with Y-axis and X-axis; TR$_A$ and TR$_B$ stand for the transverse reinforcement in directions of sharp angle with Y-axis and X-axis.

5.5   New crack width model for slabs under uniaxial and biaxial bending

Original crack width formulas in current codes, such as FIB Model Code 2010 (draft), DIN EN 1992-1-2011 and DIN1045-1-2008, neglect the influence of TR-parameters. However, the experimental results verify that TR has a significant restraining influence on crack spacing and width. Thus, Eq. (2-22) must be heavily modified by adding the TR strain at crack, ε_{TR}, in the average concrete strain between adjacent cracks, ε_{cm}.

5.5.1   New crack width model for the slab under uniaxial bending

The maximum crack width is:

$$w_k = S_{r,max} \cdot (\varepsilon_s - \varepsilon_{cm}) \qquad (5\text{-}37)$$

where

$S_{r,max}$ is the maximum crack spacing given by Model-4, according to Eq.(5-7). In this equation, $S_{r,max-EN}$ is calculated by the predicted maximum crack spacing equation according to Eq. (2-41);

ε_{cm} is the average concrete strain between adjacent cracks, which is obtained by Eq. (5-27).

Eq. (5-37) is denominated as Model-6. It is used to predict the maximum crack width for the slab under uniaxial bending considering the influence of TR-parameters. The

maximum crack spacing is predicted by Model-4 (Eq.**(5-7)**).

5.5.2 New crack width model for the slab under biaxial bending

The maximum crack width is:

$$w_{k-Y} = 2 \cdot S_{r,m-Y} \cdot (\varepsilon_{s-LR_A} - j_3 \cdot \varepsilon_{cm-X})$$
$$w_{k-X} = 2 \cdot S_{r,m-X} \cdot (\varepsilon_{s-LR_B} - j_3 \cdot \varepsilon_{cm-Y})$$

(5-38)

where

$S_{r,m-Y}$ and $S_{r,m-X}$ are the average crack spacing in Y-axis and X-axis, as given by Model-5, according to Eq. (5-12);

ε_{cm-X} and ε_{cm-Y} are the average concrete strain between adjacent cracks in X-axis and Y-axis, given by Eq. (5-28) and (5-29).

$j_3 = 0.32$ is the coefficient value considering the influence of decreased bond strength on reduced steel stress at crack. According to the test results in Section 4.4 (refer to Page 97), comparing to one-way slabs-strips, the Cracking Rate of average crack width of the slab under biaxial bending increases by 32%. The reason of the increase is due to the decreased bond stress between the LR and the sounding concrete leads to a decrease of the average concrete strain in the tension zone, ε_{cm}. Thus, a coefficient value of 0.32 is used to consider the decrease of average concrete strain in directions of X-axis and Y-axis, ε_{cm-X} and ε_{cm-Y}.

The average crack spacing turns into the maximum crack spacing by a coefficient of 2. According the bond-slip mechanism, this increase coefficient is 1.35. Adding the influence of decrease of bond strength of the slab under biaxial stress on increasing crack spacing is taken into account as a coefficient of 1.5 according the test results in Section 4.3.2. Therefore, the coefficient of 1.35 grows to 2.

Eq. (5-38) is denominated as Model-7. It is used to predict the maximum crack width for two-way slabs considering the influence of TR-parameters and bending stress in two orthogonal directions based on formulas in DIN EN 1992-1-2011. The maximum crack spacing is predicted by Model-5 (Eq.**(5-12)**).

So far, the proposed crack width models were established for one-way slabs, Model-6 (Eq.(5-37)) and for two-way slabs, Model-7 (Eq.(5-38)). A further comparison of the predicted crack width between the proposed models and current codes with the measured results will be conducted in Chapter 7.

5.6 Chapter Summary

In last two chapters, the influence of TR on crack spacing and width in one-way and two-way slabs has been investigated. A series of new analytical expressions are recommended for one-way and two-way slabs subjected to uniaxial and biaxial bending.

The proposed methods not only consider the influence of TR-cover, TR-spacing and TR-direction on TR forming cracks, but also consider the influence of TR-parameters on restraining influence and hence crack spacing and width.

The main conclusions can be summarized as follows:

- Model-1 and Model-2 in Section 5.2.1 give a good estimate for the ratio of TR-induced cracks to all cracks with a given TR-cover, TR-spacing and TR-direction in one-way and two-way slabs.

- Model-4 (Eq.(5-7)) gives a good prediction for the slab under uniaxial bending by considering the influence of TR-induced cracks with a given TR-cover, -spacing and –direction. The predicted values calculated by this model are much closer to the experimental results with approximately from 1% to 27% error than those values calculated by DIN EN 1992-1-2011 with approximately from 32% to 158% error.

- For two-way slabs, an additional influence of TR in directions of X-axis and Y-axis is considered by the superposition method in two orthogonal directions. Because the formulas in DIN EN 1992-1-2011 neglect the influence of TR on crack spacing, Model-5 (Eq.(5-12)) can better predict the average crack spacing with only approximately 7% error than that using DIN EN 1992-1-2011 with approximately -23% errors.

- The proposed average TR strain model at crack under f_{ctm} in one-way and two-way slabs is presented in Section 5.3.2.

- Models-6 (Eq.(5-37)) and Model-7 (Eq.(5-38)) for one-way and two-way slabs are respectively presented by considering the additional restraining influence of TR on crack width in two orthogonal directions. A comparison of the predicted crack width between the proposed models and current codes with the measured results is conducted in Chapter 7.

6 Theoretical modeling of flexural crack

6.1 Introduction

Crack width prediction models in current codes, such as FIB Model Code 1990, DIN EN 1992-1-2011 and DIN 1045-1-2008, are mostly developed based on Bond-slip mechanism or empirical equations for RC elements subjected to uniaxial tensile forces. The crack behavior of reinforced concrete slabs under the bending is different from that of tensile forces. A special focus is given to calculate the height of compressive zones at cracked and uncracked sections and the average bending strains of flexural TR-elements. Because of the analysis results and the direct relationship between the curvature and the crack width, a specific flexural crack model is developed for slabs under uniaxial and biaxial bending by using the geometric relationship between the curvature and the average strain of flexural TR- elements. The proposed model takes into account of the influence of TR on crack spacing and width according to the equations in Chapter 5.

This proposed flexural crack width model will be analyzed by a comparison of crack width between the predicted values in the proposed models and current codes and the measured values in Chapter 7. Equation Chapter (Next) Section 1

6.2 An assumption model for the evaluation of stresses

The following assumptions are the basis of equations and calculations of the proposed models in this Chapter:

(a) Steel and concrete are assumed to be homogeneous and isotropic;

(b) Concrete stresses due to shrinkage and temperature changes are negligible;

(c) The bond strength varies probably along steel bars and is calculated according to DIN1045-1-2008, as described in Section 6.3.

(d) Plane sections remain plane at all sections before the first cracking and at cracked section afterwards.

6.3 The height of compressive zone between adjacent cracks

The flexural stress distribution between two adjacent cracks in a RC element subjected to a moment is shown in Figure 6-1. The height of the neutral axis denominated as h_1, (see Figure 6-1 (a)), closes to the peak of the flexure crack at the cracked section. With the increased distance away from a crack, the concrete in tensile zone bears the tension force and the neutral axis is closer to the tensile surface, in this case, the height of the neutral axis is a variable, which is denominated as h_i (see Figure 6-1 (b)). In the mid section

between adjacent cracks, the neutral axis is the closest point to tensile surface, the height of the neutral axis at the mid section is denominated as h_m (see Figure 6-1 (b)). Therefore, the average height of the neutral axis between adjacent cracks h_c equals to the average value of the summation of i values of the height of the neutral axis:

$$h_c = \frac{h_1 + h_2 + \cdots + h_{i-1} + h_i}{i} \tag{6-1}$$

The curve of the neutral axis closes to a cosine curve. Therefore, the average value of the height of neutral axis between adjacent cracks approximately equals to half of h_1 and h_m:

$$h_{c,ave} = \frac{h_1 + h_m}{2} \tag{6-2}$$
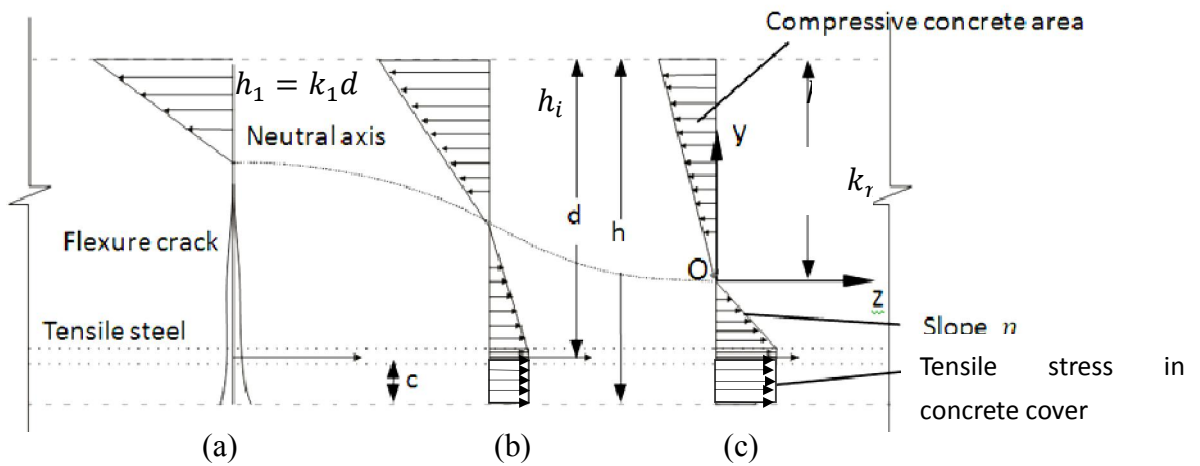
Figure 6-1: Model of stress distribution in the concrete; (a) cracked section; (b) uncracked section; (c) mid section between adjacent cracks.

6.3.1 The height of the neutral axis at crack section h_1 for a cracked RC element

Under the service load, as concrete stress is less than approximately $0.5 \cdot f_c$, the steel stress has not reached the yield point. Both materials concrete and steel behave elastically or very nearly so (see (a) to (c) in Figure 6-1). This situation commonly appears in structures under normal conditions and loads. At this stage, it is assumed that tension cracks have been generated to the neutral axis and that cross sections before bending are plane in the deformed member. The height of the neutral axis is calculated according to the standard elastic theory. To determine the location of the neutral axis, the moment of tension area about the neutral axis is equal to the moment of the compression area[106]. This relationship is shown in Figure 6-2. In this figure, at cracked section (Figure 6-2 (a)), the cross sectional area of the steel is transformed to the concrete area according to the Young's modulus ratio of the steel to the concrete, $n = \frac{E_s}{E_c}$. This relationship can be expressed as:

$$b\frac{k_1 d}{2} - nA_s(d - k_1 d) = 0 \qquad (6\text{-}3)$$

where

$k_1 d$ is the height of compressive zone, as shown in Figure 6-2 (a);

b is the width of cross-section;

$n = \dfrac{E_s}{E_c}$ is the Young's modulus ratio of the steel to the concrete.

Having obtained $k_1 d$ to solve this Eq.(6-3), a positive value of solution can be used to determine the moment of inertia at the cracked section. The solution is

$$k_1 = \sqrt{(\rho n)^2 + 2\rho n} - \rho n \qquad (6\text{-}4)$$

where ρ is the reinforcement ratio of cross-section

Eq. (6-4) is adopted according to ACI 318-2008 to calculate the height of effective compressive zone.

(a) cracked section   **(b) uncracked section**
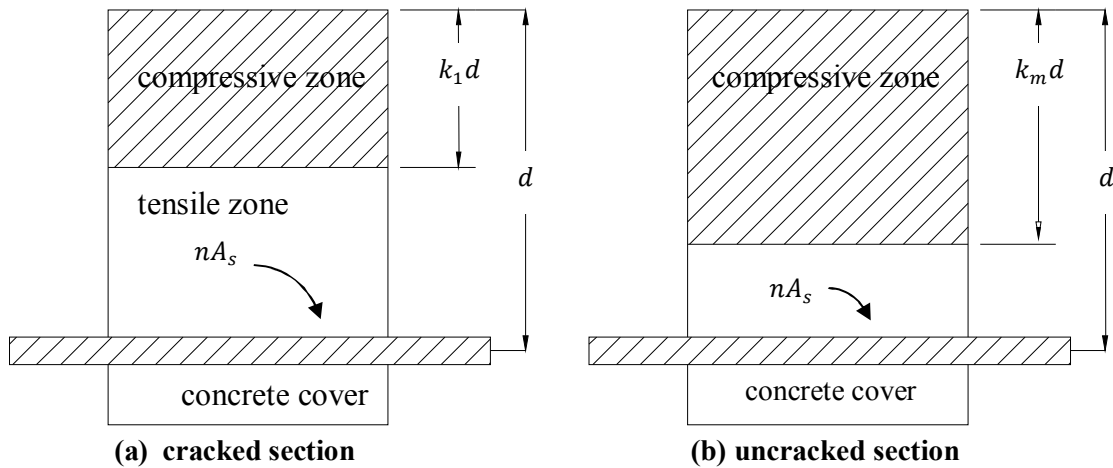
Figure 6-2: The cross sectional area of the steel transformed to the concrete area at (a) the cracked section (see Figure 6-1 (a)) and (b) uncracked section (see Figure 6-1 (c)).

6.3.2 The height of the neutral axis at the uncracked section h_m for a cracked RC element

According to a moment equilibrium, the moment of the tension area about the axis is set equal to the moment of the compression area (as shown in Figure 6-1(c) and Figure 6-2 (b)), which gives:

$$b \cdot k_m \cdot d \frac{k_m d}{2} - b \cdot \frac{\left(d - k_m d - \frac{\phi}{2}\right)^2}{2} - n \cdot A_s \cdot (d - k_m d) - b \cdot c$$

$$\cdot \left(d - k_m d + \frac{c}{2} + \frac{\phi}{2}\right) = 0 \tag{6-5}$$

where

b is the width of a RC element. The width of one-way slab-strips is 300mm and the width of two-way slab is 1200mm;

d is the distance from the extreme compression fiber to the centroid of longitudinal tension reinforcement;

k_m is the effective length factor in the compression zone at the mid section of adjacent cracks;

ϕ is the diameter of reinforcement;

c is the button concrete cover; and $n = \frac{E_s}{E_c}$ is the ratio of steel elastic modulus to concrete elastic modulus. The expression of factor k_m is derived from Eq.(6-5),

$$k_m = \frac{1}{4} \cdot \frac{4bd^2 - 4bd\phi + b\phi^2 + 8nA_s d + 8bcd + 4bc^2 + 4bc\phi}{d(2bd - \phi b + 2nA_s + 2cb)} \tag{6-6}$$

The height of compressive zone at the mid cross-section between adjacent cracks is calculated by Eq. (6-6). Then substituting Eq.(6-4) and (6-6) into Eq. (6-2), the average height of neutral axis between adjacent cracks can be given as:

$$h_{c,ave} = \frac{k_1 d + k_m d}{2} \tag{6-7}$$

The average height of neutral axis between adjacent cracks can be calculated by Eq.(6-7). This average height is an important factor to calculate the average inertia moment of the cross-section between two adjacent cracks in Section 6.6.

6.4 The curvature of the RC element subjected to pure bending

6.4.1 Estimation of the effective inertia moment

Almost all flexural RC-members show cracking under service loads. After cracking, the bending stiffness decreases along the direction of bending moment. In a cracked section, the bending stiffness B can be calculated by:

$$B = E_{cs}I \tag{6-8}$$

where I is the average inertia moment of all RC elements. E_{cs} is the Young's modulus with the weighted average value of the concrete and reinforcement areas.

$$E_{cs} = \frac{A - A_s}{A} E_c + \frac{A_s}{A} \cdot E_s \qquad (6-9)$$

In a cracked RC element, the bending stiffness has its largest value at the uncracked region B_{ut} and the smallest value at the cracked section B_{cr}. The average moment of inertia for all RC elements depends on the load intensity between the gross moment of inertia I_{ut} at the uncracked section and the inertia moment I_{cr} at the cracked section. Many other researchers have proposed various formulas to predict the effective moment of inertia I_e. For example, Branson [107] developed the following equation to compute the effective inertia moment of a cracked RC-beam and one-way slabs based on the experimental results.

$$I_e = \left(\frac{M_{cr}}{M_a}\right)^3 I_{ut} + \left(1 - \left(\frac{M_{cr}}{M_a}\right)^3\right) I_{cr} \leq I_{ut} \qquad (6-10)$$

where

M_a is the maximum bending moment;

M_{cr} is the cracking moment of a RC-member;

I_{cr} is the inertia moment at the cracked section;

I_{ut} is the gross inertia moment at the uncracked section. This formula has been recommended by ACI 318-2008 [108] to calculate short term deflections. Branson's formula has been further developed by many other researchers, such as Al Zaid 1991[109], Al shaik Al zaid 1993[110], Grossmann [111] and Rangan 1982[104]. Among these researchers, Rangans' formulas [104] computed the effective moment of inertia I_e, which is based on test results of a number of simply supported rectangular beams and one way slabs under service load. The proposed formulas by Rangan [104] is given:

If $n\rho > 0.0045$,

$$\frac{I_e}{bd^3} = 0.1599\sqrt{n\rho} \qquad (6-11)$$

If $n\rho \leq 0.045$,

$$\frac{I_e}{bd^3} = 0.0019/n\rho \qquad (6-12)$$

where

$n = \frac{E_s}{E_c}$ is the modular ratio of the steel and the concrete;

ρ is the effective reinforcement ratio in the effective tension zone of the concrete, $\rho = \frac{A_s}{A_{c,eff}}$.

The above equations of I_e have been adopted by the Standard Association of Australia

(AS3600(2001)) to develop the formulas of Eq. (6-11) and (6-12). These two equations calculate the span-to-effective depth ratio in order to control the deflection of the beam and the one-way slab. Moreover, the average curvature, κ can be calculated by the average effective moment of inertia, I_e,

$$\kappa = \frac{M_a}{E_{cs} \cdot I_e} \qquad (6\text{-}13)$$

6.4.2 Examination of the predicted curvature accuracy in two models with the measured curvature values

The code of ACI 318-2008 and Rangan's formulas [104] are used to calculate the bending stiffness of selected specimens. The curvatures of selected 12 one-way slab-strips and 9 two-way slabs were calculated and are presented in Table 6-1 and

Table 6-2. It is necessary to note that for two-way slabs, the projection area of reinforcement in the direction of X-axis was adopted to calculate the effective reinforcement area, $A_{s,eff-X}$.

Table 6-1 Comparison between the predicted and the measured curvatures of one-way slab specimens in Series 1

No.	Curvatures (1/mm)			Predicted percentage errors	
	Measured values	Predicted by ACI code	Predicted by Rangan	ACI code	Rangan
A1C1	1.48E-05	1.36E-05	7.39E-06	-8%	-50%
A2C1	1.30E-05	1.38E-05	7.56E-06	6%	-42%
A3C2	1.43E-05	1.23E-05	8.03E-06	-14%	-44%
A4C2	1.44E-05	1.24E-05	8.16E-06	-14%	-43%
A5C3	7.78E-06	8.09E-06	6.95E-06	4%	-11%
A6C3	7.95E-06	8.05E-06	6.83E-06	1%	-14%
B1C1	1.62E-05	1.34E-05	7.18E-06	-17%	-56%
B2C1	1.42E-05	1.37E-05	7.54E-06	-3%	-47%
B3C2	1.56E-05	1.13E-05	7.47E-06	-27%	-52%
B4C2	1.22E-05	1.13E-05	7.35E-06	-7%	-40%
B5C3	1.00E-05	7.97E-06	6.63E-06	-20%	-34%
B6C3	1.00E-05	7.89E-06	6.42E-06	-21%	-36%
Average percentage errors				-10%	-39%

Table 6-2 Comparison between the predicted and the measured curvatures of two-way slab specimens

No.	Curvature (1/mm)			Predicted percentage errors	
	Measured values	Predicted by ACI code	Predicted by Rangan	ACI code	Rangan
P01	1.81E-05	2.28E-05	2.23E-05	26%	23%
P02	3.24E-05	3.18E-05	3.26E-05	-2%	1%

P03	2.60E-05	1.83E-05	2.24E-05	-30%	-14%
P04	7.82E-06	1.05E-05	3.11E-05	-37%	86%
P05	1.64E-05	1.35E-05	3.02E-05	-17%	85%
P06	3.91E-06	1.31E-05	2.63E-05	236%	572%
P07	3.91E-05	3.40E-05	4.34E-05	-13%	11%
P08	4.30E-05	4.10E-05	4.72E-05	-5%	10%
P09	1.64E-05	4.70E-05	5.08E-05	187%	210%
Average absolute percentage errors				38%	109%

Figure 6-3 and Figure 6-4 present comparisons of the trend of curvatures between the ACI code's and Rangans' formulas [104] (Eq.(6-11) and (6-12)) and the measured results. These two figures indicate that the average curvature values estimated by using the ACI code's formula were much closer to the experimental results with approximately from -10% to 38% percentage error than that using the Rangans' formulas [104] (Eq.(6-11) and (6-12)) with approximately -34% to 109% percentage error. The comparison result shows that the ACI code's formula (Eq.(6-10)) provides a better estimate for the effective inertia moment, and hence the average curvature for slabs under uniaxial and biaxial bending. Therefore, the formula of ACI318-2008 (Eq.(6-10)) is adopted in the new model of Section 6.6.2. It has to be noted that for slab under uniaxial and biaxial bending, the calculated values of curvature according to ACI code's formula (Eq.(6-10)) is recommended to multiply a unified factor of 1.15.
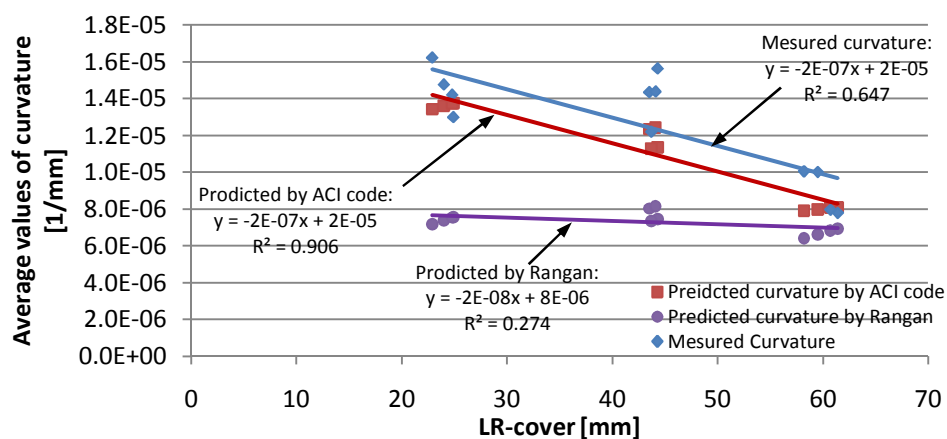
Figure 6-3: Comparison between the predicted and the measured curvature for the slab under uniaxial bending
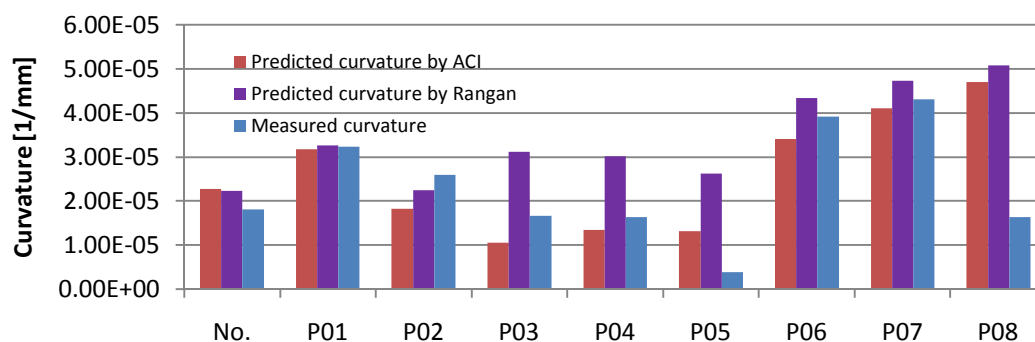
Figure 6-4: Comparison between the predicted and the measured curvature for the slab under biaxial bending

6.5 The average bending strain of a RC element subjected to pure bending

According to the assumptions in Section 6.2, two materials steel and concrete are assumed as homogeneous and isotropic, which is in accordance with the plane-section assumption. When a RC element is subjected to a pure bending moment M as shown in Figure 6-5, the upper surface of the RC element bears a tension force and the lower surface of RC element bears compressive force, as shown in Figure 6-5. In the figure, The average bending strain $\varepsilon_{f,m}$ of the whole flexural RC element is equal to ratio of extension length to the original length, it can be given by:

$$\varepsilon_{f,m} = \frac{\Delta l}{l} \tag{6-14}$$

where

Δl is the extension length of the concrete tensile fiber in the tension zone of the whole flexural RC element after cracking;

l is the original length of the whole flexural RC element before RC element cracking.

The extension length of the tensile fiber Δl is equal to the difference value between the length of the tensile fiber after cracking and that of before cracking, Δl can be calculate by

$$\Delta l = (\rho + h')\theta - l = \rho\theta + h'\theta - l \tag{6-15}$$

where

θ is the rotation angle (see Figure 6-5);

ρ is the radius of curvature;

and h' is the average height of tensile zone,

$$h' = h - h_{c,ave} = h - \frac{h_1 + h_m}{2} \tag{6-16}$$

According to the geometric relationship $l = \rho\theta$, Eq.(6-15) can be expressed as:

$$\Delta l = h'\theta = h'\frac{l}{\rho} = h'l\kappa \tag{6-17}$$

where

κ is the average curvature of the RC element;

Substituting Eq. (6-17) into Eq.(6-14), the average strain of the whole RC element is

$$\varepsilon_{f,m} = \frac{\Delta l}{l} = h'\kappa \qquad (6\text{-}18)$$

Eq.(6-18) presents a relationship between the average bending strain, $\varepsilon_{f,m}$ and the curvature of the whole flexural RC element. The average height of tensile zone between adjacent cracks is considered in the equation. This equation provides an approach to calculate the crack width with the curvature and the average height of tensile zone. It is presented in next sections.
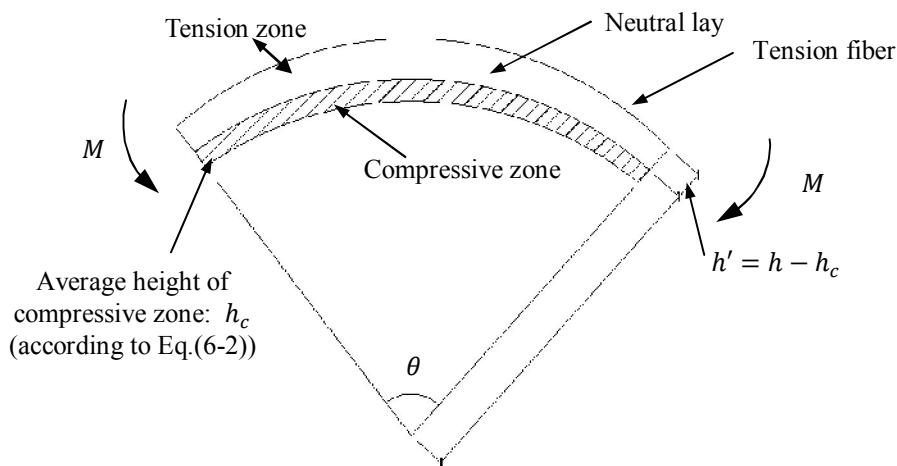
Figure 6-5: The geometric relationship of a RC element subjected to pure bending moment

6.6 Determination of the maximum flexure crack width

6.6.1 Maximum crack width model

The relationship between the average bending strain and the curvature of the whole flexural RC element is presented in the last section. In this section, the whole flexural RC element is transformed to the individual element between two adjacent cracks. In other words, the length of a RC element l is recognized as the length of adjacent cracks, which is equal to crack spacing, S_r. The average extension length between these two adjacent cracks, Δl, is equal to the summation of flexural crack width (w_f) and the concrete extension, $\varepsilon_{cm} \cdot S_r$. This summation relationship can be expressed by:

$$\Delta l = w_f + \varepsilon_{cm} \cdot S_r \qquad (6\text{-}19)$$

where

ε_{cm} is the average bending strain of tension fiber on the tensile concrete surface between adjacent cracks;

Then substituting Eq. (6-19) into Eq. (6-14), the full length of RC element, l is replaced by the crack spacing, S_r. Thus the average bending strain on tensile surface, $\varepsilon_{f,m}$ can be obtained from:

$$\varepsilon_{f,m} = \frac{\Delta l}{l} = \frac{w_f + \varepsilon_{cm} \cdot S_r}{S_r} \tag{6-20}$$

The crack width w_f can be derived from Eq. (6-20):

$$w_f = S_r \cdot (\varepsilon_{f,m} - \varepsilon_{cm}) \tag{6-21}$$

According to Eq.(6-21), the flexural crack width can be calculated with the RC element curvature, which can be obtained from experimental results or calculated by predicted values of curvature according to Eq.(6-13). Eq. (6-21) shows a basic formation to predict the crack width based on the average bending strain of tension fiber on the concrete tensile surface. This expression is the basic form of the new flexural crack model, which is presented in the next two sections.

6.6.2 Flexural maximum crack width model for the slab under uniaxial bending

In the limited cases of one-way slabs, with a given size of cross section and reinforcement layout, Eq. (6-21) can be used to calculate the maximum crack width as given:

$$w_{f,max} = S_{r,max} \cdot (1.15 \cdot \varepsilon_{f,m} - \varepsilon_{cm}) \tag{6-22}$$

Where

$\varepsilon_{f,m}$ is the average flexural strain on tensile surface given by Eq. (6-20);

$S_{r,max}$ is the maximum crack spacing given by Eq.(5-7);

$S_{r,max-EN}$ is calculated by the predicted maximum crack spacing given by Eq. (2-41);

ε_{cm} is the average steel strain at crack under f_{ctm}, which is obtained by Eq.(5-27).

The coefficient of 1.15 in Eq.(6-22) derives from the ratio of the measured to the computed bending stiffness according to the comparison results in Section 6.4.2 (refer to Page 125) for the slab under uniaxial bending.

Substituting Eq.(6-18) into (6-22), the maximum crack width can be expressed as:

$$w_{max} = S_{r,max} \cdot (1.15 \cdot h_m{}'\kappa_m - \varepsilon_{cm}) \tag{6-23}$$

where

$h_m{}'$ is the average height of tensile zone, given by Eq.(6-16);

κ_m is the predicted curvature, given by Eq. (6-13).

Eq. (6-23) is denominated as Model-8. This model is used to predict the maximum crack width of the slab under uniaxial bending based on the relationship between the crack width and the average bending strain of flexural TR-element. The maximum crack spacing was predicted by Model-4 (Eq.(5-7)).

6.6.3 Flexural crack width model for slabs under biaxial bending

The maximum crack width for the slab under biaxial bending is derived from the Eq.(6-23). The crack width of this slab is calculated in two orthogonal directions of Y-axis and X-axis respectively (see Figure 5-5). The crack width equation can be expressed by:

$$w_{k-Y} = 2 \cdot S_{r,m-Y} \cdot (\varepsilon_{f,m-X} - j_3 \cdot \varepsilon_{cm-X})$$
$$w_{k-X} = 2 \cdot S_{r,m-X} \cdot (\varepsilon_{f,m-Y} - j_3 \cdot \varepsilon_{cm-Y})$$

(6-24)

where

$S_{r,m-Y}$ and $S_{r,m-X}$ are the average crack spacing in Y-axis and X-axis, as given by Eq. (5-12);

The coefficient of 2 takes into account of two variables. One is the extension of the average crack spacing to the maximum crack spacing. The other is the enlarged crack spacing resulted from decreased bond strength. This coefficient is in accordance with that of Model-7 (see Eq.(5-38)).

$\varepsilon_{f,m-Y}$ and $\varepsilon_{f,m-X}$ are the average flexural strains on tensile surface;

ε_{cm-X} and ε_{cm-Y} are steel strains at the crack under f_{ctm} in two directions of X-axis and Y-axis, given by Eq. (5-28) and (5-29);

j_3 is the coefficient of decreased bond strength between the steel and the concrete due to the bending stress in two orthogonal direction. $j_3=0.32$ is in accordance with that of Eq. (5-38) in Section 5.5.2.

Substituting Eq. (6-18) into (6-24), the maximum crack width can be expressed as:

$$w_{k-Y} = 2 \cdot S_{r,m-Y} \cdot (h_{m-X}{}' \kappa_{m-X} - j_3 \cdot \varepsilon_{cm-X})$$
$$w_{k-X} = 2 \cdot S_{r,m-X} \cdot (h_{m-Y}{}' \kappa_{m-Y} - j_3 \cdot \varepsilon_{cm-Y})$$

(6-25)

h_{m-X}' and h_{m-Y}' is the average height of tensile zone, given by Eq. (6-16);

κ_{m-Y} and κ_{m-Y} is the predicted curvature, given by Eq. (6-13).

Eq. (6-25) is denominated as Model-9. It is used to predict the maximum crack width of the slab under biaxial bending based on the relationship between the crack width and the average bending strain of flexural TR-element in two directions. The maximum crack spacing was predicted by Model-5 (Eq.(5-12)).

So far, the proposed crack width Models-8 was established for the slab under uniaxial bending (see Eq.(6-23)) and Model-9 (Eq.(6-25)) for the slab under biaxial bending (see Eq.(6-25)). By using flexural crack Model-8and Model-9, the crack width and the whole curvature of a RC element, and hence their bending stiffness at the cracked state are connected directly. A further comparison of the predicted crack width between Model-8 and Model-9 and current codes and the measured experimental results will be conducted in Chapter 7.

7 Examples of calculating the crack spacing and width and comparisons between the predicted and the measured values

7.1 Introduction

In Chapter 5, Model-4 (Eq.(5-7)) and Model-5 (Eq.(5-12)) to the predict the average crack spacing and Model-6 (Eq.(5-37)) and Model-7 (Eq.(5-38)) to predict the maximum crack width are developed for slabs under uniaxial and biaxial bending with consideration of restraining influence of TR. In Chapter 6, Model-8 (Eq.(6-23)) and Model-9 (Eq.(6-25)) are developed for slabs under uniaxial and biaxial bending by means of a theoretical analysis of the average bending strain of flexural TR-elements.

In this chapter, two examples of calculating the crack spacing and width of a selected one-way slab specimen and a two-way slab specimen are presented in Section 7.2 and 7.3.

Subsequently, based on the experimental results of 33 slab-strips, 9 test slabs and more than 8000 recorded crack spacing and width, a comparison is conducted for the predicted crack width between the proposed models and current codes, such as FIB Model Code 2010 (draft), DIN EN 1992-1-2011, DIN 1045-1-2008 and ACI 318-2008.

7.2 Examples of calculating crack spacing and width according to models proposed in Chapter 5

7.2.1 Example of calculating crack spacing and width for the slab under uniaxial bending according to Model-4 and Model-6

The slab-strip of A3c2 has the dimensions of (see Figure 3-1) b=300mm, h=200mm, and d=156.5mm, and is reinforced with three ϕ=10mm longitudinal reinforcement bars with 38.5 concrete cover ($c = 38.5$mm) so that A_s=235.6mm². The concrete cylinder strength $f_c{}'$ is 30.1MPa. The specimen has ϕ=8mm transverse reinforcements with 100mm spacing ($s_{TR} = 100$mm), and 29mm clear concrete cover ($c_{TR} = 29$mm) as shown in Figure 7-1. It is subjected to the load of 35kN in each cylinder, and longitudinal reinforcement bearing stress of 345 MPa. More details of geometrical sizes and reinforcement of A3c1 refer to Table 3-2. According to equations in EN DIN 1991-1-2011, $f_{ctm} = 2.5$ MPa, $E_c = 27000$ MPa, and E_s=201053 MPa. The symbols of variables and their values are listed in Table 7-1.
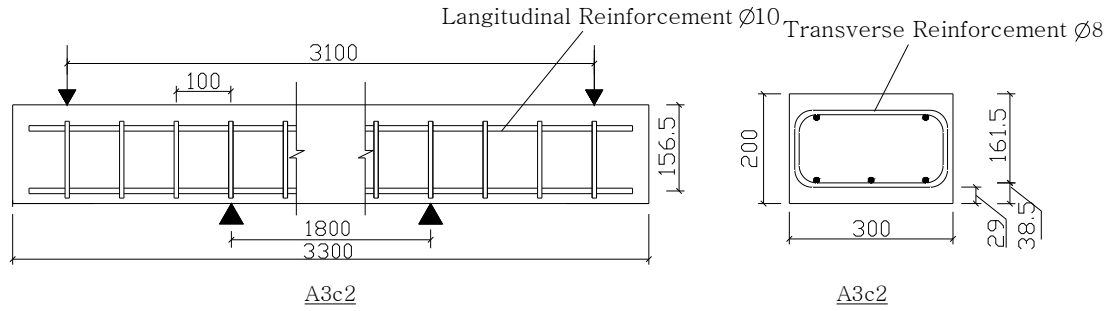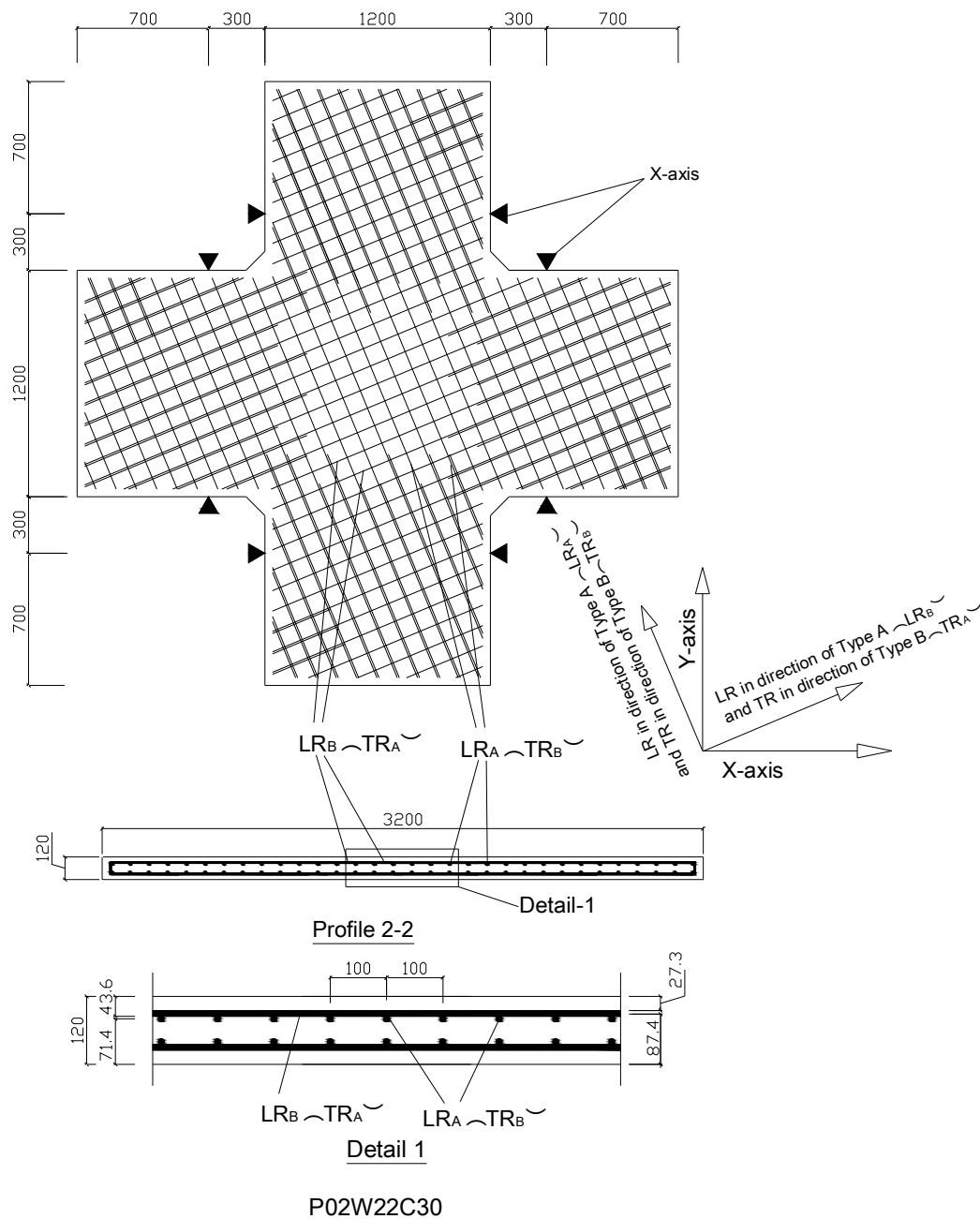
Figure 7-1: The reinforcement layout of test specimen A3c2 of Example 7.2.1

Table 7-1: Symbols of Variables and their values of Example 7.2.1

symbols	Variables	Values
b	Width of section	300 mm
c_{TR}	TR-cover	29 mm
c	LR-cover	38.5 mm
s_{TR}	TR-spacing	100mm
α_{TR}	The angle between the TR and TR-induced crack	5.7°
d	Effective height of section	156.5 mm
kd	The effective height of compressive zone	24.9 mm
ϕ	The diameter of LR	10 mm
ϕ_{TR}	The diameter of TR	8 mm
A_s	The area of LR	235.6 mm^2
f_c'	Concrete cylinder strength	30.1 Mpa
f_{ctm}	Concrete tensile strength	2.5 Mpa
E_c	Young's modulus of concrete	27000 Mpa
E_s	Young's modulus of steel	201053 Mpa

➢ **Calculation of the crack spacing according to Model-4**

Firstly, determine the ratio of TR-induced cracks to all cracks, η, from Eq.(5-3),

$$\eta = -\frac{353}{27736}c_{TR} + \frac{5}{48538}s_{TR} + 1.0993$$

$$= -\frac{353}{27736} \times 29 + \frac{5}{48538} \times 100 + 1.0993 = 74\%$$

The coefficient of TR-intersected cracks, j, can be calculated by η and α_{TR} according to Eq.(5-6). Here α_{TR}=5.7° and η=74%. Thus j is

$$j = \eta \times \frac{tan\,\alpha_{TR} \cdot b}{s_{TR}} = 74\% \times \frac{tan\,5.7° \cdot 300}{100} = 22\%$$

The reinforcement ratio of the effective cross-section, ρ is

$$\rho = \frac{A_s}{bd} = \frac{235.6}{300 \times 156.5} = 0.005$$

The coefficient of the height of compressive zone k_1 can be calculated by Eq. (6-4)

according to ACI318-2001:

$$k_1 = \sqrt{(\rho n)^2 + 2\rho n} - \rho n$$

$$= \sqrt{0.005 \times 3)^2 + 2 \times 0.005 \times 3} - 0.005 \times 3 = 0.16$$

Thus, the height of compressive zone x is

$$x = k_1 d = 0.16 \times 156.5 = 29.4 \text{ mm}$$

According to Figure 2-17 in Chapter 2, the effective height of tension zone $h_{c,eff}$ is the larger value chosen from $2.5 \cdot (c + \phi/2)$ and $\frac{h-x}{3}$, which are calculated as:

$$2.5 \cdot \left(c + \frac{\phi}{2}\right) = 2.5 \cdot \left(29 + \frac{10}{2}\right) = 108.8 \text{ mm}$$

$$\frac{h-x}{3} = \frac{200 - 29.4}{2} = 58.4 \text{ mm}$$

Thus, the effective height of tension zone is $h_{c,eff} = \frac{h-x}{3} = 58.4$ mm.

The reinforcement ratio in the effective concrete tensile zone, $\rho_{s,eff}$ can be calculated as:

$$\rho_{s,eff} = \frac{A_s}{b \cdot h_{c,eff}} = \frac{235.6}{300 \cdot 58.4} = 1.35\%$$

The minimum crack spacing l_e is given by Eq. (2-37),

$$l_e = \frac{\phi}{7.2 \cdot \rho_{s,eff}} = \frac{10}{7.2 \times 0.0135} = 82.6 \text{ mm}$$

The coefficient of j_1 is given by Eq. (5-4),

$$j_1 = \frac{1.5 \cdot l_e}{s_{TR}} = \frac{123.9}{100} = 1.24$$

The predicted maximum crack spacing, $S_{r,max}$, according to DIN EN 1992-1-2011, is given by Eq. (2-41),

$$S_{r,max} = 3.4 \cdot c + 0.425 \cdot 0.8 \cdot 0.5 \cdot \frac{\phi}{\rho_{s,eff}}$$

$$= 3.4 \cdot 38.5 + \frac{0.425 \cdot 0.8 \cdot 0.5 \cdot 10}{0.0135} = 257.2 \text{ mm}$$

The predicted average crack spacing, which equals to the maximum crack spacing divided by a coefficient of "2", is

$$S_{r,m-EN} = \frac{1}{2} \times S_{r,max} = \frac{1}{2} \cdot 257.2 = 125.1 \text{ mm}$$

The average crack spacing considered crack-forming influences of TR, is given by Eq.(5-7) of Model-4,

$$S_{r,m} = (1 - 0.74) \cdot 125.1 + 0.74 \cdot 100 \cdot \left(\frac{123.9}{100}\right) = 125.1\text{mm}$$

The maximum crack spacing, $S_{r,max}$ is

$$S_{r,max} = (1 - 0.74) \cdot 257.2 + 0.74 \cdot 100 \cdot \left(\frac{123.9}{100}\right) = 158.5\text{mm}$$

➢ **Calculation of the maximum crack width according to Model-6**

The effective projection area of TR in the bending direction, from Eq.(5-23), is

$$A_{s,eff-TR} = \eta_a \cdot \frac{A_{s-TR}}{\sin \alpha_{TR}} = \eta_a \times \frac{3.14 \cdot 4^2}{\sin 5.7°} = 506.1 \text{ mm}^2$$

and the effective reinforcement ratio in the effective concrete area of TR gives,

$$\rho_{s,eff-TR} = \frac{A_{s,eff-TR}}{A_{c,eff-TR}} = \frac{506.1}{29 \times 100} = 17.4\%$$

TR strains at crack, from Eq.(5-25), is

$$\varepsilon_{TR} = j \cdot \frac{f_{ctm} \cdot A_{c,eff-TR} \cdot \sin \alpha_{TR}}{E_s \cdot A_{s-TR}} = 1.04 \times \frac{2.5}{201053 \times 0.174} = 6.72 \times 10^{-5}$$

The average bond strength is calculated by Eq. (5-16) and (5-17),

$$\tau_m = 2.25 \cdot f_{cm,0.05} = 2.25 \times 0.7 \times 2.27 = 3.57 \text{ MPa}$$

The average concrete strain between adjacent flexural cracks, ε_c can be expressed by Eq.(5-18),

$$\varepsilon_c = \frac{4 \cdot \tau_m \cdot A_s \cdot S_{r,max}}{A_{eff} \cdot E_c \cdot \phi} = \frac{4 \times 3.57 \times 235.6 \times 158.5}{17509 \times 27000 \times 10} = 1.13 \times 10^{-4}$$

Hence, as given by Eq.(5-27),

$$\varepsilon_{cm} = \varepsilon_{TR} + \varepsilon_c = 6.72 \times 10^{-5} + 1.13 \times 10^{-4} = 1.80 \times 10^{-4}$$

and the maximum crack width can be calculated by Eq. (5-37) of Model-6,

$$w_k = S_{r,max} \cdot (\varepsilon_s - \varepsilon_{cm}) = 158.5 \times \left(\frac{345}{27000} - 1.43 \times 10^{-5} - 1.11 \times 10^{-4}\right)$$
$$= 0.25 \text{ mm}$$

Thus, the predicted maximum crack width of A3c2 is 0.25mm. The comparison results of cracking width between the predicted and measured values (referring to Table 3-3, the maximum crack width of A3c2 is 0.21mm) indicate that the prediction of crack width for the slab under uniaxial bending overestimates about 19%.

7.2.2 Example of calculating crack spacing and width for the slab under biaxial bending according to Model-5 and Model-7

The specimen P02W22C30 (refers to Section 4.2 and Table 4-1) has the dimensions of (see Figure 3-1) b=1200mm, h=120mm. Considering different concrete covers in the orthogonal direction ($\varphi = 22.5°$), the measured values of crack spacing and width of this slab specimen are analyzed in Y-axis (direction of LR_A) and X-axis (direction LR_B)

respectively. This specimen has a concrete cover of LR$_A$, $c_{LR_A}(c_{TR_B})$=43.6mm, and LR$_B$, $c_{LR_B}(c_{TR_A})$=27.3mm; and an effective depth of height, $d_{LR_A}(d_{TR_B})$=71.4mm and $d_{LR_B}(d_{TR_A})$=87.7mm, as shown in Figure 7-2. It reinforces with ϕ=10mm bars at 10cm spacing in both directions, so that A_s=942.5mm^2, and the effective reinforcement area in X-axis and Y-axis is $A_{s,eff}$=123.4mm^2. The concrete cylinder strength f_c' is 27.6MPa. The specimen is subjected to a load of 40kN in each cylinder in the orthogonal direction, and thus $M = 5.23 \times 10^7$ N·m . More details of the geometrical sizes and the reinforcement of P02W22C30 refer to Table 4-1. According to equations in EN DIN 1991-1-2011, $f_{ctm} = 3.33$ MPa, $E_s = 201053$ MPa and E_c=30457 MPa. The symbols of variables and their values are listed in Table 7-2.

Figure 7-2: The reinforcement layout of test specimen P02W22C30 of Example 7.2.2

Table 7-2: Symbols of Variables and their values of Example 7.2.2

symbols	Varables	Values
b	Width of slab section	1200 mm
h	Height of slab section	120 mm
c_{LR_A}	LR-cover in direction of LR$_A$	43.6 mm
c_{LR_B}	LR-cover in direction of LR$_B$	27.3 mm
c_{TR_A}	TR-cover in direction of TR$_A$	27.3 mm
c_{TR_B}	TR-cover in direction of TR$_B$	43.6 mm
s_{TR}	TR-spacing in two directions	100 mm
α_{TR}	The angle between the TR and TR-induced crack	5.7°
d_Y	Effective height of section on direction of the Y-axis	87.7 mm
d_X	Effective height of section on direction of the X-axis	71.4 mm
x_{TR_B}	The effective height of compressive zone in the direction of TR$_B$	28.5 mm
x_{TR_A}	The effective height of compressive zone in the direction of TR$_A$	32.3 mm
ϕ	The diameter of LR	10 mm
A_s	The area of LR	235.6 mm^2
$A_{s,eff-Y}$	the projection of 12 reinforcement area in overall width on direction of the Y-axis	1231.4 mm^2
$A_{s,eff-X}$	The projection of 12 reinforcement area on direction of the X-axis	1231.4 mm^2
$\rho_{s,eff-Y}$	The reinforcement ratio of the effective reinforcement area in overall width on direction of the Y-axis	0.0144
$\rho_{s,eff-X}$	The reinforcement ratio of the effective reinforcement area in overall width on direction of the X-axis	0.0117
$I_{e,Y}$	The effective inertia moment on direction of the Y-axis	21512806 mm^4
$I_{e,X}$	The effective inertia moment on direction of the Y-axis	21512806 mm^4
f'_c	Concrete cylinder strength	27.6 Mpa
f_{ctm}	Concrete tensile strength	3.33 Mpa
E_c	Young's modulus of concrete	30457 Mpa
E_s	Young's modulus of steel	201053 Mpa

➢ **Redistribution of the moment in two orthogonal directions**

It is noted that the longitudinal reinforcements of P02W22C30 are calculated in Y-axis and X-axis, defined as LR$_B$ and LR$_A$, respectively. The moment in two directions is calculated according to equations in Section 4.2.3.

As the orthogonal reinforcement net to bending direction at angle of 22.5°, reinforcement areas in two directions of LR$_A$ and LR$_B$ (A_s) are calculated with the projection in Y-axis, $A_{s,eff-X}$, and X-axis, $A_{s,eff-Y}$. The projection areas of reinforcement in X-axis and Y-axis are

$$A_{s,eff-X} = 12 \times 3.14 \times 5^2 \times \cos(67.5°) + 12 \times 3.14 \times 5^2 \times \cos(22.5°)$$
$$= 1231.4 \text{ mm}^2$$

$$A_{s,eff-Y} = 12 \times 3.14 \times 5^2 \times \cos(22.5°) + 12 \times 3.14 \times 5^2 \times \cos(67.5°)$$
$$= 1231.4 \text{ mm}^2$$

and Young's modulus ratio of the steel to the concrete is

$$n = E_s/E_c = 201053/30457 = 6.60$$

and the reinforcement ratio of overall cross section in X-axis and Y-axis, is

$$\rho_{s,eff-Y} = \frac{1231.4}{71.4 \times 1200} = 0.0144$$

$$\rho_{s,eff-X} = \frac{1231.4}{87.7 \times 1200} = 0.0117$$

$$n\rho_{s,eff-Y} = 6.60 \cdot 0.0144 = 0.0949 > 0.045$$

$$n\rho_{s,eff-X} = 6.60 \cdot 0.0117 = 0.0772 > 0.045$$

The effective moment of inertia I_e, from Eq. (6-11) and (6-12), is

$$I_{e,Y} = 0.1599 \times \sqrt{0.0949} \times 1200 \times 71.4^3 = 21512806 \text{ mm}^4$$

$$I_{e,X} = 0.1599 \times \sqrt{0.0772} \times 1200 \times 87.7^3 = 35970835 \text{ mm}^4$$

Then substituting the computed values of $I_{e,X}$ and $I_{e,Y}$ into Eq. (4-5),

$$\therefore \frac{M_X}{M_Y} = \frac{I_{e,X}}{I_{e,Y}} = \frac{35790834}{21512806} = 1.67$$

$$M_X + M_Y = 1.67 \times M_Y + M_Y = 5.23 \times 10^7 \text{ N·m}$$

And solving for M_X and M_Y,

$$M_X = 32722438.1 \text{ N·m}$$

$$M_Y = 19570061.9 \text{ N·m}$$

➤ **Calculation of the crack spacing according to Model-5**

Firstly, determining the ratios of TR-induced cracks to all cracks in both directions, η_{TR_A} and η_{TR_B}, from Eq.(5-9), are

$$\eta_{TR_A} = -\frac{353}{27736}c_{TR_A} + \frac{5}{48538}s_{TR} + 1.0993$$

$$= -\frac{353}{27736} \times 27.3 + \frac{5}{48538} \times 100 + 1.0993 = 76\%$$

$$\eta_{TR_B} = -\frac{353}{27736}c_{TR_B} + \frac{5}{48538}s_{TR} + 1.0993$$

$$= -\frac{353}{27736} \times 43.6 + \frac{5}{48538} \times 100 + 1.0993 = 55\%$$

when TR-direction is 22.5°, α_{TR}=22.5-5.7°=16.5°, then from Eq.(5-36), j_{TR_A} and j_{TR_B} are

$$j_{TR_A} = \eta_{TR_A} \times \frac{\tan\alpha_{TR} \cdot b_X}{s_{TR_A}} = 0.76 \times \frac{\tan 22.5° \times 1200}{100} = 276\%$$

$$j_{TR_B} = \eta_{TR_B} \times \frac{\tan\alpha_{TR} \cdot b_Y}{s_{TR_B}} = 0.55 \times \frac{\tan 22.5° \times 1200}{100} = 201\%$$

The reinforcement ratios in the effective concrete tensile zone in both directions, from Figure 2-17 in Chapter 2, are

$$\rho_{s,eff-LR_A} = \frac{A_{s-LR_A}}{b \cdot h_{c,eff-LR_A}} = \frac{942.8}{1200 \cdot 30.5} = 2.57\%$$

$$\rho_{s,eff-LR_B} = \frac{A_{s-LR_B}}{b \cdot h_{c,eff-LR_B}} = \frac{942.8}{1200 \cdot 29.2} = 2.69\%$$

The maximum crack width in both directions according to EN DIN 1992-1-2011, from Eq. (2-41), are

$$S_{r,m-LR_A} = S_{r,m-TR_B} = 3.4 \cdot 43.6 + \frac{0.425 \cdot 0.8 \cdot 0.5 \cdot 10}{0.0257} = 214.3\text{mm}$$

$$S_{r,m-LR_B} = S_{r,m-TR_A} = 3.4 \cdot 27.3 + \frac{0.425 \cdot 0.8 \cdot 0.5 \cdot 10}{0.0269} = 156.1\text{mm}$$

According to Eq.(2-42), as

$$5 \times \left(c_{LR_A} + \frac{\phi}{2}\right) = 243\text{mm} > 214.3 \text{ mm}$$

$$5 \times \left(c_{LR_B} + \frac{\phi}{2}\right) = 161.5\text{mm} > 156.1 \ mm$$

Hence,

$$S_{r,m-LR_A} = S_{r,m-TR_B} = 1.3 \times (120 - 28.5) = 119.0\text{mm}$$

$$S_{r,m-LR_B} = S_{r,m-TR_A} = 1.3 \times (120 - 32.3) = 114.0\text{mm}$$

The average crack spacing of LR_A and TR_A in the direction of the Y-axis can be obtained from Eq.(5-10),

$$S_{rm-Y-LR_A} = \left(\frac{\cos 22.5°}{119.0} + \frac{\sin 22.5°}{114.0}\right)^{-1} = 113.7 \text{ mm}$$

$$S_{rm-Y-TR_A} = \left(\frac{\cos 22.5°}{114.0} + \frac{\sin 22.5°}{119.0}\right)^{-1} = 109.7 \text{ mm}$$

The average crack spacing of LR_B and TR_B in the direction of X-axis can be calculated by Eq.(5-11),

$$S_{rm-X-LR_B} = \left(\frac{\cos 22.5°}{114.0} + \frac{\sin 22.5°}{119.0}\right)^{-1} = 109.7 \text{ mm}$$

$$S_{rm-X-TR_B} = \left(\frac{\cos 22.5°}{119.0} + \frac{\sin 22.5°}{114.0}\right)^{-1} = 113.7 \text{ mm}$$

The average crack spacing with consideration of the influence of TR-induced cracks in directions of TR_A and TR_B, from Eq.(5-12), are:

$$S_{rm-Y} = (1 - 0.76) \times 113.7 + 0.76 \times 109.7 = 110.6 \text{ mm}$$

$$S_{rm-X} = (1 - 0.55) \times 109.7 + 0.55 \times 113.7 = 111.9 \text{ mm}$$

➢ **Calculation of the maximum crack width according to Model-7**

The depths of compressive zone in both directions, from Eq. (6-4), are

$$x_{TR_A} = 0.40 \times 71.4 = 28.5 \text{ mm}$$

$$x_{TR_B} = 0.37 \times 87.7 = 32.3 \text{ mm}$$

The effective depths of tension zone, from Figure 2-17, are

$$h_{c,eff-LR_A} = h_{c,eff-TR_B} = \frac{120 - 28.5}{3} = 30.5 \text{ mm}$$

$$h_{c,eff-LR_B} = h_{c,eff-TR_A} = \frac{120 - 32.3}{3} = 29.2 \text{ mm}$$

The converted diameter in the projection area of LR_A and LR_B, from Eq. (5-32), is

$$\phi_{s,eff-LR_A} = \phi_{s,eff-LR_B} = 2 \cdot \sqrt{\frac{A_{s,eff-LR_A}}{\pi \cdot n}} = 2 \cdot \sqrt{\frac{1231.4}{3.14 \times 12}} = 11.43 \text{ mm}$$

The steel strain of LR_A and LR_B in X-axis and Y-axis, ε_{c-LR_A} and ε_{c-LR_B} from Eq. (5-30) and (5-31) are,

$$\varepsilon_{LR_A} = \frac{4 \times 5.24 \times 1231.4 \times 111.6}{11.43 \times 30457 \times 1231.4} = 0.00062$$

$$\varepsilon_{LR_B} = \frac{4 \times 5.24 \times 1231.4 \times 111.9}{11.43 \times 30457 \times 1231.4} = 0.00059$$

TR_A and TR_B strains at crack from Eq. (5-34) and (5-35), are

$$\varepsilon_{TR_A} = j_{TR_A} \cdot \frac{f_{ctm} \cdot A_{c,eff-TR_A} \cdot \sin\alpha_{TR}}{E_s \cdot A_{s-TR_A}} = 2.76 \times \frac{3.33 \times 29.2 \times 1200 \times \sin 22.5°}{201053 \times 942.48}$$
$$= 0.00014$$

$$\varepsilon_{TR_B} = j_{TR_B} \cdot \frac{f_{ctm} \cdot A_{c,eff-TR_B} \cdot \sin\alpha_{TR}}{E_s \cdot A_{s-TR_B}} = 2.01 \times \frac{3.33 \times 30.5 \times 1200 \times \sin 22.5°}{201053 \times 942.48}$$
$$= 0.000103$$

Along X-axis, the average strain at the crack from Eq.(5-28), is

$$\varepsilon_{cm-Y} = \varepsilon_{LR_A} + \varepsilon_{TR_A} = 0.00062 + 0.00014 = 0.00076$$

Along Y-axis, the average strain at the crack from Eq.(5-29), is

$$\varepsilon_{cm-X} = \varepsilon_{LR_B} + \varepsilon_{TR_B} = 0.00059 + 0.00010 = 0.00069$$

Hence, the maximum crack width in Y-axis and X-axis from Eq.(5-38), are

$$w_{k-Y} = 2.2 \times 110.62 \times \left(\frac{260.8}{201053} - 0.32 \times 0.000752\right) = 0.25 \text{ mm}$$

$$w_{k-X} = 2.2 \times 111.9 \times \left(\frac{350.7}{201053} - 0.32 \times 0.000693\right) = 0.35 \text{ mm}$$

Thus, the predicted maximum crack widths of P02W22C30 are $w_{k-Y} = 0.25$ and w_{k-X}=0.35 mm. A comparison of cracking width between the predicted and the measured values as shown in Table 4-2 presents that the maximum crack width in Y-axis and X-axis are w_{o-Y}=0.32mm and w_{o-X}=0.40 mm. Thus, the predicted maximum crack width for the slab under biaxial bending underestimates about -23% in Y-axis and -12% in X-axis.

7.3 Examples of calculating crack width according to proposed models in Chapter 6

7.3.1 Example of calculating crack width for the slab under uniaxial bending according to Model-8

Using the same concrete dimensions as were used for one-way slab-strips of Section 7.2.1, find the specimen is subjected to $M_a = 1.137 \times 10^7 \, \text{N} \cdot \text{mm}$, which is equal to a load of 35kN in each cylinder.

According to the maximum crack spacing in Section 7.2.1, $S_{r,max} = 158.5$mm.

➤ **Solution of the effective moment of inertia I_e**

In the uncracked state, according to geometrical relationship of cross-section, the height of neutral axis, y_{ut}, is

$$y_{ut} = 101.6 \, \text{mm}$$

The moment of inertia, I_{ut}, is

$$I_{ut} = 2.05 \times 10^8 \, \text{mm}^4$$

The cracking moment of section, M_{cr}, is

$$M_{cr} = \frac{f_{ctm} I_{ut}}{h - y_{ut}} = \frac{3.33 \times 2.05 \times 10^8}{(200 - 101.6)} = 4.74 \times 10^6 \, \text{N} \cdot \text{m}$$

In the cracked state, the height of neutral axis, y_{cr}, is

$$y_{cr} = 39.8 \, \text{mm}$$

The inertia moment at the cracked section, I_{cr}, is

$$I_{cr} = 2.95 \times 10^7 \, \text{mm}^4$$

Hence, from the formula in ACI 318-2008, I_e, is

$$I_e = \left(\frac{4.74 \times 10^6}{1.137 \times 10^7}\right)^3 2.05 \times 10^8 + \left(1 - \left(\frac{4.74 \times 10^6}{1.137 \times 10^7}\right)^3\right) 2.95 \times 10^7$$

$$= 4.23 \times 10^7 \, \text{mm}^4$$

➤ **Calculation of the average bending strain on tensile surface between adjacent cracks**

The longitudinal reinforcement ratio in the effective depth area is,

$$\rho = \frac{A_s}{bd} = \frac{235.6}{157 \times 300} = 0.005$$

The height of neutral axis at the cracked section $h_1 = k_1 d$, from Eq. (6-4), is

$$k_1 = \sqrt{(0.005 \cdot 3)^2 + 2 \cdot 0.005 \cdot 3} - 0.005 \cdot 3 = 0.16$$

Hence

141

$$h_1 = k_1 d = 0.16 \times 156.5 = 24.90 \text{ mm}$$

The height of neutral axis at the uncracked section $h_m = k_m d$, from Eq.(6-6), is

$$k_m = 0.631 \text{ mm}$$

Hence

$$h_m = k_m d = 0.631 \times 157 = 98.80 \text{ mm}$$

The height of average tensile zone h', from Eq. (6-2), is

$$h' = 200 - \left(\frac{24.9}{2} + \frac{98.8}{2}\right) = 138.15 \text{ mm}$$

The Young's modulus with the weighted average concrete and reinforcement areas, from (6-9), is

$$E_{cs} = \frac{A-A_s}{A} E_c + \frac{A_s}{A} \cdot E_s = \frac{60000-235.6}{60000} \cdot 27000 + \frac{235.6}{60000} \cdot 201053 = 27683 \text{ MPa}$$

And the curvature κ, from Eq. (6-13), is

$$\kappa = \frac{1.137 \times 10^7}{27683 \times 4.23 \times 10^7} = 9.72 \times 10^{-6} \text{ 1/mm}$$

The average bending strain on tensile surface between adjacent cracks from Eq.(6-18), is

$$\varepsilon_{f,m} = h' \kappa = 138.15 \times 9.72 \times 10^{-6} = 1.34 \times 10^{-3}$$

➢ **Calculation of the maximum crack width according to Model-8**

Based on the calculated results of TR, LR and the overall strain in concrete between adjacent cracks, ε_{cm}, is

$$\varepsilon_{cm} = 1.80 \times 10^{-4}$$

The maximum crack width can be calculated by Eq.(6-22),

$$w_{max} = 158.5 \times (1.34 \times 10^{-3} - 1.80 \times 10^{-4}) = 0.225 \text{ mm}$$

Thus, the predicted maximum crack width of A3c2 is 0.25mm. A comparison of crack width between the predicted and measured values, as shown in Table 3-3, presents that the maximum crack width of A3c2 is 0.21mm. Therefore, the predicted crack width for the slab under uniaxial bending overestimates about 7%.

7.3.2 Example of calculating crack width for the slab under biaxial bending according to Model-9

The specimen of P02W22C30, using the same concrete dimensions as were used for the two-way slab in Section 7.2.2, is a two-way slab subjected to two orthogonal directions set at a load of 35kN in each cylinder. It can be found in Section 7.2.2 that the moment in Y-axis, $M_y = 19570061.9$ N·m and in X-axis, $M_x = 32722438.1$ N·m , and the average crack spacing in two directions along Y-axis, $S_{rm-Y} = 110.6$ mm and along X-axis, $S_{rm-X} = 111.9$ mm.

➢ **Calculation of the effective inertia moment I_e**

In the uncracked state, according to geometrical relationship of cross-section, the height

of neutral axis in Y-axis and X-axis, y_{ut-Y} and y_{ut-X} are

$$y_{ut-Y} = 60.61 \text{ mm}$$

$$y_{ut-X} = 61.48 \text{ mm}$$

The inertia moment in corresponding axes, I_{ut-Y} and I_{ut-X} are

$$I_{ut-Y} = 1.74 \times 10^8 \text{ mm}^4$$

$$I_{ut-X} = 1.79 \times 10^8 \ mm^4$$

The cracking moment in Y-axis and X-axis, M_{cr-Y} and M_{cr-X} are

$$M_{cr-Y} = \frac{f_{ctm} I_{ut-Y}}{h - y_{ut-Y}} = \frac{3.33 \times 1.74 \times 10^8}{(200 - 60.61)} = 9.75 \times 10^6 \text{ N} \cdot \text{m}$$

$$M_{cr-X} = \frac{f_{ctm} I_{ut-X}}{h - y_{ut-X}} = \frac{3.33 \times 1.79 \times 10^8}{(200 - 61.48)} = 1.02 \times 10^7 \ N \cdot m$$

In the cracked state, the height of neutral axis in Y-axis and X-axis, y_{cr-Y} and y_{cr-X} are

$$y_{cr-Y} = 25.58 \text{ mm}$$

$$y_{cr-X} = 29.00 \text{ mm}$$

The inertia moment at the crack conversion sections in Y-axis and X-axis, I_{cr-Y} and I_{cr-X} are

$$I_{cr-Y} = 2.12 \times 10^7 \text{ mm}^4$$

$$I_{cr-X} = 3.40 \times 10^7 \text{ mm}^4$$

Hence, the effective inertia moment in two directions of Y-axis and X-axis, I_{e-Y} and I_{e-X} are

$$I_{e-Y} = \left(\frac{9.75 \times 10^6}{2.12 \times 10^7}\right)^3 1.74 \times 10^8 + \left(1 - \left(\frac{9.75 \times 10^6}{2.12 \times 10^7}\right)^3\right) 2.12 \times 10^7$$

$$= 2.66 \times 10^7 \text{ mm}^4$$

$$I_{e-X} = \left(\frac{1.02 \times 10^7}{1.79 \times 10^8}\right)^3 1.79 \times 10^8 + \left(1 - \left(\frac{1.02 \times 10^7}{1.79 \times 10^8}\right)^3\right) 3.40 \times 10^7$$

$$= 4.86 \times 10^7 \text{ mm}^4$$

➤ **Calculation of the average strain between adjacent cracks**

The longitudinal reinforcement ratio in two directions of Y-axis and X-axis are

$$\rho_Y = \frac{1231.4}{71.4 \times 1200} = 0.014$$

$$\rho_X = \frac{1231.4}{87.7 \times 1200} = 0.012$$

The height of neutral axis at the cracked section $h_1 = k_1 d$, from Eq. (6-4), is

$$k_{1,Y} = \sqrt{(0.014 \cdot 12)^2 + 2 \cdot 0.014 \cdot 12} - 0.014 \cdot 12 = 0.44$$

$$k_{1,X} = \sqrt{(0.012 \cdot 12)^2 + 2 \cdot 0.012 \cdot 12} - 0.012 \cdot 12 = 0.41$$

and

$$h_{1,Y} = 31.4 \text{ mm}$$
$$h_{1,X} = 35.8 \text{ mm}$$

The height of neutral axis at the uncracked section $h_m = k_m d$, from Eq.(6-6), is

$$k_{m-Y} = 0.836 \text{ mm}$$
$$k_{m-X} = 0.675 \text{ mm}$$

Hence

$$h_{m-Y} = 0.836 \times 71.4 = 59.69 \text{ mm}$$
$$h_{m-X} = 0.675 \times 87.7 = 59.23 \text{ mm}$$

The height of the average tensile zone h', from Eq.(6-2), is

$$h_Y' = 120 - \left(\frac{31.4}{2} + \frac{59.69}{2}\right) = 74.46 \text{ mm}$$

$$h_X' = 120 - \left(\frac{35.8}{2} + \frac{59.23}{2}\right) = 72.50 \text{ mm}$$

Young's modulus with the weighted average concrete and reinforcement areas is

$$E_{cs} = \frac{A - A_s}{A} E_c + \frac{A_s}{A} \cdot E_s = \frac{180000 - 1231.4}{180000} \cdot 30457 + \frac{1231.4}{180000} \cdot 201053$$
$$= 31915 \text{ } MPa$$

and the curvature, κ, from Eq.(6-13), is

$$\kappa_Y = \frac{19570061.9}{31915 \times 21512806} = 1.53 \times 10^{-5} \text{ 1/mm}$$

$$\kappa_X = \frac{32722438.1}{31915 \times 35790834} = 2.68 \times 10^{-5} \text{ 1/mm}$$

The average bending strain on tensile surface between adjacent cracks in Y-axis and X-axis from Eq.(6-18), are

$$\varepsilon_{f,m-Y} = h_Y' \kappa_Y = 74.46 \times 1.53 \times 10^{-5} = 1.14 \times 10^{-3}$$
$$\varepsilon_{f,m-X} = h_X' \kappa_X = 72.50 \times 2.68 \times 10^{-5} = 1.94 \times 10^{-3}$$

➢ **Calculation of the maximum crack width according to Model-9**

In Section 7.2.2, when the calculated values of TR, LR and concrete strain along X-axis and Y-axis, the average concrete strain between adjacent cracks can be calculated as follows:

Along X-axis, the average strain of the concrete from Eq.(5-28), is

$$\varepsilon_{cm-Y} = \varepsilon_{LR_A} + \varepsilon_{TR_A} = 0.00062 + 0.00014 = 0.00076$$

Along Y-axis, the average strain of the concrete from Eq. (5-29), is

$$\varepsilon_{cm-X} = \varepsilon_{LR_B} + \varepsilon_{TR_B} = 0.00059 + 0.00010 = 0.00069$$

Hence, the maximum crack width can be calculated by Eq. (6-22),

$$w_{max} = 2 \times 110.6 \times (1.14 \times 10^{-3} - 0.32 \times 7.6 \times 10^{-4}) = 0.214 \text{ mm}$$

$$w_{max} = 2 \times 111.9 \times (1.94 \times 10^{-3} - 0.32 \times 6.9 \times 10^{-4}) = 0.394 \text{ m}$$

Thus, the predicted maximum crack widths of P02W22C30 are $w_{k-Y} = 0.214$ and w_{k-X}=0.394 mm. A comparison of cracking width between the predicted and the measured values as shown in Table 4-2 presents that the maximum crack width in Y-axis and X-axis are w_{o-Y}=0.32mm and w_{o-X}=0.40 mm. Thus, the predicted maximum crack width for the slab under biaxial bending underestimate about 33% in Y-axis and overestimate 1% in X-axis.

7.4 Comparison of crack spacing and width for slabs under uniaxial bending between the predicted and the measured values

7.4.1 Comparison of predicted and observed crack spacing for slabs under uniaxial bending

7.4.1.1 *Influence of concrete cover and TR-spacing on crack spacing (Series 1)*

Figure 7-3 and Figure 7-5 indicate that similar values of the average predicted crack spacing are obtained from FIB Code Model 2010 (draft) and DIN EN 1992-1-2011. These values are approximately 50% larger than those of the measured values. The DIN 1045-1-2008 and Model-4 (Eq.(5-7)) provide better estimate for the average crack spacing values with -5% and 1% percentage error. These values are in good agreement with those obtained experimentally, which can be seen in Figure 7-4. This figure illustrates that an increase of concrete cover resulted in an increase of the predicted crack spacing. This increasing tendency in DIN 1045-1-2008 and Model-4 (Eq.(5-7)) presents a better agreement with the experimental tendency than that in other codes.

Table 7-3 Comparison of predicted and observed average crack spacing in Series1

No.	Obers-ved Av. crack spacing * [mm]	Crack spacing [mm]							
		Predicted by FIB Model Code 2010		Predicted by DIN EN 1992-1-2011		Predicted by DIN1045-1		by Model-4 (Eq.(5-7))	
		Values	Percenta-ge errors	Values	Percenta ge errors	Values	Percentage errors	Predicted values	Percentag-e errors
A1C1	100	121	22%	132	32%	107	7%	109	10%
A2C1	100	121	22%	134	35%	107	7%	109	10%
A3C2	112	167	50%	199	72%	119	7%	125	12%

Comparison of crack spacing and width for slabs under uniaxial bending between the predicted and the measured values

A4C2	104	169	63%	194	87%	119	15%	125	21%
A5C3	167	223	34%	249	49%	131	-21%	148	-11%
A6C3	161	222	38%	247	54%	131	-18%	149	-7%
B1C1	100	121	22%	129	30%	107	7%	101	1%
B2C1	100	121	22%	134	34%	107	7%	102	2%
B3C2	123	169	38%	195	59%	119	-3%	127	4%
B4C2	145	168	16%	193	33%	119	-18%	126	-13%
B5C3	158	219	39%	244	55%	131	-17%	148	-6%
B6C3	137	216	58%	240	76%	131	-4%	145	6%
C1c2	130	184	41%	211	62%	119	-9%	132	2%
C2c2	157	179	14%	206	31%	119	-24%	130	-17%
Av.**	128	171	34%	193	51%	119	-5%	127	1%
Std.***	25.96	39.05	0.15	44.83	0.19	9.36	0.13	16.73	0.11
C.V.****	0.20	0.23	-	0.23	-	0.08	-	0.13	-

* The average observed crack spacing are according to Table 3-3Table 3-3 in Section 3.3.2.

** Av. stand for average values

*** Std. stand for standard diviation;

****C.V. stand for coefficient of variation.
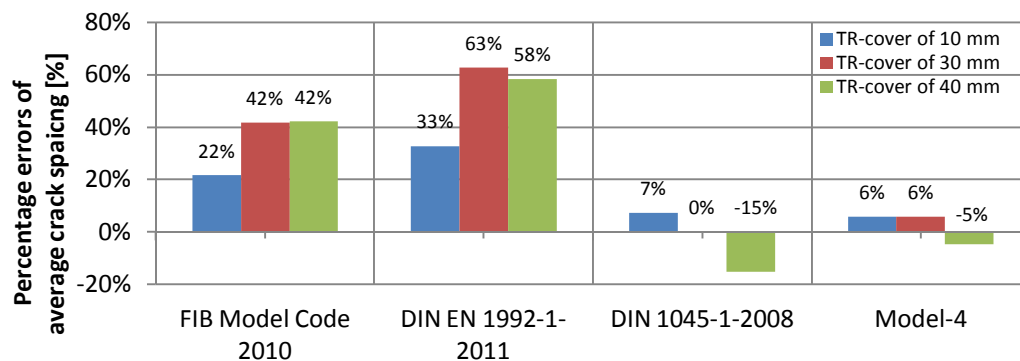
Figure 7-3 Comparison of predicted and observed average crack spacing with various TR-cover in Series 1
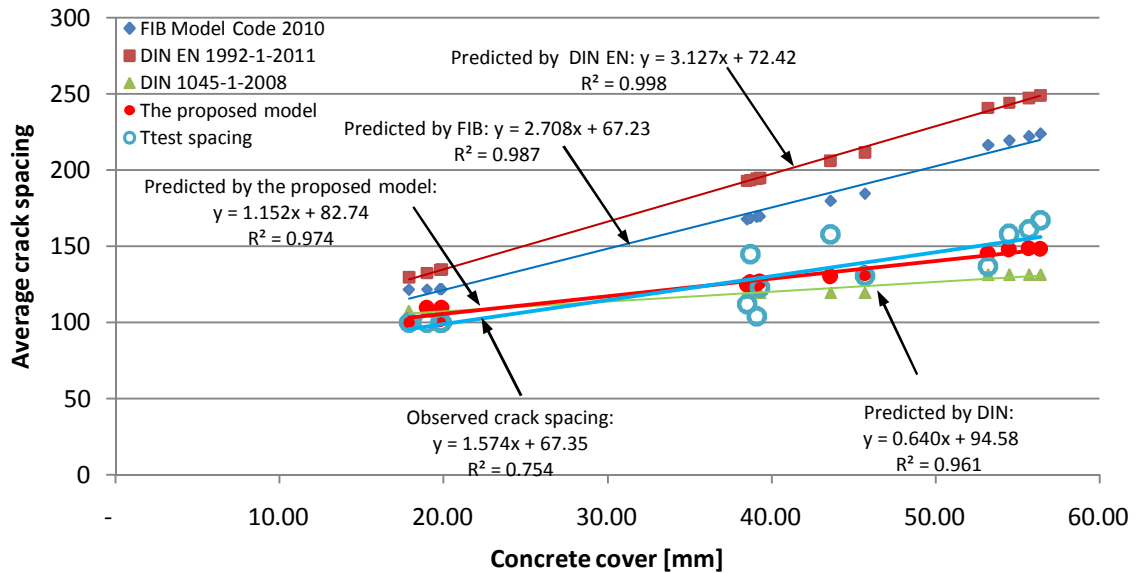
Figure 7-4 Comparison of predicted and observed average crack spacing tendency with various TR-cover in Series 1
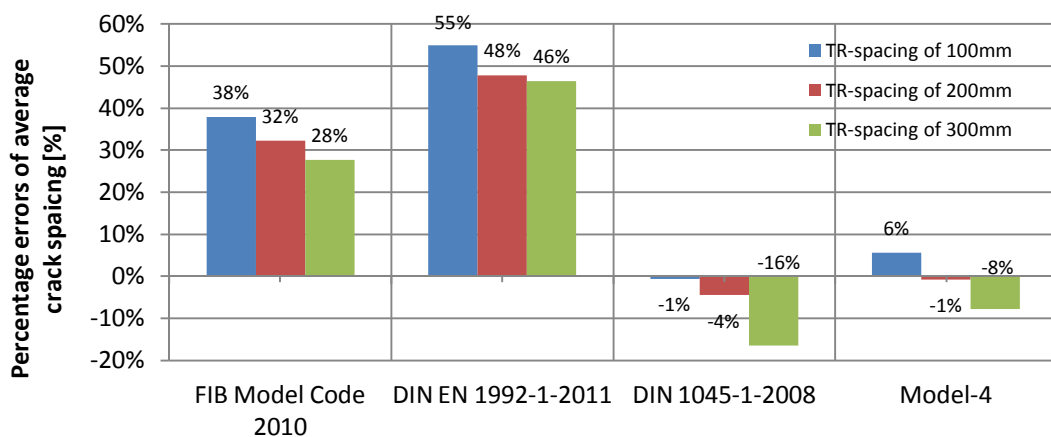
Figure 7-5 Comparison of predicted and observed average crack spacing with various TR-spacing in Series 1

7.4.1.2 *Influence of the TR-direction on crack spacing (Series 2)*

In Series 2, specimens were tested to investigate the influence of TR-direction on the average crack spacing. Table 7-4 presents comparison results of predicted and observed crack spacing according to FIB Model Code 2010 (draft), DIN EN 1992-1-2011, DIN 1045-1-2008 and Model-4 (Eq.(5-7)). Figure 7-6 presents that when TR-direction of LC increases from 0° to 45°, all current codes and Model-4 (Eq.(5-7)) overestimate the average crack spacing by a large percentage error. This figure further indicates that when TR-direction increases from 0° to 45°, FIB model code 2010 (draft) and DIN EN 1992-1-2011 have similar predicted average crack spacing values. The predicted average crack spacing values of normal-strength concrete (NC) overestimates from 80% to 120% approximately, and for high-strength concrete (HC) overestimates from 40% to 120%

approximately. Values in DIN 1045-1-2008 overestimate from -13% to 30% approximately for both concrete types. However, Model-4 (Eq.(5-7)) provides better-predicted average crack spacing values than those of three current codes. When TR-direction=0°, Model-4 (Eq.(5-7)) underestimates crack spacing by 6%, and when TR-direction=45°, it overestimates crack spacing by 10%.

The comparison shows that an increase of TR-direction from 0° to 45° results in an increase of overestimation of average crack spacing. Model-4 (Eq.(5-7)) gives a better understanding of the predicted crack spacing with the consideration of the influence of TR-direction on crack spacing than other three codes. Therefore, Model-4 (Eq.(5-7)) is recommended to estimate average crack spacing of flexural RC element for NC and HC.

Table 7-4 Comparison of predicted and observed average crack spacing in Series 2

No.	Observed Av. crack spacing* [mm]	Predicted crack width [mm]							
		by FIB Model Code 2010		by DIN EN 1992-1-2011		by DIN1045-1		by Model-4 (Eq.(5-7))	
		Values	Percentage errors	Values	Percentage errors	Values	Percentage errors	Values	Percentage errors
N1w1	112	185	66%	213	90%	119	7%	98	-12%
N2w1	104	184	77%	211	103%	119	15%	99	-4%
N3w2	100	183	83%	210	110%	119	19%	99	-1%
N4w2	106	186	76%	213	102%	119	13%	101	-4%
N5w3	89	191	115%	219	147%	119	34%	101	14%
N6w3	94	179	91%	206	120%	119	27%	99	5%
H1w1	120	188	46%	216	67%	119	-7%	100	-22%
H2w1	140	187	26%	214	45%	119	-19%	100	-32%
H3w2	128	192	50%	220	72%	119	-7%	102	-20%
H4w2	96	197	106%	225	135%	119	24%	103	7%
H5w3	109	202	86%	231	113%	119	10%	104	-4%
H6w3	82	200	145%	229	180%	119	46%	103	27%
L3S2	56	178	219%	204	266%	119	113%	141	152%
L4S2	86	183	114%	210	145%	119	39%	148	73%
L3w2	52	172	231%	197	280%	119	130%	99	92%
L4w2	51	194	282%	222	337%	119	134%	109	114%
L5w2	58	182	215%	209	262%	119	106%	101	75%
L6w2	48	186	288%	213	345%	119	149%	102	114%
Aver.	91	187	129%	215	162%	119	46%	106	32%
Std.	29	7.79	0.82	8.68	0.94	0.00	0.54	14.27	0.56
C.V.	0.32	0.04	-	0.04	-	0.00	-	0.13	-

* The observed average crack spacing is according to Table 3-5 in Section 3.4.2
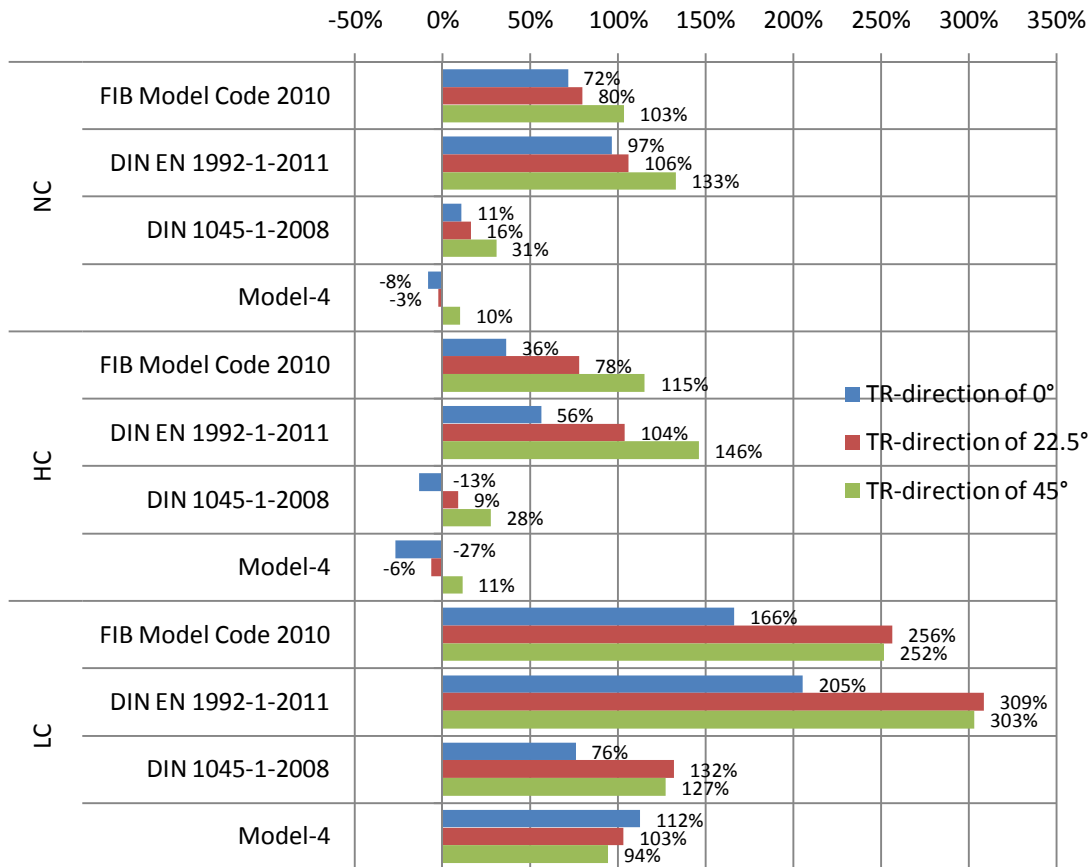
Figure 7-6 Comparison of predicted and observed average crack spacing with various TR-direction in Series 2

7.4.2 Comparison of predicted and observed maximum crack width for slabs under uniaxial bending

7.4.2.1 Influence of TR-cover on crack width (Series 1)

Table 7-5 presents a comparison of predicted and observed crack width according to FIB Model Code 2010 (draft), DIN EN 1992-1-2011, DIN 1045-1-2008, ACI 318-2008, Model-6 (Eq.(5-37)) and the proposed Model-8 (Eq.(6-23)).

Figure 7-7 indicates that for TR-spacing of 100mm, FIB Code Model 2010 (draft), DIN EN 1992-1-2011 and DIN 1045-1-2008 have similar predicted maximum crack width. These values are larger than the test results by 35% approximately. The ACI 318-2008 overestimates the maximum crack width for specimens with a TR-cover of 40mm by a large percentage error. However, comparing to these codes，Model-6 (Eq.(5-37)) and Modle-8 provide better predictions of the maximum crack width for specimens with TR-cover from 10mm to 40mm by approximately 1% percentage error.

Furthermore, it can be observed in Figure 7-8 that, for specimens with TR-spacing of 200mm, four current codes provide a good prediction for maximum crack width. However, for specimens with TR-spacing of 100mm, as the influence of TR on crack width is neglected, an overestimation of the average crack width from 30% to 70% is observed.

However, Model-6 (Eq.(5-37)) and Model-8 (Eq.(6-23)) observe the percentage errors by 7% and 2% by taking into account of the influence of TR.

Moreover, for TR-spacing of 200mm and 300mm，it is also presented in this figure that percentage errors of -4% and 3% can be observed by Model-6 (Eq.(5-37)). Therefore, TR-cover and -spacing are important factors in calculating the crack width in Model-6 (Eq.(5-37)) and Model-8 (Eq.(6-23)). These two proposed models give a better understanding of the predicted crack width with consideration of the influence of TR. Model-6 (Eq.(5-37)) and Model-8 (Eq.(6-23)) are recommended for flexural RC element with TR-spacing until 300 mm.

Table 7-5 Comparison of predicted and observed maximum crack width in Series 1

No.	Observed crack width[mm] *		Predicted values of crack width [mm] Values (percentage errors)**					
	Av. Values	Maximum values	by FIB Model Code 2010	by DIN EN 1992-1-2011	by DIN1045-1	by ACI318	by Model-6 (Eq.(5-37))	by Model-8 (Eq.(6-23))
A1c1	0.15	0.15	0.21 (41%)	0.20 (32%)	0.26 (72%)	0.21 (41%)	0.17 (14%)	0.16 (8%)
A2c1	0.15	0.17	0.21 (23%)	0.20 (15%)	0.25 (49%)	0.21 (26%)	0.17 (-1%)	0.16 (-3%)
A3c2	0.17	0.21	0.31 (46%)	0.30 (42%)	0.30 (41%)	0.36 (73%)	0.25 (20%)	0.22 (7%)
A4c2	0.23	0.28	0.30 (8%)	0.30 (6%)	0.29 (5%)	0.36 (30%)	0.25 (-9%)	0.23 (-17%)
A5c3	0.26	0.21	0.28 (34%)	0.26 (24%)	0.28 (31%)	0.42 (102%)	0.27 (30%)	0.18 (-15%)
A6c3	0.24	0.17	0.30 (78%)	0.28 (65%)	0.29 (70%)	0.44 (158%)	0.30 (74%)	0.18 (7%)
B1c1	0.14	0.16	0.16 (2%)	0.15 (-9%)	0.21 (34%)	0.17 (6%)	0.17 (5%)	0.19 (19%)
B2c1	0.14	0.20	0.21 (6%)	0.20 (0%)	0.26 (28%)	0.22 (8%)	0.21 (4%)	0.20 (0%)
B3c2	0.29	0.35	0.30 (-15%)	0.29 (-17%)	0.30 (-15%)	0.37 (6%)	0.31 (-11%)	0.24 (-30%)
B4c2	0.21	0.25	0.28 (14%)	0.28 (10%)	0.30 (18%)	0.36 (43%)	0.30 (20%)	0.24 (-4%)
B5c3	0.32	0.31	0.32 (4%)	0.30 (-3%)	0.30 (-3%)	0.45 (45%)	0.31 (-1%)	0.18 (-42%)
B6c3	0.31	0.32	0.31 (-3%)	0.29 (-10%)	0.30 (-7%)	0.43 (35%)	0.29 (-11%)	0.17 (-47%)
C1c2	0.26	0.25	0.33 (33%)	0.32 (30%)	0.30 (18%)	0.42 (69%)	0.32 (26%)	0.30 (20%)
C1c2	0.29	0.27	0.32 (18%)	0.32 (20%)	0.29 (8%)	0.40 (48%)	0.30 (12%)	0.28 (5%)
Av.	0.23	0.31	0.34(15%)	0.33(11%)	0.33(13%)	0.40(33%)	0.31(2%)	0.29(-1%)
Std.	0.07	0.10	0.08(0.20)	0.08(0.19)	0.04(0.25)	0.12(0.30)	0.08(0.17)	0.08(0.22)
C.V.	0.29	0.32	0.23	0.25	0.11	0.30	0.25	0.28

* The observed crack width is according to Table 3-3 in Section 3.3.3

**Values (percentage errors) is the example of values in this table.
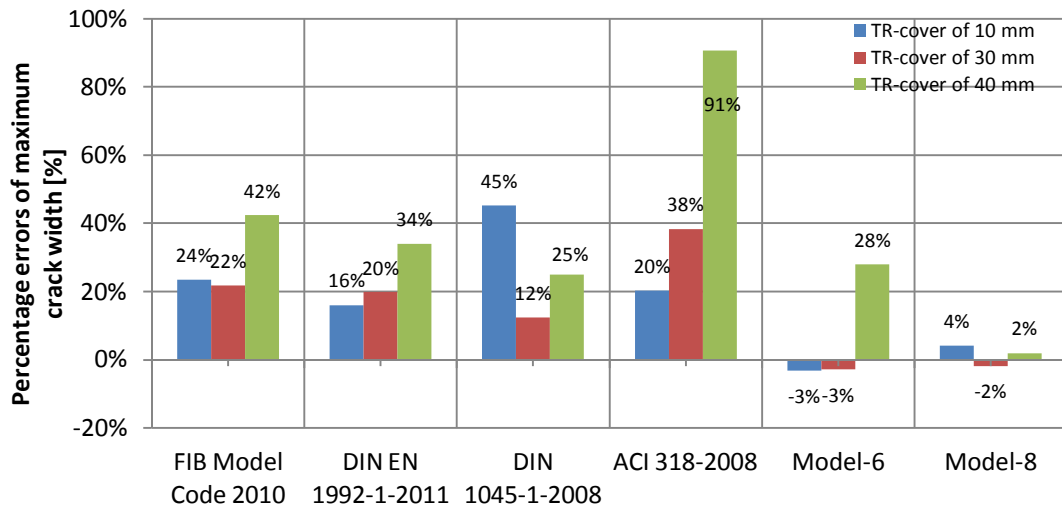
Figure 7-7 Comparison of predicted and observed maximum crack width at the load level of 0.625 f_y with various TR-cover in Series 1
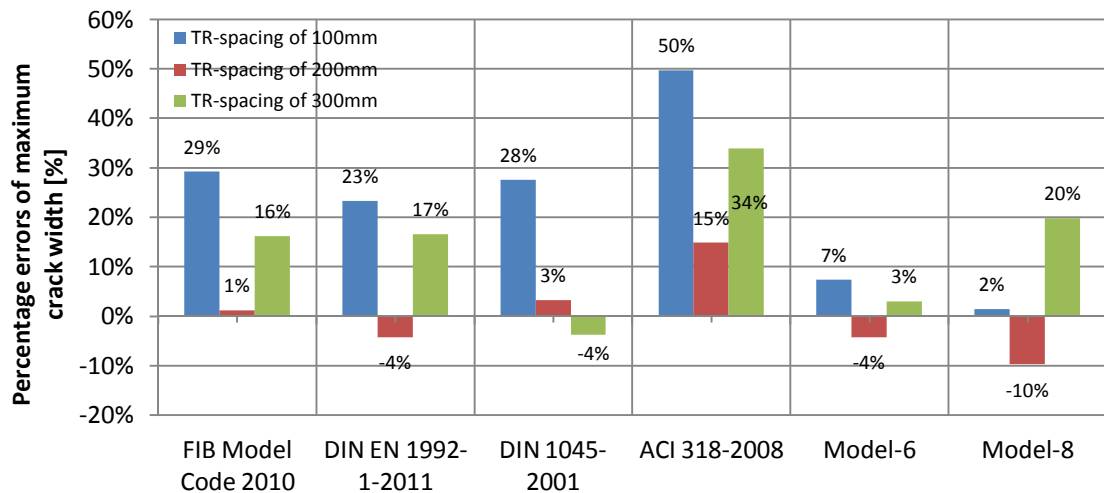
Figure 7-8 Comparison of predicted and observed maximum crack width at the load level of 0.625 f_y with various TR-spacing in Series 1

7.4.2.2 *Influence of TR-direction on crack width (Series 2)*

In Series 2, the influence of TR-direction on crack behavior has been investigated. Table 7-6 shows a comparison of predicted and observed maximum crack width according to four current codes, Model-6 (Eq.(5-37)) and Model-8 (Eq.(6-23)). Figure 7-9 through Figure 7-11 illustrate that for a TR-direction of 45°, four current codes overestimate the maximum crack width by extremely large percentage errors. The reason for this overestimate is that the restraining influence of TR-direction on crack width is neglected by current four codes. Model-6 (Eq.(5-37)) and Model-8 (Eq.(6-23)) taking into account of TR-direction give closer estimates of the maximum crack width for three concrete types of HC, LC and NC, except that NC specimens with TR-direction of 45° provide

151

larger overestimates by 180% and 129% percentage error.

Both Model-6 (Eq.(5-37)) and Model-8 (Eq.(6-23)) give better understanding of the predicted crack width with consideration to the influence of TR-direction. These two models are recommended for flexural RC element with various concrete types with consideration of TR-direction.

Table 7-6 Comparison of predicted and observed maximum crack width at the load level of 0.625 f_y in Series 2

No.	Observed crack width [mm]*		Predicted values of maximum crack width [mm]					
			Values (percentage crack width)					
	Av. values	Max. values	by FIB Model Code 2010	by DIN EN 1992-1-2011	by DIN1045-1	by ACI318	by Model-6 in Chapter 5	by Model-8 (Eq.(6-23))
N1w1	0.17	0.30	0.42 (40%)	0.41 (38%)	0.34 (14%)	0.43 (43%)	0.25 (-16%)	0.30 (-1%)
N2w1	0.26	0.30	0.41 (36%)	0.40 (34%)	0.34 (12%)	0.42 (41%)	0.26 (-15%)	0.30 (1%)
N3w2	0.15	0.26	0.41 (56%)	0.40 (54%)	0.34 (29%)	0.42 (61%)	0.24 (-8%)	0.28 (10%)
N4w2	0.15	0.28	0.42 (50%)	0.42 (48%)	0.34 (22%)	0.43 (54%)	0.25 (-9%)	0.30 (8%)
N5w3	0.04	0.06	0.44 (640%)	0.44 (629%)	0.35(480%)	0.45 (652%)	0.24 (292%)	0.29 (379%)
N6w3	0.16	0.32	0.39 (23%)	0.39 (21%)	0.33 (4%)	0.41 (27%)	0.21 (-33%)	0.26 (-20%)
H1w1	0.31	0.36	0.33 (-9%)	0.32 (-12%)	0.34 (-7%)	0.44 (22%)	0.26 (-29%)	0.13 (-64%)
H2w1	0.24	0.26	0.33 (25%)	0.32 (22%)	0.34 (29%)	0.43 (67%)	0.26 (-1%)	0.13 (-50%)
H3w2	0.20	0.26	0.33 (28%)	0.32 (24%)	0.33 (29%)	0.45 (75%)	0.24 (-9%)	0.11 (-59%)
H4w2	0.15	0.22	0.35 (58%)	0.34 (54%)	0.34 (54%)	0.47 (115%)	0.24 (10%)	0.11 (-50%)
H5w3	0.10	0.12	0.36 (196%)	0.34(187%)	0.34(181%)	0.49 (312%)	0.20 (69%)	0.07 (-40%)
H6w3	0.08	0.10	0.36 (261%)	0.35 (250%)	0.34(243%)	0.49 (387%)	0.21 (106%)	0.07 (-30%)
L3S2	0.13	0.30	0.35 (16%)	0.33 (10%)	0.29 (-3%)	0.39 (31%)	0.28 (-7%)	0.41 (38%)
L4S2	0.26	0.39	0.43 (9%)	0.41 (5%)	0.33 (-14%)	0.37 (-6%)	0.34 (-12%)	0.54 (39%)
L3w2	0.15	0.26	0.38 (47%)	0.37 (41%)	0.32 (24%)	0.0 (-100%)	0.25 (-6%)	0.38 (48%)
L4w2	0.17	0.29	0.43 (48%)	0.41 (41%)	0.32 (10%)	0.0 (-100%)	0.26 (-10%)	0.49 (70%)
L5w2	0.13	0.19	0.36 (87%)	0.34 (77%)	0.29 (52%)	0.42 (120%)	0.18 (-3%)	0.31 (61%)
L6w2	0.14	0.22	0.63 (187%)	0.62 (181%)	0.46(109%)	0.43 (96%)	0.33 (51%)	0.32 (46%)
Aver.	0.17	0.25	0.40 (100%)	0.38 (95%)	0.34 (70%)	0.43 (123%)	0.25 (20%)	0.27 (22%)
Std.	0.07	0.09	0.07 (1.53)	0.07 (1.51)	0.03(1.22)	0.03 (1.66)	0.04 (0.76)	0.14 (1.99)
C.V.	0.41	0.35	0.18	0.18	0.10	0.08	0.16	0.53

* The observed crack width is according to Table 3-5 in Section 3.4.3.
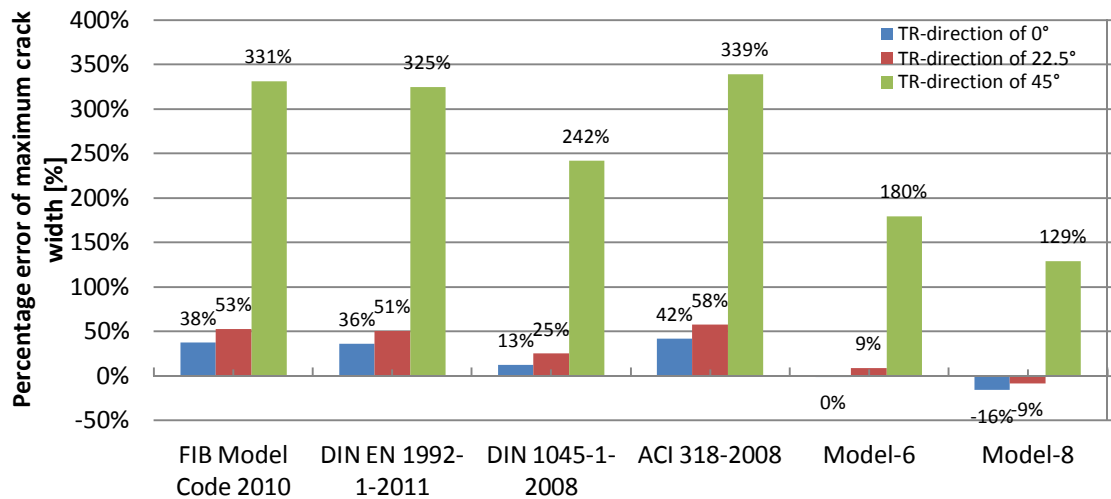
Figure 7-9 Comparison of predicted and observed maximum crack width at the load level of 0.625 f_y with variousTR-direction in Series 2 for NC
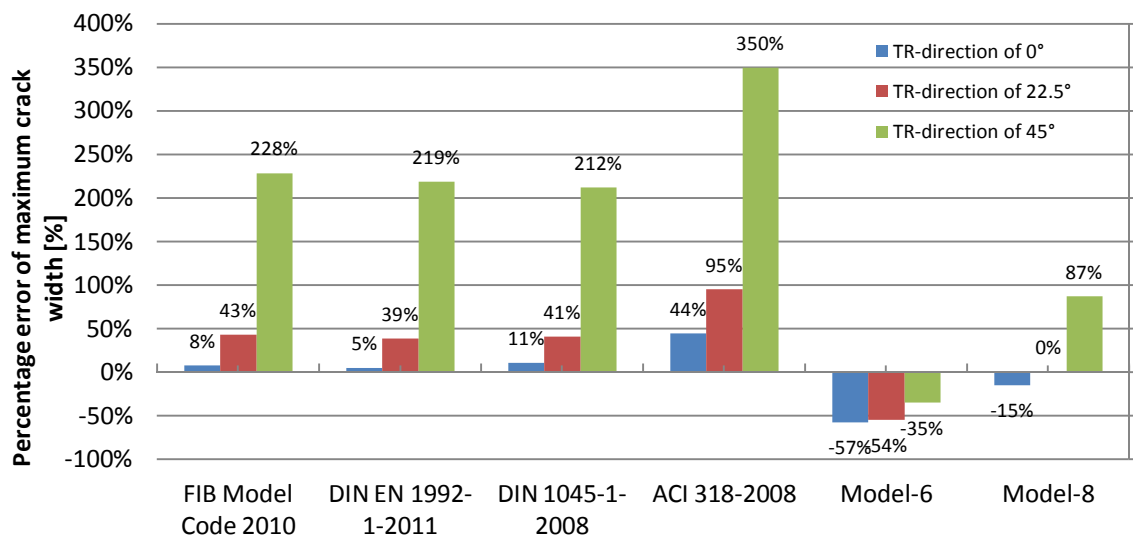
Figure 7-10 Comparison of predicted and observed maximum crack width at the load level of 0.625 f_y with various TR-direction in Series 2 for HC
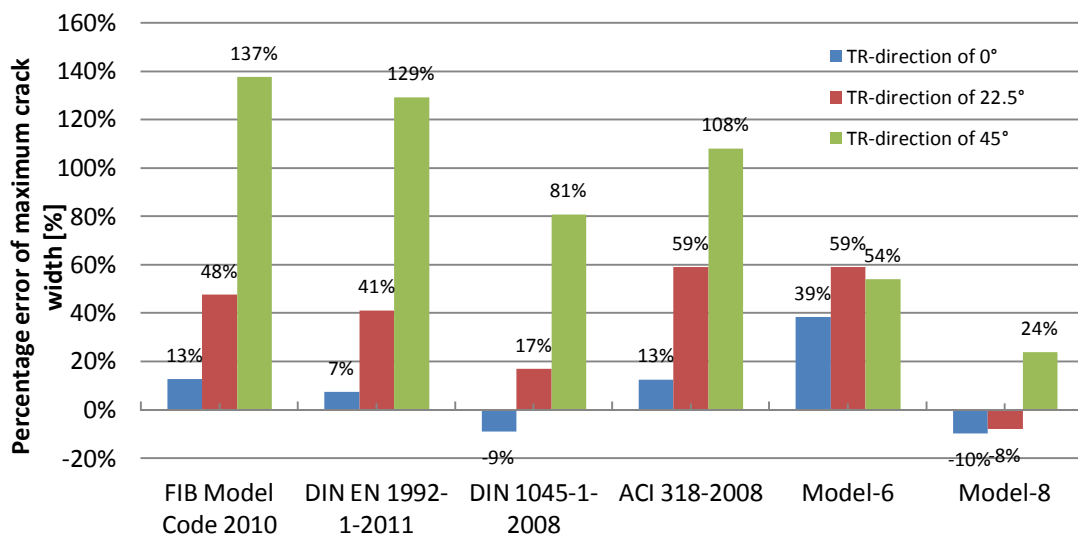
Figure 7-11 Comparison of predicted and observed maximum crack width at the load level of 0.625 f_y with various TR-direction in Series 2 for LC

7.5 Comparison of predicted and observed crack spacing and width for slabs under biaxial bending

7.5.1 Comparison of predicted and observed crack spacing for slabs under biaxial bending

Table 7-7 presents a comparison of predicted and observed crack spacing according to FIB Model Code 2010 (draft), DIN EN 1992-1-2011, DIN 1045-1-2008 and Model-5 (Eq.(5-12)). It can be observed from Figure 7-12 and Figure 7-13 that FIB Model Code 2010, DIN EN 1992-1-2011 and DIN1045-1 similarly underestimate about 20% and 40% in directions of Type A and Type B, and variation coefficients in these two directions are larger than 0.16. However, Model-5 (Eq.(5-12)) gives a better estimate for the average crack spacing by a percentage error of 17% and -3%, and their variation coefficients decrease to 0.13. These values are in good agreement with those obtained experimentally and can be observed from Figure 7-14. This figure illustrates that an increase of the angle between the TR and its intersected cracks (α_{TR}) resulted in a decrease of the predicted crack spacing. This decrease tendency in Model-5 (Eq.(5-12)) presents a better agreement with the experimental results than models in the actual codes. This tendency indicates that α_{TR} and the bending stress in two orthogonal directions are important factors for calculating the crack spacing, which are neglected by the actual codes. Model-5 (Eq.(5-12)) gives a better understanding of the predicted crack spacing with consideration of these two factors. Model-5 (Eq.(5-12)) is recommended for flexural slabs subjected to biaxial bending with various angles between the OR-direction and the bending direction.

Table 7-7 Comparison of predicted and observed average crack spacing for slabs under biaxial bending. (a) is in the direction of Type A and (b) is in the direction of Type B (see Figure 5-5)

Table (a)

		Table 7-5 (a)						
Direction of Type A (a)	Observed Av. crack Spacing*	Predicted crack spacing [mm]						
		by FIB Model Code 2010		by DIN EN 1992-1-2011		by DIN1045-1		By Model-5 (Eq.(5-12))
P01-0°	100	77	-22%	85	-14%	79	-20%	102	2%
P02-22.5°	87	61	-29%	67	-21%	60	-29%	110	29%
P03-450°	75	56	-25%	62	-17%	56	-25%	83	11%
P04-0°	66	80	21%	89	34%	79	19%	106	60%
P05-22.5°	85	61	-28%	67	-21%	60	-29%	111	30%
P06-45°	85	56	-35%	61	-28%	56	-34%	82	-3%
P07-0°	85	79	-7%	87	2%	79	-7%	105	23%
P08-22.5°	120	61	-49%	67	-43%	60	-49%	111	-7%
P09-45°	75	56	-24%	62	-16%	56	-25%	83	12%
Av.	86	65	-22%	72	-14%	65	-22%	99	17%
Std.	15.67	10.48	0.20	11.56	0.22	10.69	0.19	12.64	0.21
C.V.	0.18	0.16	–	0.16	–	0.16	–	0.13	-

* The crack spacing of slab under biaxial bending is according to Table 4-2 in Section 4.3.2.

Table (b)

		Table 7-5 (b)						
Direction of Type B (b)	Observe d Av. crack*	Predicted crack spacing [mm]						
		by FIB Model Code 2010		by DIN EN 1992-1-2011		by DIN1045-1		By Model-5 (Eq.(5-12))
P01-0°	150	75	-50%	82	-45%	79	-47%	104	-30%
P02-22.5°	100	30	-69%	66	-34%	60	-39%	111	12%
P03-450°	120	56	-53%	62	-48%	56	-53%	83	-30%
P04-0°	85	77	-9%	85	0%	79	-7%	107	26%
P05-22.5°	100	31	-69%	66	-34%	60	-39%	112	12%
P06-45°	100	56	-44%	61	-38%	56	-44%	82	-17%
P07-0°	120	76	-36%	84	-29%	79	-34%	106	-11%
P08-22.5°	100	31	-69%	66	-33%	60	-39%	112	12%
P09-45°	85	56	-34%	62	-27%	56	-34%	83	-2%
Av.	106	54	-48%	71	-32%	65	-37%	100	-3%
Std.	20.28	19.77	0.20	10.22	0.14	10.69	0.13	13.17	0.20
C.V.	0.19	0.36	-	0.14	-	0.16	-	0.13	-

* The crack spacing of slab under biaxial bending is according to Table 4-2 in Section 4.3.2.
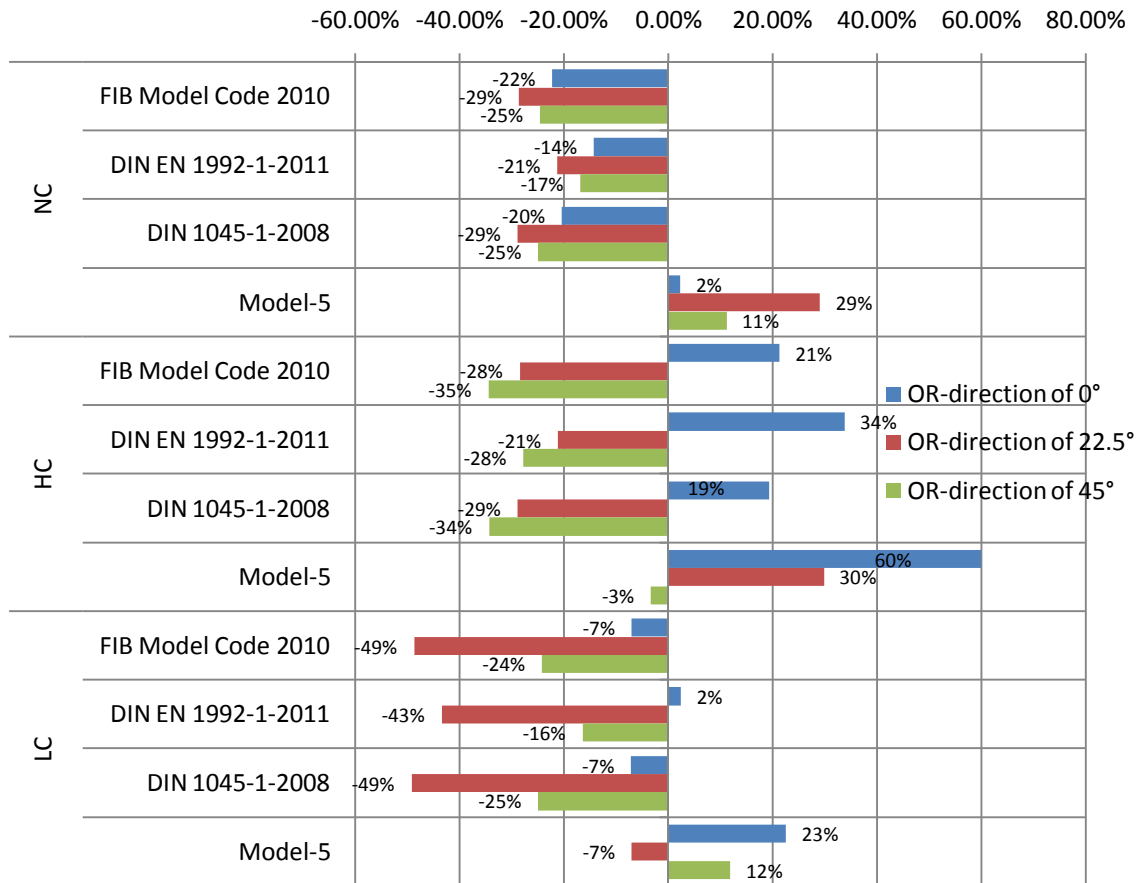
Figure 7-12 Comparison of predicted and observed average crack spacing in the direction of Type A (see Figure 5-5)
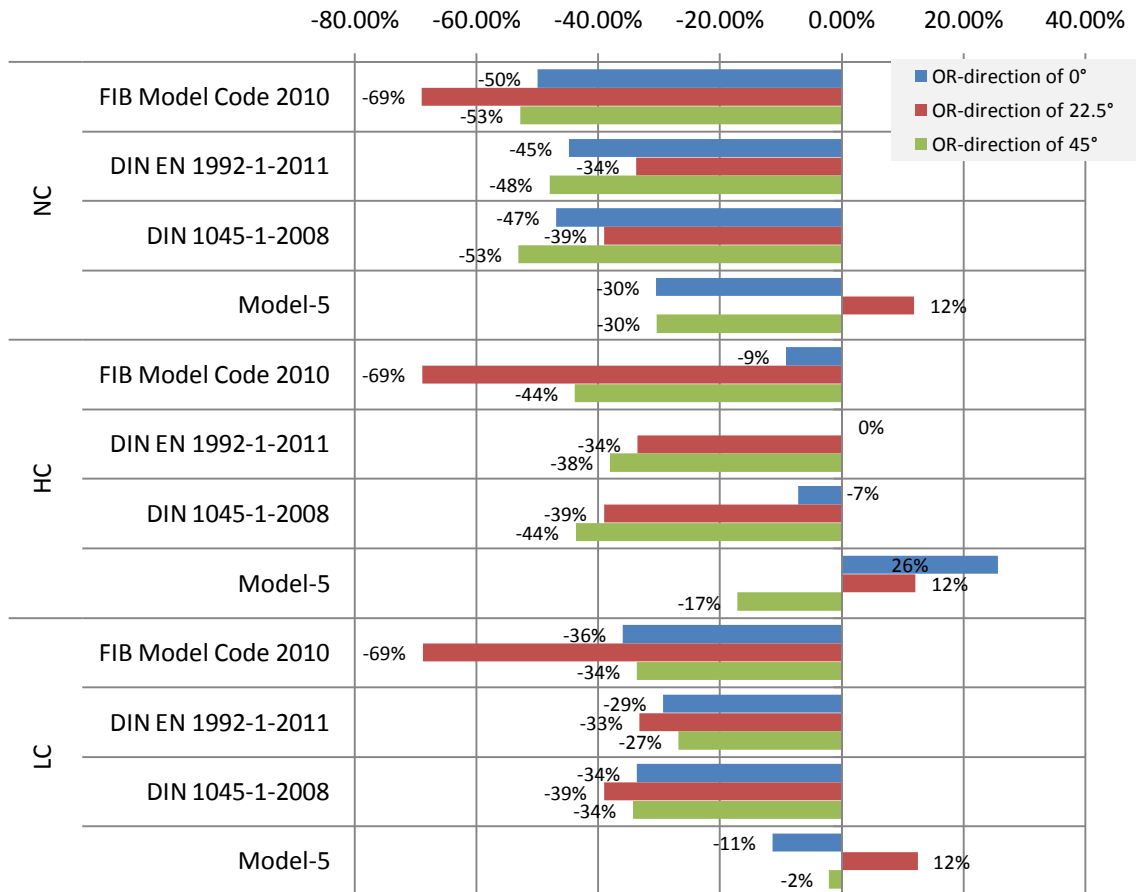
Figure 7-13 Comparison of predicted and observed average crack spacing in the direction of Type B (see Figure 5-5)
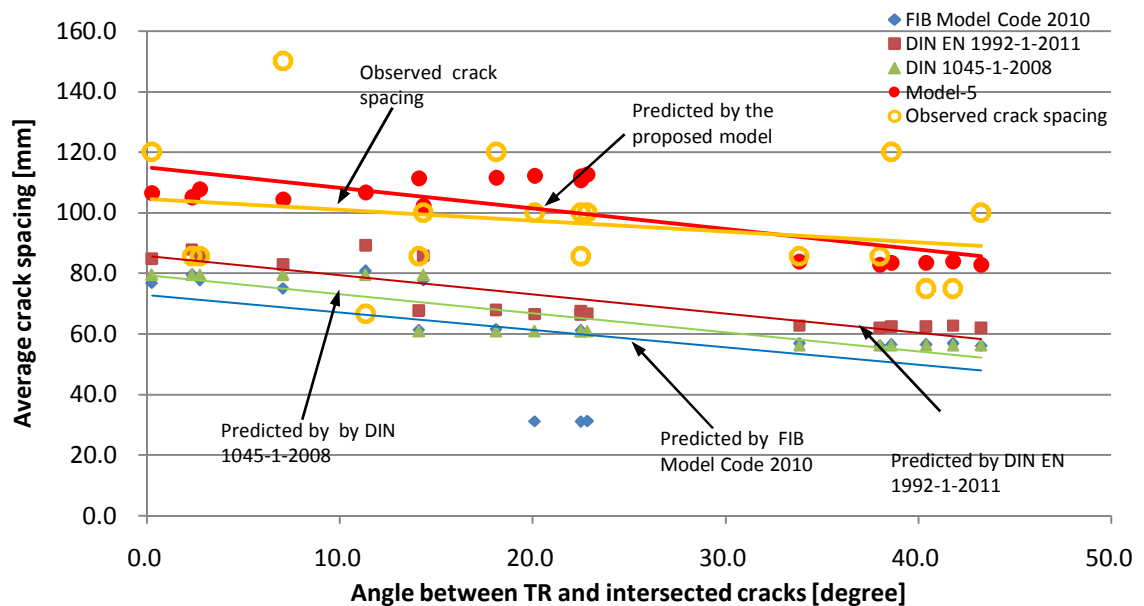
Figure 7-14 Comparison of predicted and observed average crack spacing with α_{TR}

7.5.2 Comparison of predicted and observed maximum crack width for slabs under biaxial bending

Table 7-8 presents a comparison results of predicted and observed crack width according to FIB Model Code 2010 (draft), DIN EN 1992-1-2011, DIN 1045-1-2008, ACI 318-2008, Model-7 (Eq.(5-38)) and Model-9 (Eq.(6-25)).

Figure 7-15 and Figure 7-16 indicate that DIN EN 1992-1-2011 and DIN1045-1 similarly underestimate approximately 50% and 60% of the predicted maximum crack width in two directions of Type A and Type B，and their variation coefficients are over 0.25. FIB Model Code 2010 (draft) gives closer results than other current codes, while its variation coefficients reached 0.42 and 0.54. However, Model-7 (Eq.(5-38)) and Model-9 (Eq.(6-25)) provide better predictions of the maximum crack width with three concrete types at -4% to 14% percentage error. These values are in good agreement with those obtained experimentally and can be observed from Figure 7-17. This figure illustrates that an increase of the angle between the TR and its intersected cracks (α_{TR}) resulted in a decrease of the predicted crack width. This decrease tendency in Model-7 (Eq.(5-38)) and Model-9 (Eq.(6-25)) give a better agreement with the experimental results than models in the actual codes.

This tendency indicates that α_{TR} and bending stress in two orghogonal directions are important factors for calculating the crack spacing, which are neglected by current codes. Model-7 (Eq.(5-38)) and Model-9 (Eq.(6-25)) give a better understanding of the predicted crack width with consideration of these two factors. By considering a considerable high accuracy, Model-7 (Eq.(5-38)) is recommended for flexural two-way RC element subjected to biaxial bending with various angles between the OR-direction and the bending direction.

Table 7-8 Comparison of predicted and observed maximum crack width for slabs under biaxial bending. (a) is in the direction of Type A and (b) is in the direction of Type B (see Figure 5-5)

Table (a)

Type A (a)	Obeserved crack width*		Predicted crack width [mm]										
	Av.	Max.	by FIB Model Code 2010		by DIN EN 1992-1-2011		by DIN1045-1		by ACI318		by Model-7 (Eq.(5-38))		by Model-9 (Eq.(6-25))	
P01	0.10	0.18	0.25	41%	0.12	-33%	0.15	-14%	0.32	78%	0.28	54%	0.22	22%
P02	0.25	0.32	0.26	-18%	0.08	-76%	0.10	-68%	0.48	49%	0.25	-23%	0.21	-35%
P03	0.10	0.31	0.33	8%	0.10	-69%	0.12	-62%	0.59	91%	0.23	-25%	0.38	24%
P04	0.18	0.31	0.41	32%	0.14	-56%	0.18	-43%	0.62	100%	0.33	7%	0.14	-55%
P05	0.14	0.27	0.28	4%	0.08	-70%	0.11	-58%	0.55	103%	0.28	3%	0.17	-37%
P06	0.07	0.11	0.21	90%	0.06	-44%	0.09	-14%	0.44	303%	0.18	61%	0.11	3%
P07	0.22	0.28	0.37	31%	0.14	-51%	0.15	-47%	0.44	57%	0.27	-4%	0.49	75%
P08	0.33	0.40	0.34	-15%	0.09	-77%	0.10	-74%	0.53	32%	0.25	-38%	0.54	34%
P09	0.16	0.20	0.34	70%	0.09	-54%	0.10	-49%	0.55	176%	0.20	0%	0.45	123%
Av.	0.17	0.26	0.31	27%	0.10	-59%	0.12	-48%	0.50	110%	0.25	4%	0.37	27%
Std.	0.08	0.09	0.06	0.37	0.03	0.15	0.03	0.21	0.09	0.84	0.05	0.34	0.32	0.01
C.V.	0.49	0.33	0.20	-	0.27	-	0.23	-	0.18	-	0.18	-	0.39	−

* The crack width of slab under biaxial bending is according to Table 4-2 in Section 4.3.3.

Table (b)

Type B (b)	Obsered crack width*		Predicted Crack width [mm]										
	Av	Max.	by FIB Model Code 2010		by DIN EN 1992-1-2011		by DIN1045-1		by ACI318-2008		by Model-7 (Eq.(5-38))		by Model-9 (Eq.(6-25))	
P01	0.14	0.25	0.30	18%	0.16	-37%	0.19	-23%	0.22	-10%	0.36	42%	0.32	27%
P02	0.25	0.40	0.12	-69%	0.12	-71%	0.14	-65%	0.36	-9%	0.35	-13%	0.39	-1%
P03	0.09	0.13	0.20	57%	0.07	-42%	0.10	-25%	0.30	131%	0.19	49%	0.16	24%
P04	0.31	0.59	0.41	-31%	0.13	-77%	0.23	-61%	0.49	-17%	0.34	-43%	0.39	-34%
P05	0.23	0.27	0.12	-54%	0.11	-59%	0.14	-48%	0.39	44%	0.35	31%	0.30	11%
P06	0.15	0.21	0.21	-1%	0.08	-60%	0.11	-46%	0.38	79%	0.22	6%	0.21	2%
P07	0.33	0.50	0.34	-33%	0.18	-65%	0.19	-62%	0.34	-32%	0.35	-29%	0.52	4%
P08	0.48	0.54	0.16	-71%	0.13	-75%	0.14	-74%	0.42	-23%	0.35	-36%	0.55	2%
P09	0.22	0.34	0.33	-2%	0.11	-67%	0.12	-65%	0.49	44%	0.20	-41%	0.45	33%
Av.	0.25	0.36	0.24	-21%	0.12	-62%	0.15	-52%	0.38	23%	0.30	-4%	0.37	8%
Std.	0.12	0.16	0.10	0.42	0.03	0.14	0.04	0.18	0.08	0.56	0.07	0.37	0.13	0.20
C.V.	0.48	0.44	0.42	-	0.26	-	0.29	-	0.23	-	0.24	-	0.36	-

* The crack width of slab under biaxial bending is according to Table 4-2 in Section 4.3.3.
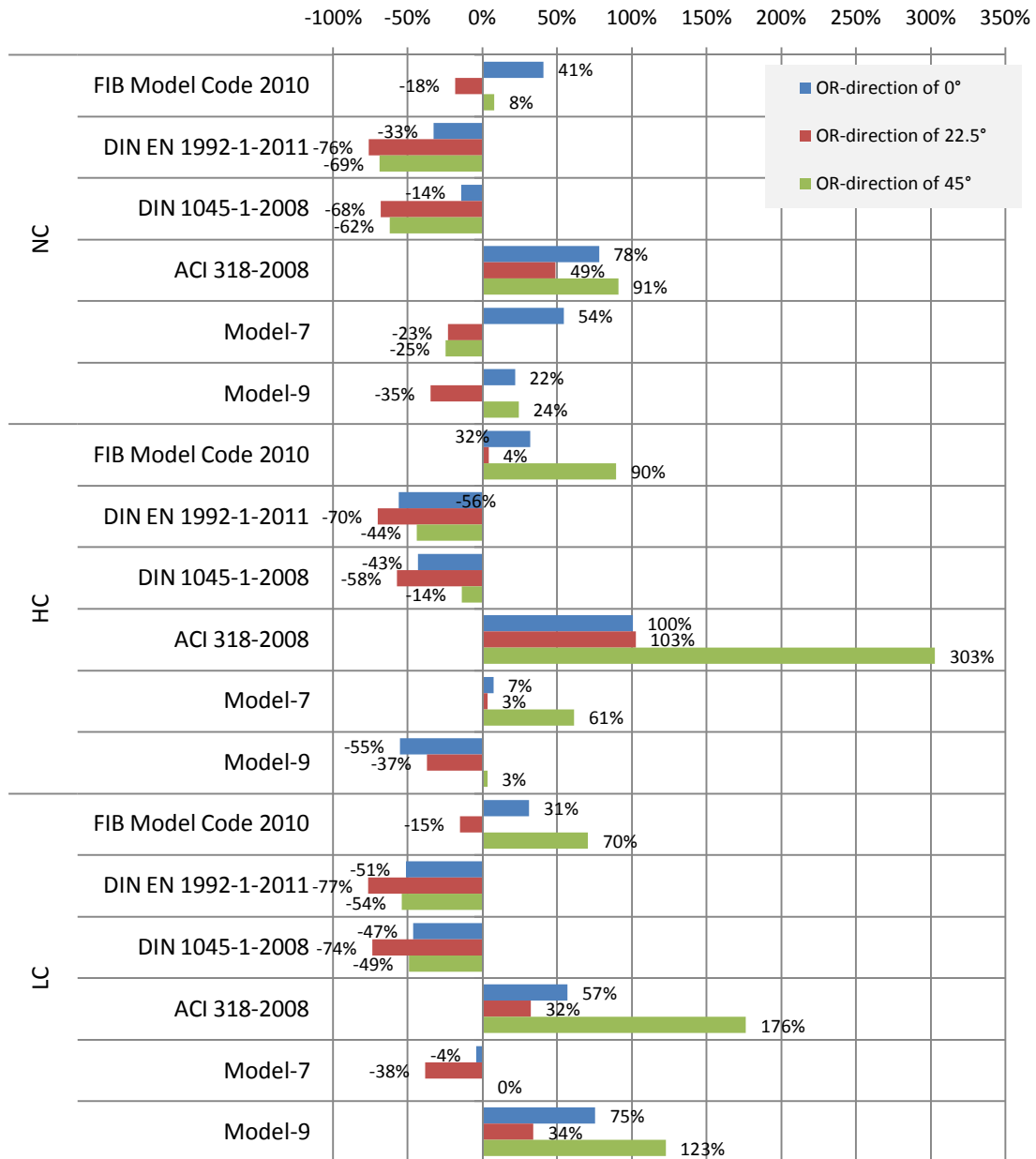
Figure 7-15 Comparison of predicted and observed maximum crack width at the load level of serviceability limit state in the direction of Type A (see Figure 5-5)
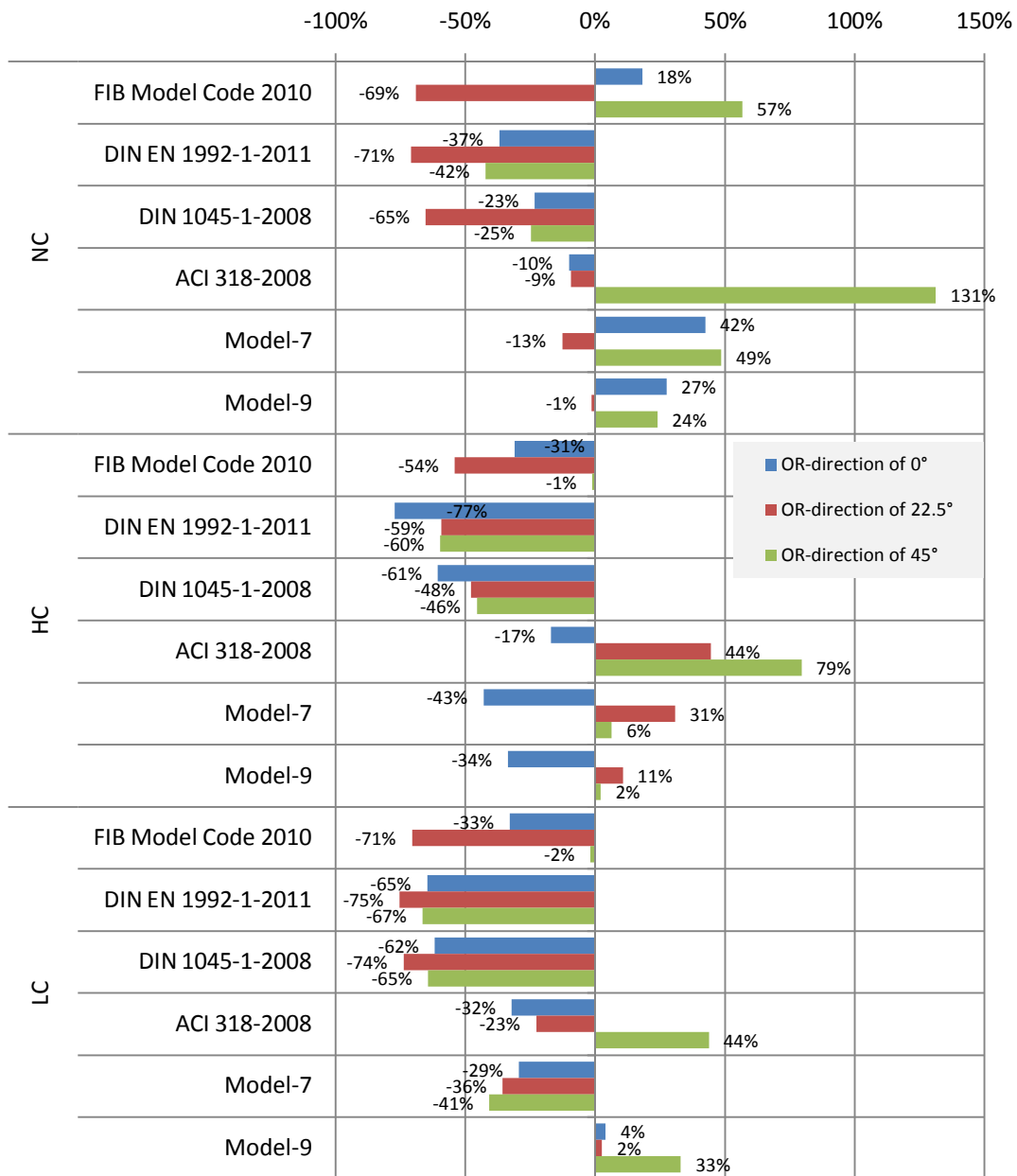
Figure 7-16 Comparison of predicted and observed maximum crack width at the load level of serviceability limit state in the direction of Type B (see Figure 5-5)
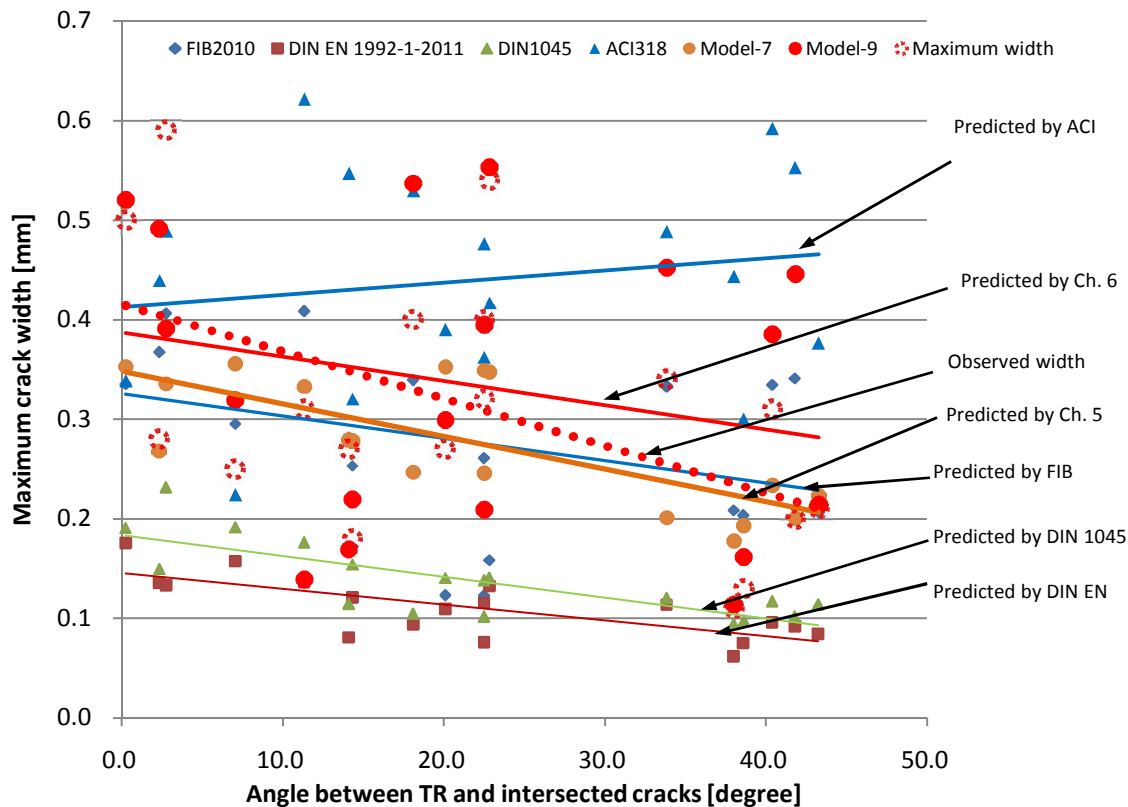
Figure 7-17 Comparison of predicted and observed maximum crack width with α_{TR} at the load level of serviceability limit state

7.6 Chapter summary

In this chapter, the average crack spacing and the maximum crack width of slab specimens under uniaxial and biaxial bending were calculated according to Model-4 (Eq.(5-7)), Model-5 (Eq.(5-12)), Model-6 (Eq.(5-37)), Model-7 (Eq.(5-38)), Model-8 (Eq.(6-23)) and Model-9 (Eq.(6-25)). The calculating procedures of these 6 proposed models for slabs under uniaxial and biaxial bending were presented as examples in Section 7.2 and 7.3. The crack spacing and width of 33 slab-strips and 9 slabs were calculated according to the actual codes, such as FIB Mode Code 2011, DIN EN 1992-1-2011, DIN 1045-1-2008 and ACI 318-2008.

A comparison of predicted and observed average crack spacing and maximum crack width for slab under uniaxial bending indicates that, TR-cover, -spacing and -direction are important factors in calculating the crack spacing and width, which were not sufficiently considered by current codes. For slabs under biaxial bending, α_{TR} and bending stress in two orghogonal directions are important factors in calculating the crack spacing and width, which were neglected by current codes. Model-4 (Eq.(5-7)) and Model-5 (Eq.(5-12)) for slabs under uniaxial and biaxial bending gave better understanding of the predicted crack spacing and width with consideration of the influence of these TR-parameters. These two models are recommended for flexural RC-slabs subjected to uniaxial and biaxial bending

with various TR.

Moreover, a direct connection between the crack width and the bending stiffness was developed by Model-7 (Eq.(5-38)) and Model-9 (Eq.(6-25)) to avoid calculating the steel stress, which was difficult to be predicted suitably for RC elements subjected to multiaxial bending. The comparison results show that these two models better estimate the maximum crack width for RC elements subjected to biaxial bending moment. The influence of TR-parameters on crack spacing and crack width must be taken into account of predicting the crack spacing and width for slabs under uniaxial and biaxial bending.

8 Conclusion and recommendations

8.1 Conclusions

The flexural cracking behavior of reinforced concrete (RC) members, such as beams and slabs, is an important issue for serviceability limit state design. It has also a significant influence on the load bearing capacity of the structures. To date, the influence of the transverse reinforcement (TR) on the crack behaivor of RC slabs subjected to uniaxial and biaxial bending has not been well understood. No experimental investigations of the influencing mechanism of TR parameters on the cracks have been carried out. Hence, design equations involving the influence of TR for the flexural cracking behavior are not available in the current codes of practice. This thesis presented a comprehensive study on the influence of transverse reinforcement on the cracking patterns of RC slabs, including both slab-strips under uniaxial bending and also slabs subjected to biaxial bending. The variations in the tests include: TR-cover, TR-spacing, TR-direction and TR-position. For each case, three different concrete types, including normal strength concrete, high strength concrete and lightweight concrete were also taken into account. Two series of experimental investigations, that is, uniaxial and biaxial bending tests, were performed, respectively. More than 8000 test data for the average crack spacing and the maximum crack width were obtained from 33 slab-strips and 9 slabs.

The experimental work on slab-strips subjected to uniaxial bending reveals that the TR-cover TR-spacing as well as TR-direction has a considerable influence on the cracking behavior of the members. TR-cover and TR-spacing affect the number of TR-intersected cracks, thus affect crack spacing and width. TR-direction does not obviously make the crack inclining, but an increase of TR-direction results in a significant decrease of crack width. The influence of concrete types on crack behavior is related to the bond-slip relationship between steel and concrete. Based on the experimental observations and theoretical analysis, new calculation equations for the average crack spacing and maximum crack width of RC slabs subjected to uniaxial bending were proposed. These equations take into account the influence of the transverse reinforcement and concrete types.

A comparison of the calculated and experimental data indicates that the proposed design models for average crack spacing and maximum crack width succeed to better predict averagely 17% and 11% percentage errors compared to 68% and 58% errors according to FIB Model Code 2010, DIN EN 1992-1-2011, DIN 1045-1-2008 and ACI 318-2008.

In the experiment on RC slabs subjected biaxial bending, the experimental observations verify that the different TR-cover in two orthogonal directions result in a different numbers of TR-induced cracks. The inclined orthogonal reinforcement net from 0° to 45° does not lead to a change of overall direction of cracks. In general, the influence of TR on

the crack behavior of the slab under biaxial bending is in good agreement with that in uniaxial bending. Moreover, due to the biaxial bending stress, a reverse relationship of decreasing bond-slip stress on perpendicular direction and increasing crack spacing and width was found in the experiment. Based on the mechanism analysis of interaction between TR and the surrounding concrete, new models were developed to predict the average crack spacing and the maximum crack width of RC slabs under biaxial bending taking into account the TR-cover and TR-direction in two orthogonal directions and concrete types.

In comparison with the design provisions, the new design equations can describe the cracking behavior of RC slabs subjected to biaxial bending in a more accurate way. Numerically, The proposed design models for average crack spacing and maximum crack width succeed to better predict averagely 7% and 4% percentage errors compared to -29% and 50% errors according to accrual codes.

Moreover, experimentally, a direct correlation between the curvature and the average crack width has been verified by test results of one-way and two-way slab.

Furthermore, two flexural crack design models were presented to calculate maximum crack width of slabs under uniaxial and biaxial bending. These two model are based on a series of theoretical analysis, such as analyzing the bond strength at cracked and uncracked sections, deriving equation of the compressive zone height at both sections, establishing a geometry equilibrium equations at cracked section and etc. The proposed flexural crack width models provides a prediction averagely 12% and 17.5% percentage errors for slabs under uniaxial and biaxial bending, respectively. These models not only provide a better prediction, but also present a direct connection between crack width and bending stiffness was developed in order to avoid calculating the steel stress, which was difficult to be predicted accurately for RC element subjected to multi-axial forces.

8.2 Recommendations

The proposed average crack spacing and maximum crack width design models in Chapter 5 and 6 give good predictions for maximum crack width. However, the formulae need to be simplified to apply in construction. For further research, the simplified models can be developed on the basis of these expressions.

The proposed flexural maximum crack width design models in Chapter 6 gives a reasonable approach to predict the crack width based on bending stiffness in the elastic and plastic stage. However, the prediction accuracy of these models depends on the prediction accuracy of bending stiffness of RC element subjected to multi-axial bending. Therefore, for further research, bending stiffness is one of the main directions to increase the prediction accuracy of the flexural model and the predicted maximum crack width for RC element with various bending loads.

A two-way slab subjected to uniform load is one of the most general load situations. The

application of the proposed crack spacing and width design models in these load situations can be verified and modified by the test results from other researchers in future research.

In the experimental work of this thesis, the displacement cloudy on one-way and two-way slabs was acquired and processed by Laser-scanner and MATLAB. This acquisition data can be used for further research on nonlinear behaviors of one- and two-way slab specimens, especially research on curvature and bending stiffness in different complicated areas. This investigation can increase the prediction accuracy of bending stiffness; hence, the prediction accuracy of the proposed flexural maximum crack width design models in Chapter 6 can be enhanced as well.

As the proposed the proposed flexural maximum crack width design models of Chapter 6 confirmed the correlation between the bending stiffness and the crack width, which gives a possibility to connect the stiffness matrix with the crack spacing and width in Finite Element Method. This connection can be applied to predict crack position and width and hence can be implemented in a visual crack pattern in FEM software

Reference

1. Nilson, A.H., D. Darwin, and W.D. Dolan, *Design of Concrete Structures (13th edition).* Singapore: Mc Graw Hill Higher Education., 2004: p. 203-204.

2. Gergely, P. and L.A. Lutz, *Maximum Crack Width in Reinforced Concrete Flexural Members. in Causes, Mechanisms, and Control of Cracking in Concrete.* SP-20, American Concrete Insitute, Deroit, 1968: p. pp 1-17.

3. Kaar, P.H. and A.H. Mattock, *High-Strength Bars as Concrete Reinforcement-Part 4: Control of Cracking.* Journal, PCA Research and Development Laboratories, 1963. **vol. 5(1)**: p. pp 15-38.

4. Broms, B.B., *Width and Crack Spacing in Reinforced Concrete Member.* ACI Structureal Journal, 1965. **vol. 62(10)**: p. pp 1237-1256.

5. Saliger, R., *High-grade steel in reinforced concrete.* Proceedings Second Congress of the International Association for Bridge and Structureal Engineering, Berlin-Munich., 1936.

6. FIB2010, *Model Code 2010 (Draft).* 2010.

7. Beeby, A.W., *The Prediction of Crack widths in Hardened concrete.* The Structural Engineer (UK), 1979. **Vol. 57A, No. 1, January 1979**: p. pp. 9-17.

8. Noesterle, R.G. and H.G. Russell, *Tangential Shear Tests of Reinforced Concrete Containment Elements,.* Nuclear Engineering and Design 1980. **59**: p. 99-122.

9. Lee, S.L., et al., *Cracking Behavior of Concrete Tension Members Reinforced with Welded Wire Fabric.* ACI Structural Journal, 1987. **11-12**.

10. Rizkalla, S.H., L.S. Hwang, and M. El Shahawi, *Transverse reinforcement effect on cracking behaviour of R.C. members.* Canadian Journal of Civil Engineering, 1983. **10**: p. 566-581.

11. Purainer, R., *Last- und Verformungsverhalten von Stahlbetonflächentragwerken unter zweiaxialer Zugbeanspruchung.* Dissertation. Universität der Bundeswehr München, 2005.

12. Nawy, E.G. and G.S. Orensteln, *Crack Width Control in Reinforced Concrete Two Way Slabs.* ASCE, 1970. **93**: p. 701-721.

13. Nawy, E.G. and K.W. Blair, *Further Studies on Flexural Crack Control in Structural Slab Systems.* ACI special Publication 30, 1971: p. 1-41.

14. Clark, L.A., *Flexural Cracking in slab Bridge.* Technical Report of Cement and Concrete Association, London., 1973. **1973**.

15. Purainer, R. and M. Keuser, *Versuche and Stahlbetonscheiben und -platten unter Zugbeanspruchung.* Berichte aus dem Konstruktiven Ingenieurbau, 2006. **Vol. 06/3**.

16. Keuser, M. and R. Purainer, *Cracking and Load-carrying Behavior of Reinforced Concrete Planels Subjected to Biaxial Tension.* 5th International PhD-Symposium in

Civil Engineering 2004.

17. Keuser, M., L. Ruediger, and N. Hallermann, *Platten aus Stahlbeton unter zweiaxialer Biegebeanspruchung.* Beton-und Stahlbetonbau, 2007. **Vol.102, No. 5**: p. 14.

18. Xiao, S. and H. Li, *Experimental study of biaxial compressive damage behaviour of concrete at different strain rates.* Materials Research Innovations, 2011. **15**: p. S266-S269.

19. Zhou, X.Q. and H. Hao, *Modelling of compressive behaviour of concrete-like materials at high strain rate.* International Journal of Solids and Structures, 2008. **45**(17): p. 4648-4661.

20. Ding, Y.N. and W. Kusterle, *Compressive stress-strain relationship of steel fibre-reinforced concrete at early age.* Cement and Concrete Research, 2000. **30**(10): p. 1573-1579.

21. Kim, Y.R., et al., *Micromechanical Model for Heterogeneous Asphalt Concrete Mixtures Subjected to Fracture Failure.* Journal of Materials in Civil Engineering, 2011. **23**(1): p. 30-38.

22. Li, K.F. and C.S. Zhou, *Numerical and statistical analysis of permeability of concrete as a random heterogeneous composite.* Computers and Concrete, 2010. **7**(5): p. 469-482.

23. Wang, J.S., et al., *Adhesive-Bonded Anchorage Pullout Test to Estimate In-Place Concrete Compressive Strength.* Journal of Testing and Evaluation, 2008. **36**(6): p. 500-505.

24. Huon, V., O. Maisonneuve, and B. Cousin, *Thermomechanical behaviour of a plain concrete in compressive test: experimentation and modelling.* Comptes Rendus De L Academie Des Sciences Serie Ii Fascicule B-Mecanique, 2001. **329**(12): p. 889-896.

25. Bishr, H.A.M., et al., *Assessment of Concrete Compressive Strength Using the Lok Test.* Construction and Building Materials, 1995. **9**(4): p. 227-237.

26. König, G., N.V. Tue, and M. Zink, *Hochleistungsbeton.* Ernst & Sohn Verlag, Berlin, 2001.

27. Rüsch, H., *Versuche zur Festigkeit der Biegedruckzone.* Heft 120 Deutscher Ausschuss für Stahlbeton, Verlag Ernst & Sohn, Berlin, 1955.

28. Heft-525-DAfStb, *Erläuterungen zu DIN 1045-1. .* Deutscher Ausschuss für Stahlbeton Beuth Verlad, Berlin, 2003.

29. DIN-1045-1-2008, *Tragwerke aus Beton, Stahlbeton und Spannbeton, Bemessung und Ausführung.* Beuth Verlag, Berlin, 2008.

30. Grübl, P., J. Weigler, and S. Karl, *Beton, Arten - Herstellung - Eigenschaften.* 2. Auflage, Verlag Ernst & Sohn, Berlin, 2001.

31. DIN-EN-12390, *Prüfung von Festbeton.* Beuth Verlag, Berlin, 2001.

32. Li, Z.J., et al., *Uniaxial tensile behavior of concrete reinforced with randomly*

distributed short fibers. Aci Materials Journal, 1998. **95**(5): p. 564-574.

33. Ferreira, M., et al., *Tensile and uniaxial fatigue behavior of poly(p-phenylene-co-3,4 '-oxydiphenylene terephthalamide) fibers: Relationship with chain orientation.* Textile Research Journal, 1999. **69**(1): p. 30-37.

34. Lin, Z.H. and L. Wood, *Concrete uniaxial tensile strength and cylinder splitting test.* Journal of Structural Engineering-Asce, 2003. **129**(5): p. 692-698.

35. L'vov, V.A. and N. Glavatska, *Theoretical consideration of the time-dependent deformation of ferromagnetic Ni-Mn-Ga martensite.* Materials Science and Engineering a-Structural Materials Properties Microstructure and Processing, 2008. **481**: p. 279-282.

36. Alcan, T., C. Ceylanoglu, and B. Baysal, *The Relationship between Digital Model Accuracy and Time-Dependent Deformation of Alginate Impressions.* Angle Orthodontist, 2009. **79**(1): p. 30-36.

37. Tokatly, I.V., *Time-dependent current density functional theory via time-dependent deformation functional theory: a constrained search formulation in the time domain.* Physical Chemistry Chemical Physics, 2009. **11**(22): p. 4621-4630.

38. Zhang, X.C., et al., *Time-dependent creep deformation of the coating-based system under in-plane bending moment.* Materials & Design, 2009. **30**(10): p. 4543-4547.

39. Wittmann, F.H., *Corrosion of cement-based materials under the influence of an electric field.* Electrochemical Methods in Corrosion: Research and Application, 1997. **247**: p. 107-126.

40. Bazant, P., et al., *Guidelines for Characterizing Concrete Creep and Shrinkage in Structural Design Codes or Recommendations.* Materials and Structures, 1995. **28**(175): p. 52-55.

41. DIN-EN-1992-1-2011, *Teil 1-1: Allgemeine Bemessungsrregeln und Regeln für den Hochbau Deutsche Fassung EN 1992-1-1:2004+AC:2010.* Eurocode 2: Bemmessung und Konstruktion von Stahlbeton- und Spannbetontragwerken, 2011.

42. HEFT-425-DAfStb, *Bemessungshilfen zu Eurocode 2 Teil 1.* Deutscher Ausschuss für Stahlbeton, Beuth Verlag, Berlin, 1992.

43. Lockner, D.A. and T.R. Madden, *A Multiple-Crack Model of Brittle-Fracture .1. Non Time-Dependent Simulations.* Journal of Geophysical Research-Solid Earth, 1991. **96**(B12): p. 19623-19642.

44. Lockner, D.A. and T.R. Madden, *A Multiple-Crack Model of Brittle-Fracture .2. Time-Dependent Simulations.* Journal of Geophysical Research-Solid Earth, 1991. **96**(B12): p. 19643-19654.

45. Filiatrault, A. and M. Holleran, *Stress-strain behavior of reinforcing steel and concrete under seismic strain rates and low temperatures.* Materials and Structures, 2001. **34**(238): p. 235-239.

46. Ting, S.C., A.S. Nowak, and K.S. Li, *Effect of Reinforcing Steel Area Loss on Flexural Behavior of Reinforced-Concrete Beams - Discussion.* ACI Structural Journal, 1992.

89(2): p. 216-217.

47. Jo, B.W., Y.H. Shon, and Y.J. Kim, *The evalution of elastic modulus for steel fiber reinforced concrete.* Russian Journal of Nondestructive Testing, 2001. **37**(2): p. 152-161.

48. Kankam, C.K., *Relationship of bond stress, steel stress, and slip in reinforced concrete.* Journal of Structural Engineering-Asce, 1997. **123**(1): p. 79-85.

49. Tang, D.L., et al., *Influence of Surface Crack Width on Bond Strength of Reinforced Concrete.* Aci Materials Journal, 2011. **108**(1): p. 29-37.

50. Dai, J.G., T. Ueda, and Y. Sato, *Development of the nonlinear bond stress-slip model of fiber reinforced plastics sheet-concrete interfaces with a simple method.* Journal of Composites for Construction, 2005. **9**(1): p. 52-62.

51. Lyons, J. and D. Huang, *Numerical stress analysis of the bond between a reinforced concrete T-Beam and FRP sheets.* Journal of Reinforced Plastics and Composites, 2007. **26**(12): p. 1225-1237.

52. Harajli, M.H., M. Hout, and W. Jalkh, *Local Bond Stress-Slip Behavior of Reinforcing Bars Embedded in Plain and Fiber Concrete.* Aci Materials Journal, 1995. **92**(4): p. 343-354.

53. Giuriani, E., G. Plizzari, and C. Schumm, *Role of Stirrups and residual Tensile Strength of Cracked Concrete on Bond.* Journal of the Structural Division, Proceeding, American Society of Civil Engineers, 1991. **117**(1): p. 1-18.

54. Carpinteri, A., J.R. Carmona, and G. Ventura, *Propagation of flexural and shear cracks through reinforced concrete beams by the bridged crack model.* Magazine of Concrete Research, 2007. **59**(10): p. 743-756.

55. Kulkarni, N., et al., *Fatigue crack growth and life prediction of foam core sandwich composites under flexural loading.* Composite Structures, 2003. **59**(4): p. 499-505.

56. Kolluru, S.V., et al., *Crack propagation in flexural fatigue of concrete.* Journal of Engineering Mechanics-Asce, 2000. **126**(9): p. 891-898.

57. Toumi, A., A. Bascoul, and A. Turatsinze, *Crack propagation in concrete subjected to flexural-cyclic loading.* Materials and Structures, 1998. **31**(211): p. 451-458.

58. Shiah, Y.C., *Transverse flexural fracture of a plate containing an arc crack.* Journal of the Chinese Institute of Engineers, 2002. **25**(2): p. 189-198.

59. Makhlouf, H.M. and F.A. Malhas, *The effect of thick concrete cover on the maximum flexural crack width under service load.* ACI Structural Journal, 1996. **93**(3): p. 257-265.

60. Warner, R.F., et al., *Concrete Structures.* Addison Wesley Lonmen Australia Pty. Ltd., South Melbourne, Australia, 1998.

61. Marchenko, A., *Parametric excitation of flexural-gravity edge waves in the fluid beneath an elastic ice sheet with a crack.* European Journal of Mechanics B-Fluids, 1999. **18**(3): p. 511-525.

62. Zhang, J. and H. Stang, *Applications of stress crack width relationship in predicting the flexural behavior of fibre-reinforced concrete.* Cement and Concrete Research, 1998. **28**(3): p. 439-452.

63. El-Ariss, B., *Behavior of beams with dowel action.* Engineering Structures, 2007. **29**(6): p. 899-903.

64. Martin-Perez, B. and S.J. Pantazopoulou, *Effect of bond, aggregate interlock and dowel action on the sheer strength degradation of reinforced concrete.* Engineering Structures, 2001. **23**(2): p. 214-227.

65. Soroushian, P., K.B. Choi, and A. Ahlhamad, *Dynamic Constitutive Behavior of Concrete.* ACI Journal, 1986. **83**: p. 251-259.

66. Soroushian, P., K. Obaseki, and M.C. Rojas, *Bearing Strength and Stiffness of Concrete under Reinforcing Bars.* Aci Materials Journal, 1987. **84**: p. 179-184.

67. Huang, X.M. and C.Y. Yang, *Early-age concrete cover crack and its effects on concrete cover.* Environmental Ecology and Technology of Concrete, 2006. **302-303**: p. 630-636.

68. Tae, S.H., et al., *Corrosion resistance of Cr-bearing rebar to macrocell corrosion caused by concrete cover crack.* Isij International, 2006. **46**(7): p. 1086-1092.

69. Ryu, J.S., *Influence of crack width, cover depth, water-cement ratio and temperature on the formation of electrodeposits on the concrete surface.* Magazine of Concrete Research, 2003. **55**(1): p. 35-40.

70. Makhlouf, H.M. and F.A. Malhas, *The effect of thick concrete cover on the maximum flexural crack width under service load.* ACI structural journal, 1996. **93**: p. 257-265.

71. Frosch, R., *Another Look at Cracking and Crack Control in Reinforced Concrete.* Aci Structural Journal, 1999. **96**: p. 437-442.

72. Leevers, P.S., P.N. Freeman, and M.M. Arthur, *Rapid Crack-Propagation in Small-Diameter Thermoplastic Pipe.* Plastics Rubber and Composites Processing and Applications, 1995. **24**(3): p. 113-121.

73. Clark, A.P., *Cracking in Reinforced Concrete Flexural Members.* Journal of the American Concrete Institute, 1956. **V. 27, No. 8**.

74. ACI-318-05, *Building Code Requirements for Structural Concrete.* American Concrete Institute, Farmington Hills, , 2005.

75. Muttoni, A. and M.F. Ruiz, *Shear strength of members without transverse reinforcement as function of critical shear crack width.* ACI Structural Journal, 2008. **105**(2): p. 163-172.

76. Sahmaran, M. and I.O. Yaman, *Influence of transverse crack width on reinforcement corrosion initiation and propagation in mortar beams.* Canadian journal of civil engineering, 2008. **35**(3): p. 236-245.

77. Cho, S.H. and L.H. Lee, *Rotating- and fixed-angle crack models in beams without transverse reinforcement.* ACI Structural Journal, 2000. **97**(5): p. 757-764.

78. Ruedier, L. and M. Keuser, *Numerische Berechnungen zur Untersuchung des Einflusses der Bewehrungsrichtung auf das Last-Verformungsverhalten von Stahlbetonplatten.* Beton-und Stahlbetonbau, 2008. **Vol. 103, No. 6**: p. 10.

79. Radaj, D., *Ermüdungsfestigkeit - Grundlagen für Leichtbau, Maschinen- und Stahlbau. 2. Auflage,.* Springer- Verlag, Berlin Heidelberg New Zork, 2003.

80. Petersen, S.B., J.M.C. Rodrigues, and P.A.F. Martins, *Extended Formability Limits for Tubular Components through Combined Injection Forming Upsetting - a Finite-Element Analysis.* Proceedings of the Institution of Mechanical Engineers Part B-Journal of Engineering Manufacture, 1995. **209**(2): p. 107-114.

81. Ruediger, L., *Zum Tragverhalten von Stahlbetonplatten unter Berücksichtigung der Steifigkeitsänderung im gerissenen Zustand.* Dissertation. Universität der Bundeswehr München, 2008.

82. Hughes, B.P. and C.V. Cifuentes, *Comparison of Early-age Crack Width Formulas for Reinforced Concrete.* ACI Structural Journal, 1988. **Vol. 85, No. 2, March-April 1988**: p. pp. 158-166.

83. CEB(1990), *Behavior and Analysis of Reinforced Concrete Structures under Alternate Actions Including Inelastic Response.* Bulletin d'Information No.210, Comite Euro-International du Beton, Lausanne, 1990.

84. Fantilli, A.P., H. Mihashi, and P. Vallini, *Effect of bond-slip on the crack bridging capacity of steel fibers in cement-based composites.* Journal of Materials in Civil Engineering, 2008. **20**(9): p. 588-598.

85. Dominguez, N., et al., *Prediction of crack pattern distribution in reinforced concrete by coupling a strong discontinuity model of concrete cracking and a bond-slip of reinforcement model.* Engineering Computations, 2005. **22**(5-6): p. 558-582.

86. Chen, G. and G. Baker, *Influence of bond slip on crack spacing in numerical modeling of reinforced concrete.* Journal of Structural Engineering-Asce, 2003. **129**(11): p. 1514-1521.

87. Rizza, R. and K. Meade, *No-slip crack model for damaged bone/cement interface.* Engineering Fracture Mechanics, 2003. **70**(6): p. 757-773.

88. Jirasek, M., *Embedded crack model: II. Combination with smear cracks.* International Journal for Numerical Methods in Engineering, 2001. **50**(6): p. 1291-1305.

89. Beeby, A.W., *An Investigation of cracking in Slabs Spanning One Way* Technical Report TRA 433, Cement and Concrete Association, London, 1970. **33**.

90. Beeby, A.W., *Prediction and Control of Flexural Cracking in Reinforced Concrete Members.* Cracking, Deflection and Ultimate Load of Concrete Slab System, SP-30, American Concrete Institute, Detroit, 1971: p. 55-75.

91. 50010-2002, G., *Code for Design of Concrete Structure.* National Standard of The People's Republic of China, 2002: p. 86-96.

92. 2000, I., *Plain and Reinforced Concrete Code of Practice [Fouth Revision].* 2000.

93. ACI-318-08, *Building Code Requirements for Structural Concrete.* American Concrete Institute, Farmington Hills, , 2008.

94. Venkateswarlu, B. and H. Gesund, *Cracking and Bond Slip in Concrete Beams.* Journal of the Structural Division, Proceeding, American Society of Civil Engineers, 1972. **98**(ST11): p. 2663-2885.

95. Bazant, Z.P. and B.H. Oh, *Spacing of Cracks in Reinforced Concrete.* Journal of the Structural Engineering, ASCE, 1983. **109**(9): p. 2066-2085.

96. ACI-318-95, *Building Code Requirements for Structural Concrete.* American Concrete Institute, Farmington Hills, , 1995.

97. ACI-318-99, *Building Code Requirements for Structural Concrete.* American Concrete Institute, Farmington Hills, , 1999.

98. Clark, A.L., *Crack similitude in 1:3.7 Scale Models of Slabs Spanning One Way.* Technical Report 43.455, Cement and Concrete Association, London, 1972: p. 24.

99. MacGregor, J.G. and A.O. Aghayere, *Analysis of Concrete Plates under Combined Inplane and Transverse Loads.* ACI Structural Journal, 1990. **87**(5): p. 539-547.

100. Rizk, E. and H. Marzouk, *A New Formula to Calculate Crack Spacing for Concrete Plates.* ACI Structureal Journal, 2010. **107, No.1**: p. 47-52.

101. DIN1048, *Prüfverfahren für Beton.* Beuth Verlag, Berlin, 1991.

102. Marzouk, A.M., M. Hossin, and A. Hussein, *Crack Width Estimation for Concrete Plates.* ACI Journal, 2010. **107**(3): p. 282-290.

103. Castel, A., T. Vidal, and R. FranÇOis, *Effective Tension Active Cross-Section of Reinforced Concrete Beams After Cracking.* MATERIALS AND STRUCTURES, 2006. **39**: p. 115-126.

104. Rangan, B.B., *Control of Beam Deflection by Allowable Span-Depth Ratios,.* ACI Journal, Proceedings, 1982. **79**(5): p. 372-377.

105. Baumann, T., *Tragwirkung orthogonaler Bewehrungsnetze beliebiger Richtung in Flächentragwerken aus Stahlbeton.* Heft 217 Deutscher Ausschuss Fär Stahlbeton, Verlag Ernst & Sohn, Berlin - München - Düsseldorf, 1972.

106. Nilson, A.H., D. Darwin, and C.W. Dolan, *Design of Concrete Structures.* 2004: p. 71-73.

107. Branson, D.E., *Instantaneous and Time-dependent Deflections of Simple and Continuos Reinforced Concrete Beams.* HPR Report No. 7 Part 1, Alabama Highway Department/ U.S. Bureauof Public Roads,, 1963: p. 78.

108. ACI-Committe-318, *Building Code Requirements for Reinforced Concrete (ACI318-2008).* American Concrete Institute, 2008.

109. Al-Zaid, R.Z., A.H. Al-Shaikh, and M.M. Abu-Hussein, *Effect of Loading Type on the Effective Moment of Inertia of Reinforced Concrete Beams.* ACI Structureal Journal, 1991. **88**(2): p. 184-190.

110. Al-Shaikh, A.H. and R.Z. Al-Zaid, *Effect of Reinforcement Ratio on the Effective Moment of Inertia of Reinforced Concrete Beam.* ACI Structural Journal, 1993. **90**(2): p. 144-149.

111. Grossmann, J.S., *Simplified Computations for Effective Moment of Inertia Ie and Minimum Thickness to Avoid Deflection Computation, Proceedings.* ACI Journal, 1981. **78**(6): p. 423-439.

Index

Figure Index

Table Index

Appendix A   Symbols Index

Abbreviations

TR	Transverse reinforcement
LR	Longitudinal reinforcement
DIN	Deutscher Ausschuss für Normung e.V.
FE	Finite Element
HC	High-strength concrete
LC	Light-weight concrete
NB	Normal-strength concrete
OR	Orthogonal reinforcement concrete of slab
RC	Reinforced concrete
Type A	Transverse reinforcement is outside of longitudinal reinforcement
Type B	Transverse reinforcement is inside of longitudinal reinforcement
Av.	Average values
Std.	Standard deviation
C.V.	Coefficient of variability

Symbols

Latin small letters

b	Width
c	Concrete cover
d_a	Maximum aggregate size
f	Strength
j	Influence coefficient of TR
l	Clear spacing
n	Number
r	Diameter
s	Reinforcement spacing
S	Crack spacing
w	Crack width

Latin large letters

A	Area
B	Bending stiffness
E	Young's module
M	Moment
N	Normal forces
X	X-axis
Y	Y-axis

Greek letters

η	The ratio of the number of TR-induced cracks to all cracks
θ	The angle between the reinforcement and bending direction
α	The angle between TR and TR-intersected cracks
ε	Strain
σ	Stress

186

κ	Curvature
ϕ	Diameters of reinforcement
π	Value of π
τ	Bond strength

Indices$(\dots)$

$(\dots)_c$	Concrete
$(\dots)_{cover}$	Transverse reinforcement cover
$(\dots)_{cube}$	Cube
$(\dots)_{ctm}$	Average tensile strength
$(\dots)_{direction}$	Transverse reinforcement direction
$(\dots)_{eff}$	Effective
$(\dots)'$	characteristic compressive strength
$(\dots)_m$	Average values
$(\dots)_{min}$	Minimum value
$(\dots)_{max}$	Maximum values
$(\dots)_s$	Steel
$(\dots)_{spacing}$	Transverse reinforcement spacing
$(\dots)_A$	In on the direction of Type A of two-way slabs
$(\dots)_B$	In on the direction of Type B of two-way slabs
$(\dots)_{TR}$	Transverse reinforcement direction
$(\dots)_{LR}$	Transverse reinforcement direction
$(\dots)_X$	In the direction of X-axis of two-way slabs
$(\dots)_Y$	In on the direction of Y-axis of two-way slabs

Proposed models list

Model-1: The model to predict the ratio of TR-induced crack to all cracks with considering parameters of TR-cover and TR-spacing. Refer to Eq. (5-4)

Model-2: The model to predict the ratio of TR-induced crack to all cracks with considering parameters of TR-cover and TR-spacing for two-way slab. Refer to Eq. (5-9)

Model-3: The model to predict the percentage of cracks intersecting TR with considering TR-parameters, including TR-cover, TR-spacing and TR-direction. Refer to Eq. (5-6).

Model-4: The model to predict average crack spacing for one-way slab with consideration of TR-parameters influence (refer to Model-3 Eq. (5-6) on the basic of formulas of DIN EN 1992-1-2011. Model-4 (refers to Eq. (5-7))

Model-5: The model to predict average crack spacing for two-way slab width consideration of TR-parameters influence and bending stress in to orthogonal directions on the basic of formulas of DIN EN 1992-1-2011. Model-5 refers to Eq. (5-12)

Model-6: The model to predict maximum crack width for one-way slab with consideration of TR-parameters influence on the basic of the crack model (according to Eq. (5-7)). The maximum crack spacing was predicted by the proposed Model-4 (see Eq. (5-7)). Model-6 refers to Eq. (5-37)

Model-7: The model to predict maximum crack width for two-way slab with consideration of TR-parameters influence and bending stress in two orthogonal directions on the basic of formulas of DIN EN 1992-1-2011. The maximum crack spacing was predicted by the proposed Model-5 (see Eq. (5-12)). Model-7 refers to Eq. (5-38).

Model-8: The model to predict maximum crack width for one-way slab on the basic of the relationship between the crack width and the average bending strain of flexural TR-element. The maximum crack spacing was predicted by the proposed Model-4 (see Eq. (5-7)). Model-8 refers to Eq. (6-23).

Model-9: The model to predict maximum crack width for two-way slab on the basic of the relationship between the crack width and the average bending strain of flexural TR-element in two directions. The maximum crack spacing was predicted by the proposed Model-5 (see Eq. (5-12)). Model-9 refers to Eq. (6-25).

Appendix B Material properties

Appendix B.1   Reinforcement

Figure B-1: Steel reinforcement properties in the beam and slab test

Test specimens	f_{yk} [N/mm^2]	f_{uk} [N/mm^2]	E_s [N/mm^2]
BStZP01	595.56	693.19	198138
BStZP01	595.12	696.59	204842
BStZP01	602.58	699.45	204355
BStZP01	602.58	693.10	202000
BStZP01	602.32	698.24	195931
BStZP01	599.63	696.12	201053

Appendix B.2   Concrete

➢ Calculation the material parameters according to DIN 1045-1-2008

The assessment of concrete properties is according to the the Eq. (1) to (4). In DIN 1045-1, the average tangent modul (E_{c0m}) can be calculated by

$$E_{c0m} = 9500 \cdot (f_{ck} + 8)^{1/3} \tag{1}$$

f_{ck} is the characteristic cylinder compressive strength of concrete in 28 days;

The elastic module can be obtained by Eq. (2)

$$E_{cm} = \alpha_i \cdot E_{c0m}$$
$$mit : \alpha_i \cdot 0,8 + 0,2 \cdot \frac{f_{cm}}{88} \leq 1,0 \tag{2}$$

For lightweight concrete, the coefficient η_E is considered:

$$\eta_E = (\rho / 2200)^2 \tag{3}$$

with ρ in kg/m^3 and Eq. (4), The characteristic compressive strength of concrete f_{ck} can be considered as the test average cube compressive strength $f_{cm,cube,15}$

$$f_{ck} = 0,92 \cdot \frac{f_{cm,cube,15}}{1,25} - 8 \tag{4}$$

The formula of average tensile strength according to DIN-1045-1-2008 for normal concrete is

$$f_{ctm} = 0,30 \cdot f_{ck}^{\,2/3} \tag{5}$$

For high-strength concrete, the f_{ctm} can be calculated by

$$f_{ctm} = 2,12 \cdot \ln\left(1 + \frac{f_{cm}}{10}\right) \tag{6}$$

For light-weight concrete coefficient η_1 is combined:

$$\eta_1 = 0,40 + 0,60\rho / 2200 \tag{7}$$

with ρ in kg/m^3

The fossicked scattering of tensile strength by 5% and 95% is

$$f_{ctk;0,05} = 0,70 \cdot f_{ctm}$$
$$f_{ctk;0,95} = 1,30 \cdot f_{ctm} \tag{8}$$

Figure B-2 Test group with various of TR-concrete cover – Serien-1

Test No.	TR-spacing [mm]	TR-direction	Concrete types	Age old test [d]	Density [kg/m^3]	$f_{ck.cube}$ [N/mm^2]	$f_{ck.cyl}$ [N/mm^2]	f_{ctm} [N/mm^2]	E_c [N/mm^2]
A1C1	100	0°	NB	118	2451	51.65	30.01	2.90	283135
A2C1	100	0°	NB	121	2451	51.65	30.01	2.90	283135
A3C2	100	0°	NB	215	2311	34.00	26.01	2.63	270002
A4C2	100	0°	NB	216	2311	34.00	26.01	2.63	270002
A5C3	100	0°	NB	116	2451	51.65	30.01	2.90	283135
A6C3	100	0°	NB	117	2451	51.65	30.01	2.90	283135
B1C1	200	0°	NB	118	2451	51.65	30.01	2.90	283135
B2C1	200	0°	NB	120	2451	51.65	30.01	2.90	283135
B3C2	200	0°	NB	121	2451	51.65	30.01	2.90	283135
B4C2	200	0°	NB	123	2451	51.65	30.01	2.90	283135
B5C3	200	0°	NB	124	2451	51.65	30.01	2.90	283135
B6C3	200	0°	NB	126	2451	51.65	30.01	2.90	283135
C1C2	300	0°	NB	126	2451	51.65	30.01	2.90	283135
C2C2	300	0°	NB	127	2451	51.65	30.01	2.90	283135

Figure B-3: Test group with various of TR-direction – Serien-2

Test No.	Beton types	Age old test [d]	Density [kg/m³]	$f_{ck,cube}$ [N/mm²]	$f_{ck,cyl}$ [N/mm²]	f_{ctm} [N/mm²]	E_c [N/mm²]
N1w1	NC	215	2311	34.00	26.01	2.63	270002
N2w1	NC	216	2311	34.00	26.01	2.63	270002
N3w2	NC	218	2311	34.00	26.01	2.63	270002
N4w2	NC	220	2311	34.00	26.01	2.63	270002
N5w3	NC	211	2311	34.00	26.01	2.63	270002
N6w3	NC	213	2311	34.00	26.01	2.63	270002
H1w1	HC	118	2454	81.77	73.77	4.70	406493
H2w1	HC	120	2454	81.77	73.77	4.70	406493
H3w2	HC	121	2454	81.77	73.77	4.70	406493
H4w2	HC	123	2454	81.77	73.77	4.70	406493
H5w3	HC	124	2454	81.77	73.77	4.70	406493
H6w3	HC	126	2454	81.77	73.77	4.70	406493
L1w1	LB	68	1536	39.60	21.15	1.81	121799
L1w1	LC	67	1536	39.60	21.15	1.81	121799
L3w2	LC	72	1536	39.60	21.15	1.81	121799
L4w2	LC	73	1536	39.60	21.15	1.81	121799
L5w2	LC	74	1536	39.60	21.15	1.81	121799
L6w2	LC	75	1536	39.60	21.15	1.81	121799

➢ Consideration of shrinkage for concrete tensile strength

The phenomenon of shrinkage is caused by self-stress in concrete element, which can decrease tension strength of concrete, and then lead to decrease the load of the first crack. Such an influence has been presented in Chapter 2. Test specimens were performed in 31-123 days after the production of slab-strips. Comparison first cracking moment between measurement and calculation Figure B-4
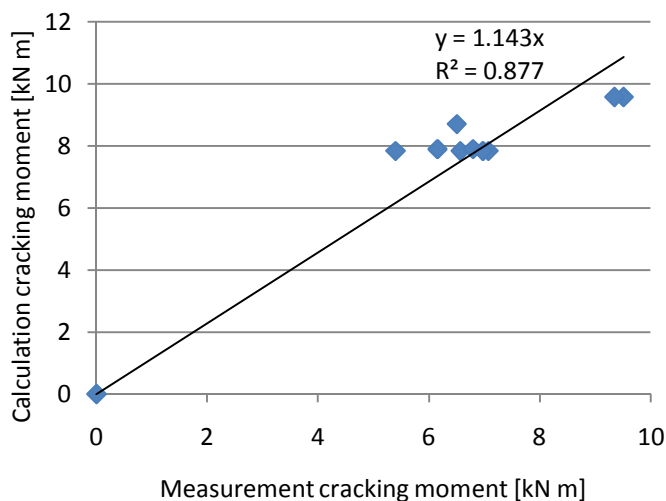
Figure B-4 linear regression to consider the influence of the shrinkage.

The figure result a equation:

$$M_{calculated} = 1.196 M_{measured} \qquad (0\text{-}9)$$

The determination value is $R^2 = 0.775$, which the relationships can be used with great accuracy. Consequently, consideration of the influence of shrinkage on the concrete tensile strength (α_s):

$$f_{ct,S} = \underbrace{1.196^{-1}}_{\alpha_S} \cdot f_{ctm}$$

$$= 0.836 \cdot f_{ctm} \qquad (0\text{-}10)$$

This mitigating factor is that in a similar area of the (Empelmann 1995)(α_S=0,73), (Maurer 1992)(α_S=0,85), (Purainer and Keuser 2006) (α_S=0,784) and (Ruediger 2008)(α_S=0,90).

Table B-1 Reduction factors of concrete tension strength with consideration of shrinkage for four test series

	Concrete types	R^2*	α_S**
Series-1 with TR-cver	NC	0.775	0.863
Series-2 with TR-direction	NC	0.980	0.781
	HC	0.979	0.740
	LC	-	-
Series-3 with TR-position	NC	0.981	0.792

* determination value

** Decrement factor of concrete tensile strength $f_{ct,S} = \alpha_s \cdot f_{ctm}$

Appendix C Test setup

In the inner region of the test structure have the necessary measuring equipment for recording deformation of the plate can be accommodated. More detailed information will follow in the next section.

For the introduction of point loads, the hydraulic cylinders stand as a line load in the specimens. It also had a special device to be manufactured. On the first test a 50mm wider and 5mm flat heavysteel was secured with clamps. Then a strong 60mm solid steel tube was placed, which was secured by the side walls at the underlying flat steel to prevent evasion in the longitudinal and transverse directions. As a final component is a 100 HEB was placed on the role, which was also provided with side cheeks, to prevent an escape from the stress processes. The hydraulic cylinders were finally shut down so far that the hydraulic cylinders were connected to each other, but were not taken any loading from the presses in the test sample. The arrangement of the load transfer design is shown in the figure below.

Hydraulic cylinder

Fix steel palte

I-steel

Steel roll
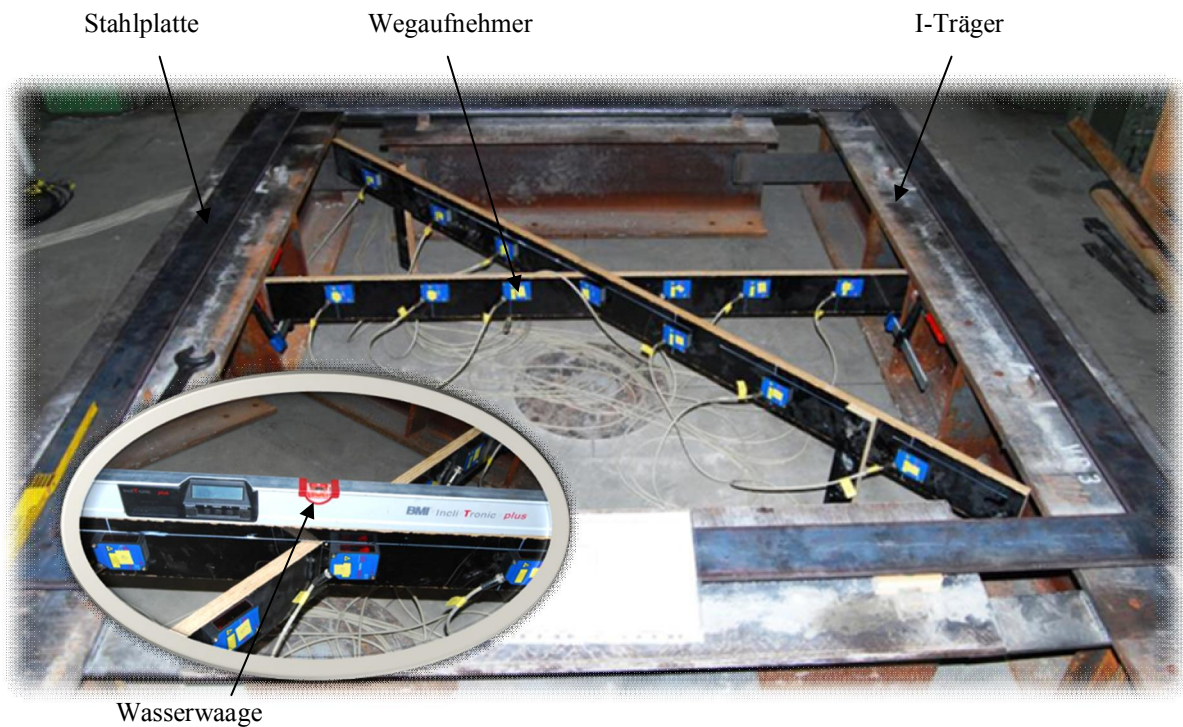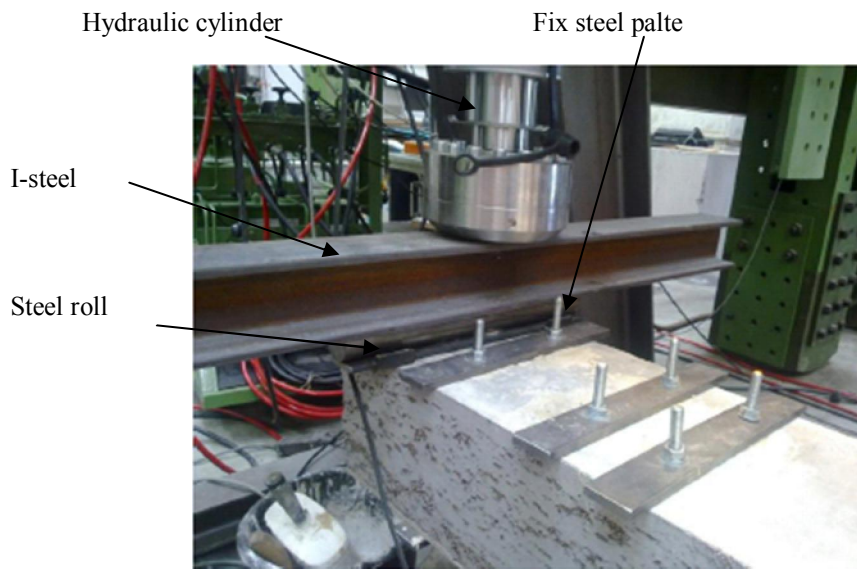
Figure C-1: Load application design

Appendix C.1   Measurement displacement and force

As described in experimental design, statements to the load-displacement behavior are made by boards. In Figure C-2, the arrangement of the 7 laser displacement measurement instrument (LWA) is shown. Here were arranged in longitudinal transducers each 7. The spacing is equated with record attempts, as will compare with plate tests. The measurement accuracy of laser-controlled displacement transducer was 15μm.

Appendix C.2   Detecting reinforcement

With this HILTI Ferroscan PS200, it is possible to detect steel reinforcement in the finished part to determine (Figure C-3). This scanner is on a fixed grid over the surface of the specimens. The collected data is stored on it and can then be analyzed on the PC. It is possible at the device to adjust various types of scans. In the tests conducted here, the image scan function was used. This allowed the subsequent location of the reinforcement in the component and control that determine the real existing concrete cover. With the scanner, it is possible to separate ferrous reinforcement with a minimum depth of 10 mm and a distance to determine steel of 36 mm. While the use of itself after the device was taken to ensure that no interference from magnetic fields affects the measurement. The measured positions of reinforcement are given with an accuracy of ± 3 mm. The following figure shows the scanner with the appropriate grid. To derive a better relationship between the direction and position of the transverse reinforcement and the crack formation can, the top transverse reinforcement with "Ferro PS 200" scanned on the plate before loading strips, and set to "block scan" is used
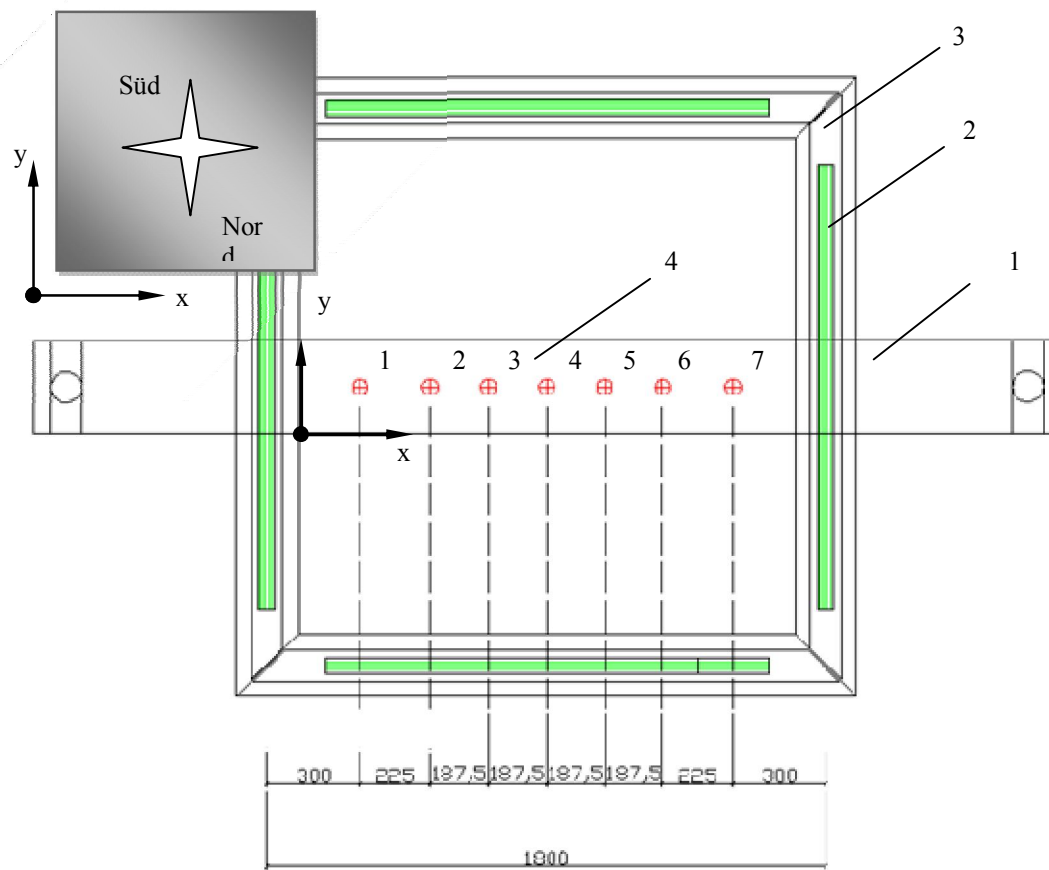
Figure C-3: HILTI Ferroscanner PS200

Appendix C.3   Moment measurement value

The required constant bending moment in the area to be investigated was the vertical force generated by four hydraulic cylinder-cylinders with type PL250N. The bending moment can be calculated by Eq. (11).

$$M_i = \frac{F_i}{2} \cdot l_M \qquad (11)$$

where l_M is the clear span between two cylinders, here is 65cm

The force was initiated by a hydraulic cylinder mounted on the load cell (type: PM250K) were measured. The force acting in the measurement program is automatically recorded to the respective deformations of the plate and recorded in the load-deformation diagram. It should be noted that the additional weight to be considered by the load
introduction with construction needs.

In order to make statements about the load-deformation behavior of the test strip can drive, have more than measure the deformations along the longitudinal axis at the bottom of the test strip plate seven laser rangefinders (Figure C-2) were measured. The measurement of the deformation took place at seven different points with a defined distance, so that later from the measured deformations, the corresponding "Extensive shifts" could be compared.

The bottom plate was used as a reflector strip for measurement
instruments. By withdrawn during concreting bottom of the test specimen was a
good reflection of the laser beams can be guaranteed. The measurement accuracy of laser-controlled displacement transducer was 15 mm. The aforementioned
measures cylinder pressure force and deformation were continuously during the experiments were conducted by the measurement program DIA-DEM recorded. The program automatically measured the pressure force acting cylinders; each of the
corresponding deformation of the test specimen was assigned and recorded in a load-deformation diagram. Since this was an attempt at implementing a path-controlled trial, the piston stroke to 0.05 mm was increased every two seconds. The recording of the individual measurement values were also per second.

Appendix C.4   Measurement of Cracks pattern, cracks spacing and cracks width

For further analysis of the influence of transverse reinforcement on the structural behavior of reinforced concrete slabs subjected to bending load, recruiting cracks were documented at the top of each test specimen by photos Figure C-4. During the experiment, the first cracking load and further loading were reached. Each load steps were marked with different colors (green, blue and red and dark) after the failure of the component. The crack spacing were measured by AutoCAD software at each load and recorded in Excel files.

With this optical digital crack width measurement instrument, all cracks were measured along the central axis specimens. It is also possible to make every tear from a photo that can be processed in the port on the PC. With the camera of the device, the crack under the display of the measuring instrument can take the real-time image, which automatically captures and displays the crack whose width in [mm]. The accuracy in the range of 0.01 mm to 2.0 mm amounts to about 0.01 mm. Figure 4 shows this crack width measurement instrument with the camera image. Cracks were measured one by one by this instrument and recorded on the surface of specimens. After recorded crack width, the top of specimen was photographed. Later, the crack width measurement was read from the digital photos and then, records the data with PC

Figure C-4: Measurement instruments with digital camera and Laserscanner

Figure C-5: Crack width measurement instrument PTS-C10

Appendix D Test Specimen
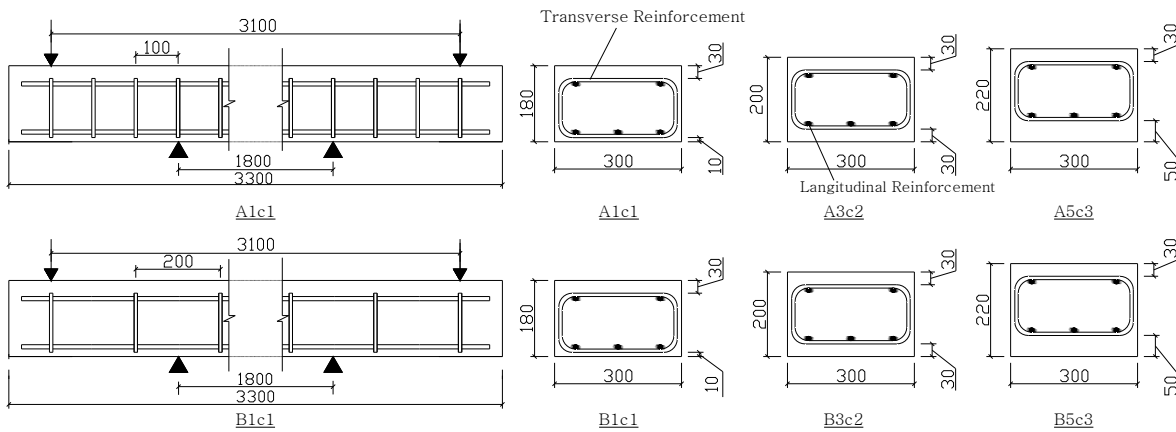
Figure D-1 Geometry and steel plan of test specimens in Series 1 (TR-cover)
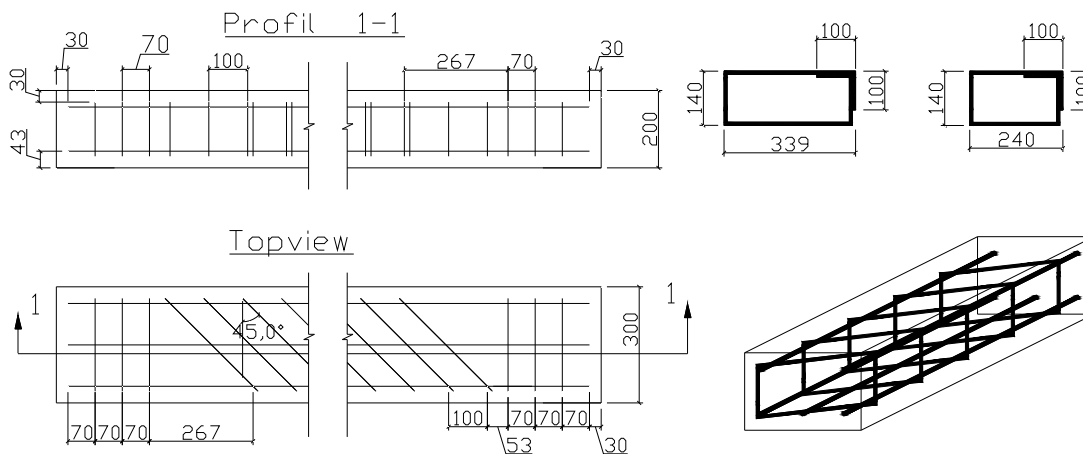
Figure D-2: Geometry and steel plan of test specimens in Series 2 (TR-direction spacing)
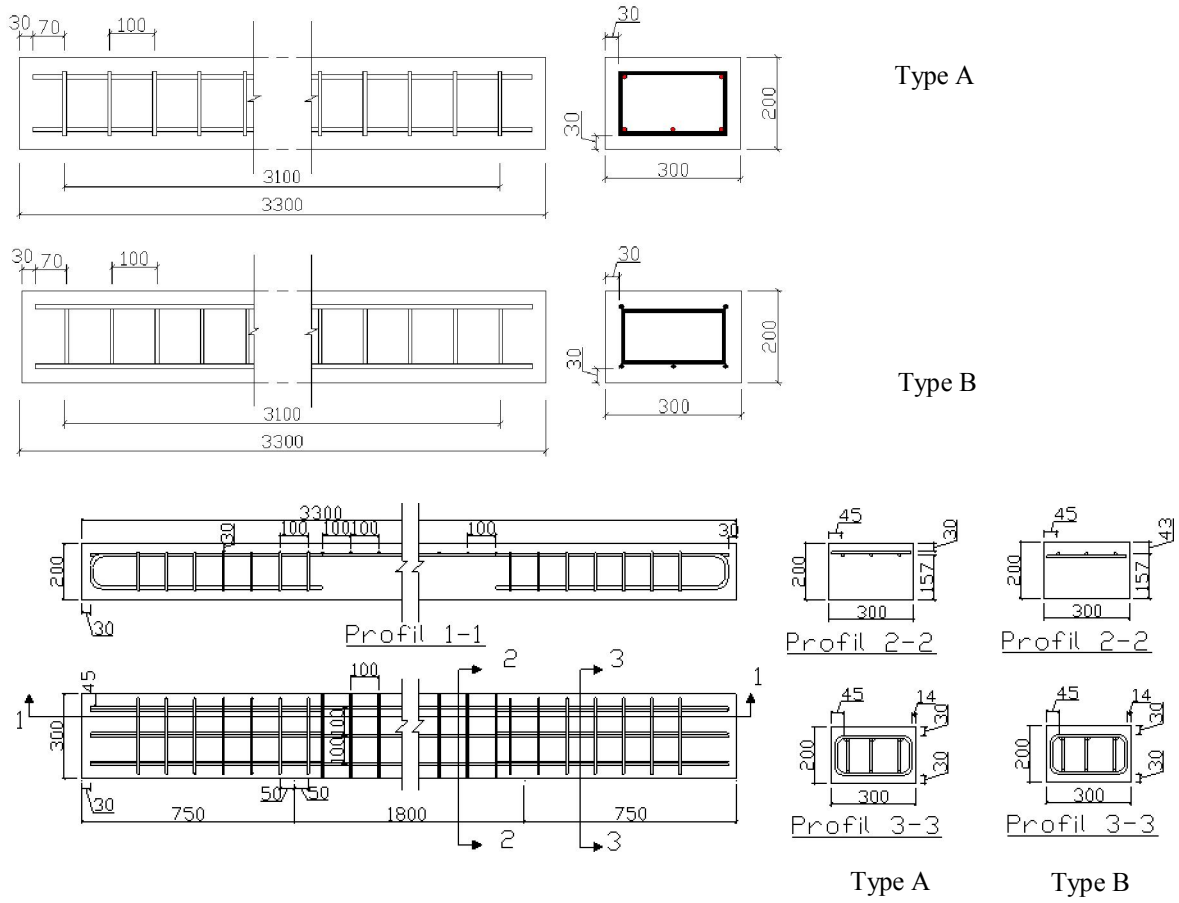
Figure D-3: Geometry and steel plan of test specimens in Series 3 (TR-position)

Concrete cover=10mm

Concrete cover=50mm

Figure D-4 Formwork and reinforcement of test specimens in Series-1 (a)

Abstand= 200mm

Abstand=300mm

Figure D-5: Formwork and reinforcement of test specimens in Series-1 (b)
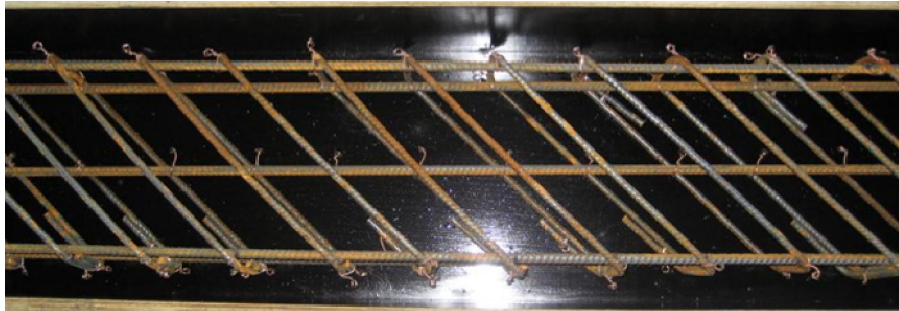
Winkel= 22,5°
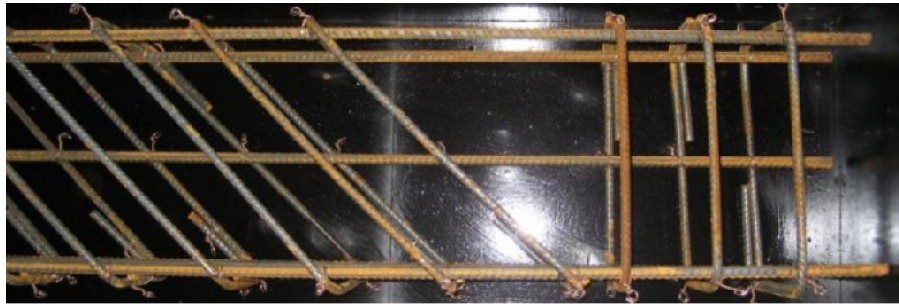
Winkel=45°

Figure D-6: Formwork and reinforcement of test specimens in Series-2

Typ A

Winkel=0° Abstand=10 cm

Typ B

Winkel=0° Abstand=10 cm

Figure D-7: Formwork and reinforcement of test specimens in Series-3

Appendix E   Test results of strips under uniaxial bending

Appendix E.1   Final crack pattern overlapped with TR layout

The crack pattern were recorded by digital camera. the reinforcement were detected by HILTI PS200. With the help of Photoshop, two pictures are combined in ratio 1:1, as shown in following figures.

Appendix E.2   Parameters of TR-cover and TR-spacing – Serien-1
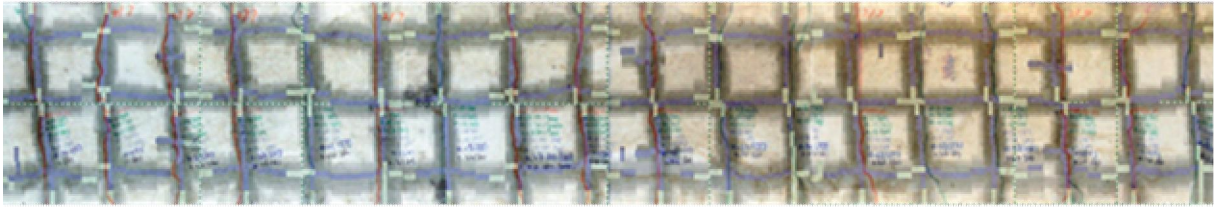
A1C1, loading 60kN, 78% of Ultimate load
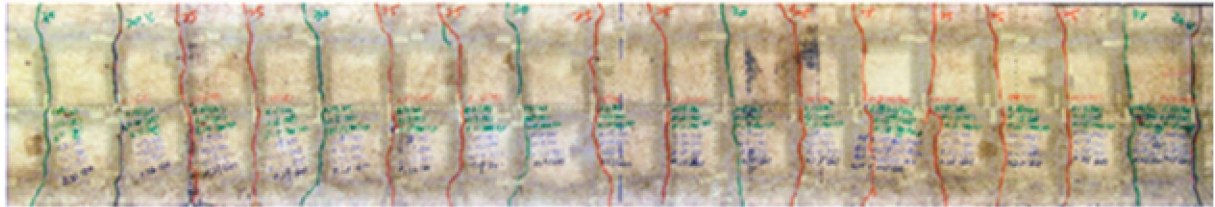
A2C1, loading 60kN, 79,1% of Ultimate load
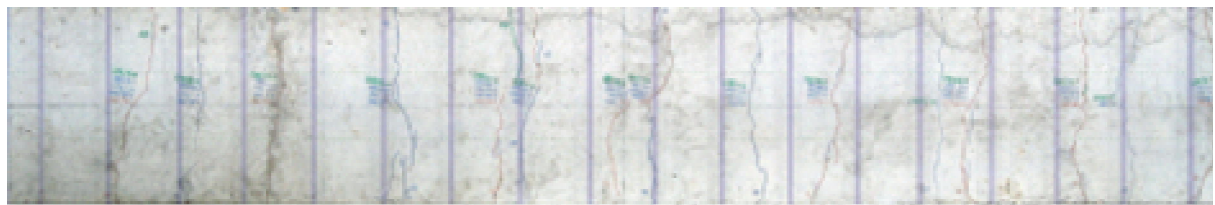
A3C2, loading 45kN, 68,4% of Ultimate load
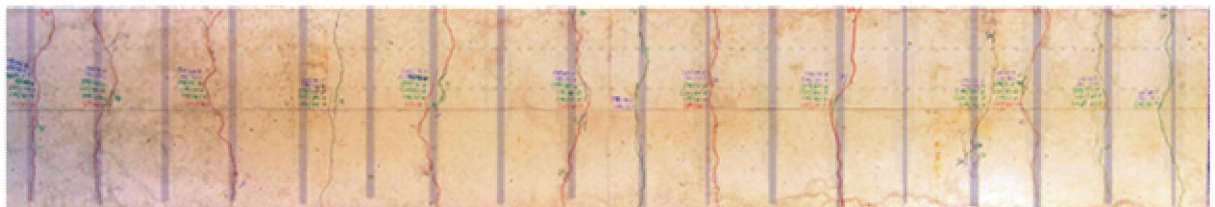
A4C2, loading 45kN, 64,5% of Ultimate load
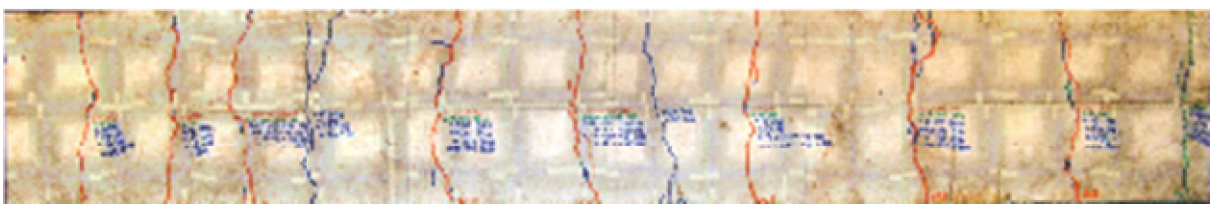
A5C3, loading 60kN, 72,4% of Ultimate load
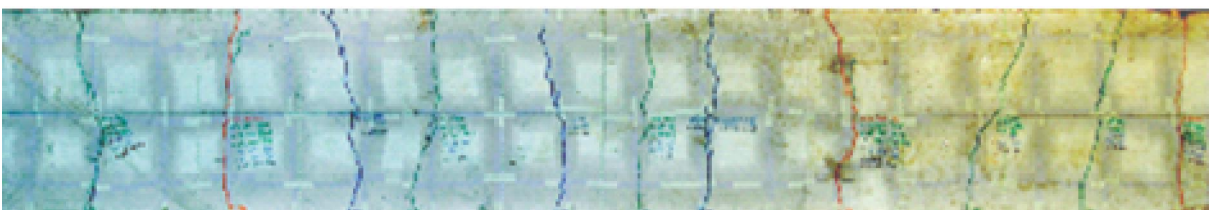
A6C3, loading 60kN, 74,4% of Ultimate load

Figure E-1 Final crack pattern overlapped with TR layout of specimens with TR-spacing of 100mm

B1C1, loading 60kN, 79% of Ultimate load
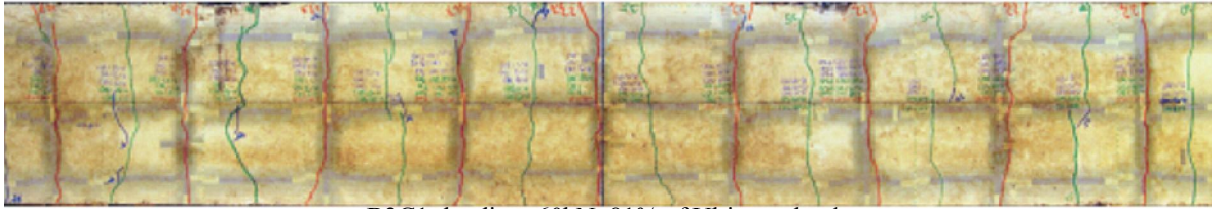
B2C1, loading 60kN, 81% of Ultimate load
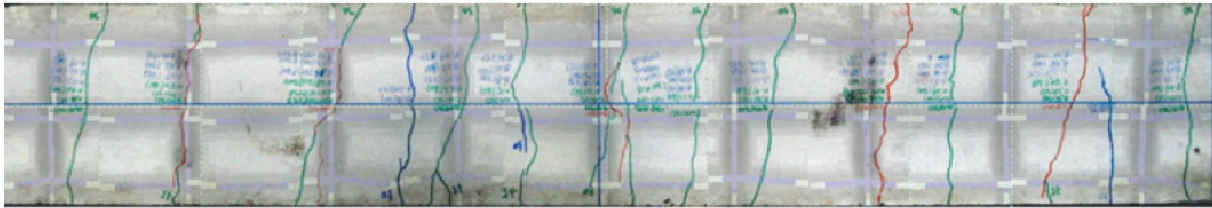
B3C2, loading 55kN, ? % of Ultimate load

B4C2, loading 55kN, ? % of Ultimate load
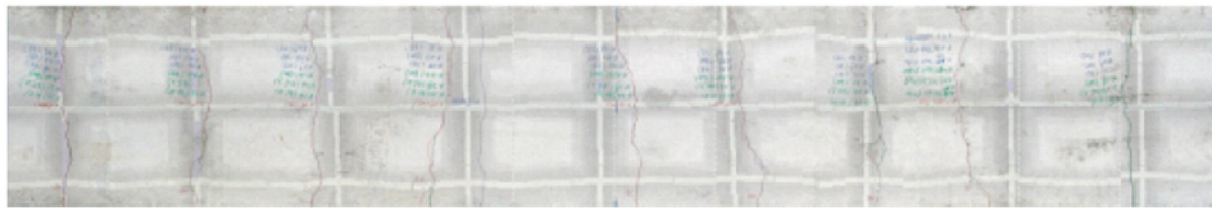
B5C3, loading 55kN, 70% of Ultimate load
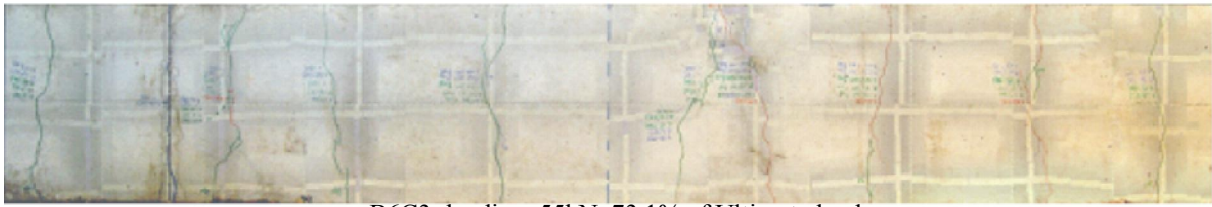
B6C3, loading 55kN, 73,1% of Ultimate load

Figure E-2 Final crack pattern overlapped with TR layout of specimens with TR-spacing of 200 mm
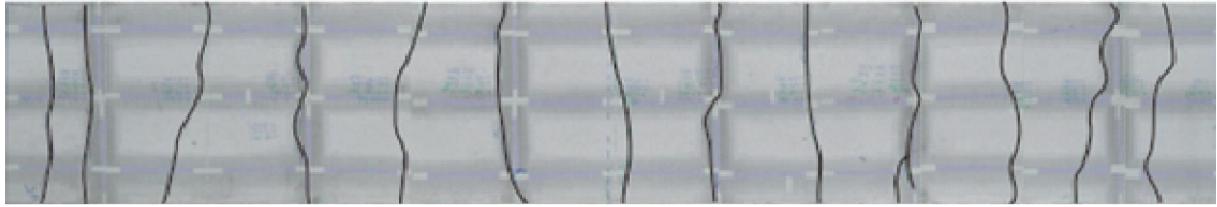
C1c2, loading 40kN, 64% of Ultimate load
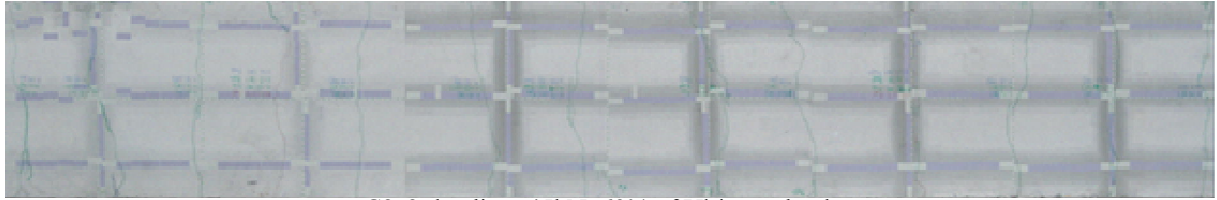
C2c2, loading 45kN, 69% of Ultimate load

Figure E-3 Final crack pattern overlapped with TR layout of specimens with TR-spacing of 300 mm

Appendix E.3   Parameters of TR-direction – Series -2

➢ **Normal-strength concrete**
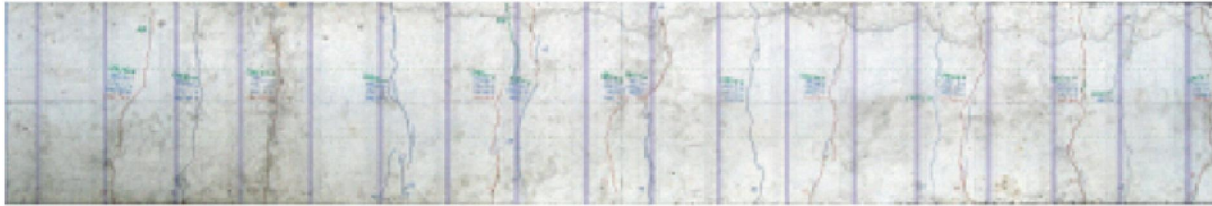
N1w1, loading 45kN, 68,4% of Ultimate load
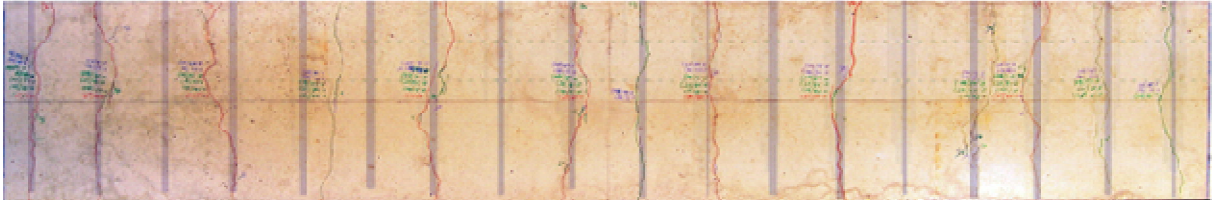
N2w1, loading 45kN, 64,5% of Ultimate load

N3w2, loading 50kN, 64 % of Ultimate load
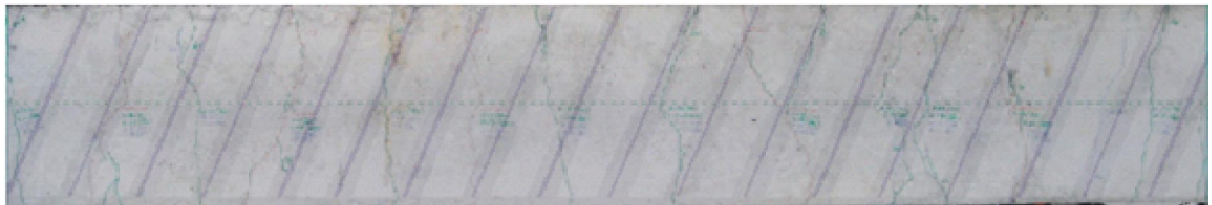
N4w2, loading 50kN, 67 % of Ultimate load

N5w3, loading 50kN, 69 % of Ultimate load
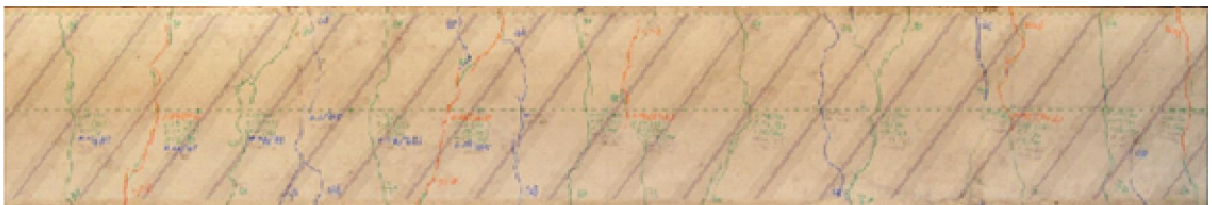
N6w3, loading 50kN, 69 % of Ultimate load

Figure E-4 Final crack pattern overlapped with TR layout of specimens of Normal-strength concrete

➢ High-strength concrete
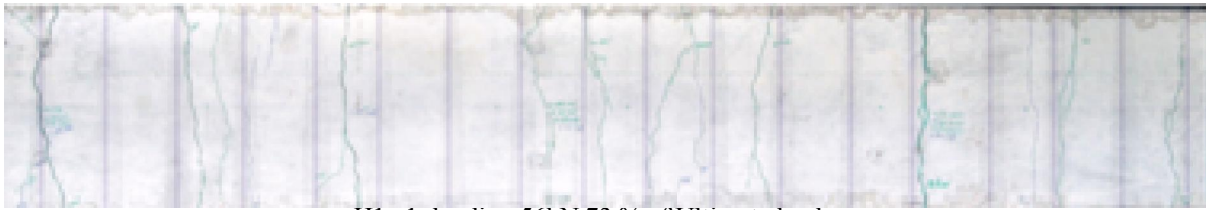
H1w1, loading 56kN,73 % of Ultimate load
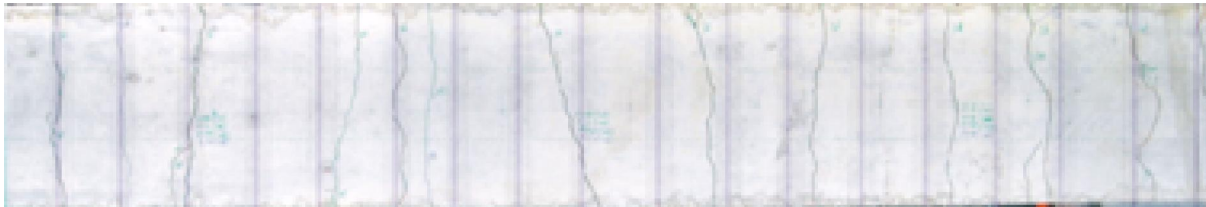
H2w1, loading 56kN,72 % of Ultimate load
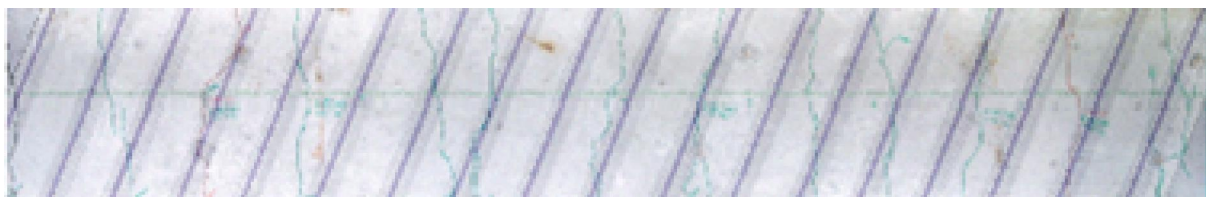
H3w2, loading 47,8kN,56 % of Ultimate load
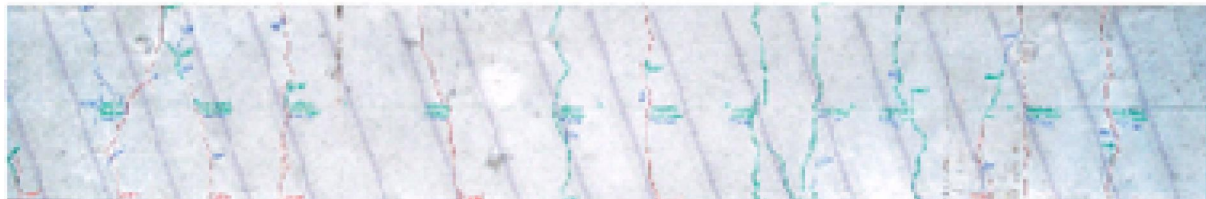
H4w2, loading 48kN, 58 % of Ultimate load
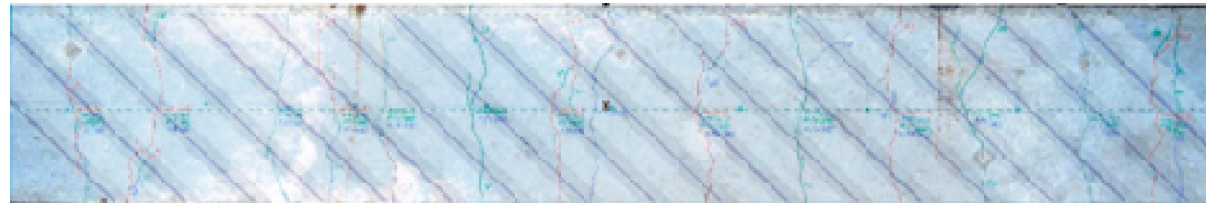
H5w3, loading 57 kN, 51 % of Ultimate load

N6w3, loading 56kN, 56 % of Ultimate load

Figure E-5 Final crack pattern overlapped with TR layout of specimens of Hight-strength concrete

➢ Lightweight concrete
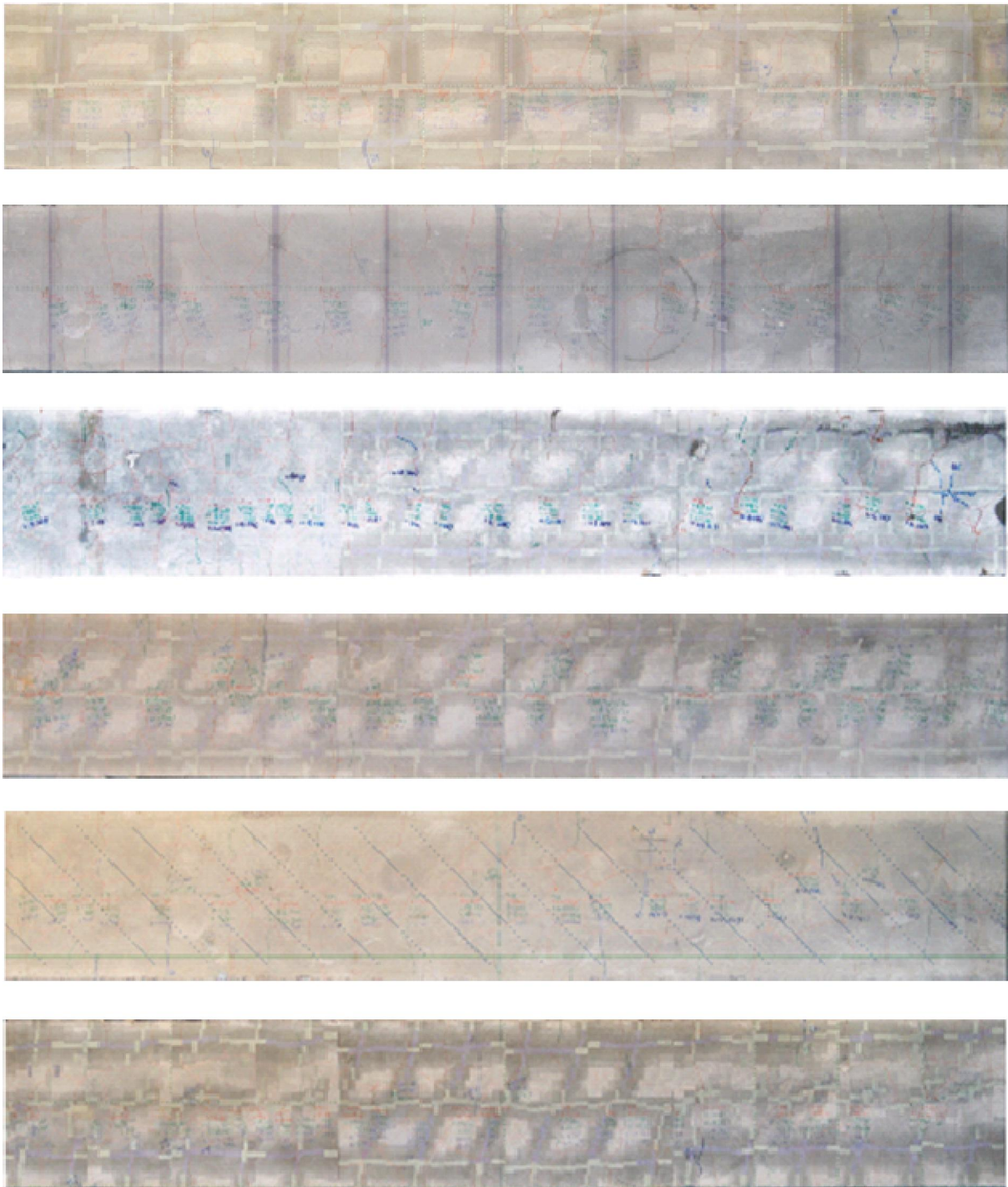
L6w2, loading 45kN, 61 % of Ultimate load

Figure E-6 Final crack pattern overlapped with TR layout of specimens of lightweight concrete

Appendix E.4   *Load-deformation behavior*

The deformation was measured by laser displacement measurement instruments. the middle points deformation were used. The load-deformation figure were plotted as following parts.

➢ **Series 1**
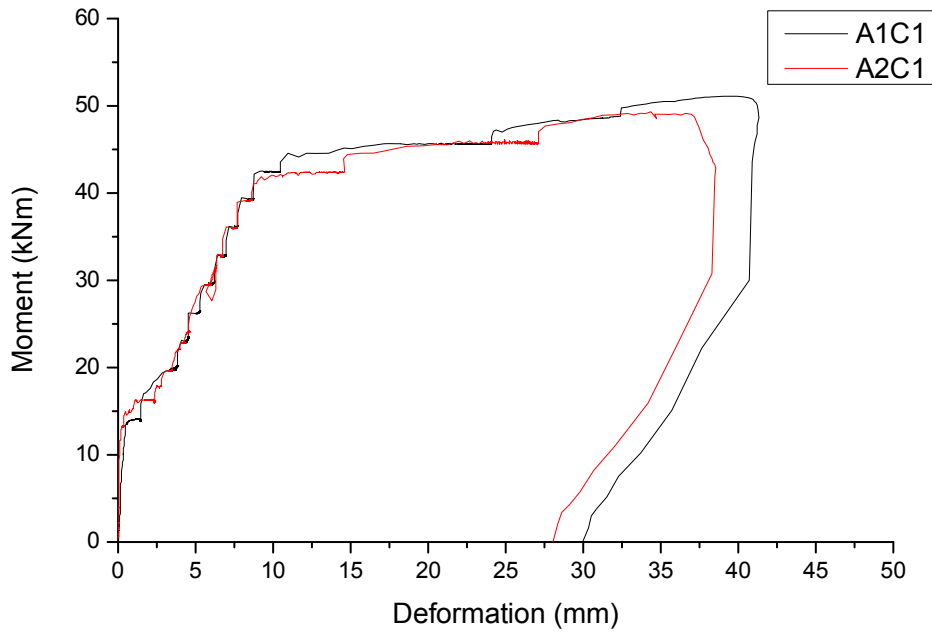
Figure E-7 Load-deformation curves of A1C1, A2C1 with TR-spacing of 100mm in Series 1
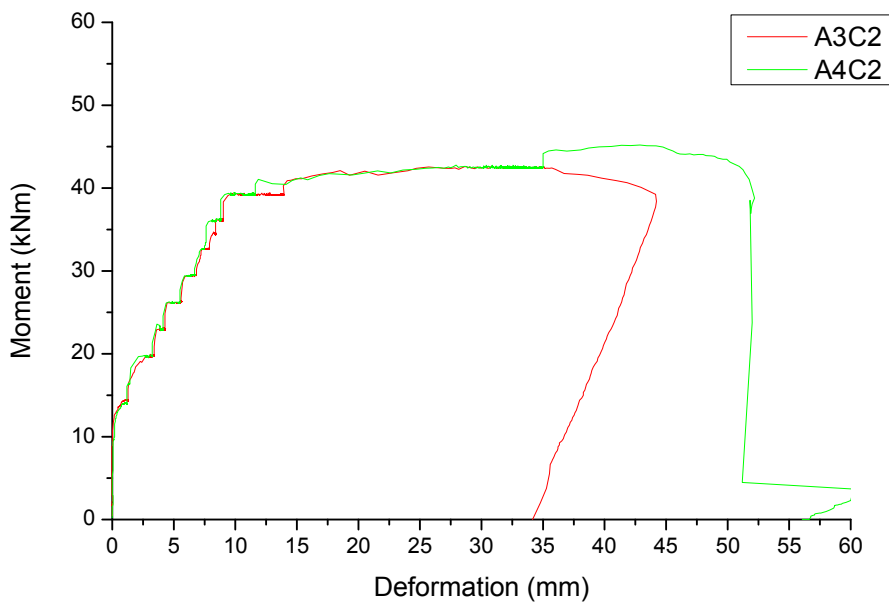
Figure E-8 Load-deformation curves of A3C2 and A4C2 with TR-spacing of 100mm in Series 1
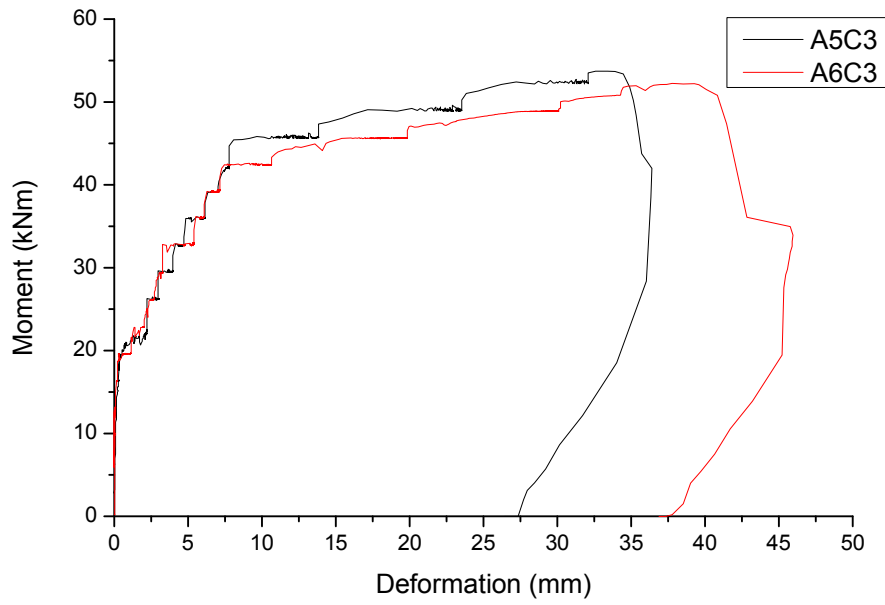
Figure E-9 Load-deformation curves of A5C3 and A6C3 with TR-spacing of 100mm in Series 1
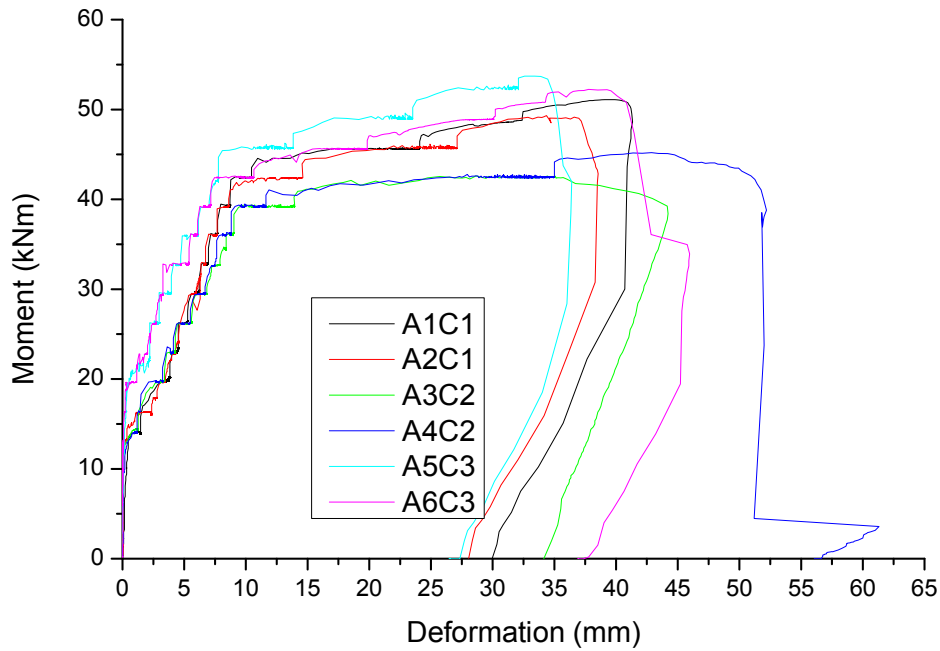
Figure E-10 Load-deformation curves of 6 specimens with TR-spacing of 100mm in Series 1
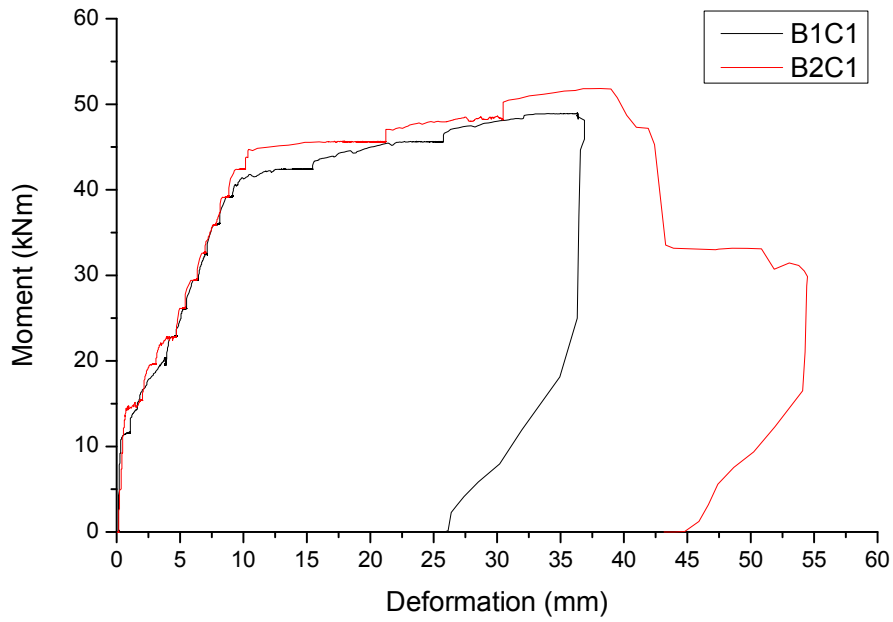
Figure E-11 Load-deformation curves of B1C1 and B2C1 with TR-spacing of 200mm in Series 1
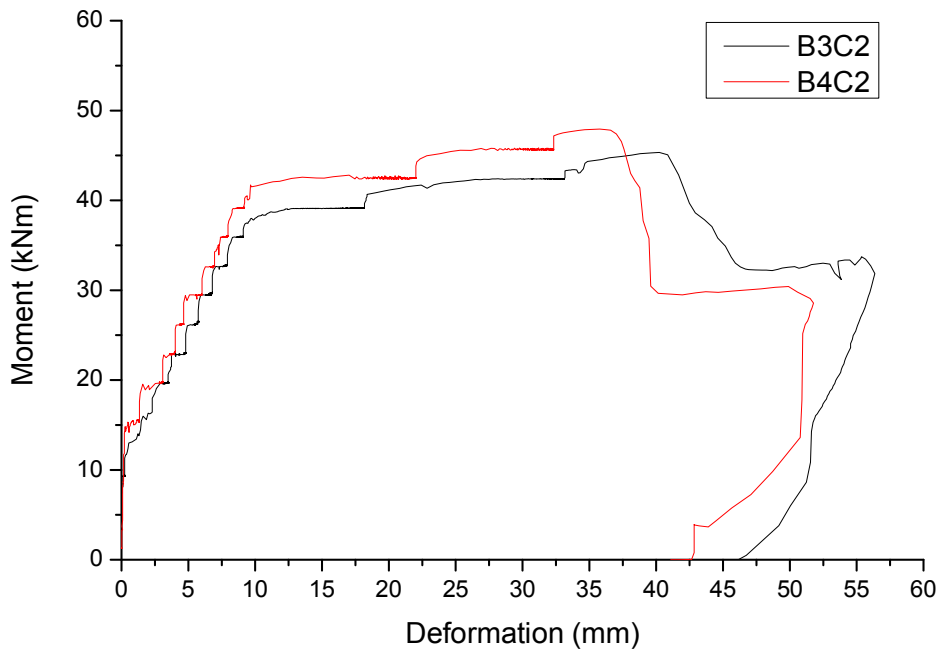
Figure E-12 Load-deformation curves of B3C2 and B4C2 with TR-spacing of 200mm in Series 1
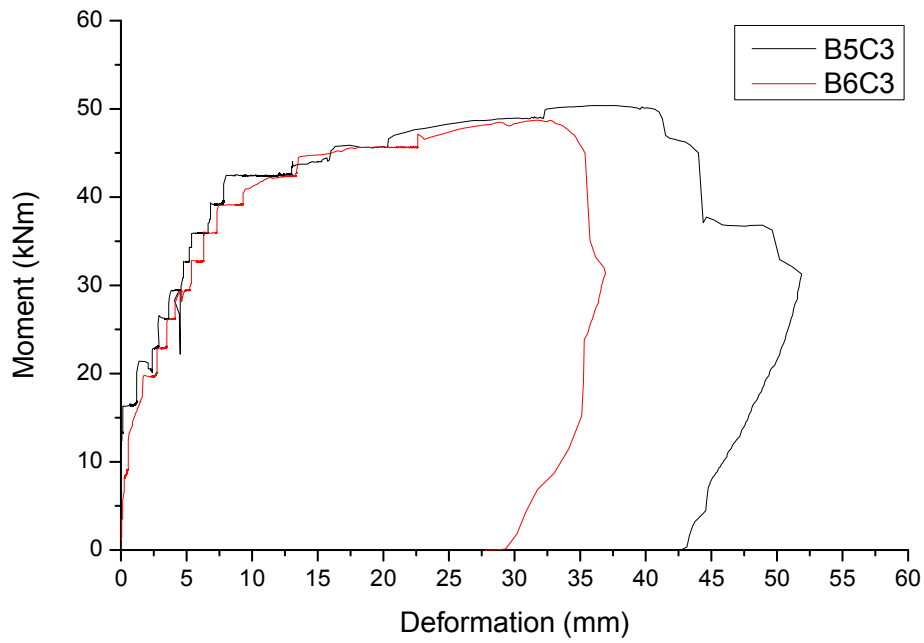
Figure E-13 Load-deformation curves of B5C3 and B6C3 with TR-spacing of 200mm in Series 1
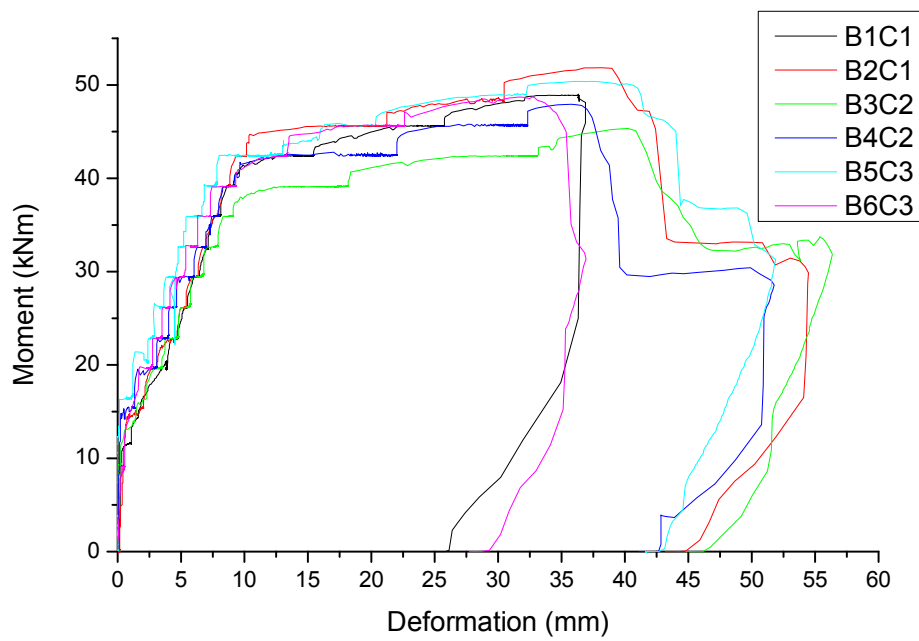
Figure E-14 Load-deformation curves of 6 specimens with TR-spacing of 200mm in Series 1
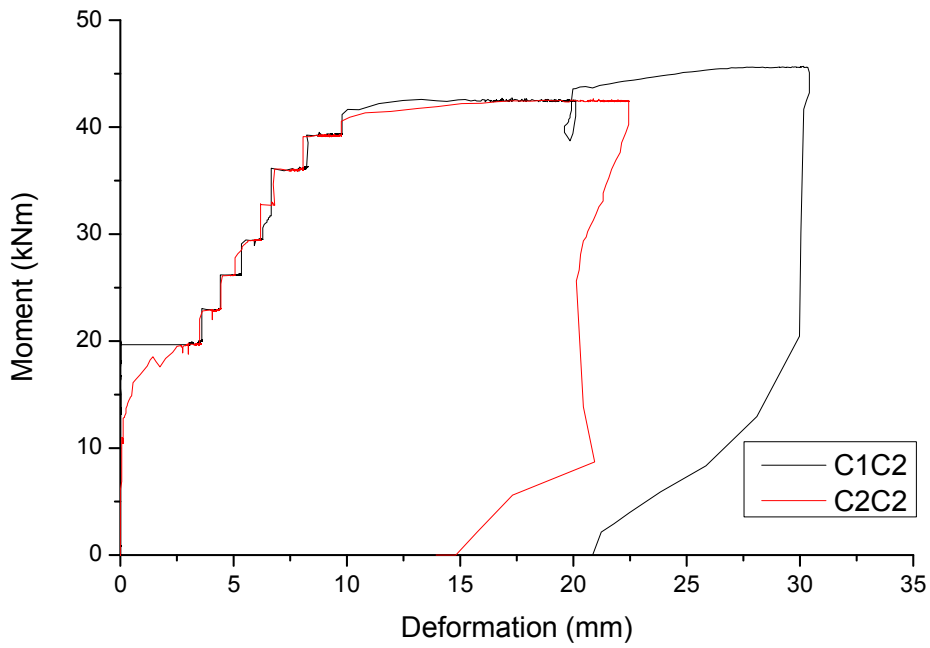
Figure E-15 Load-deformation curves of 2 specimens with TR-spacing of 300mm in Series 1

➢ **Series 2**
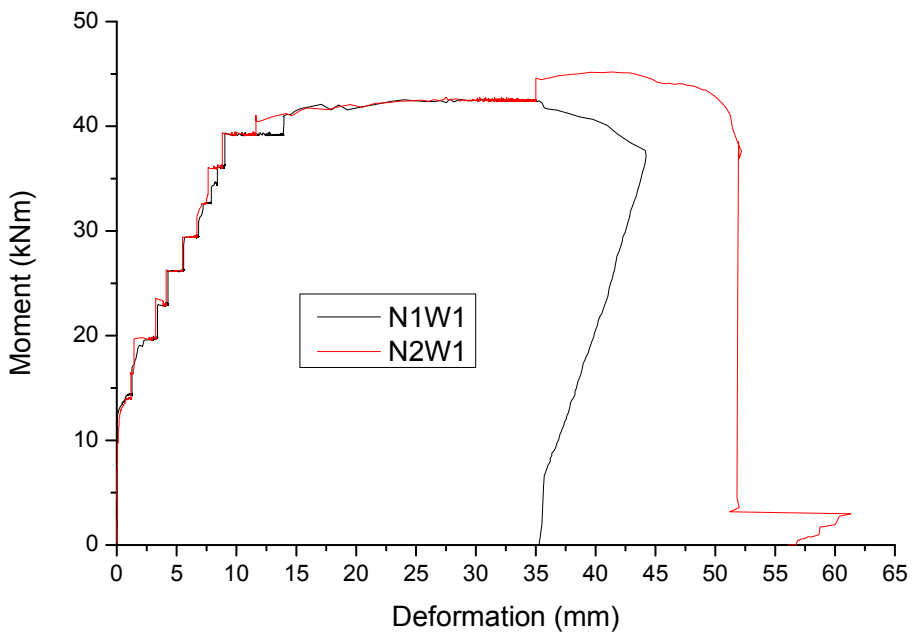
Figure E-16 Load-deformation curves of 0° TR-direction of normal-strength concrete specimens in Series 2
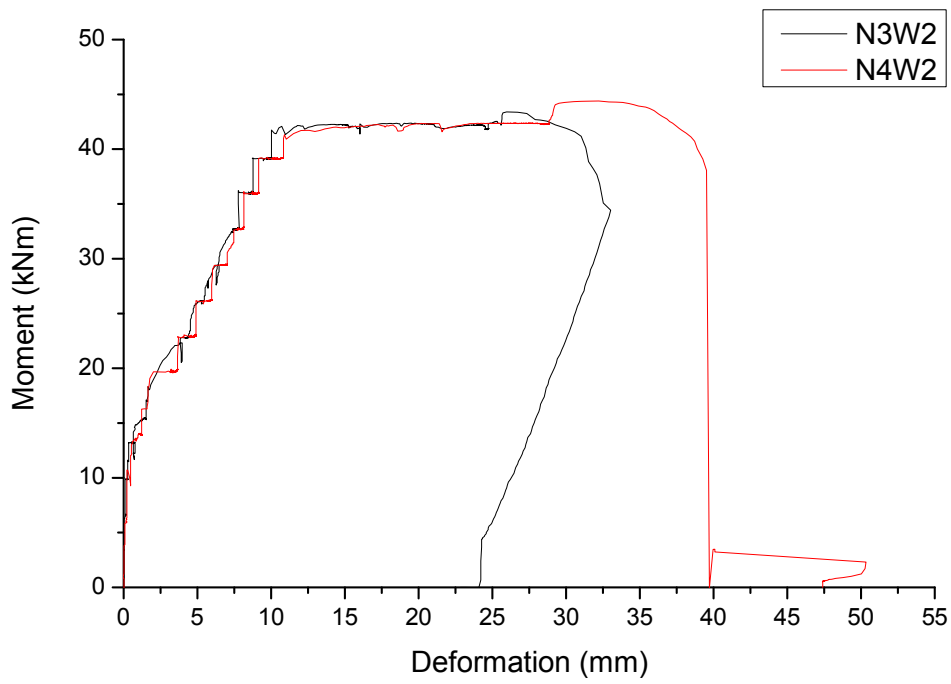
Figure E-17 Load-deformation curves of 22.5° TR-direction of normal-strength concrete specimens in Series 2
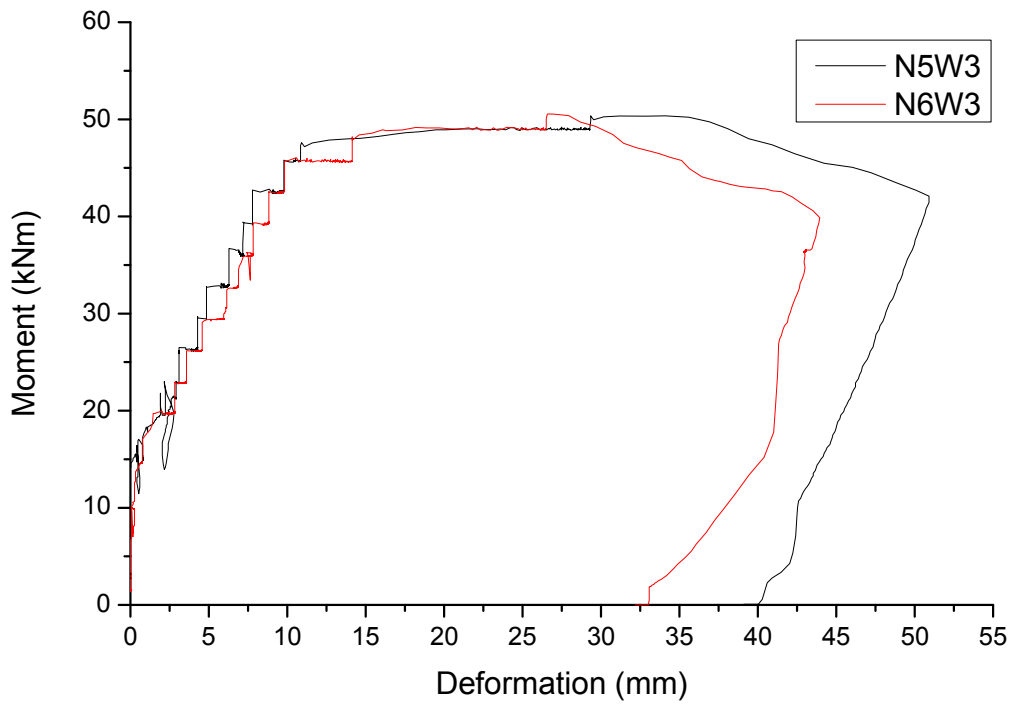
Figure E-18 Load-deformation curves of 45° TR-direction of normal-strength concrete specimens in Series 2
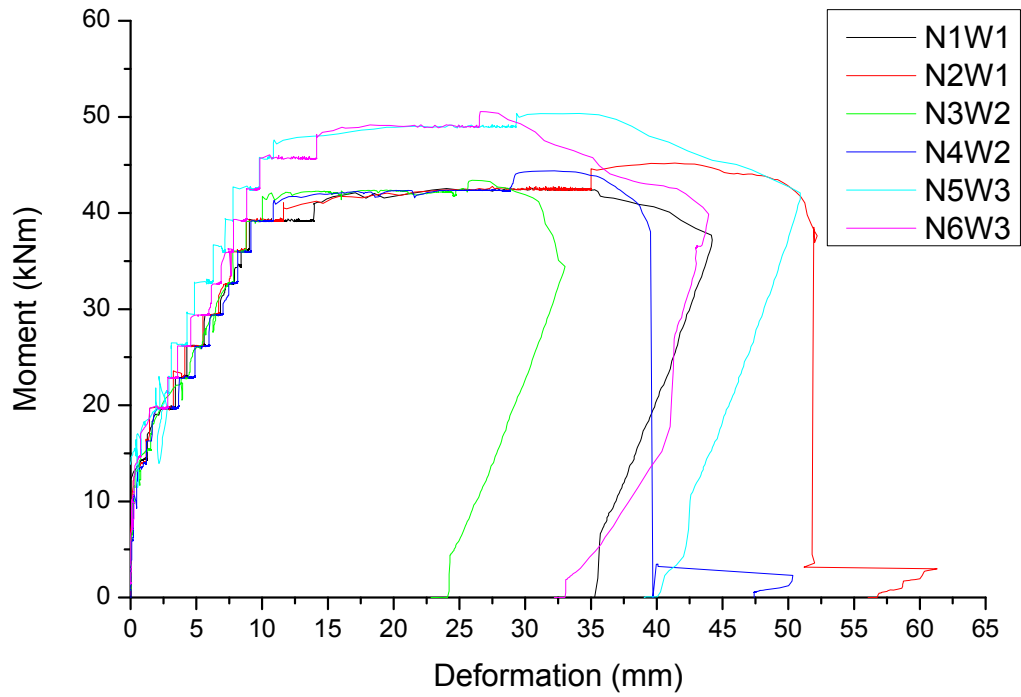
Figure E-19 Load-deformation curves of 6 normal-strength concrete specimens in Series 2
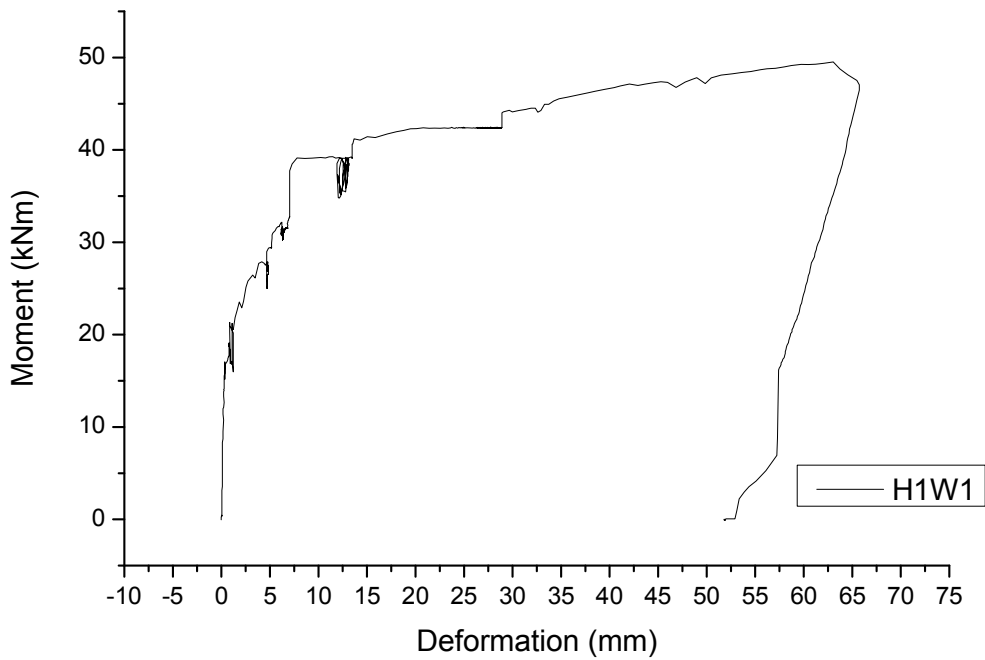
Figure E-20 Load-deformation curves of 0° TR-direction of high-strength concrete specimens in Series 2
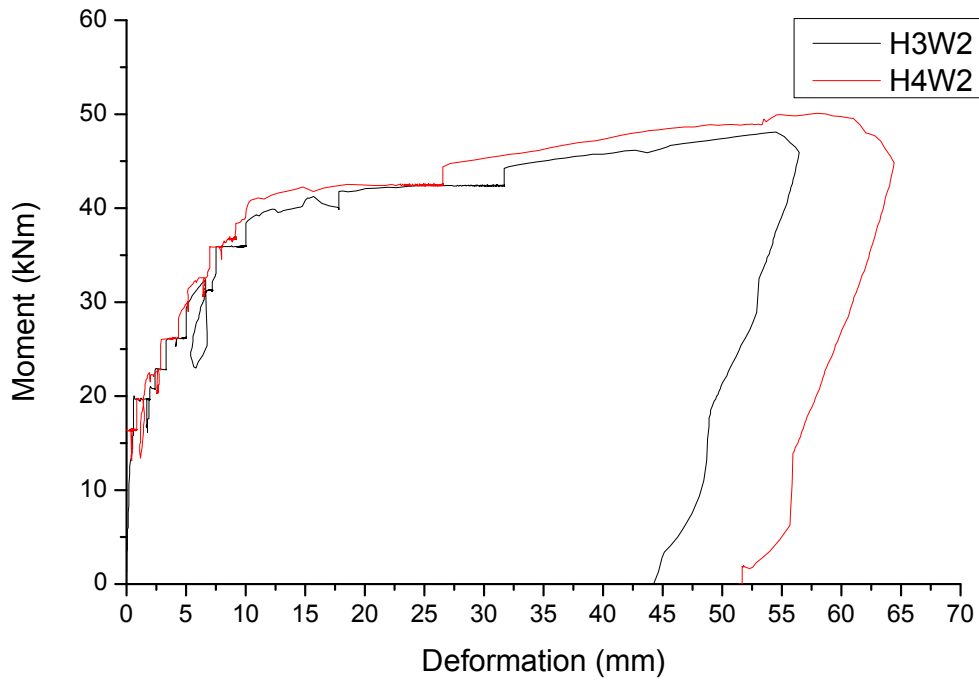
Figure E-21 Load-deformation curves of 22.5° TR-direction of high-strength concrete specimens in Series 2
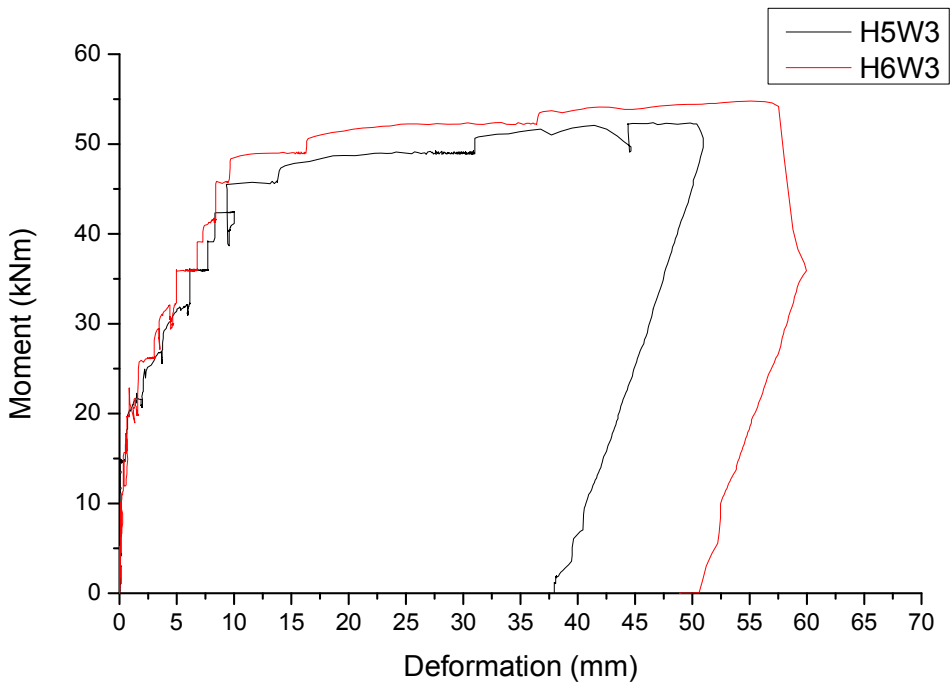
Figure E-22 Load-deformation curves of 45° TR-direction of high-strength concrete specimens in Series 2
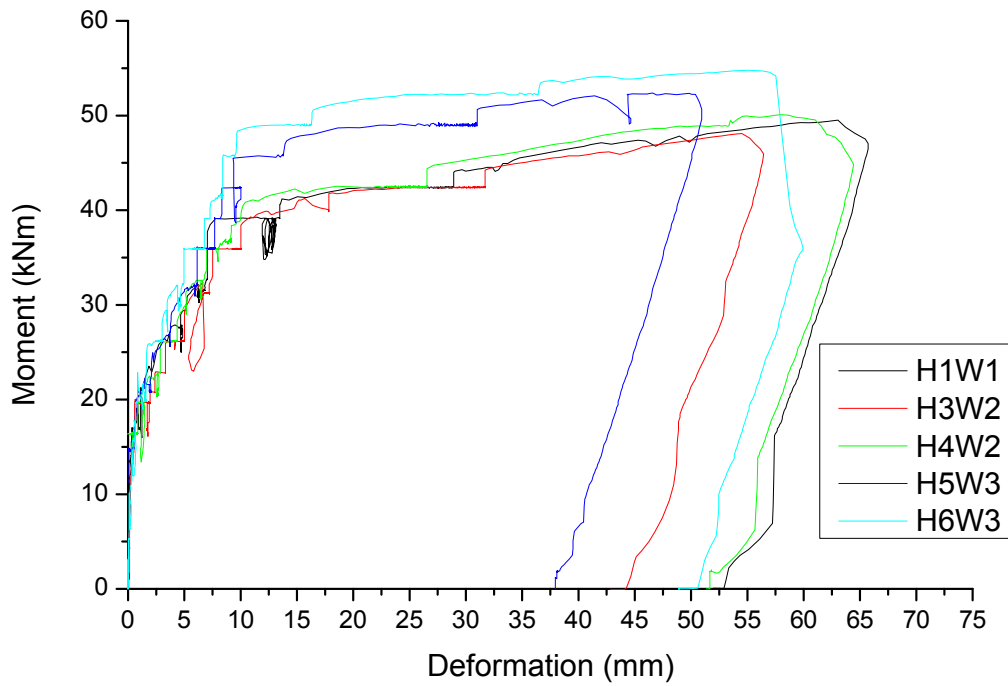
Figure E-23 Load-deformation curves of 6 high-strength concrete specimens in Series 2 (without data of H2W1)
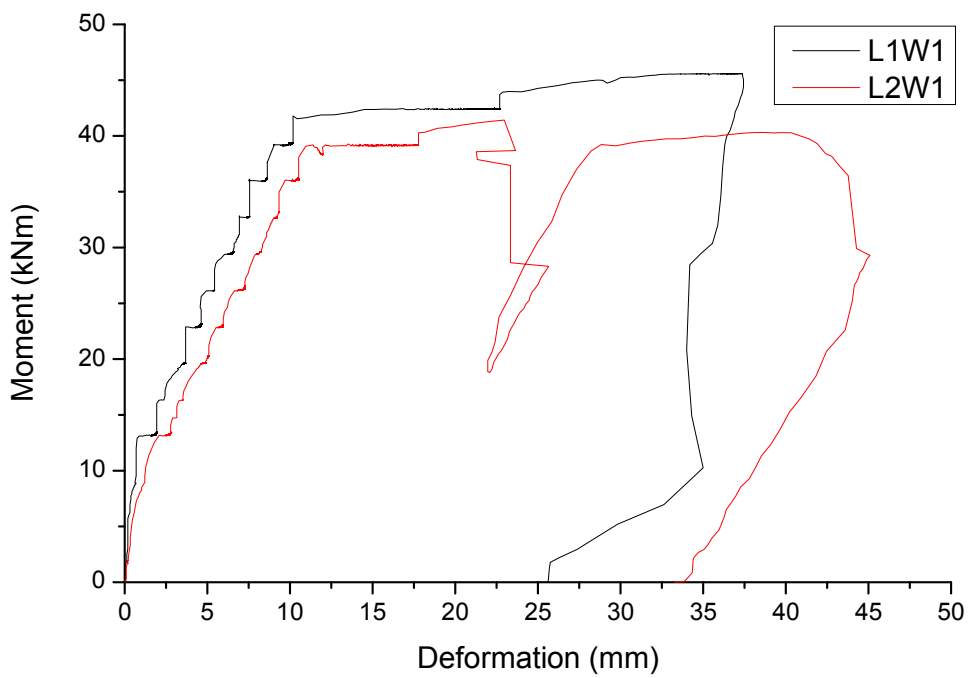
Figure E-24 Load-deformation curves of 0° TR-direction of lightweight concrete specimens in Series 2
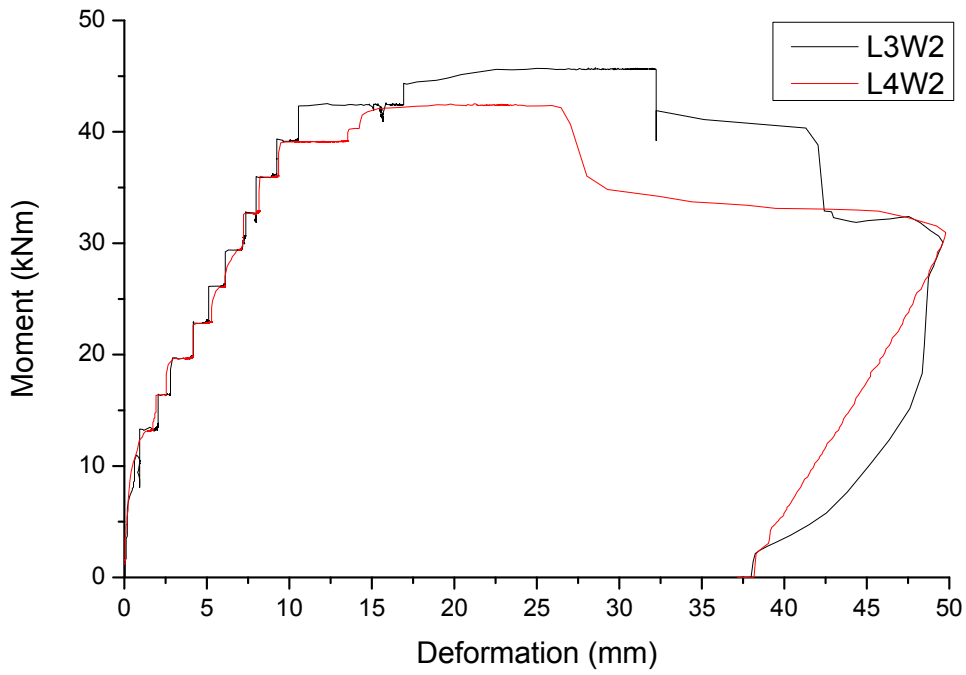
Figure E-25 Load-deformation curves of 22.5° TR-direction of lightweight concrete specimens in Series 2
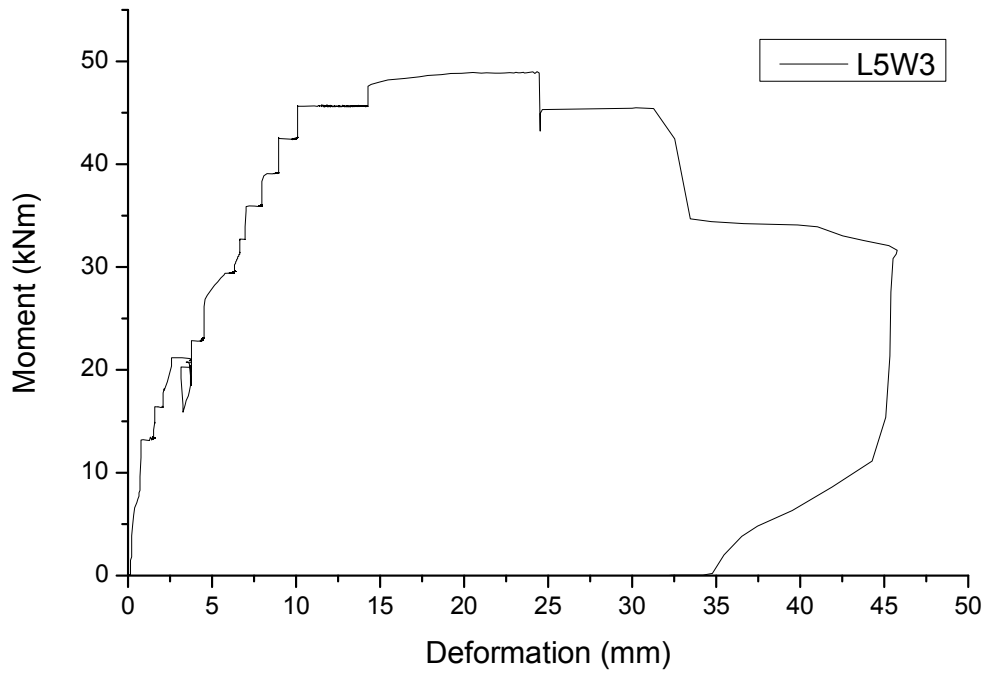
Figure E-26 Load-deformation curves of 45° TR-direction of lightweight concrete specimens in Series 2
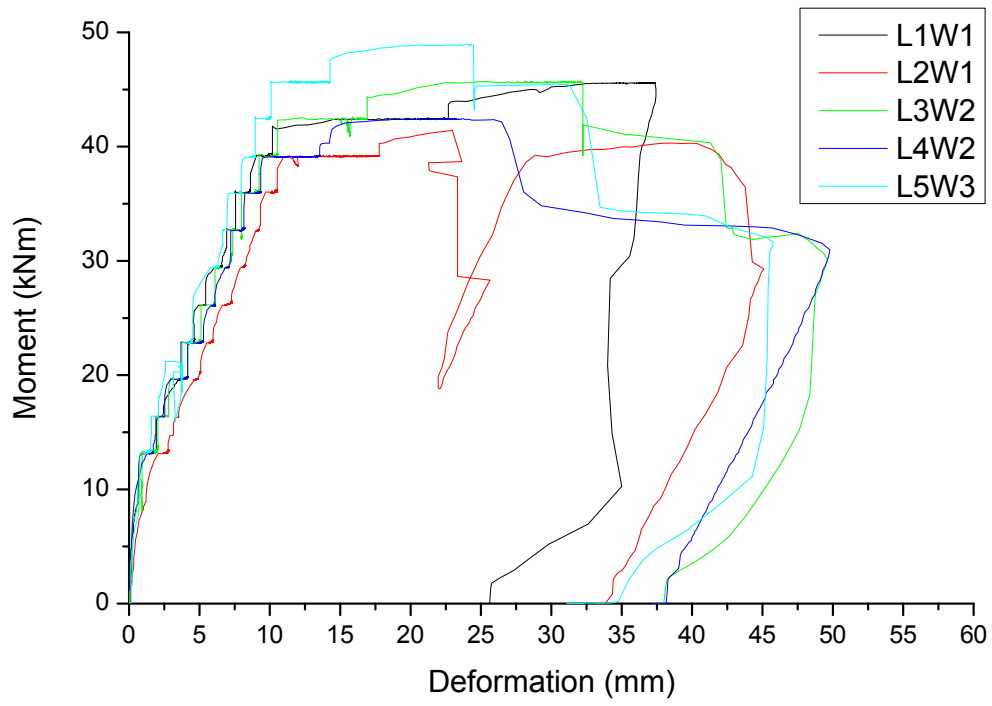
Figure E-27 Load-deformation curves of 6 lightweight concrete specimens in Series 2 (without data of L6W3)

Appendix E.5 *Crack spacing data of slab-strip specimens*

➢ **Series 1**

Table E-1 Crack spacing data of slab-strips test specimens of Series 1

No.	Mean crack spacing [mm]	Crack spacing [mm]							
		Computed by FIB Model Code 2010		Computed by DIN EN 1992-1-2011		Computed by DIN1045-1		Computed by Model-5	
A1C1	100	122	22%	132	32%	107	7%	110	10%
A2C1	100	122	22%	135	35%	107	7%	110	10%
A3C2	112	168	50%	193	72%	119	7%	125	12%
A4C2	104	169	63%	194	87%	119	15%	126	21%
A5C3	167	224	34%	249	49%	131	-21%	149	-11%
A6C3	161	222	38%	247	54%	131	-18%	149	-7%
B1C1	100	122	22%	130	30%	107	7%	101	1%
B2C1	100	122	22%	134	34%	107	7%	102	2%
B3C2	123	170	38%	195	59%	119	-3%	127	4%
B4C2	145	168	16%	193	33%	119	-18%	127	-13%
B5C3	158	219	39%	244	55%	131	-17%	148	-6%
B6C3	137	216	58%	241	76%	131	-4%	146	6%
C1C2	131	185	41%	212	62%	119	-9%	133	2%
C2C2	158	180	14%	206	31%	119	-24%	131	-17%
Av.	128	172	34%	193	51%	119	-5%	127	1%
Std.	26	39.05	0.15	44.83	0.19	9.36	0.13	16.73	0.11
C.V.	0.20	0.23	0.45	0.23	0.37	0.08	-2.93	0.13	11.83

➤ Series 2

Table E-2 Crack spacing data of slab-strips test specimens of Series 2

No.	Mean crack spacing [mm]	Crack spacing [mm]						
		Computed by FIB Model Code 2010		Computed by DIN EN 1992-1-2011		Computed by DIN1045-1		Computed by Model-5	
N1w1	112	186	66%	213	90%	119	7%	98	-12%
N2w1	104	184	77%	211	103%	119	15%	99	-4%
N3w2	100	183	83%	210	110%	119	19%	99	-1%
N4w2	106	187	76%	214	102%	119	13%	101	-4%
N5w3	89	192	115%	219	147%	119	34%	102	14%
N6w3	94	180	91%	206	120%	119	27%	99	5%
H1w1	129	189	46%	216	67%	119	-7%	100	-22%
H2w1	148	187	26%	214	45%	119	-19%	101	-32%
H3w2	128	192	50%	220	72%	119	-7%	102	-20%
H4w2	96	197	106%	226	135%	119	24%	103	7%
H5w3	109	203	86%	232	113%	119	10%	104	-4%
H6w3	82	201	145%	230	180%	119	46%	104	27%
L3S2	56	179	219%	205	266%	119S2	113%	141	152%
L4S2	86	184	114%	211	145%	119	39%	149	73%
L3w2	52	172	231%	198	280%	119	130%	100	92%
L4w2	51	195	282%	223	337%	119	134%	109	114%
L5w2	58	183	215%	210	262%	119	106%	101	75%
L6w2	48	186	288%	213	345%	119	149%	103	114%
Aver.	92	188	129%	215	162%	119	46%	106	32%
Std.	29.43	7.79	0.82	8.68	0.94	0.00	0.54	14.27	0.56
C.V.	0.32	0.04	0.64	0.04	0.58	0.00	1.18	0.13	1.76

Appendix E.6   *Crack width data of slab-strip specimens*

➤ **Series 1**

Table E-3 Crack width data of slab-strips test specimens of Series 1 at 35kN of two cylinders

No.	Steel stress [MPa]	Av. crack width [mm]**	Max. crack width [mm]**	Computed by FIB Model Code 2010		Computed by DIN EN 1992-1-2011		Computed by DIN1045-1		Computed by ACI318		Computed by Model-6		Computed by Model-8	
A1c1	334.3	0.12	0.15	0.21	41%	0.20	32%	0.26	72%	0.21	41%	0.17	14%	0.16	8%
A2c1	329.0	0.14	0.17	0.21	23%	0.20	15%	0.25	49%	0.21	26%	0.17	-1%	0.16	-3%
A3c2	345.0	0.13	0.21	0.31	46%	0.30	42%	0.30	41%	0.36	73%	0.25	20%	0.22	7%
A4c2	341.0	0.23	0.28	0.30	8%	0.30	6%	0.29	5%	0.36	30%	0.25	-9%	0.23	-17%
A5c3	292.6	0.17	0.21	0.28	34%	0.26	24%	0.28	31%	0.42	102%	0.27	30%	0.18	-15%
A6c3	306.1	0.17	0.17	0.30	78%	0.28	65%	0.29	70%	0.44	158%	0.30	74%	0.18	7%
B1c1	278.8	0.11	0.16	0.16	2%	0.15	-9%	0.21	34%	0.17	6%	0.17	5%	0.19	19%
B2c1	332.8	0.12	0.20	0.21	6%	0.20	0%	0.26	28%	0.22	8%	0.21	4%	0.20	0%
B3c2	345.6	0.20	0.35	0.30	-15%	0.29	-17%	0.30	-15%	0.37	6%	0.31	-11%	0.24	-30%
B4c2	337.3	0.20	0.25	0.28	14%	0.28	10%	0.30	18%	0.36	43%	0.30	20%	0.24	-4%
B5c3	320.3	0.27	0.31	0.32	4%	0.30	-3%	0.30	-3%	0.45	45%	0.31	-1%	0.18	-42%
B6c3	315.6	0.24	0.32	0.31	-3%	0.29	-10%	0.30	-7%	0.43	35%	0.29	-11%	0.17	-47%
C1c2	343.3	0.18	0.25	0.33	33%	0.32	30%	0.30	18%	0.42	69%	0.32	26%	0.30	20%
C1c2	339.2	0.21	0.27	0.32	18%	0.32	20%	0.29	8%	0.40	48%	0.30	12%	0.28	5%
Aver.		0.18	0.24	0.28	21%	0.26	15%	0.28	25%	0.35	49%	0.26	12%	0.21	-7%
Std.				0.05	0.23	0.05	0.22	0.02	0.26	0.09	0.40	0.05	0.21	0.04	0.20
C.V.				0.19	1.12	0.20	1.50	0.09	1.03	0.27	0.81	0.21	1.73	0.20	-3.09

Table E-4 Crack width data of slab-strips test specimens of Series 1 at 40kN of two cylinders

No.		Av. crack width [mm]**	Max. crack width [mm]**	Crack width [mm] 40kN												
				Computed by FIB Model Code 2010		Computed by DIN EN 1992-1-2011		Computed by DIN1045-1		Computed by ACI318		Computed by Model-6		Computed by Model-8	
A1c1	378.7	0.15	0.18	0.29	64%	0.28	54%	0.33	84%	0.27	49%	0.22	23%	0.20	12%
A2c1	346.7	0.15	0.21	0.30	41%	0.28	34%	0.33	57%	0.28	32%	0.22	5%	0.20	-3%
A3c2	393.9	0.17	0.3	0.43	43%	0.42	41%	0.38	27%	0.47	55%	0.33	9%	0.29	-3%
A4c2	389.0	0.23	0.3	0.43	42%	0.42	41%	0.38	26%	0.47	56%	0.33	11%	0.30	0%
A5c3	349.2	0.26	0.28	0.45	61%	0.43	53%	0.37	33%	0.57	104%	0.38	36%	0.27	-5%
A6c3	350.5	0.24	0.25	0.45	79%	0.43	70%	0.37	49%	0.56	126%	0.39	56%	0.27	9%
B1c1	324.8	0.14	0.18	0.25	38%	0.23	25%	0.29	60%	0.23	25%	0.23	27%	0.24	31%
B2c1	382.3	0.14	0.23	0.30	31%	0.29	24%	0.33	45%	0.28	22%	0.27	19%	0.25	8%
B3c2	394.7	0.29	0.47	0.42	-10%	0.42	-12%	0.38	-18%	0.48	1%	0.41	-13%	0.33	-30%
B4c2	386.1	0.21	0.31	0.41	31%	0.40	29%	0.38	23%	0.46	48%	0.40	28%	0.32	4%
B5c3	363.3	0.32	0.35	0.47	33%	0.44	26%	0.39	10%	0.57	63%	0.40	14%	0.27	-24%
B6c3	359.6	0.31	0.47	0.45	-3%	0.43	-8%	0.38	-18%	0.55	18%	0.37	-20%	0.25	-47%
C1c2	438.8	0.26	0.37	0.46	26%	0.46	24%	0.38	3%	0.54	46%	0.41	11%	0.39	6%
C1c2	435.9	0.29	0.42	0.45	7%	0.46	9%	0.38	-10%	0.51	22%	0.40	-5%	0.37	-11%
Aver.		0.23	0.23	0.40	55%	0.38	49%	0.36	46%	0.45	70%	0.34	23%	0.28	2%
Std.				0.07	0.25	0.08	0.22	0.03	0.30	0.12	0.33	0.07	0.19	0.06	0.19
C.V.				0.18	0.45	0.20	0.46	0.08	0.65	0.27	0.47	0.21	0.82	0.20	12.47

Table E-5 Crack width data of slab-strips test specimens of Series 1 at 45kN of two cylinders

No.	Steel stress	Av. crack width [mm]**	Max. crack width [mm]**	Crack width [mm] 45kN Computed by FIB Model Code 2010		Computed by DIN EN 1992-1-2011		Computed by DIN1045-1		Computed by ACI318		Computed by Model-6		Computed by Model-8	
A1c1	425.5	0.2	0.23	0.29	28%	0.28	21%	0.33	44%	0.27	17%	0.19	-19%	0.21	-9%
A2c1	424.9	0.2	0.21	0.30	41%	0.28	34%	0.33	57%	0.28	32%	0.19	-12%	0.21	1%
A3c2	441.9	0.2	0.38	0.43	13%	0.42	11%	0.38	0%	0.47	23%	0.28	-27%	0.31	-19%
A4c2	439.0	0.2	0.32	0.43	34%	0.42	32%	0.38	19%	0.47	46%	0.28	-12%	0.32	-1%
A5c3	394.3	0.3	0.33	0.45	37%	0.43	30%	0.37	13%	0.57	73%	0.30	-9%	0.31	-6%
A6c3	394.1	0.3	0.33	0.45	36%	0.43	29%	0.37	13%	0.56	71%	0.31	-6%	0.32	-4%
B1c1	371.4	0.2	0.29	0.25	-15%	0.23	-22%	0.29	-1%	0.23	-22%	0.19	-35%	0.25	-14%
B2c1	430.4	0.2	0.27	0.30	12%	0.29	6%	0.33	24%	0.28	4%	0.23	-15%	0.26	-4%
B3c2	443.7	0.3	0.53	0.42	-20%	0.42	-22%	0.38	-28%	0.48	-10%	0.34	-35%	0.36	-32%
B4c2	434.7	0.3	0.37	0.41	10%	0.40	8%	0.38	3%	0.46	24%	0.33	-11%	0.35	-5%
B5c3	407.8	0.4	0.43	0.47	8%	0.44	3%	0.39	-10%	0.57	33%	0.31	-27%	0.30	-31%
B6c3	404.5	0.4	0.54	0.45	-16%	0.43	-20%	0.38	-29%	0.55	2%	0.29	-46%	0.28	-49%
C1c2	438.8	0.3	0.37	0.46	26%	0.46	24%	0.38	3%	0.54	46%	0.35	-6%	0.41	11%
C1c2	435.9	0.3	0.42	0.45	7%	0.46	9%	0.38	-10%	0.51	22%	0.33	-20%	0.39	-8%
Aver.		0.26	0.36	0.40	31%	0.38	26%	0.36	24%	0.45	44%	0.28	-14%	0.30	-6%
Std.				0.07	0.20	0.08	0.20	0.03	0.24	0.12	0.27	0.06	0.12	0.06	0.15
C.V.				0.18	0.65	0.20	0.75	0.08	0.97	0.27	0.62	0.20	-0.84	0.19	-2.49

Table E-6 Crack width data of slab-strips test specimens of Series 1 at 50kN of two cylinders

No.	Steel stress	Av. crack width [mm]**	Max. crack width [mm]**	Computed by FIB Model Code 2010		Computed by DIN EN 1992-1-2011		Computed by DIN1045-1		Computed by ACI318		Computed by Model-6		Computed by Model-8	
A1c1	468.5	0.2	0.25	0.33	33%	0.32	26%	0.36	46%	0.30	18%	0.24	-2%	0.27	9%
A2c1	472.4	0.2	0.25	0.34	36%	0.32	30%	0.37	47%	0.31	23%	0.25	-1%	0.28	11%
A3c2	489.4	0.2	0.38	0.49	28%	0.48	27%	0.42	11%	0.52	36%	0.37	-4%	0.42	9%
A4c2	486.0	0.3	0.4	0.49	22%	0.48	21%	0.42	5%	0.52	30%	0.37	-7%	0.43	7%
A5c3	436.3	0.3	0.43	0.52	21%	0.50	16%	0.41	-4%	0.63	47%	0.42	-1%	0.45	6%
A6c3	438.9	0.3	0.41	0.52	28%	0.50	22%	0.42	2%	0.63	53%	0.44	7%	0.46	13%
B1c1	420.2	0.2	0.29	0.29	1%	0.27	-8%	0.33	12%	0.26	-12%	0.26	-10%	0.32	11%
B2c1	476.4	0.2	0.28	0.34	23%	0.33	17%	0.37	32%	0.31	11%	0.30	9%	0.34	21%
B3c2	492.1	0.3	0.58	0.48	-17%	0.48	-18%	0.43	-27%	0.53	-9%	0.46	-21%	0.49	-15%
B4c2	480.6	0.3	0.43	0.46	8%	0.46	7%	0.42	-2%	0.51	18%	0.44	3%	0.48	13%
B5c3	452.4	0.5	0.52	0.54	4%	0.51	-1%	0.43	-17%	0.63	22%	0.45	-14%	0.45	-13%
B6c3	450.0	0.5	0.61	0.53	-14%	0.50	-17%	0.43	-30%	0.62	1%	0.42	-31%	0.42	-31%
C1c2	–	–	-	–	-	–	-	–	-	–	-	–	-	–	-
C1c2	–	–	-	–	-	–	-	–	-	–	-	–	-	–	-
Aver.		0.29	0.40	0.45	28%	0.43	24%	0.40	18%	0.48	35%	0.37	-1%	0.40	9%
Std.				0.09	0.17	0.09	0.17	0.03	0.25	0.14	0.20	0.08	0.11	0.08	0.14
C.V.				0.19	0.62	0.20	0.72	0.08	1.37	0.29	0.57	0.22	-7.89	0.19	1.56

Table E-7 Crack width data of slab-strips test specimens of Series 1 at 55kN of two cylinders

No.	Steel stress	Av. crack width [mm]	Max. crack width [mm]	Computed by FIB Model Code 2010		Computed by DIN EN 1992-1-2011		Computed by DIN1045-1		Computed by ACI318		Computed by Model-6		Computed by Model-8	
				Crack width [mm] 55kN											
A1c1	515.8	0.2	0.28	0.38	34%	0.36	27%	0.40	43%	0.33	16%	0.27	-3%	0.31	10%
A2c1	518.7	0.2	0.27	0.38	42%	0.37	35%	0.40	50%	0.34	25%	0.27	1%	0.31	16%
A3c2	541.7	0.3	0.4	0.55	38%	0.55	38%	0.47	17%	0.57	43%	0.41	2%	0.48	19%
A4c2	540.0	0.4	0.5	0.56	11%	0.55	11%	0.47	-6%	0.58	15%	0.42	-17%	0.49	-2%
A5c3	479.7	0.4	0.62	0.59	-4%	0.57	-8%	0.46	-26%	0.70	12%	0.47	-24%	0.55	-12%
A6c3	484.0	0.4	0.47	0.60	27%	0.57	22%	0.46	-2%	0.69	47%	0.49	4%	0.56	19%
B1c1	461.3	0.3	0.37	0.33	-11%	0.30	-18%	0.36	-3%	0.28	-24%	0.29	-22%	0.36	-2%
B2c1	523.5	0.2	0.33	0.39	17%	0.37	12%	0.41	24%	0.34	3%	0.34	2%	0.38	15%
B3c2	539.9	0.4	0.72	0.54	-25%	0.54	-25%	0.47	-35%	0.58	-20%	0.51	-30%	0.57	-21%
B4c2	530.4	0.3	0.48	0.53	10%	0.52	9%	0.47	-3%	0.56	17%	0.49	2%	0.56	17%
B5c3	547.2	0.6	0.75	0.69	-7%	0.67	-11%	0.52	-30%	0.77	2%	0.55	-27%	0.55	-27%
B6c3	–	---	--	–	–	–	–	–	–	–	–	–	–	–	–
C1c2	537.5	0.3	0.46	0.60	31%	0.60	30%	0.47	2%	0.66	44%	0.51	11%	0.66	43%
C1c2	535.1	0.4	0.47	0.58	24%	0.60	27%	0.46	-1%	0.63	34%	0.50	5%	0.62	32%
Aver.		0.33	0.47	0.52	25%	0.51	21%	0.45	13%	0.54	27%	0.42	-6%	0.49	8%
Std.				0.11	0.20	0.11	0.20	0.04	0.25	0.16	0.22	0.10	0.14	0.11	0.19
C.V.				0.21	0.82	0.22	0.98	0.09	1.99	0.29	0.82	0.23	-2.15	0.23	2.31

➢ Series 2

Table E-8 Crack width data of slab-strips test specimens of Series 2 at 40kN of two cylinders

No.	Steel stress [MPa]	Av. crack width [mm]	Max. crack width [mm]	Computed by FIB Model Code 2010		Computed by DIN EN 1992-1-2011		Computed by DIN1045-1		Computed by ACI318		Computed by Model-6		Computed by Model-8	
N1w1	393.91	0.17	0.30	0.420	40%	0.414	38%	0.341	14%	0.430	43%	0.251	-16%	0.296	-1%
N2w1	389.00	0.26	0.30	0.409	36%	0.403	34%	0.337	12%	0.423	41%	0.255	-15%	0.302	1%
N3w2	388.00	0.15	0.26	0.406	56%	0.400	54%	0.336	29%	0.419	61%	0.240	-8%	0.285	10%
N4w2	393.74	0.15	0.28	0.421	50%	0.415	48%	0.341	22%	0.432	54%	0.254	-9%	0.304	8%
N5w3	402.00	0.04	0.06	0.444	640%	0.438	629%	0.348	480%	0.451	652%	0.235	292%	0.288	379%
N6w3	384.00	0.16	0.32	0.393	23%	0.387	21%	0.332	4%	0.407	27%	0.214	-33%	0.257	-20%
H1w1	388.18	0.31	0.36	0.328	-9%	0.318	-12%	0.335	-7%	0.439	22%	0.255	-29%	0.128	-64%
H2w1	388.18	0.24	0.26	0.325	25%	0.316	22%	0.335	29%	0.434	67%	0.259	-1%	0.129	-50%
H3w2	386.73	0.20	0.26	0.332	28%	0.322	24%	0.334	29%	0.455	75%	0.236	-9%	0.107	-59%
H4w2	391.95	0.15	0.22	0.348	58%	0.338	54%	0.339	54%	0.474	115%	0.243	10%	0.111	-50%
H5w3	390.67	0.10	0.12	0.355	196%	0.344	187%	0.338	181%	0.495	312%	0.202	69%	0.072	-40%
H6w3	396.68	0.08	0.10	0.361	261%	0.350	250%	0.343	243%	0.487	387%	0.206	106%	0.070	-30%
L3S2	342.13	0.13	0.30	0.349	16%	0.331	10%	0.290	-3%	0.393	31%	0.279	-7%	0.413	38%
L4S2	391.25	0.26	0.39	0.426	9%	0.408	5%	0.334	-14%	0.368	-6%	0.342	-12%	0.543	39%
L3w2	377.59	0.15	0.26	0.382	47%	0.366	41%	0.322	24%	0.399	53%	0.245	-6%	0.384	48%
L4w2	376.14	0.17	0.29	0.429	48%	0.409	41%	0.320	10%	0.477	65%	0.261	-10%	0.494	70%
L5w2	341.27	0.13	0.19	0.356	87%	0.337	77%	0.290	52%	0.418	120%	0.183	-3%	0.307	61%
L6w2	341.00	0.14	0.22	0.632	187%	0.617	181%	0.460	109%	0.430	96%	0.333	51%	0.322	46%
Aver.		0.17	0.25	0.40	100%	0.38	95%	0.34	70%	0.43	123%	0.25	20%	0.27	22%
Std.		0.07	0.09	0.07	1.53	0.07	1.51	0.03	1.22	0.03	1.66	0.04	0.76	0.14	0.99
C.V.		0.41	0.35	0.18	1.53	0.18	1.59	0.10	1.74	0.08	1.34	0.16	3.73	0.53	4.61

Table E-9 Crack width data of slab-strips test specimens of Series 2 at 50kN of two cylinders

No.	Steel stress [MPa]	Av. crack width [mm]	Max. crack width [mm]	Computed by FIB Model Code 2010		Computed by DIN EN 1992-1-2011		Computed by DIN1045-1		Computed by ACI318		Computed by Model-6		Computed by Model-8	
N1w1	489.4	0.2	0.38	0.55	45%	0.55	44%	0.43	12%	0.43	13%	0.32	-17%	0.41	9%
N2w1	486.0	0.3	0.4	0.54	36%	0.54	35%	0.42	6%	0.42	6%	0.32	-19%	0.42	5%
N3w2	485.0	0.2	0.3	0.54	80%	0.53	78%	0.42	40%	0.42	40%	0.31	2%	0.40	34%
N4w2	490.6	0.3	0.42	0.56	33%	0.55	32%	0.43	1%	0.43	3%	0.32	-23%	0.43	2%
N5w3	500.0	0.1	0.12	0.58	387%	0.58	384%	0.43	262%	0.45	276%	0.31	155%	0.42	249%
N6w3	483.0	0.2	0.32	0.53	64%	0.52	63%	0.42	31%	0.41	27%	0.28	-11%	0.37	17%
H1w1	474.5	0.4	0.42	0.45	7%	0.44	5%	0.41	-2%	0.44	5%	0.32	-25%	0.24	-42%
H2w1	474.5	0.4	0.46	0.45	-3%	0.44	-5%	0.41	-11%	0.43	-6%	0.32	-30%	0.25	-47%
H3w2	461.1	0.4	0.4	0.44	10%	0.43	8%	0.40	0%	0.45	14%	0.29	-28%	0.23	-43%
H4w2	462.8	0.2	0.36	0.45	26%	0.44	23%	0.40	11%	0.47	32%	0.29	-18%	0.24	-34%
H5w3	473.9	0.1	0.2	0.48	141%	0.47	136%	0.41	105%	0.49	147%	0.26	32%	0.20	2%
H6w3	453.5	0.1	0.22	0.45	103%	0.44	99%	0.39	79%	0.49	121%	0.25	13%	0.20	-9%
L3S2															
L4S2		0.3	0.45	-0.08	-119%	-0.14	-132%	-0.01	-102%	0.37	-18%	-0.03	-107%	0.47	5%
L3w2	461.2	0.2	0.3	0.49	63%	0.48	59%	0.40	32%	-	-100%	0.31	2%	0.51	69%
L4w2	473.1	0.2	0.37	0.57	54%	0.55	49%	0.41	10%	-	-100%	0.34	-8%	0.66	79%
L5w2															
L6w2															
Aver.		0.24	0.34	0.47	62%	0.46	59%	0.38	32%	0.38	31%	0.28	-5%	0.36	20%
Std.				0.16	1.07	0.17	1.08	0.11	0.78	0.16	0.94	0.09	0.54	0.13	0.73
C.V.				0.34	1.73	0.38	1.84	0.29	2.47	0.41	3.06	0.32	-9.81	0.37	3.71

Table E-10 Crack width data of slab-strips test specimens of Series 2 at 55kN of two cylinders

No.	Steel stress [MPa]	Av. crack width [mm]	Max. crack width [mm]	Computed by FIB Model Code 2010		Computed by DIN EN 1992-1-2011		Computed by DIN1045-1		Computed by ACI318		Computed by Model-6		Computed by Model-8	
N1w1	542	0.3	0.4	0.63	56%	0.62	56%	0.47	18%	0.43	7%	0.35	-12%	0.47	17%
N2w1	540	0.4	0.5	0.62	23%	0.61	23%	0.47	-6%	0.42	-15%	0.36	-28%	0.48	-4%
N3w2	534	0.2	0.36	0.61	68%	0.60	68%	0.46	29%	0.42	16%	0.34	-5%	0.46	27%
N4w2	542	0.3	0.52	0.63	21%	0.62	20%	0.47	-9%	0.43	-17%	0.36	-31%	0.49	-6%
N5w3	550	0.1	0.18	0.66	265%	0.65	263%	0.48	166%	0.45	151%	0.34	90%	0.48	167%
N6w3	532	0.2	0.34	0.59	74%	0.59	74%	0.46	36%	0.41	20%	0.32	-7%	0.43	26%
H1w1	540	0.7	0.82	0.54	-34%	0.54	-35%	0.47	-43%	0.44	-46%	0.36	-56%	0.31	-63%
H2w1	540	0.5	0.52	0.54	3%	0.53	2%	0.47	-10%	0.43	-17%	0.37	-29%	0.31	-41%
H3w2	530	0.7	1.38	0.54	-61%	0.53	-61%	0.46	-67%	0.45	-67%	0.34	-75%	0.30	-79%
H4w2	553	0.3	0.5	0.59	17%	0.58	16%	0.48	-4%	0.47	-5%	0.36	-28%	0.31	-39%
H5w3	546	0.1	0.26	0.59	127%	0.58	124%	0.47	82%	0.49	90%	0.32	23%	0.28	6%
H6w3	544	0.1	0.34	0.58	71%	0.57	69%	0.47	39%	0.49	43%	0.32	-7%	0.27	-20%
L3S2	499	0.2	0.38	0.56	47%	0.54	43%	0.43	13%	0.39	3%	0.41	9%	0.72	90%
L4S2	518	0.3	0.48	0.60	25%	0.59	22%	0.45	-7%	0.37	-23%	0.46	-4%	0.80	66%
L3w2	521	0.2	0.51	0.57	11%	0.55	9%	0.45	-12%	0.58	14%	0.35	-32%	0.57	11%
L4w2	519	0.2	0.38	0.64	68%	0.62	63%	0.45	17%	0.63	66%	0.38	0%	0.74	95%
L5w2	535	0.2	0.6	0.62	4%	0.61	1%	0.46	-23%	0.42	-30%	0.32	-46%	0.58	-4%
L6w2	535	0.2	0.45	0.63	40%	0.62	37%	0.46	2%	0.43	-4%	0.33	-26%	0.61	35%
Aver.		30%	50%	60%	46%	59%	44%	46%	12%	45%	10%	36%	-15%	48%	16%
Std.		0.17	0.26	0.04	0.69	0.04	0.69	0.01	0.50	0.06	0.51	0.04	0.35	0.17	0.60
C.V.		0.58	0.53	0.06	1.51	0.06	1.57	0.03	4.11	0.14	4.99	0.10	-2.39	0.35	3.79

Appendix F   Results of slabs under biaxial bending

Appendix F.1   Final crack pattern overlapped with TR layout

➢ **Normal-strength concrete**
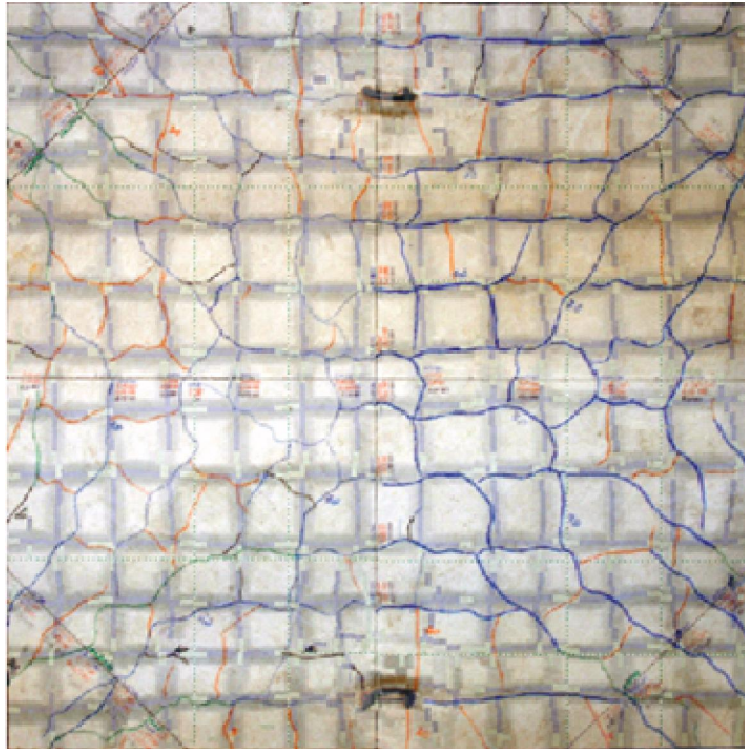
P01 W1 C30 , loading 60kN, 63% of Ultimate load
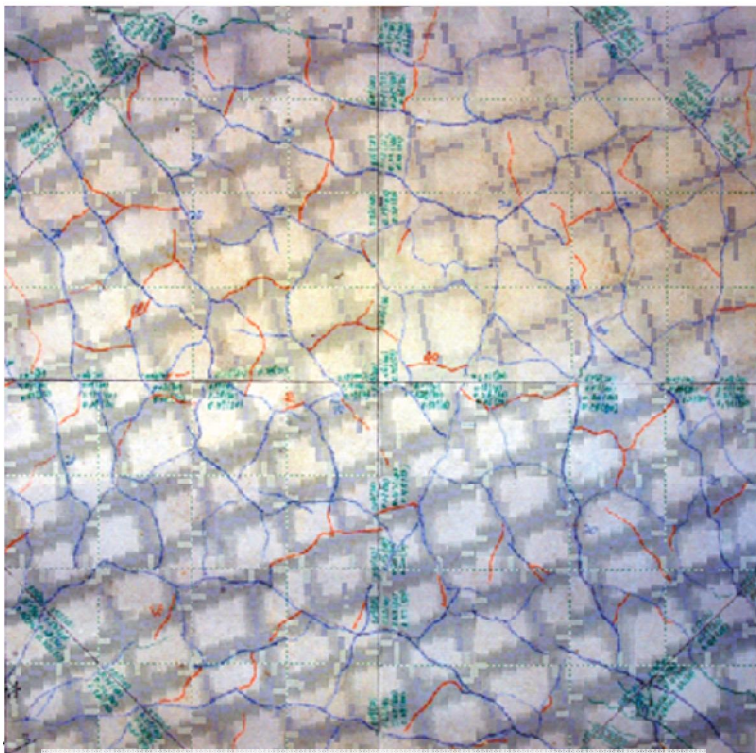
P01 W2 C30 , loading 60kN, 63% of Ultimate load
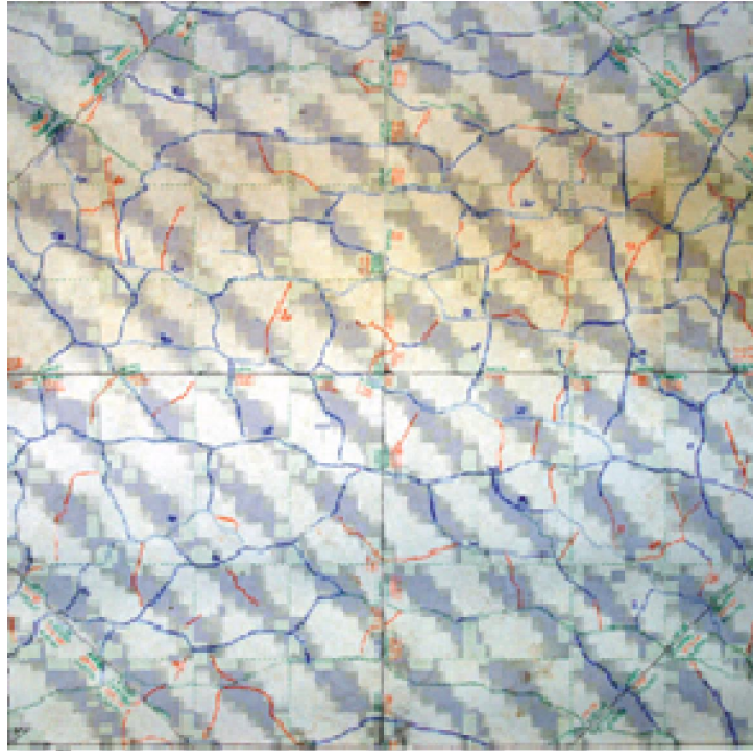
P03 W3 C30 , loading 60kN, 63% of Ultimate load

Figure F-1 Final crack pattern overlapped with TR layout of slabs of normal-strength concrete

➢ **High-strength concrete**
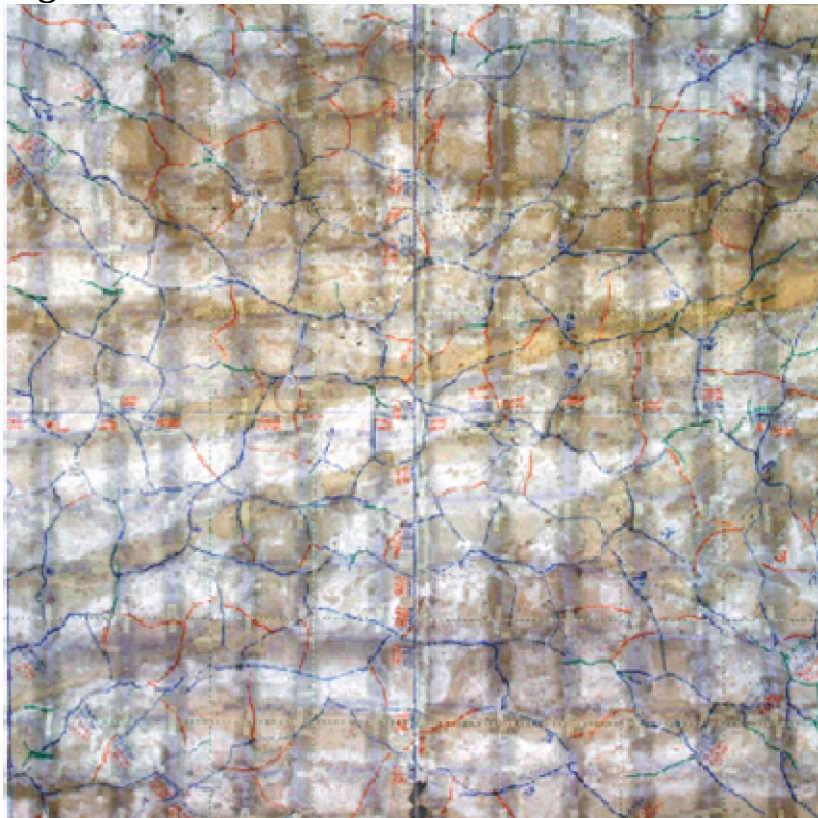
P04 W1 C100 , loading 60kN, 60 % of Ultimate load
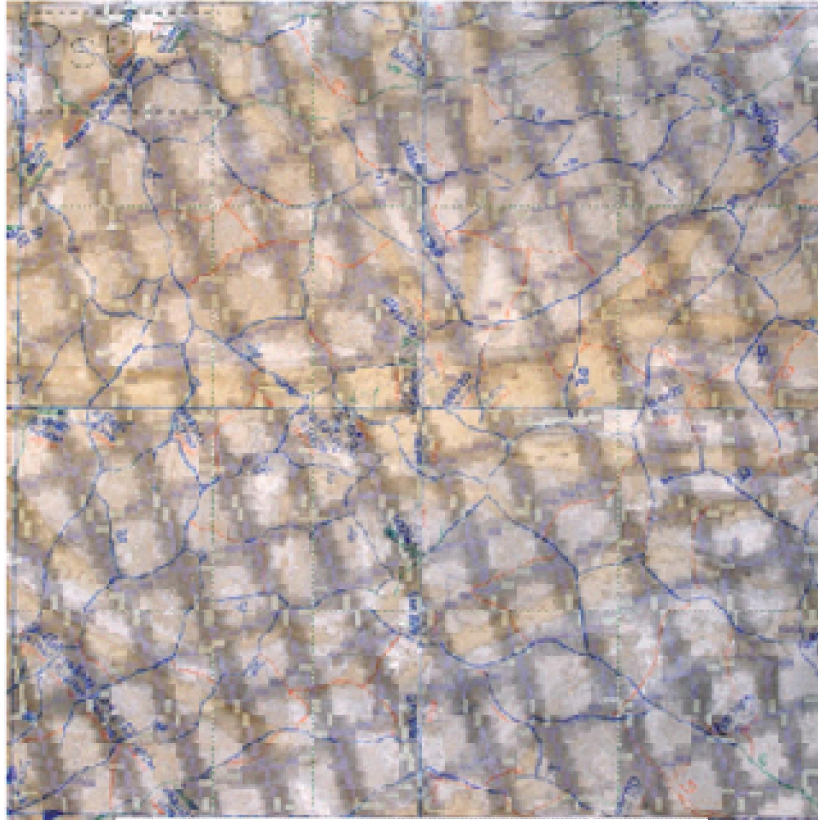
P05 W2 C100 , loading 60kN, 60 % of Ultimate
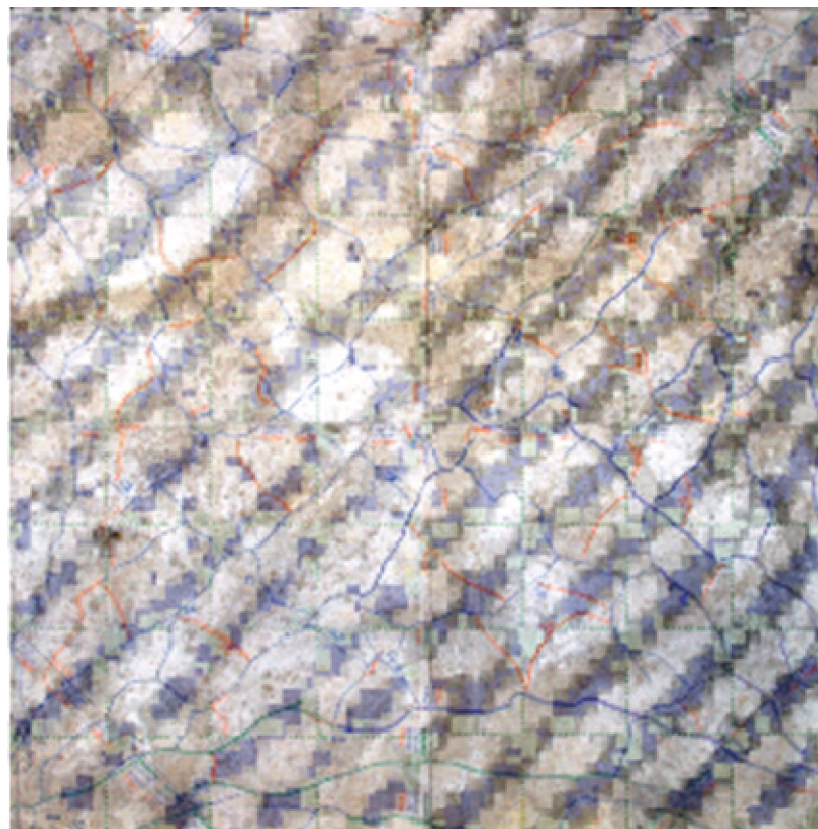
P06 W3 C100 , loading 60kN, 60 % of Ultimate load

Figure F-2 Final crack pattern overlapped with TR layout of slabs of high-strength concrete

➢ **Lightweight –concrete**
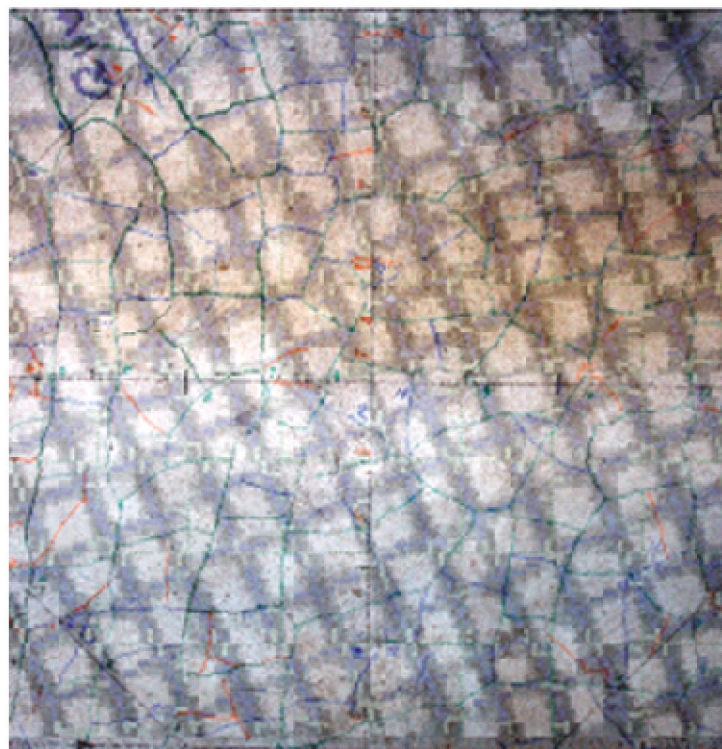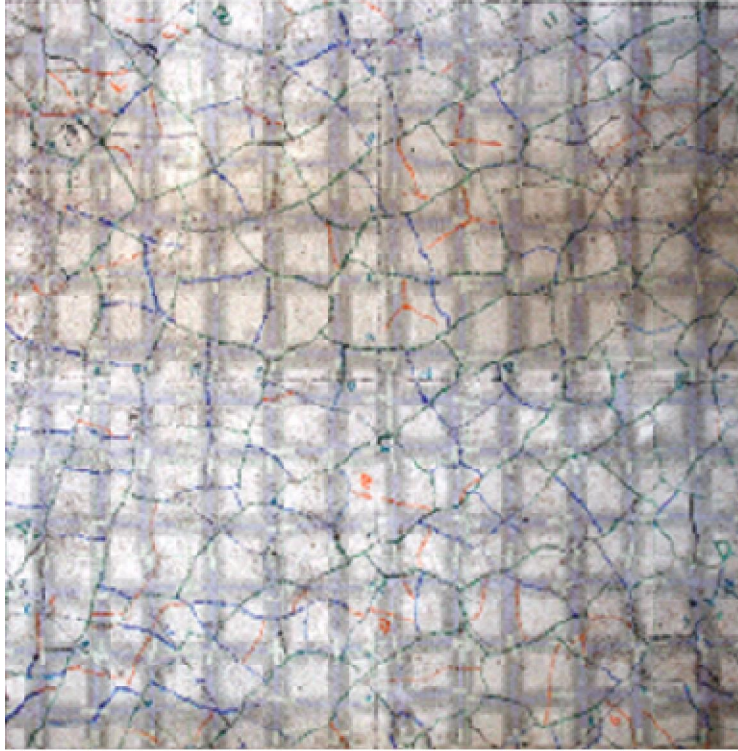
P08 W2 LC33 , loading 60kN, 70 % of Ultimate load
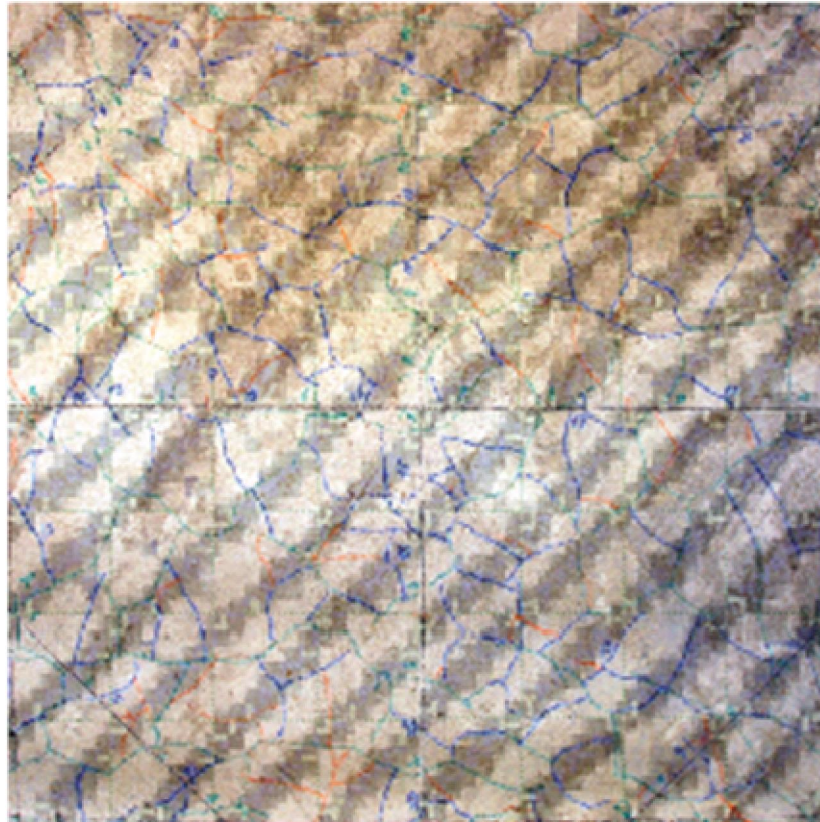
P09 W3 LC33 , loading 60kN, 70 % of Ultimate load

Figure F-3 Final crack pattern overlapped with TR layout of slabs of lightweight concrete

Appendix F.2 Load-deformation behavior
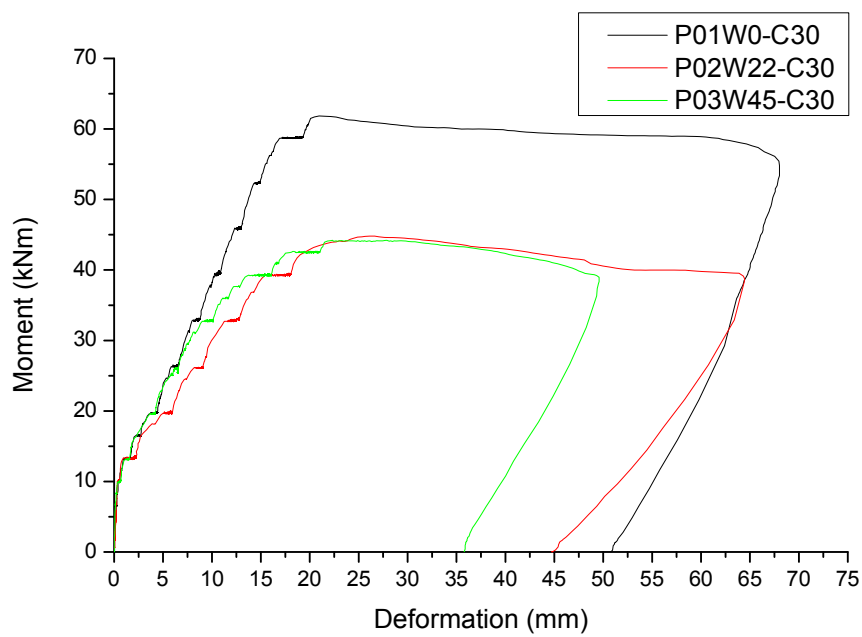
Figure F-4 Load-deformation curves of 3 normal-strength concrete specimens with 3 kinds of TR-direction
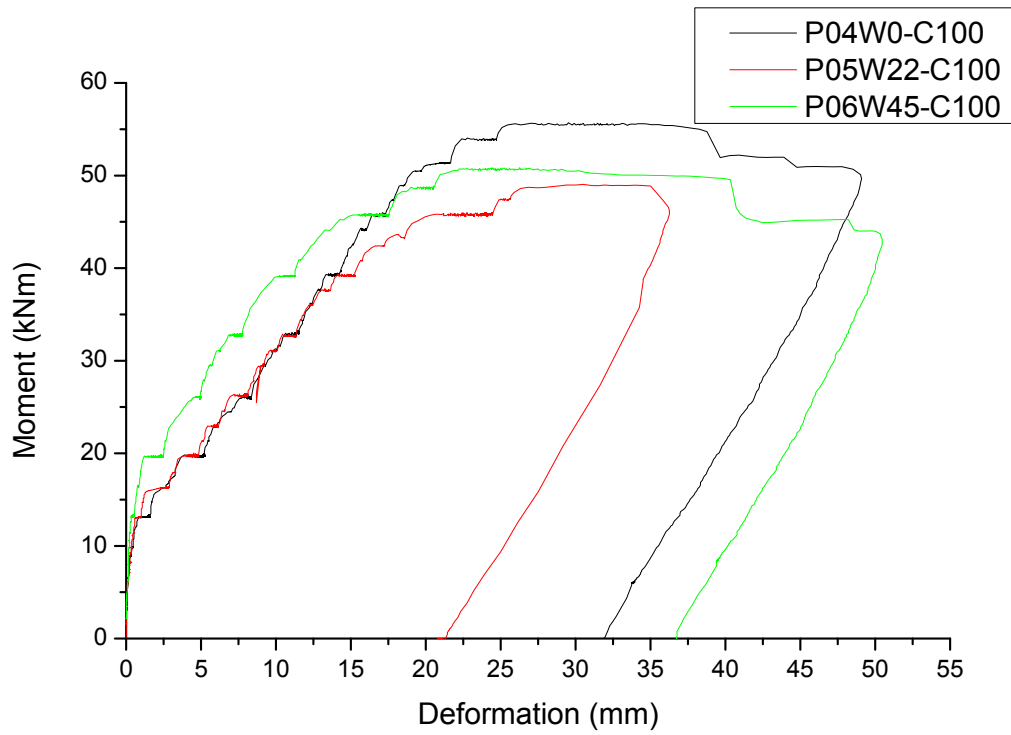
Figure F-5 Load-deformation curves of 3 high-strength concrete specimens with 3 kinds of TR-direction
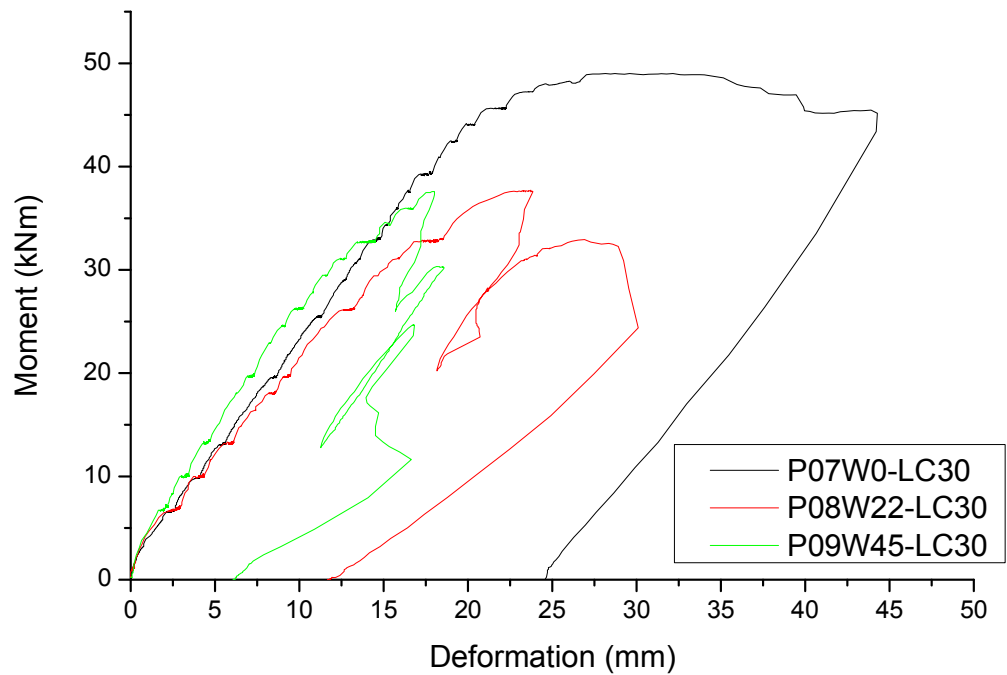
Figure F-6 Load-deformation curves of 3 lightweight concrete specimens with 3 kinds of TR-direction

Appendix F.3   *Crack spacing data of slab specimens*

Table F-1 Crack spacing data of slab test specimens in direction of Type A

Direction of Type A	Av. crack	Predicted crack spacing [mm]							
		by FIB Model Code 2010		by DIN EN 1992-1-2011		by DIN1045-1		By proposed model	
P01-0°	100.00	77.70	-22%	85.68	-14%	79.58	-20%	102.26	2%
P02-22.5°	85.71	61.16	-29%	67.45	-21%	60.91	-29%	110.62	29%
P03-45°	75.00	56.53	-25%	62.34	-17%	56.27	-25%	83.41	11%
P04-0°	66.67	80.88	21%	89.19	34%	79.58	19%	106.68	60%
P05-22.5°	85.71	61.30	-28%	67.60	-21%	60.91	-29%	111.29	30%
P06-45°	85.71	56.13	-35%	61.89	-28%	56.27	-34%	82.81	-3%
P07-0°	85.71	79.60	-7%	87.78	2%	79.58	-7%	105.02	23%
P08-22.5°	120.00	61.51	-49%	67.83	-43%	60.91	-49%	111.52	-7%
P09-45°	75.00	56.84	-24%	62.68	-16%	56.27	-25%	83.88	12%
Av.	86.61	65.74	-22%	72.49	-14%	65.58	-22%	99.72	17%
Std.	15.67	10.48	0.20	11.56	0.22	10.69	0.19	12.64	0.21
C.V.	0.18	0.16	-0.89	0.16	-1.55	0.16	-0.86	0.13	1.20

Table F-2 Crack spacing data of slab test specimens in direction of Type B

Direction of Type B	Av. crack	Predicted crack spacing [mm]							
		by FIB Model Code 2010		by DIN EN 1992-1-2011		by DIN1045-1		By proposed model	
P01-0°	150.00	75.05	-50%	82.81	-45%	79.58	-47%	104.26	-30%
P02-22.5°	100.00	30.98	-69%	66.25	-34%	60.91	-39%	111.89	12%
P03-450°	120.00	56.53	-53%	62.34	-48%	56.27	-53%	83.46	-30%
P04-0°	85.71	77.82	-9%	85.82	0%	79.58	-7%	107.73	26%
P05-22.5°	100.00	31.03	-69%	66.47	-34%	60.91	-39%	112.15	12%
P06-45°	100.00	56.13	-44%	61.89	-38%	56.27	-44%	82.87	-17%
P07-0°	120.00	76.83	-36%	84.72	-29%	79.58	-34%	106.41	-11%
P08-22.5°	100.00	31.13	-69%	66.71	-33%	60.91	-39%	112.49	12%
P09-45°	85.71	56.84	-34%	62.68	-27%	56.27	-34%	83.91	-2%
Av.	106.83	54.71	-48%	71.08	-32%	65.58	-37%	100.57	-3%
Std.	20.28	19.77	0.20	10.22	0.14	10.69	0.13	13.17	0.20
C.V.	0.19	0.36	-0.42	0.14	-0.43	0.16	-0.34	0.13	-6.23

Appendix F.4   Crack width data of slab specimens

Table F-3 Crack width data of slab test specimens in direction of Type A at load of 30kN at each cylinder

Direction of Type A	Steel stress [MPa]	Crack width [mm] 30kN														
		Av	Max.	Computed by FIB Model Code 2010		Computed by DIN EN 1992-1-2011		Computed by DIN1045-1		Computed by ACI318		Computed by Model-7		Computed by Model-9	
P01	224.5	0.07	0.13	0.17	28%	0.08	-40%	0.11	-12%	0.24	84%	0.20	54%	0.10	-26%
P02	196.3	0.17	0.27	0.17	-38%	0.05	-83%	0.08	-72%	0.36	33%	0.17	-35%	0.08	-71%
P03	246.4	0.10	0.25	0.23	-9%	0.06	-74%	0.09	-65%	0.45	81%	0.17	-32%	0.23	-10%
P04	340.7	0.11	0.20	0.27	34%	0.09	-56%	0.13	-34%	0.47	136%	0.24	22%	0.04	-81%
P05	268.9	0.10	0.14	0.17	24%	0.05	-66%	0.09	-39%	0.41	194%	0.20	42%	0.04	-70%
P06	237.1	0.12	0.19	0.12	-35%	0.03	-82%	0.07	-63%	0.33	76%	0.12	-35%	0.03	-84%
P07	289.7	0.16	0.24	0.27	11%	0.10	-60%	0.11	-53%	0.34	41%	0.20	-18%	0.34	43%
P08	272.1	0.21	0.26	0.24	-9%	0.06	-76%	0.08	-70%	0.40	53%	0.17	-34%	0.36	37%
P09	252.5	0.11	0.12	0.24	98%	0.06	-48%	0.07	-38%	0.41	245%	0.14	17%	0.31	156%
Av.		0.13	0.20	0.21	12%	0.06	-65%	0.09	-49%	0.38	105%	0.18	-2%	0.17	-12%
Std.		0.04	0.06	0.05	0.42	0.02	0.15	0.02	0.20	0.07	0.73	0.04	0.36	0.14	0.79
C.V.		0.34	0.29	0.25	3.54	0.31	######	0.24	-0.41	0.19	0.70	0.20	-17.78	0.82	-6.65

Table F-4 Crack width data of slab test specimens in direction of Type B at load of 30kN at each cylinder

Direction of Type B	Steel stress [MPa]	Crack width [mm] 30kN													
		Av	Max.	Computed by FIB Model Code 2010		Computed by DIN EN 1992-1-2011		Computed by DIN1045-1		Computed by ACI318		Computed by Model-7		Computed by Model-9	
P01	277.4	0.09	0.15	0.20	34%	0.11	-30%	0.14	-5%	0.17	12%	0.26	72%	0.19	28%
P02	263.9	0.12	0.19	0.08	-56%	0.08	-59%	0.10	-46%	0.27	43%	0.25	33%	0.24	28%
P03	206.2	0.07	0.12	0.14	13%	0.05	-60%	0.07	-39%	0.23	91%	0.14	17%	0.07	-38%
P04	260.8	0.20	0.30	0.28	-6%	0.09	-71%	0.17	-42%	0.37	24%	0.25	-18%	0.20	-32%
P05	220.8	0.20	0.26	0.08	-69%	0.07	-73%	0.10	-60%	0.29	13%	0.25	-2%	0.14	-46%
P06	197.5	0.27	0.53	0.13	-75%	0.05	-90%	0.08	-84%	0.28	-47%	0.16	-70%	0.10	-80%
P07	229.4	0.28	0.46	0.25	-46%	0.13	-72%	0.15	-68%	0.26	-43%	0.26	-43%	0.38	-17%
P08	205.1	0.25	0.32	0.11	-65%	0.09	-71%	0.10	-67%	0.31	-2%	0.25	-23%	0.40	24%
P09	214.3	0.15	0.20	0.24	18%	0.08	-61%	0.09	-56%	0.37	83%	0.14	-30%	0.32	62%
Av.		0.18	0.28	0.17	-28%	0.08	-65%	0.11	-52%	0.28	19%	0.22	-7%	0.23	-8%
Std.		0.08	0.14	0.07	0.42	0.02	0.16	0.03	0.23	0.06	0.48	0.05	0.43	0.12	0.46
C.V.		0.43	0.49	0.45	-1.52	0.30	-0.25	0.29	-0.44	0.22	2.50	0.25	-5.98	0.51	-5.86

Table F-5 Crack width data of slab test specimens in direction of Type A at load of 40kN at each cylinder

Direction of Type A	Steel stress [MPa]	Av	Max.	Computed by FIB Model Code 2010		Computed by DIN EN 1992-1-2011		Computed by DIN1045-1		Computed by ACI318		Computed by Model-7		Computed by Model-9	
P01	300.9	0.1	0.18	0.25	41%	0.12	-33%	0.15	-14%	0.32	78%	0.28	54%	0.22	22%
P02	260.8	0.2	0.32	0.26	-18%	0.08	-76%	0.10	-68%	0.48	49%	0.25	-23%	0.21	-35%
P03	323.0	0.1	0.31	0.33	8%	0.10	-69%	0.12	-62%	0.59	91%	0.23	-25%	0.37	19%
P04	448.8	0.2	0.31	0.41	32%	0.14	-56%	0.18	-43%	0.62	100%	0.33	7%	0.14	-55%
P05	357.4	0.1	0.27	0.28	4%	0.08	-70%	0.11	-58%	0.55	103%	0.28	3%	0.16	-39%
P06	315.3	0.1	0.11	0.21	90%	0.06	-44%	0.09	-14%	0.44	303%	0.18	61%	0.11	-1%
P07	375.5	0.2	0.28	0.37	31%	0.14	-51%	0.15	-47%	0.44	57%	0.27	-4%	0.49	75%
P08	362.3	0.3	0.40	0.34	-15%	0.09	-77%	0.10	-74%	0.53	32%	0.25	-38%	0.52	30%
P09	337.2	0.2	0.20	0.34	70%	0.09	-54%	0.10	-49%	0.55	176%	0.20	0%	0.43	114%
Av.		0.17	0.26	0.31	27%	0.10	-59%	0.12	-48%	0.50	110%	0.25	4%	0.29	14%
Std.		0.08	0.09	0.06	0.37	0.03	0.15	0.03	0.21	0.09	0.84	0.05	0.34	0.16	0.55
C.V.		0.49	0.33	0.20	1.36	0.27	-0.26	0.23	-0.45	0.18	0.76	0.18	8.40	0.54	3.81

Table F-6 Crack width data of slab test specimens in direction of Type B at load of 40kN at each cylinder

Direction of Type B	Steel stress [MPa]	Av	Max.	Crack width [mm] 40kN											
				Computed by FIB Model Code 2010		Computed by DIN EN 1992-1-2011		Computed by DIN1045-1		Computed by ACI318		Computed by Model-7		Computed by Model-9	
P01	371.7	0.14	0.25	0.30	18%	0.16	-37%	0.19	-23%	0.22	-10%	0.36	42%	0.32	27%
P02	350.7	0.25	0.40	0.12	-69%	0.12	-71%	0.14	-65%	0.36	-9%	0.35	-13%	0.38	-5%
P03	270.3	0.09	0.13	0.20	57%	0.07	-42%	0.10	-25%	0.30	131%	0.19	49%	0.15	19%
P04	343.6	0.31	0.59	0.41	-31%	0.13	-77%	0.23	-61%	0.49	-17%	0.34	-43%	0.39	-34%
P05	293.5	0.23	0.27	0.12	-54%	0.11	-59%	0.14	-48%	0.39	44%	0.35	31%	0.29	7%
P06	262.7	0.15	0.21	0.21	-1%	0.08	-60%	0.11	-46%	0.38	79%	0.22	6%	0.21	-2%
P07	297.4	0.33	0.50	0.34	-33%	0.18	-65%	0.19	-62%	0.34	-32%	0.35	-29%	0.52	4%
P08	273.1	0.48	0.54	0.16	-71%	0.13	-75%	0.14	-74%	0.42	-23%	0.35	-36%	0.54	-1%
P09	286.2	0.22	0.34	0.33	-2%	0.11	-67%	0.12	-65%	0.49	44%	0.20	-41%	0.43	28%
Av.		0.25	0.36	0.24	-21%	0.12	-62%	0.15	-52%	0.38	23%	0.30	-4%	0.36	5%
Std.		0.12	0.16	0.10	0.42	0.03	0.14	0.04	0.18	0.08	0.56	0.07	0.37	0.13	0.19
C.V.		0.48	0.44	0.42	-2.05	0.26	-0.23	0.29	-0.35	0.23	2.42	0.24	-9.72	0.36	4.00

Table F-7 Crack width data of slab test specimens in direction of Type A at load of 50kN at each cylinder

Direction of Type A	Steel stress [MPa]	Av	Max.	Crack width [mm] 50kN												
				Computed by FIB Model Code 2010		Computed by DIN EN 1992-1-2011		Computed by DIN1045-1		Computed by ACI318		Computed by Model-7		Computed by Model-9	
P01	373.8	0.13	0.24	0.34	40%	0.16	-32%	0.19	-20%	0.40	66%	0.35	47%	0.34	41%
P02	313.6	0.28	0.45	0.34	-25%	0.10	-78%	0.12	-73%	0.57	27%	0.30	-33%	0.37	-19%
P03	412.6	0.14	0.37	0.46	24%	0.13	-64%	0.15	-59%	0.76	104%	0.31	-17%	0.53	45%
P04	569.8	0.21	0.35	0.57	61%	0.19	-45%	0.23	-36%	0.79	125%	0.43	23%	0.30	-14%
P05	443.9	0.25	0.35	0.39	10%	0.11	-68%	0.14	-59%	0.68	94%	0.36	2%	0.32	-9%
P06	397.2	0.12	0.19	0.30	56%	0.09	-53%	0.12	-37%	0.56	194%	0.23	23%	0.22	13%
P07	488.1	0.29	0.34	0.50	47%	0.19	-45%	0.20	-42%	0.57	68%	0.36	6%	0.67	98%
P08	454.6	0.45	0.52	0.44	-14%	0.12	-76%	0.13	-74%	0.66	28%	0.32	-38%	0.69	32%
P09	419.7	0.24	0.32	0.44	38%	0.12	-62%	0.13	-60%	0.69	115%	0.26	-19%	0.55	73%
Av.		0.23	0.35	0.42	26%	0.14	-58%	0.16	-51%	0.63	91%	0.33	-1%	0.44	29%
Std.		0.10	0.10	0.09	0.30	0.04	0.15	0.04	0.18	0.12	0.52	0.06	0.28	0.17	0.40
C.V.		0.45	0.28	0.21	1.16	0.27	-0.43	0.24	-0.36	0.19	0.57	0.18	-54.56	0.39	1.39

Table F-8: Crack width data of slab test specimens in direction of Type B at load of 50kN at each cylinder

Directi on of Type B	Steel stress [MPa]	Av	Max.	Crack width [mm] 50kN										
				Computed by FIB Model Code 2010		Computed by DIN EN 1992-1-2011		Computed by DIN1045-1		Computed by ACI318		Computed by Model-7		Computed by Model-9	
P01	461.9	0.16	0.26	0.39	48%	0.21	-20%	0.24	-8%	0.28	7%	0.45	73%	0.43	65%
P02	422.0	0.34	0.56	0.16	-72%	0.15	-74%	0.17	-70%	0.44	-22%	0.43	-23%	0.52	-8%
P03	345.3	0.15	0.19	0.28	49%	0.11	-44%	0.13	-34%	0.38	102%	0.26	34%	0.25	32%
P04	436.2	0.31	0.61	0.55	-10%	0.19	-69%	0.30	-52%	0.62	2%	0.43	-29%	0.59	-3%
P05	364.5	0.32	0.43	0.16	-62%	0.15	-66%	0.18	-59%	0.48	13%	0.45	4%	0.43	0%
P06	330.9	0.19	0.34	0.29	-16%	0.12	-65%	0.14	-57%	0.47	40%	0.29	-14%	0.31	-7%
P07	386.5	0.44	0.80	0.45	-44%	0.24	-70%	0.25	-69%	0.44	-45%	0.47	-41%	0.70	-13%
P08	342.6	0.50	0.54	0.20	-62%	0.17	-68%	0.18	-67%	0.52	-3%	0.45	-17%	0.69	27%
P09	356.1	0.22	0.34	0.43	26%	0.15	-57%	0.15	-55%	0.61	79%	0.26	-24%	0.55	62%
Av.		0.29	0.45	0.32	-16%	0.16	-59%	0.19	-52%	0.47	19%	0.39	-4%	0.50	17%
Std.		0.12	0.19	0.14	0.48	0.04	0.17	0.06	0.20	0.11	0.47	0.09	0.36	0.15	0.31
C.V.		0.41	0.43	0.43	-3.01	0.26	-0.29	0.30	-0.38	0.23	2.46	0.23	-8.96	0.31	1.77

Curriculum Vitae

Personal information

Daguang Han

Margreider platz 1, 85521 Ottobrunn

Tel.: 017640258738

E-mail:daguang.han@gmail.com

Date of Birth 21. July 1982

Education:

09.1995 – 07.1998	Fuxin 26th Middle school, Liaoning P.R. China
09.1998 – 06.2001	Fuxinxian High middle school, Liaoning P.R. China
09.2001 – 07.2005	Shenyang Jianzhu University, Liaoning, P.R. China Major:Civil Engineering, Bachelor Thesis: "Architecture and Structure Design for an Office Building"
09.2005 – 02.2008	Shenyang Jianzhu University, Liaoning, P.R. China Major:Structural Engineering, Master Thesis: "Experiment and Theoretical Research on Multi-ribbed Reinforced Concrete Slab System"
07.2008 – Now	Research assistant, UniBwM, Institute for Construction Engineering. Prof. Dr.-Ing Manfrd Keuser

Neubiberg 2011